



universität  
wien

# DISSERTATION

Titel der Dissertation

Molecular, structural, and in vivo analysis of the  
dominant plectin mutation EBS-Ogna

Verfasserin

Nevena Jaksic

angestrebter akademischer Grad

Doctor of Philosophy (PhD)

Wien, 2015

Studienkennzahl lt.  
Studienblatt:

A >091 490<

Dissertationsgebiet lt.  
Studienblatt:

Molecular Biology

Betreut von:

Emer. o. Univ.-Prof. Dr. Gerhard Wiche



## ACKNOWLEDGEMENTS

I would like to thank Prof. Gerhard Wiche for giving me the opportunity to carry out my PhD work in his group on this interesting and exciting project, for his supervision and support.

Thanks to the members of my PhD committee, Prof. Roland Foisner and Prof. Robert Konrat for their valuable suggestions during the course of this work. I am also thankful to the reviewers of my PhD thesis Prof. Marcel F. Jonkmann and Prof. Matthias Schmuth for taking the time to read and evaluating my work.

I am very grateful to M. Castañón for continuous support, encouragement and endless motivation. Her knowledge, experience and work with me resulted in my scientific development and finalization of this thesis.

Many thanks go to all lab members, and collaborators, especially to Peter Fuchs for his great support by the generation of transgenic mice, and to my lab colleagues Selma, Reinhard, Gernot, and Günther for creating an excellent working atmosphere and for many scientific discussions. Irmi and Karin provided valuable technical assistance, Ute advice with the statistics and Siegfried precious expertise on electron microscope.

I am grateful to my family for their endless patience, support and love during this thesis.

## CONTRIBUTIONS

Peter Fuchs designed the targeting construct.

Siefrid Reipert performed the electron microscopy shown in Figures 24-26 and 30, except for the analysis of the micrographs which was done in full by myself.

Ute Jungwirth (Medical University of Vienna) helped with statistical analysis.

Mass spectrometry was performed by the MFPL Mass Spectrometry Facility.

### Manuscript

*Targeted proteolysis of plectin isoform 1a accounts for hemidesmosome dysfunction in mice mimicking the dominant skin blistering disease EBS-Ogna.*

Walko G, **Vukasinovic N**, Gross K, Fischer I, Sibitz S, Fuchs P, Reipert S, Jungwirth U, Berger W, Salzer U, Carugo O, Castañón MJ, Wiche G.  
PLoS Genet. 7, e1002396, 2011.

Own contribution:

First part of results, including chapters:

EBS-Ogna mouse lines mimic the human disease

Altered morphology and decreased numbers of HDs in Ogna epidermis

Cultured Ogna keratinocytes show impaired formation of HD-like protein complexes

Reduced osmotic shock resistance, and increased migration potential

The Ogna mutation decreases the stability of the dimeric plectin RD

and Figures 1-6 in the main text, and S1-S2, S5-S6, S7A,B and S8 in Supporting Information.



# TABLE OF CONTENTS

Acknowledgements.....	i
Contributions.....	ii
Table of Contents.....	iii
Table of Figures.....	vi
Abbreviations.....	viii
Summary.....	1
Zusammenfassung.....	3
Introduction.....	5
The Skin.....	5
Epidermal homeostasis.....	6
Cell junctions in the epidermis.....	7
The cytoskeleton.....	9
Cytolinker proteins.....	11
Plectin.....	12
<i>The gene</i> .....	13
<i>Structural properties, interactions and cellular localization of the protein</i> .....	14
<i>Plectin deficiency</i> .....	16
<i>EBS-Ogna – an autosomal dominant disease</i> .....	19
<i>Animal models in the study of plectin function</i> .....	20
Aim of thesis.....	22
Results.....	23
I. Generation of an EBS-Ogna plectin knock-in mouse line.....	23
Construction of the targeting vector.....	24
Gene targeting in mouse embryonic stem cells.....	24
Generation of mice with a targeted plectin locus.....	27
Removal of the neomycin resistance cassette.....	28
Generation of a homozygous Ogna plectin knock-in mouse line.....	31
II. Expression of Ogna plectin mRNA in mouse tissues and primary keratinocytes...32	
Transcript levels of plectin isoforms in mouse epidermis and primary keratinocytes.....	33
III. Phenotypic analysis of Ogna mice.....	35
1. Skin Phenotype.....	35
<i>Macroscopic analysis</i> .....	35
<i>Skin integrity</i> .....	36
<i>Histological analysis of the skin</i> .....	38
<i>Ultrastructural analysis of skin lesions</i> .....	39
<i>Ultrastructural and morphometric analyses of hemidesmosomes</i> .....	40
<i>Ultrastructural analysis of desmosomes</i> .....	44
<i>Expression of hemidesmosomal components</i> .....	44
<i>Expression of epidermal stratification markers</i> .....	50
2. Muscle phenotype.....	51
<i>Voluntary wheel running</i> .....	51
<i>Expression of plectin, desmin, and <math>\alpha</math>-actinin in skeletal and cardiac muscle</i> .....	52
<i>Expression of plectin and desmoplakin in cardiac muscle</i> .....	55
IV. Ex vivo analysis of primary keratinocytes.....	56
Expression of hemidesmosomal proteins in primary keratinocytes.....	56
Keratin network organization.....	57
Attempted rescue of the abnormal HPC phenotype.....	58
Response to hypo-osmotic shock.....	59
Migration behavior.....	61

V. The plectin rod: structure and interactions.....	64
Expression and purification of the rod domain.....	66
Oligomeric state of the plectin rod.....	67
Differential stability of the RD oligomers.....	71
Binding affinity.....	72
Hetero-oligomer formation.....	73
Identification of novel binding partners.....	75
Discussion.....	80
The Ogn mouse mimics the human disease.....	80
P1a but not P1c is the isoform missing in the basal cell layer of the Ogn epidermis.....	81
Absence of P1a correlates with rudimentary HDs at the dermo-epidermal junction.....	81
Impact of the Ogn mutation on the plectin rod.....	82
Spatiotemporal regulation of P1a degradation.....	83
Impact of the mutated rod on hemidesmosome formation.....	84
Ethiopathogenesis/molecular basis of EBS-Ogn.....	85
Conclusions.....	85
Materials & Methods.....	87
Materials.....	87
1. Buffers and Solutions.....	87
2. Bacterial strains.....	92
3. Baculoviruses.....	93
4. Plasmids, cloning and expression vectors used for preparation of new constructs.....	93
5. Primers.....	94
6. Antibodies and enzyme conjugates.....	95
Methods.....	96
1. Molecular Biology: DNA and RNA.....	96
<i>Isolation of genomic DNA from cells and mouse tails.....</i>	96
<i>Phenol-purification and precipitation of DNA.....</i>	96
<i>Quantification of DNA and RNA.....</i>	96
<i>Polymerase chain reaction.....</i>	96
<i>Preparation of plasmid DNA.....</i>	97
<i>Digestion of DNA with restriction enzymes.....</i>	97
<i>Dephosphorylation of vector DNA.....</i>	97
<i>Separation of DNA by agarose gel electrophoresis.....</i>	98
<i>Recovery of DNA from agarose gels.....</i>	98
<i>Ligation.....</i>	98
<i>Preparation of competent bacteria and transformation.....</i>	98
<i>Preparation of bacterial stocks.....</i>	99
<i>DNA sequencing.....</i>	99
<i>Southern blot analysis.....</i>	100
<i>Isolation of RNA.....</i>	100
<i>RNA electrophoresis.....</i>	100
<i>Reverse Transcription and RT-PCR.....</i>	101
<i>Real Time quantitative PCR (RT-qPCR).....</i>	101
2. Biochemistry: protein expression, purification, and interactions.....	102
<i>Expression of recombinant proteins in insect cells.....</i>	102
<i>Purification of recombinant proteins.....</i>	102
<i>Preparation of cell and tissue extracts.....</i>	103
<i>Protein quantification.....</i>	103
<i>SDS-polyacrylamide gel electrophoresis (PAGE).....</i>	104
<i>Native and blue native (BN) – PAGE.....</i>	104

Size exclusion chromatography (SEC) – gel filtration.....	104
Buffer exchange and microdialysis.....	104
Cross-linking experiments.....	105
Immunoblotting.....	105
Quantification of protein bands in gels and immunoblots.....	105
Pull-downs.....	105
Overlay binding assay.....	106
3. Cell Culture.....	107
Insect cell culture.....	107
Mammalian cell culture.....	107
4. Histology.....	109
Preparation of tissue sections.....	109
Staining of tissue sections.....	110
5. Immunofluorescence and cell assays.....	110
Immunofluorescence and phase contrast microscopy of tissue sections and cells ...	110
Electron microscopy.....	110
Time-lapse video microscopy of single cells.....	111
Scratch wound closure assay.....	111
Morphometric analysis of Hemidesmosomes.....	111
Quantification of HPC formation in cultured keratinocytes.....	112
Hypo-osmotic shock.....	112
6. Mice.....	112
Generation of heterozygous and homozygous mice.....	112
Dye penetration assay.....	112
Tape stripping and transepidermal water loss (TEWL).....	113
Voluntary wheel-running.....	113
7. Statistics.....	113
References.....	114
Appendix.....	122
Cloning of the targeting vector.....	122
Plasmids generated in this work.....	126
Sequence of mouse plectin Ex1a.....	127
Sequence of mouse plectin from exon 2 to end.....	127
Curriculum Vitae.....	132

## TABLE OF FIGURES

Figure 1. The layers of the epidermis .....	5
Figure 2. Main types of cell junctions in the epidermis.....	7
Figure 3. The hemidesmosome, a cell-matrix junction.....	9
Figure 4. The plakin family of cytolinker proteins .....	12
Figure 5. IF-microtubule cross-linking via plectin .....	13
Figure 6. Schematic representation of the plectin gene .....	14
Figure 7. Schematic representation of plectin and some of its interaction domains .....	15
Figure 8. Plectin mutations .....	17
Figure 9. Clinical phenotype of EBS-Ogna patients.....	20
Figure 10. Schematic representation of the Ogna plectin gene knock-in strategy .....	23
Figure 11. Southern blot analysis of targeted ES clones.....	25
Figure 12. DNA sequencing of targeted ES clones E14.1/59neo and E14.1/71neo.....	26
Figure 13. Different phases in generation of knock-in mice using coat color as a marker .....	28
Figure 14. Southern blot analysis of knock-in Ogna mice.....	29
Figure 15. Verification of the PlectOgna/+ mouse genotype by PCR analysis and sequencing .....	30
Figure 16. Verification of the plectinOgna/Ogna mouse genotype by PCR analysis .....	31
Figure 17. Expression of Ogna plectin mRNA in various tissues and in epithelial cells.....	32
Figure 18. Expression pattern of plectin isoform transcripts in wild-type and mutant mouse epidermis and in primary keratinocytes.....	34
Figure 19. Quantification of mRNA expression levels of plectin isoforms in skeletal muscle versus epidermis.....	34
Figure 20. Gross appearance of wild-type and Ogna mutant mice at various stages.....	36
Figure 21. Barrier-dependent assay .....	37
Figure 22. Mechanical resistance of the epidermis.....	38
Figure 23. Histological analysis of skin from newborn mice .....	39
Figure 24. Ultrastructural analysis of newborn mouse skin.....	39
Figure 25. Ultrastructural analysis of hemidesmosomes in newborn mouse skin .....	40
Figure 26. Ultrastructural analysis of hemidesmosomes in adult mouse skin.....	41
Figure 27. Hemidesmosome size distribution in wild-type and mutant mice.....	42
Figure 28. Morphometric analysis of hemidesmosomes from adult mouse skin.....	43
Figure 29. Quantification of hemidesmosomes with inner plates.....	43
Figure 30. Ultrastructural analysis of desmosomes in mouse skin .....	44
Figure 31. Immunolocalization of plectin on frozen sections of leg skin from 1-day-old wild-type and mutant mice.....	46
Figure 32. Immunolocalization of plectin isoforms P1c and P1a on frozen sections of leg skin from 1-day-old wild-type and mutant mice.....	47
Figure 33. Immunolocalization of plectin on frozen sections of foot pad skin from 2-month-old mice.....	47
Figure 34. Immunolocalization of hemidesmosomal proteins on frozen sections of leg skin from 1-day-old mice .....	48
Figure 35. Immunolocalization of hemidesmosomal proteins on frozen sections of footpad skin from 2-month-old mice .....	49
Figure 36. Detection of integrin $\beta$ 4, keratin 5, and plectin in skin lesions inflicted by mechanical injury.....	50
Figure 37. Voluntary wheel-running of 2-month-old mice.....	51
Figure 38. Immunolocalization of plectin in skeletal and cardiac muscle .....	52
Figure 39. Immunolocalization of desmin in skeletal and cardiac muscle .....	53
Figure 40. Colocalization of plectin and desmin in skeletal and cardiac muscle.....	54
Figure 41. Detection of $\alpha$ -actinin in EDL and heart using immunofluorescence microscopy.....	55
Figure 42. Immunolocalization of desmoplakin and plectin in cardiac muscle.....	55

Figure 43. Immunolocalization of plectin and integrin $\alpha 6$ in primary keratinocytes and quantification of integrin clustering. ....	56
Figure 44. Keratin network organization in primary keratinocytes.....	57
Figure 45. Colocalization of K5 with ITG $\alpha 6$ and plectin in primary mouse keratinocytes.....	58
Figure 46. Wild-type and Ogna plectin P1a restores normal keratin network cytoarchitecture in plectin-null keratinocytes.....	59
Figure 47. Effect of hypo-osmotic shock on integrin clustering. ....	60
Figure 48. Effect of hypo-osmotic shock on the keratin network .....	61
Figure 49. Migration of primary keratinocytes in response to scratch wounding .....	62
Figure 50. Migration velocities of mouse keratinocytes expressing wild-type or Ogna P1a.....	63
Figure 51. Schematic presentation of plectin rod variants expressed in insect cells.....	65
Figure 52. Optimization of recombinant His-tagged protein expression.....	66
Figure 53. SDS-PAGE of fractions obtained during the purification of HIS-tagged rod fusion proteins .....	67
Figure 54. Chemical cross-linking of the plectin's rod domain. ....	68
Figure 55. BN-PAGE analysis of the oligomeric state of the plectin rod. ....	69
Figure 56. Elution profile of plectin's rod domain on a Superose-6 column .....	70
Figure 57. Dissociation of plectin rod domain oligomers as a function of temperature and urea concentration .....	71
Figure 58. Schematic representation of minirod. ....	72
Figure 59. Formation and detection of plectin rod hetero-oligomers .....	73
Figure 60. Pull-down analysis of oligomer complexes formed in vitro upon mixing wild-type and Ogna rod domains.....	74
Figure 61. Quantification of pulled-down oligomeric complexes formed upon coexpression of wild-type and Ogna minirods.....	75
Figure 62. Analysis of pull-down complexes and protein overlay assay. ....	76
Figure 63. SDS-PAGE analysis of proteins pulled pulled down by GST-RodOgna after subtraction of GST-Rodwt-bound proteins from the keratinocyte lysate .....	77
Figure 64. Detection of eEF1 $\beta$ protein in mouse keratinocytes and proteins pulled-down by plectin's rod domain .....	79
Figure 65. Molecular modeling of RD fragments harboring the p.Arg2000Trp mutation .....	82
Figure 66. Model of HD stabilization through plectin multimerization.....	84
Figure 67. Construction of the targeting vector.....	123

## ABBREVIATIONS

ANOVA	analysis of variance
ABD	actin-binding domain
BHK	baby hamster kidney cells
BPAG	bullous pemphigoid antigen
DP	desmoplakin
EBS	epidermolysis bullosa simplex
EBS-MD	epidermolysis bullosa simplex-muscular dystrophy
ES cells	embryonic stem cells
GFAP	glial fibrillary acidic protein
GFP	green fluorescent protein
GST	glutathione S-transferase
HDs	hemidesmosomes
HPC	hemidesmosome-like protein complexes
IF	intermediate filament
ITGa6	integrin $\alpha 6$
ITGb4	integrin $\beta 4$
K5, K14	keratin 5, keratin 14
LIF	leukemia inhibitory factor
LoxP	locus of X over P1
mAbs	monoclonal antibodies
MAPs	microtubule associated proteins
MCK	muscle creatin kinase
MTs	microtubules
P1a	plectin isoform 1a
P1c	plectin isoform 1c
PRD	plectin repeat domain
SD	standard deviation
SH2	src homology 2 domain
SH3	src homology 3 domain
TEWL	transepidermal water loss

## SUMMARY

Plectin is a large multifunctional cytoskeletal protein that cross-links intermediate filaments and mediates their interaction with actin filaments and microtubules, the other two major cytoskeletal filament systems. Plectin also anchors intermediate filaments at strategic cellular sites, such as hemidesmosomes in basal keratinocytes, costamers, Z-disks, and the neuromuscular junction in muscle cells, the abaxonal membrane of Schwann cells, focal adhesions, mitochondria, and the nucleus. Due to these functions, and the additional ability to form compact oligomeric structures, plectin stabilizes cells and tissues, maintaining tissue integrity, particularly of tissues subjected to great mechanical stress, such as skin, skeletal muscle, and blood vessels. Plectin is expressed in a wide range of cell types and tissues in form of several protein isoforms that are generated by differential alternative first exon splicing from a single gene (*PLEC*). The use of alternative first exons, endowed with their own promoters, allows for cell-type specific expression of the isoforms.

Mutations in the plectin gene are inherited in an autosomal recessive manner and result in epidermolysis bullosa simplex (EBS) combined with muscular dystrophy and/or myasthenic syndrome, pyloric atresia, ptosis and ophthalmoplegia. The only autosomal dominant mutation identified in the plectin gene, known as the “Ogna mutation”, is due to a missense mutation in a domain of the protein common to all isoforms. Its carriers exhibit a skin-only phenotype. The study of this naturally occurring mutation, thus represents an ideal system, to reveal skin-specific functions of plectin, and to explain the pathomechanism of the mutation on the molecular level.

In the first part of this thesis, I describe the generation of a mouse line carrying the Ogna mutation. This work included the construction of a targeting vector, growing, electroporation and selection of ES cells carrying the mutation in only one allele, production of chimeric mice by blastocyst injection and confirmation of germ line transmission. I also confirmed the expression of the mutation in different mouse tissues and primary keratinocytes.

In the second part, I present the phenotypic characterization of the Ogna knock-in mouse line. As its main pathological features, I found skin fragility, and less, smaller, and non-functional hemidesmosomes characterized by impaired attachment of keratin filaments to the inner hemidesmosome plaque. Using isoform-specific antibodies I could

show that plectin isoform P1a was missing in the skin of Ogn mice and in monolayers of cultured primary keratinocytes. Additional *ex vivo* studies with primary keratinocytes showed that keratinocytes isolated from Ogn mice are less resistant to stress (eg. hypo-osmotic shock), migrate faster than their wild-type counterparts, and fail to promote integrin clustering. Furthermore I found that upon transient expression only wild-type P1a was able to rescue the aberrant keratin cytoskeleton organization of plectin-null keratinocytes. Skeletal muscle and heart showed no functional or structural abnormalities. These data clearly established the importance of P1a for the structure and functionality of hemidesmosomes.

In the last, more biochemical part of my thesis I expressed plectin's rod domain in Sf9 cells using recombinant baculovirus. This enabled me to demonstrate that the plectin rod is able to dimerize and further form highly ordered oligomeric structures. However, compared to wild-type oligomers, rod oligomers carrying the Ogn mutation turned out to be less resistant towards heat and denaturing agents, such as urea. As the Ogn mutation brings about a local unfolding of the coiled-coil rod structure, its lower resistance could be attributed to a reduced stability of plectin's secondary structure. A search for binding partners of the mutated rod revealed its association with serine proteases.

The work done for this thesis led to the proposal of a novel model for the structural reinforcement/stabilization of hemidesmosomes through self-association of plectin molecules and it provided insights into the molecular basis of the skin blistering disease EBS-Ogn.



## ZUSAMMENFASSUNG

Plectin, ein großes multifunktionelles Cytoskelettprotein vernetzt Intermediärfilamente und vermittelt ihre Interaktion mit Aktinfilamenten und Mikrotubuli, den beiden anderen Cytoskelett-Filamentsystemen. Plectin verankert auch Intermediärfilamente an strategisch wichtigen Stellen der Zelle, wie Hemidesmosomen in basalen Keratinozyten, Costamere, Z-Scheiben und neuromuskuläre Endplatten in Muskelzellen, der axonalen Membran von Schwann-Zellen, fokalen Adhäsionen, Mitochondrien und dem Zellkern. Aufgrund dieser Eigenschaften und der zusätzlichen Fähigkeit kompakte oligomere Strukturen ausbilden zu können, wirkt Plectin Zell- und Gewebe-stabilisierend und zeichnet für die Aufrechterhaltung der Integrität, insbesondere von Geweben die großen mechanischen Belastung ausgesetzt sind, wie Haut, Skelettmuskel und Blutgefäße, verantwortlich. Plectin wird in einer Vielzahl von Zelltypen und Geweben exprimiert, und zwar in Form mehrerer Proteinisoformen, die durch differentielles Spleißen alternativer erster Exons aus einem einzigen Gen (PLEC) entstehen. Durch die Verwendung unterschiedlicher Promotoren für die einzelnen ersten Exons kommt es zur Zelltyp-spezifischen Expression der Isoformen.

Mutationen im Plectingen werden autosomal-rezessiv vererbt und führen zu Epidermolysis bullosa simplex (EBS) assoziiert mit Muskeldystrophie und/oder Myasthenie-Syndrom, Pylorusatresie, Ptosis und Ophthalmoplegie. Die einzige autosomal-dominante Mutation im Plectingen ist als „Ogna-Mutation“ bekannt und beruht auf einer Missense-Mutation in einer Domäne des Proteins, die in allen Isoformen vorkommt. Träger dieser Mutation zeigen einen Phänotyp, der sich nur in der Haut manifestiert. Diese natürlich vorkommende Mutation stellt somit ein ideales System dar, um etwaige Haut-spezifische Funktionen von Plectin zu identifizieren und den Pathomechanismus der Mutation auf molekularen Ebene untersuchen.

Im ersten Abschnitt meiner Dissertationsarbeit stellte ich eine („knock-in“) Mauslinie her, bei der das Plectingen in einem der beiden Allele mit einem die Ogna-Mutation enthaltendem Gen ersetzt wurde. Dieser Teil der Arbeit umfasst Kapitel über die Konstruktion des Targeting-Vektors, die Züchtung, Elektroporation, und Selektion von embryonalen Stammzellen mit nur einem mutierten Allel, die Produktion von chimären Mäusen nach Blastozysteninjektion und den Nachweis der Keimbahntransmission. Ferner

werden Versuche beschrieben, welche die Expression der Mutation in verschiedenen Mausgeweben und primären Keratinozyten bestätigen.

Im zweiten Teil der Arbeit präsentiere ich die phänotypische Charakterisierung dieser Knock-in-Mauslinie. Als wichtigste pathologische Merkmale, fand ich deutlich erhöhte Fragilität der Haut, und weniger, kleinere, und nicht-funktionelle Hemidesmosomen, gekennzeichnet durch eine Störung der Verankerung von Keratinfilamenten am inneren hemidesmosomalen Plaque. Unter Verwendung Isoform-spezifischer Antikörpern konnte ich zeigen, dass die als P1a bekannte Plectinisoform in der Epidermis von Oga-Mäusen sowie daraus isolierter primärer Keratinozyten fehlt. Weitere ex-vivo-Studien mit primären Keratinozyten zeigten, dass aus Oga-Mäusen isolierte Keratinozyten weniger widerstandsfähig gegen Stress (z.B. hypo-osmotischer Schock) sind, schneller migrieren als ihre Wildtyp-Gegenstücke, und keine Integrin-Clusterbildung aufweisen. Außerdem fand ich, dass nach transienter Expression von Wildtyp-P1a, im Gegensatz zu anderen Isoformen, die normale Keratin-Cytoskelett-Organisation in Plectin-defizienten Keratinozyten wieder hergestellt werden konnte. Skelett- und Herzmuskel zeigten keine funktionellen oder strukturellen Anomalien. Diese Daten weisen eindeutig auf eine große Bedeutung von P1a für die Struktur und Funktionalität von Hemidesmosomen hin.

Für den letzten, mehr biochemischen Teil meiner Arbeit, exprimierte ich die zentrale Stabdomain von Plectin in Sf9-Zellen mit Hilfe rekombinanter Baculoviren. Ich konnte zeigen, dass die Stabdomäne in der Lage ist zu dimerisieren und weitere Formen hochgeordneter oligomerer Strukturen zu bilden. Im Vergleich zu Wildtyp-Oligomeren, erwiesen sich die aus Oga-mutiertem Plectin gebildeten Oligomere als weniger resistent gegenüber Hitze und Denaturierungsmitteln wie Harnstoff. Die geringere Stabilität der Oga-Stabdomäne ist wahrscheinlich auf die lokale Entfaltung ihrer coiled-coil-Struktur und die damit verbundene verminderte Sekundärstruktur-Ausbildung zurückzuführen. Eine Suche nach Bindungspartnern der mutierten Stabdomäne offenbarte seine Assoziation mit Serin-Proteasen.

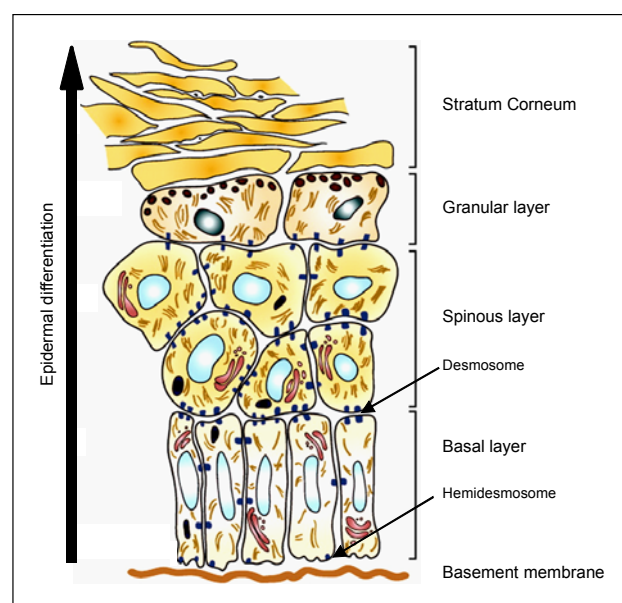
Die im Rahmen dieser Arbeit durchgeführten Experimente führten zur Entwicklung eines neuen, die Selbstassoziation von Plectinmolekülen miteinbeziehenden Strukturmodells für Hemidesmosomen, und sie geben Einblicke in die molekularen Mechanismen die zur Blasenbildung der Haut bei EBS-Oga führen.

## INTRODUCTION

### The Skin

The skin (Latin *cutis*) is the largest organ of the human body. It functions primarily as a protective layer of the underlying tissues preventing dehydration, mechanical trauma and environmental impact. It is involved in the regulation of body temperature, immunological surveillance against pathogens, sensory perception, lipid storage and synthesis of vitamin D. The skin consists of two layers: the epidermis and the dermis.

The epidermis represents the outer layer of the skin. It consists of a stratified squamous epithelium composed primarily of keratinocytes in progressive stages of differentiation arranged in layers upon a basement membrane. The different layers are distinguished on the basis of the morphological and functional features of the differentiating keratinocytes (Fig. 1). The inner most layer is the basal layer, also called stratum basale; it is made up of a single layer of basal columnar epithelial cells that lie above the dermis. These cells are attached at irregular intervals to the basement membrane by hemidesmosomes (HDs). Above the basal layer there is the stratum spinosum, also known as prickle cell layer, due to the “prickle” or spiny morphology of the cells. Keratinocytes in this layer are polyhedral in shape and are firmly held together by desmosomes. Moving upwards, the next layer is the stratum granulosum. Here the keratinocytes contain irregularly shaped granules of keratohyalin. The outermost epider-



Fuchs 2008, Fig. 1).

**Figure 1. The layers of the epidermis.**

Diagram shows the different stratified layers of the epidermis. The deepest one is the basal layer which is attached to the basement membrane through HDs (blue hemi-spheres). The suprabasal spinous and granular layers follow. In these layers the keratinocytes are connected to each other by desmosomes (blue hemispheres with the symmetrically positioned counterpart in the neighboring cell). The outermost layer is the stratum corneum. **Epidermal differentiation:** keratinocytes proliferate within the basal layer and move upwards as differentiation proceeds, losing first their proliferative potential, then the nucleus, ultimately flattening, and eventually shedding off from the skin surface. (From

mal layer is the stratum corneum, or cornified layer, where the cells, now called corneocytes, have lost their nuclei and cytoplasmic organelles, flattened out and are densely packed with keratin and skin lipids. These cells are eventually shed off from the skin surface. In addition to keratinocytes, the epidermis harbors minor cells populations with specialized functions including melanocytes (UV light protection), Langerhans cells (cutaneous immune response), and Merkel cells (mechanoreception).

The dermis is the layer beneath the epidermis. It is made up of connective tissue and remains tightly connected to the epidermis through the basement membrane, which is formed from secreted products of the cells in the two adjacent layers, such as collagen and laminin. The dermis itself consists of two layers, the upper papillary and the reticular layers. Both are filled with collagen fibers, thin and sparse in the papillary layer, thick and abundant in the reticular layer, and to a lesser degree with elastin. The primary cell type is the fibroblast which produces the structural (collagen and elastin), adhesion (fibronectin), and complex polysaccharides (glycosaminoglycans) that form the extracellular matrix (ECM). Embedded in this matrix are scattered mast cells, macrophages, blood and lymph vessels, nerve endings, hair follicles, sebaceous and sweat glands.

### **Epidermal homeostasis**

The skin has the remarkable property that the cells of the epidermal layers undergo constant renewal. This is required to maintain skin homeostasis. Thus, to compensate for the cells lost either by injury or desquamation of the cornified layer basal keratinocytes divide giving rise to two daughter cell populations, one that loses contact with the basement membrane and undergoes terminal differentiation as the cells leave the basal layer and gradually move upwards through the suprabasal layers; while the other one remain in the basal layer keeping its proliferative potential (Fig. 1). However, a tightly controlled balance between keratinocyte proliferation and terminal differentiation is required for normal epithelial function. This is indeed exerted at multiple levels including microenvironmental cues from the basement membrane, integrin signaling, growth factors, transcriptional activation or repression, etc. The switch from proliferation to differentiation is also accompanied by the reorganization of the cytoskeleton, most notably of the keratin network and changes in keratin expression. Basal keratinocytes express keratin (K) 5 and K14, while suprabasal keratinocytes express K1 and K10 (Simpson et al. 2011).

## Cell junctions in the epidermis

Cell junctions play an important role in the maintenance of tissue integrity as they connect cells with each other, mediate signals from the neighbouring cells or from the extracellular matrix to the cytoskeleton, and recruit signaling molecules. There are two main types of junctions, those that link cells together, known as intercellular junctions: tight, gap, adherens, and desmosomal junctions; and those that link cells to the ECM: focal adhesions, and HDs (Fig. 2). Tight and adherens junctions link the actin networks of two cells whereas desmosomes link their intermediate filaments; focal adhesions and HDs connect the ECM to either the actin or intermediate filament cytoskeleton (Simpson et al. 2011). Keratinocytes express different junctional molecules and form different junctions depending of the epidermal layer where they reside. A short summary follows:

**Tight junctions** form a continuous intercellular barrier between epithelial cells, beneath their apical surface, that prevents the passage of molecules through the space between cells. They are found in the granular layer of skin and are major regulators of permeability. The key transmembrane proteins of tight junctions are claudins and occludins. Both proteins associate directly with ZO proteins, intracellular plaque proteins that anchor them to the actin cytoskeleton (Furuse 2010).

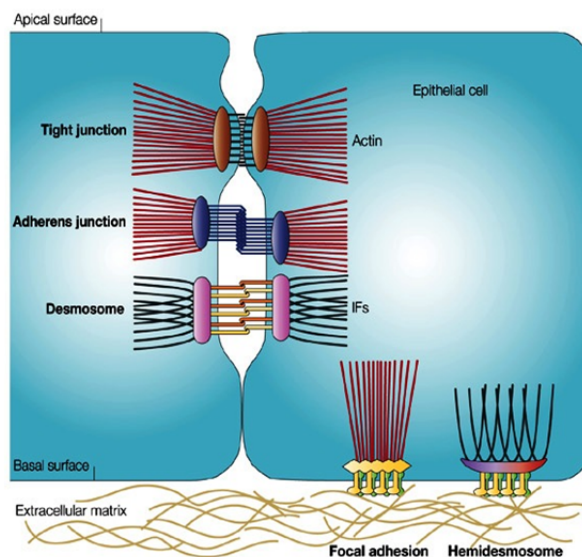


**Figure 2. Main types of cell junctions in the epidermis.** The central piece of cell junctions are transmembrane proteins that interact with similar proteins on adjacent cells and with components of the ECM via their extracellular domain, or with the actin or intermediate filament cytoskeleton via their cytoplasmic domains. Intercellular junctions: tight junctions, adherens junctions, and desmosomes. Cell-matrix junctions: focal adhesions and hemi-desmosomes. (From Jefferson et al. 2004. Fig. 1).

**Adherens junctions** provide strong mechanical attachment of adjacent cells to each other and are usually more basal than tight junctions. These junctions are formed by transmembrane molecules belonging to the cadherin family. They are connected to the actin cytoskeleton through  $\alpha$ - and  $\beta$ -catenin (Hartsock and Nelson 2008).

**Gap junctions** are intercellular channels that allow the passage of ions and small signaling molecules between adjacent cells. The building block of the junction is the connexin subunit. Six of these subunits assemble into hexameric connexons (hemichannels). Next, two connexons in the plasma membrane of adjacent cells pair end-to-end and form a hydrophilic channel. This channel allows direct cytoplasmic communication between the cells. Gap junctions are present in all layers of the epidermis and play an important role in skin development and keratinocyte homeostasis (Goudenough and Paul 2009).

**Desmosomes** are highly symmetric junctional complexes present at the basolateral membranes of epithelial cells. They mediate direct cell-cell contacts and provide anchorage sites for intermediate filaments. Desmosomes are composed of proteins from three major families: the desmosomal cadherins desmoglein and desmocollin that are the actual anchor, desmoplakin, a plakin protein that provides the link to the intermediate filaments, and the armadillo proteins plakoglobin and plakophilin that link the cadherins to desmoplakin (Green and Gaudry 2000).

**Focal adhesions** are cell-matrix junctions that consist of clustered integrin molecules, predominantly integrin  $\beta 1$ , acting as the transmembrane anchor, and the cytoplasmic adaptor proteins vinculin, talin,  $\alpha$ -actinin and paxillin that simultaneously bind to the cytoplasmic tail of the  $\beta$ -integrin subunit and to the actin cytoskeleton (Tsuruta et al. 2011).

**Hemidesmosomes** are anchoring structures that link the basement membrane to the intermediate filament cytoskeleton. They are located at the basal cell surface of basal keratinocytes and provide stable adhesion of the epidermis to the underlying dermis. The major transmembrane components of HDs are the basal keratinocyte-specific integrins  $\alpha 6$  and  $\beta 4$  and the bullous pemphigoid antigen 2 (BPAG2 or BP180). The plaque components include the plakin proteins plectin and BPAG1 (BP230) (Fig. 3A). Functionally, plectin and BP230 anchor the keratin filament network to the HD, while integrin  $\alpha 6 \beta 4$  attaches basal keratinocytes to the basement membrane by binding to the extracellular matrix component laminin 5 (Ln-332) (Walko et al. 2015). At the ultrastructure level, HDs appear as triangular shaped electron dense structures formed by an outer and an inner plaque. The outer plaque lying directly underneath the plasma membrane is larger than the inner plaque (Fig. 3A-B). HDs are classified into two types depending on whether they have (type I), or lack (type II), BPAG1 and BPAG2. Type I are found in basal keratinocytes of multilayered squamous epithelia, such as skin, type II

in simple epithelial tissues, such as the epithelia lining the digestive track (Litjens et al. 2006).

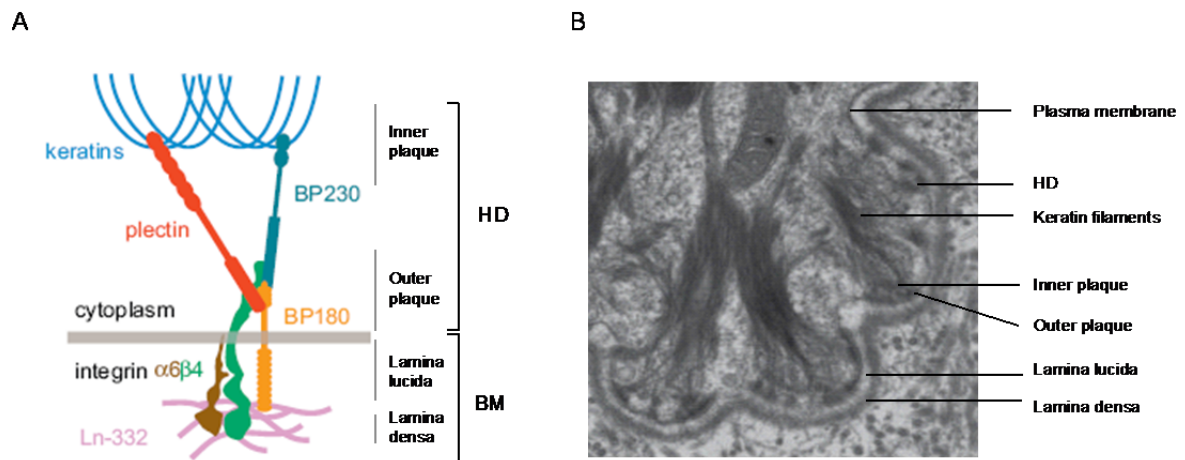


**Figure 3. The hemidesmosome, a cell-matrix junction.** (A) Schematic model of a HD showing major molecular components. Integrin  $\alpha 6 \beta 4$  and BP180 attach the cells to the basement membrane, whereas plectin and BP230 connect the transmembrane complex to intermediate filament (keratin) networks stabilizing the junction. HD, hemidesmosome; BM, basement membrane. (From Reznicek et al. 2010, Fig 1E). (B) Electron micrograph of the dermo-epidermal junction showing several HDs, the basal membrane and the two layers of the basement membrane: lamina lucida and lamina densa. (From Structure of the dermal-epidermal junction, M. Démarchez 2011).

## The cytoskeleton

The cytoskeleton is a highly organized complex network of protein filaments that extends throughout the cytoplasm of eukaryotic cells. It is required for the establishment of cell shape and polarity, for proper cell locomotion, intracellular transport of organelles, chromosome movement, cell division and adhesion. It confers cells resistance against mechanical stress and provides transient docking sites for proteins and lipids. Three main cytoskeletal networks are responsible for such diverse tasks: microfilaments, microtubules and intermediate filaments. Each filament system differs in architecture, protein composition and functional performance. Microfilaments, being made up of actin, are the thinnest (diameter  $\sim 6$  nm), microtubules which are assembled from tubulin, the largest (diameter  $\sim 25$  nm), and with a diameter of about 10 nm intermediate filaments are mid-sized, and in contrast to actin filaments and microtubules they are made of a number of structurally related proteins (Fletcher and Mullins 2010).

The subunit protein of microfilaments, actin, exists either as a globular monomer (G-actin) or filamentous polymer (F-actin). Actin filaments are polar and flexible, their structure resembles a double helix, and their ends differ in geometry, stability and growth

rate. To preserve filament length, monomers are added at the plus end and released at the minus end, a property known as treadmilling. The filaments are usually organized into larger structures such as bundles or networks depending on the proteins that bind them together. Actin filaments are essential for the formation of cellular protrusions that are involved in cell migration, for cell adhesion and morphology, the development of surface projections, cytokinesis and regulation of transcription. In muscle cells, actin in association with myosin form myofibrils that are the basis of muscle contraction; in non-muscle cells they form bundles, called stress fibers, which play a central role in cell adhesion, motility and morphogenesis (Schoenenberger et al. 2011).

Microtubules are stiff hollow cylinders, built from alternating  $\alpha$ - and  $\beta$ -tubulin subunits which spontaneously bind to each other to form a heterodimer. The  $\alpha/\beta$ -tubulin heterodimer assembles into linear protofilaments which in turn assemble into microtubules (13 protofilaments per microtubule). Like microfilaments, microtubules are polar structures that can undergo treadmilling by constantly adding and subtracting tubulin dimers at both ends of the filament. Proteins that bind to microtubules are known as microtubule associated protein (MAPs). Two major families of MAPs have been described, structural MAPs that promote assembly and stabilize microtubules and motor proteins that carry vesicles, organelles or protein complexes along the microtubules. There are two types of structural MAPs, type I (MAP1) and type II (MAP2, MAP4 and tau), both consisting of a microtubule-binding domain and a protruding arm that binds to other cellular structures. There are also two main types of microtubule motor proteins, kinesins that transports cargo towards the plus end and dyneins that do it towards the minus end. Microtubules serve as structural components within the cell, provide the internal structure of centrioles, cilia and flagella, and serve as tracks for the directional transport of organelles. During mitosis microtubules form the mitotic spindle which is required for proper segregation of chromosomes (Wade 2009).

Intermediate filaments (IFs) are strong, ropelike filaments which have a diameter intermediate between thin actin filaments and thick microtubules. IFs comprise a large and heterogeneous family of proteins sharing structural features but playing similar functions. There are currently six classes of IFs: type I and type II consists of acidic and basic keratins; type III include vimentin, desmin, glial fibrillary acidic protein, and peripherin; type IV the neurofilaments proteins; type V are the nuclear lamins; and type VI nestin. All cells have IFs, but the protein subunits vary depending on the cells in which they are expressed. Keratins are only expressed in epithelial cells, desmin in muscle cells,



and neurofilaments in neurons, whereas vimentin is expressed in fibroblasts and many other cells, and lamins in all cells. Each type of epithelial cell synthesizes at least one basic and one acidic keratin. Structurally, IFs are made up of 32  $\alpha$ -helical peptides each one consisting of a central  $\alpha$ -helical rod domain flanked by N- and C-terminal domains. Their assembly starts with the dimerization of two polypeptide chains and formation of a parallel coiled-coil dimer. Next, the dimers self-associate in an anti-parallel fashion to form a staggered tetramer. These tetramers are considered the basic subunit of the IF. Eight tetramers pack together laterally and wrap around each other to stepwise form protofilaments, protofibrils and the final filament. As a result of being assembled from antiparallel tetramers, IFs have identical ends, thus they lack intrinsic polarity in contrast to microfilaments and microtubules. IFs are involved in the maintenance of cell shape and organization of their internal three-dimensional structure; they impart mechanical stability, anchor the nucleus and other organelles within the cytoplasmic space, dock to junctions, and form the nuclear lamina (Coulombe and Wong 2004).

## Cytolinker proteins

Cytoskeletal linker proteins, or cytolinkers, bridge the three cytoskeletal filament systems promoting their cooperation in the execution of biological functions. Cytolinker was a term coined to describe plectin (Wiche 1998) but is now often applied to portray the members of the plakin family of proteins (Bouameur et al. 2014). Plakins are large multimodular proteins defined by the presence of a plakin domain. In addition they variably have an actin-binding domain (ABD), a coiled-coil rod domain (RD) or a spectrin-like rod domain, one or more plectin repeat domains (PRDs), an intermediate filament-binding domain and microtubule-binding domains (Fig. 4).

Most plakin genes encode multiple isoforms that are differentially expressed in a tissue-specific manner. The desmoplakin (DP) gene encodes two alternatively spliced isoforms, DPI and DPII differing in the size of the rod. Both isoforms are found in cells that form desmosomes, such as epithelial and endothelial cells, while DPI is also found in heart. Plectin will be described in detail below. The bullous pemphigoid antigen 1 (BPAG1) gene encodes several structurally distinct proteins, BPAG1a, 1b, 1e and 1n/dystonin. BPAG1e has a similar structure as DP; BPAG1-n/dystonin is identical to BPAG1-e, except for an ABD at the N terminus; BPAG1a and BPAG1b have a spectrin repeat-containing rod instead of the canonical coiled coil rod domain and a microtubule-

binding domain at the very C terminus. The isoforms are expressed in brain (BPAG1a), muscle (BPAG1b), epithelia (BPAG1e) and neurons (BPAG1n/dystonin). The two major isoforms of microtubule actin crosslinking factor 1 (MACF1), MACF1a and MACF1b, are similar in structure to BPAG1a and BPAG1b. Envoplakin and periplakin are very similar to desmoplakin but with a single, or no, PRD. They are both components of the cornified envelope found in the outer layer of the stratified epithelium. Epiplakin consists entirely of PDRs and is expressed in epithelial tissues (Sonnenberg and Liem 2007).

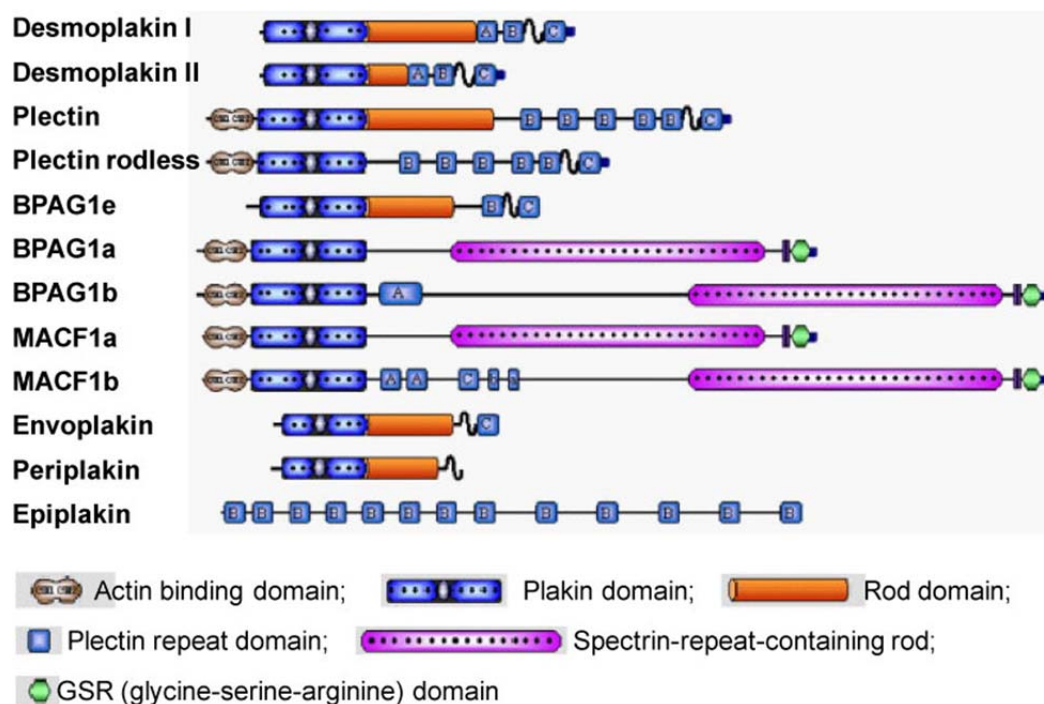


**Figure 4. The plakin family of cytolinker proteins.** Plakins are extraordinary large proteins with molecular masses ranging from 200-800 kDa. They share a common plakin domain and a similar domain organization. Desmoplakin, plectin, and bullous pemphigoid antigen 1e (BPAG1e) are the founding members of this protein family. (From Sonnenberg and Liem 2007, Fig. 1).

### Plectin

As one of the first identified members of the cytolinker protein family, plectin was originally isolated from rat glioma C6 cells in association with IF preparations (Pytela and Wiche 1980). Later the protein was shown to copurify also with microtubules (Koska et al. 1985) and eventually, using a variety of biochemical, molecular and immunological techniques, it was revealed that it can bind directly to all types of IF subunit proteins, high molecular MAPs, as well as cytoskeletal and structural proteins of the subplasma membrane skeleton, and nuclear and mitochondrial membrane scaffolds. Furthermore immunolocalization revealed its association with junctional complexes, Z-lines and sarcomeres,

bridging IF elements, microfilaments and microtubules (Wiche 1998, Boyer et al. 2009, Ketema and Sonnenberg 2011, Wiche et al. 2014) (Fig. 5). Its visualization as dense filamentous networks within the cytoplasm of the cells was the motivation for choosing its name (Wiche et al. 1982). Proteins isolated from HDs (Hieda et al. 1992) and IF-enriched cytoskeletal preparations of BHK cells (Lieska et al. 1985), were originally claimed to be different from plectin, receiving the names HD1 and IFAP300. However both were later shown to be identical to plectin (Okumura et al. 1999; Clubb et al. 2000).

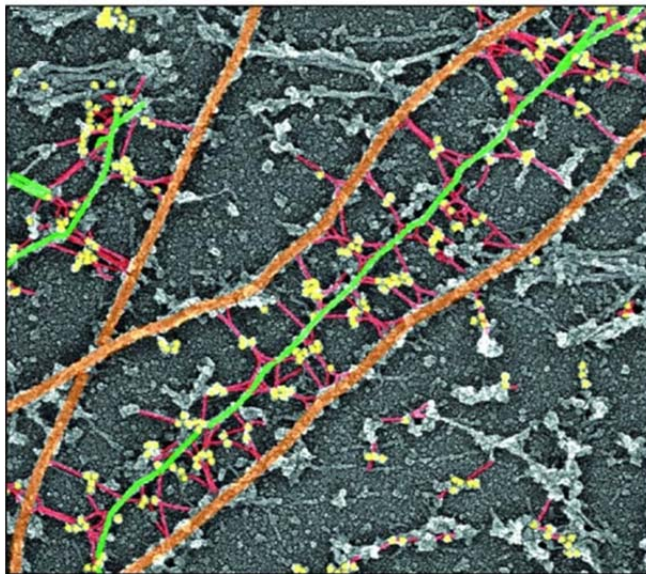
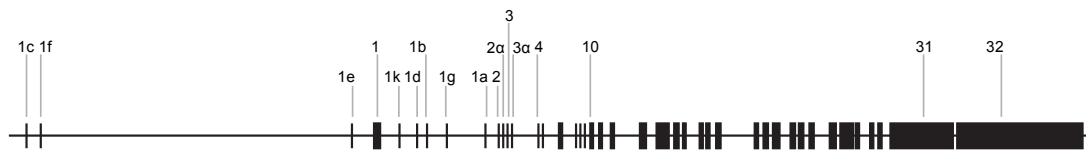


**Figure 5. IF-microtubule cross-linking via plectin.** Plectin (red) forms anastomizing bridges between IFs (green) and microtubules (orange). To unmask these bridges actin filaments were removed. The yellow dots are gold particles bound to anti-plectin antibodies. (From Svitkina et al. 1996, Fig. 5).

### ***The gene***

In humans the plectin gene (PLEC) is located in the terminal part of the long arm of chromosome 8 (8q24) (Liu et al. 1996), in mice on chromosome 15 (Fuchs et al. 1999) and in rats on chromosome 7 (7q34) (RefGene, 64204; <http://refgene.com/gene/64204>). The gene comprises more than 40 exons spanning over 62 kb of genomic DNA (Fig. 6A). The detailed characterization of the plectin gene revealed that most of the introns reside within the region encoding the N-terminal domain of plectin and that there exist alternative first exons that account for an unusual 5' transcript complexity. Twelve exons (1, 1a-1k) splice into a common exon 2, three alternative exons precede and splice into exon 1c, and two exons, 2 $\alpha$  and 3 $\alpha$ , optionally splice within exon 2-4 (Fuchs et al. 1999) (Fig. 6B). An alternative splice variant lacks exon 31 (Elliott et al. 1997). The availability of the human, mouse, and rat genomic sequences and their comparison and analysis by advanced bioinformatics tools (ENSEMBL and VEGA) revealed a similar gene organization in these organisms.

A



B

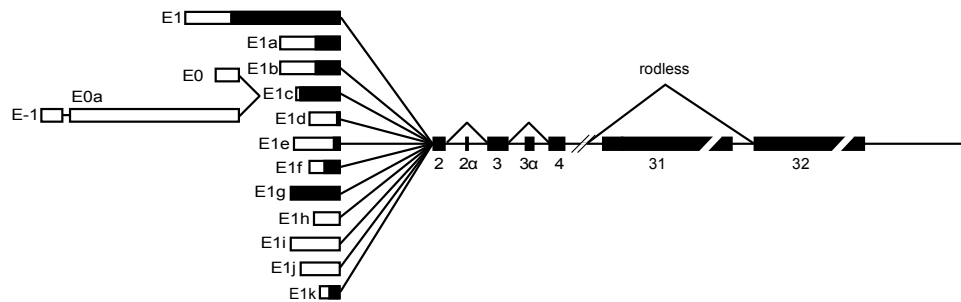


**Figure 6. Schematic representation of the plectin gene.** (A) Genomic organization. Exons are depicted by black boxes, introns by lines. (B) Transcripts generated by alternative splicing of the 5' end of the gene and its central rod domain. In total, 12 alternative first exons splice into exon 2; three non-coding exons into exon 1c, and two between either exon 2 and 3, or 3 and 4. Alternative splicing of exon 30 into exon 32 generates the rodless plectin variant. Exons are illustrated by boxes. Black boxes represent coding regions, white boxes non-coding regions. (From Fuchs et al. 1999, Figs. 1 and 3).

Transcript variants of the plectin gene encode multiple protein isoforms which differ by their N-terminal sequences. These short sequences were shown to target the isoforms to specific subcellular localizations and confer tissue specific expression (reviewed in Wiche et al. 2014). For example, plectin 1a (P1a) specifically associates with HDs, plectin 1b (P1b) with mitochondria, plectin 1c (P1c) with microtubules and plectin 1f (P1f) is present in vinculin-positive structures at actin stress fiber ends (Rezniczek et al. 2003; Wiche and Winter 2011), whereas plectin 1d (P1d) associates with Z-disks in myofibers (Konieczny et al. 2008).

### ***Structural properties, interactions and cellular localization of the protein***

Full-length plectin is expressed as a 499-533 kDa protein depending on the identity of the alternative first exon. The protein contains three structural domains: a long (190 nm) central  $\alpha$ -helical coiled-coil rod, and two flanking globular N and C termini (Wiche et al. 1991) (Fig. 7). Functionally, plectin is a multimodular protein as is typical for cytoskeletal linker proteins. The N-terminal domain harbors an actin-binding domain and a plakin domain that consists of 9 spectrin repeats interrupted by a central SH3 domain (Ortega et

al. 2011). The actin-binding domain which is similar to that of other spectrin superfamily proteins, comprises a pair of calponin-homology (CH) domains (Garcia Alvarez et al. 2003; Sevcik et al. 2004). The rod domain represents a 1127 residue-long, practically continuous stretch of heptad repeats which adopt the typical  $\alpha$ -helical conformation enabling the formation of coiled-coils. The rod domain promotes dimerization/oligomerization, and may serve as a scaffold for interactions with other proteins or to connect binding partners over relatively long distances. The C-terminal domain consists of six plectin repeat domains (PRDs), followed by a short tail region. Each PRD consist of a repetitive sequence motif called the plectin module and a linker region. Modules are each composed of five 38 residue-long motifs that are structurally similar to ankyrin repeats (Janda et al. 2001; Choi et al. 2002). The binding site for vimentin, GFAP, cytokeratins and desmin (IF-binding site) resides in the linker between PRDs 5 and 6 in the C-terminal domain (Nikolic et al. 1996).

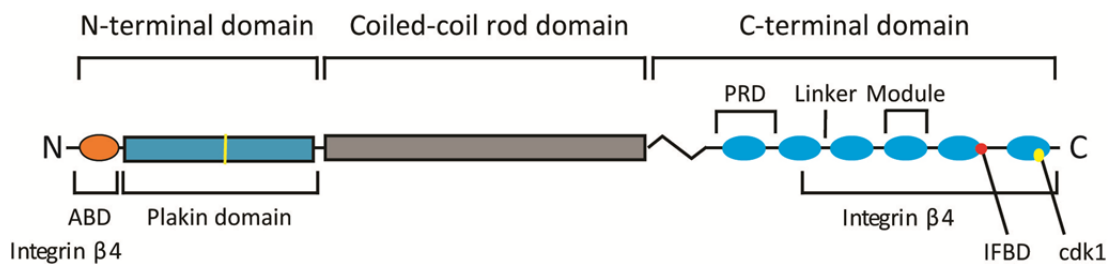


**Figure 7. Schematic representation of plectin and some of its interaction domains.** The protein consists of an N-terminal domain, a central rod domain and a C-terminal domain. The N-terminal domain contains an actin-binding domain (ABD) and a plakin domain comprising 9 spectrin repeats and an SH3 domain (yellow line). The rod domain is a long  $\alpha$ -helical coiled-coil. The C-terminal domain consists of 6 homologous repeats each one consisting of a conserved core, the plectin module (blue), and a linker region. Binding sites for integrin  $\beta 4$  and intermediate filaments (IFBD) are marked, along with the site for cdk1 phosphorylation.

Binding sites for integrin  $\beta 4$  have been mapped to the C-terminal domain (PRD 2-6) and to a region that overlaps with the actin-binding site (Reznicek et al. 1998, Geerts et al. 1999). There is an extra vimentin-binding site situated within the CH1 subdomain of the ABD (Sevcik et al. 2004). Additionally, a binding site for the nonreceptor tyrosine kinase Fer has been identified in the N-terminal region of plectin downstream of the ABD (Lunter and Wiche 2002); a unique mitosis specific phosphorylation site (threonine 4429) in plectin's repeat 6 is phosphorylated during M-phase by cdk1 (cyclin dependent kinase 1, formerly called p34<sup>cdc2</sup> kinase) (Foisner et al. 1996; Malecz et al. 1996); and a caspase 8 cleavage site (Asp 2285) that is cleaved at the early stages of apoptosis is found in the

middle of the rod domain (Stegh et al. 2000). A high affinity binding site for the SIAH E3 ubiquitin ligase has been mapped to residues 95-117 of exon 1 (House et al. 2003). Many other interaction partners of plectin have been identified, and their number is growing. Among them are cytoskeletal proteins such as all three of the neurofilament subunit proteins (NF 210/160/70), lamin B, the microtubule-associated proteins 1 and 2 (MAP1, MAP2), the membrane skeleton proteins fodrin/ $\alpha$ -spectrin (reviewed in Wiche 1998), the hemidesmosomal and desmosomal components BPAG1 and BPAG2 (Koster et al. 2003), desmoplakin (Eger et al. 1997); skeletal muscle specific ankyrins (Maiweilidan et al. 2011), and the outer nuclear membrane protein nesprin 3 (Wilhelmsen et al. 2005).

Plectin is widely expressed in practically all mammalian tissues and cell types, being particularly abundant in tissues subjected to great mechanical stress, such as striated and heart muscle, stratified and simple epithelia, and blood vessels. In such tissues, plectin is predominantly found at IF and microfilament attachment sites, for instance, Z-lines in stratified muscle, dense plaque in smooth muscle, intercalated disks in cardiac muscle, hemidesmosomal complexes in the basal cell layer of stratified epithelia, desmosomes, and focal contacts. Plectin is also very prominent in tissue layers at the interface between tissues and fluid-filled cavities, such as kidney glomeruli, liver bile canaliculi, bladder urothelium, gut villi, ependymal layers lining the cavities of brain and spinal cord and endothelial cells of blood vessels (Wiche, 1998; Wiche et al., 2014).

### ***Plectin deficiency***

In 1996 a number of groups reported that patients suffering from a skin blistering disease known as epidermolysis bullosa simplex (EBS) associated with muscular dystrophy (MD), lack plectin expression in skin and muscle tissues. Meanwhile, several nonsense and frameshift mutations in the plectin gene have been described that results in premature stop codons, mRNA decay and undetectable or very low plectin levels. Several recent reviews of plectin mutations leading to disease are available (Rezniczek et al. 2010; Chung and Uitto 2010; Chiavérini et al. 2010; Winter and Wiche 2013; Natsuga 2014). A summary of these mutations and their positions on the plectin molecule is shown in Fig. 8. As can be seen, exon 31, encoding the central rod domain of plectin, seems to be a hotspot for mutations.

Most mutations in the plectin gene are inherited in an autosomal-recessive manner and carriers of the mutations suffer from three different forms of EBS: EBS with muscu-



lar dystrophy (EBS-MD), EBS with pyloric atresia (EBS-PA) and EBS with congenital myasthenia (EBS-MD-MyS). The only known autosomal dominant plectin mutation, EBS-Ogna, is due to a missense mutation and disease symptoms are limited to the skin. Conversely, mutations in the first alternative exon 1f affect only skeletal muscle (LGMD2Q; Gundesli et al. 2010).

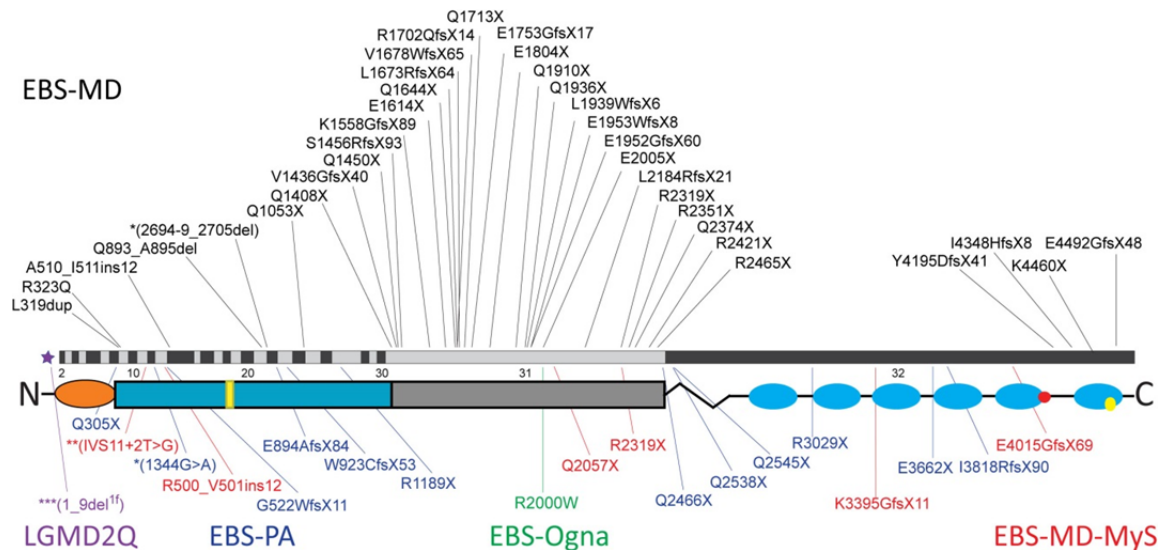


**Figure 8. Plectin mutations.** Positions of mutations reported in the literature are indicated along a schematic model of the plectin gene (upper bar) and the protein (superimposed graph). Numbers below upper bar correspond to exons; symbols in superimposed graph as in Fig. 7. Color code according to mutation phenotype. (Modified from Winter and Wiche 2013, Fig. 3).

Epidermolysis bullosa (EB) is a heterogeneous group of blistering disorders characterized by painful blister formation as a result of minor trauma to the skin. Three major types of EB have been defined based on the level at which the blisters occur (Table 1): i) within the epidermis at the level of the basal layer (EBS for EB-simplex), ii) at the interface between the epidermis and the dermis at the level of the lamina lucida (JEB for junctional EB), and iii) in the upper dermis just beneath the basement membrane (DEB, for dystrophic EB) (Fine et al. 2014). Under each main category there are numerous subtypes.

Most cases of EBS are caused by mutations in the keratin genes KRT5 and KRT14, encoding basal cell keratins K5 and K14, respectively; yet, a smaller number of cases are caused by mutations in the plectin gene (Bolling et al. 2014). While mutations in basal keratins result in skin blistering, mutations in plectin result in skin blistering accompanied by muscular, gastric and/or neuromuscular abnormalities (Table 2), reflecting the broader cellular roles of plectin (see above).

**Table 1. Major categories of EB and their genetic heterogeneity**

Major Type	Level of blistering	Mutated genes	Missing proteins
Simplex (EBS)	Basal layer of epidermis	<i>KRT5</i> , <i>KRT14</i> , <i>PLEC</i>	Keratin 5 & 14, Plectin
Junctional (JEB)	Intra-lamina lucida	<i>LAMA3</i> , <i>LAMB3</i> , <i>LAMC2</i> , <i>COL17A1</i> , <i>ITGA6</i> , <i>ITGA4</i>	Laminin 3 & 2, type XVII collagen, $\alpha 6\beta 4$ integrin
Dystrophic (DEB)	Sub-lamina densa	<i>COL7A1</i>	Type VII collagen

*KRT*, keratin 5; *KRT14*, keratin 14; *PLEC*, plectin; *LAMA3*, laminin A3; *LAMB3*, laminin B3; *LAMC2*, laminin C2; *ITGA6*, integrin  $\alpha 6$ ; *ITGB4*, integrin  $\beta 4$ ; *COL17A1*, type XVII collagen; *COLA1*, type VII collagen.

**Table 2. Major subtypes of EBS caused by plectin deficiency**

Type	Inheritance	Clinical Phenotype
EBS-MD	AR	Blistering with late onset of muscular dystrophy
EBS-PA	AR	Blistering with pyloric atresia
EBS-MD-MyS	AR	Blistering with congenital myasthenia
EBS-Ogna	AD	Blistering

AR, autosomal recessive; AD, autosomal dominant.

**EBS-MD (MIM:226670)** is characterized by generalized neonatal skin blistering and late onset of muscular dystrophy. The onset and extent of the muscle symptoms vary greatly, and eventually lead to the patients becoming wheelchair-bound and to premature death. Electron microscopy revealed that blistering occurs within the basal keratinocytes and muscle fibers have disorganized myofibrils and sarcomers. Plectin mutations detected in EBD-MD patients are mainly located within exon 31, which encodes the central rod domain of plectin.

**EBS-PA (MIM:612138)** is characterized by severe neonatal skin blistering and pyloric or duodenal atresia. Carriers of these mutations die shortly after birth. Because these clinical features are very similar to those observed in patients with defects in integrin  $\alpha 6$  and  $\beta 4$  subunits, it is believed that plectin mutations resulting in EBS-PA affect sites directly involved in the interaction between plectin and integrin  $\beta 4$ . In fact, the reported mutations are located in exons encoding the plakin and C-terminal domains (Chung and Uitto 2010).

**EBS-MD-MyS** is characterized by generalized skin blistering since birth and dysfunctional neuromuscular transmission. Responsible for this condition is the absence of plectin at the end plate of the muscle fiber. This results in the destruction of the junctional folds, loss of voltage-gated Na channels and the ability of nerves to trigger muscle activity (Banwell et al. 1999, Forrest et al. 2010, Maselli et al. 2011, Selcen et al. 2011).



**LGMD2Q** is characterized by generalized muscular weakness and loss of ambulation early in life (late twenties). These symptoms are the result of structural alterations of skeletal muscle due to the absence of plectin 1f expression. Patients with this condition do not suffer from skin disease (Gundesli et al. 2010).

### ***EBS-Ogna – an autosomal dominant disease***

EBS-Ogna (MIM 131950) was identified as a dominant trait in a Norwegian kindred in the village of Ogna (Gedde-Dahl 1971; Koss-Harnes et al. 2005). In 1973, EBS-Ogna was shown to be genetically linked to the glutamate pyruvate transaminase (GPT) locus with a maximum lod score of 11 at 5% recombination (Olaisen and Gedde-Dahl 1973). In 1982 the GPT gene was assigned to human chromosome 8 (Astrin et al. 1982; Kielty et al. 1982), in 1988 it was localized to the long arm of the chromosome, band 8q24.2 (Rocha et al. 1988), and in 1997 the locus was definitively mapped to the most distal band of the long arm of human chromosome 8, band 8q24.3 (Sohocki et al. 1997). Around this time the human plectin gene was mapped to chromosome 8q24 prompting speculation that mutations in the plectin gene could be responsible for EBS-Ogna. This was confirmed in two sequential reports. The first showed that skin biopsies from EBS-Ogna patients lacked immunoreactivity for plectin at the basal layer of epidermal cells, whereas strong immunostaining was seen in skin biopsies from healthy controls of the same family (Koss-Harnes et al. 1997). The second report proved that EBS-Ogna is due to a missense mutation, explicitly a C>T transition at cDNA position 5998 (RefSeq NM\_000445, NP\_000436) leading to a pArg2000Trp (formerly a pArg2010Trp, RefSeq NM\_201380.3, NP\_958782.1) substitution in the rod domain of plectin (Koss-Harnes et al. 2002). Immunofluorescence microscopy of EBS-Ogna skin revealed the absence of plectin expression at the basal layer of basal keratinocytes. Furthermore, ultrastructural analysis showed that cleavage occurred above the inner plates of HDs and that keratin filaments were not, or to a significantly reduced extent, inserted into the attachment plates.

The clinical phenotype is characterized by generalized epidermal fragility with frequent traumatic erosions and rare exfoliation of the epithelium, small (superficial) hemorrhagic blebs, and serous blisters of the skin (Gedde-Dahl 1971; Kiritsi et al. 2012) (Fig. 9). Skin fragility is evident within a few weeks or months after birth and is a permanent feature throughout life. Skin erosions are most frequent on the extremities, distal to elbows and knees, less frequent on the face and scalp and rare on proximal parts of extremities and on the trunk. Erosions dry up within a few hours and heal within a few

days. Small blood blebs are often present on the palms and fingers. Serous blisters are mainly restricted to hands and feet. Traumatic serous bullae occur more frequently at summertime. Nails are prone to be thickened and discolored (onychogryphosis).

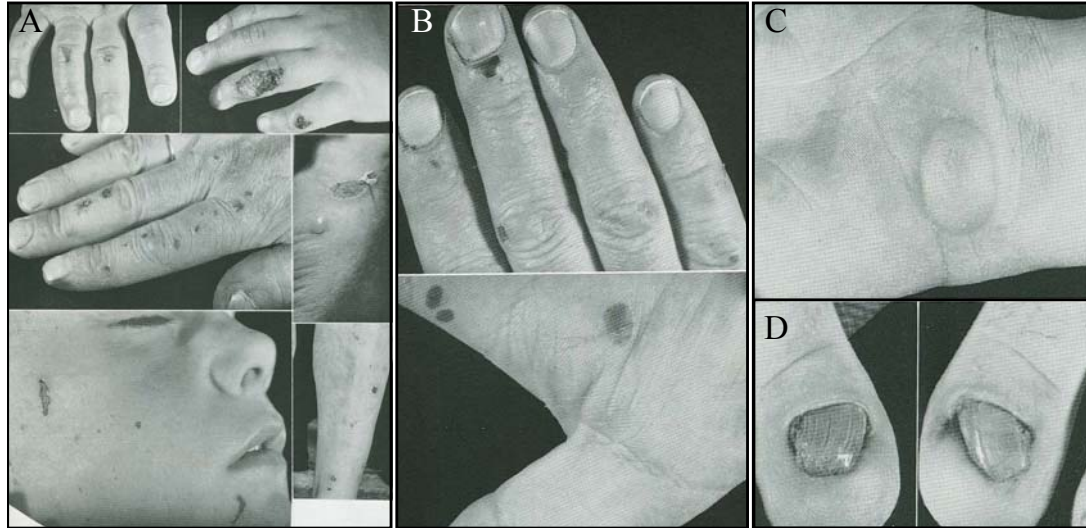


**Figure 9. Clinical phenotype of EBS-Ogna patients.** EBS-Ogna manifests with generalized epidermal fragility (A), small haemorrhagic blebs (B), serous blisters (C), and rare development of onychogryphotic nails (D). (Modified from Gedde-Dahl 1971, Figs 8 and 10).

No complaints about muscular, neurological or cardiological problems were recorded for the early EBS-Ogna patients. After it was known that plectin-deficient patients develop muscular dystrophy, muscle biopsies from 5 EBS-Ogna patients and 4 healthy controls were analyzed for plectin expression and muscle structure, but neither of them showed an aberrant muscle phenotype (Koss-Harnes et al. 2002; Bolling et al. 2014).

Nowadays it is known that EBS-Ogna is not restricted to the Norwegian kindred, since the disease has been detected also in an unrelated German family (Koss-Harnes et al. 2002), in three (also unrelated) German families (Kiritsi et al. 2012) and in three Dutch and one Iraqi families (Bolling et al. 2014), all of them unrelated.

### ***Animal models in the study of plectin function***

Animal models, in particular from mouse, are widely used to study gene function, to mimic human diseases and to investigate the etiology and mechanisms of disease. In the case of plectin, a unique collection of full (null), conditional, tissue- and isoform-specific knock out (KO) mouse lines has been generated to delineate the function of plectin in different tissues and the pathogenesis of plectin-related diseases. Plectin-null mice die two days after birth showing extensive blister formation, especially at the fore- and

hindlimbs and in the epithelial layers of the oral mucosa, and multiple structural aberrations in skeletal and cardiac muscles such as degenerated muscle fibers and partial disintegration of intercalated disks in the heart. The mice replicate the ultrastructural phenotype of EBS-MD patients including intraepidermal blister formation just above the inner hemidesmosomal plaque, impaired keratin filament anchorage into the plasma membrane of basal keratinocytes, sarcomere disruption and Z-line streaming. However, as these abnormalities were not severe enough to cause the early death of the mice, it was speculated that the severity of blistering in the oral cavity prevented food intake and death was the result of malnutrition. This was proven to be the case when an epithelia-restricted conditional KO mouse (K5-Cre/cKO) was generated and analyzed (Ackerl et al. 2007). K5-Cre/cKO died within 1-3 days after birth, exhibiting severe skin fragility, multiple mucosal blistering, skin blisters and empty stomachs. Serious disruption of nutrient intake has been reported in cases of EB-MD with oral mucosal involvement (Kunz et al., 2000; Schara et al., 2004), similar to what has been observed with K5-Cre/cKO mice.

Deletion of plectin in skeletal muscle was achieved by generation of a muscle creatine kinase (MCK)-Cre conditional KO mice (Konieczny et al. 2008). These mice, in combination with three isoform-specific KO mouse lines (plectin 1, 1b, and 1d KO) allowed to gain a comprehensive picture of the role of plectin in striated muscle. It was learned that plectin is required to preserve the integrity of skeletal muscle fibers and that a functional desmin network depends on plectin isoform-specific targeting of the filaments to specific docking sites. That is, P1d links desmin IFs to Z-disks, P1f to the sarcolemmal dystrophin-glycoprotein complex, P1b to mitochondria, and P1 to the outer nuclear/ER membrane. As a consequence, the absence of plectin results in detachment of desmin IFs from Z-disks, costameres, mitochondria, and nuclei, leading to the formation of desmin aggregates. Furthermore it also causes dysfunction and loss of mitochondria resulting in energy deprivation and fiber death (Konieczny et al. 2008).

In a similar approach, where a plectin isoform 1c-specific KO mouse line combined with a neural cell-restricted (nestin-Cre) conditional KO line were used, a specific function of p1c in motor neuron performance was discovered. In this case it was showed that the absence of plectin resulted in reduced motor neuron conduction velocity and reduced axonal caliber (Fuchs et al. 2009).

## **AIM OF THESIS**

Given the unique properties of the Ogn mutation, particularly the fact that a single amino acid substitution in a protein as large as plectin (>4500 residues), in a subdomain that is shared between the different isoforms, leads to an autosomal-dominant disease with exclusive skin involvement (in sharp contrast to most plectin mutations that affect both skin and muscle), makes this mutation a prime candidate to investigate the specific role of plectin in the basal epidermal cell layer and in maintaining skin integrity .

The main goal of this thesis was to investigate the pathogenesis of EBS-Ogn and the role of plectin in HD stabilization. To achieve this goal a genetic and a biochemical approach were to be taken. For the first part of the thesis it was planned to generate a knock-in mouse model carrying the Ogn mutation followed by its phenotypic analysis, including histological, immunological, and ultrastructural analysis. The second part of the thesis was to be based on cellular (ex vivo) approaches enabling structural and functional studies directed at assessing skin integrity. To this end, it was planned to isolate primary keratinocytes from knock-in mice to assess keratin network organization, stress resistance, and cell migration. Furthermore, questions related to the stability, interactions, oligo- and polymerization of the plectin rod should be addressed in the third and final part of the thesis.

## RESULTS

### I. Generation of an EBS-Ogna plectin knock-in mouse line

A knock-in mouse is a genetically engineered mouse with inserted genetic information into a particular locus in the genome. It contrasts a knock out mouse, where genetic information is removed from a particular locus, and a traditional transgenic mouse, in which genetic information is inserted randomly and not in a targeted fashion. The first step of my thesis work was to generate a knock-in mouse line carrying one wild-type plectin allele and one allele with the single nucleotide substitution which is the hallmark of the Ogna mutation (C>T at position 5995 in the mouse isoform 1c RefSeq NM\_011117.2, equivalent to C>T at position 5998 in the human isoform 1c RefSeq NM\_000445.3, GeneBank). An outline of the targeting strategy designed to generate such a mouse line, is given in Fig. 10. The procedure is described in detail in the following chapters. In brief, the targeting construct was introduced into embryonic stem (ES) cells by homologous recombination and successfully targeted ES cell clones were then used to generate mice with a targeted plectin locus (Fig. 10B). Subsequently, the neomycin-resistance cassette ( $neo^R$ ) was removed by the Cre recombinase (Fig. 10C). This was done by

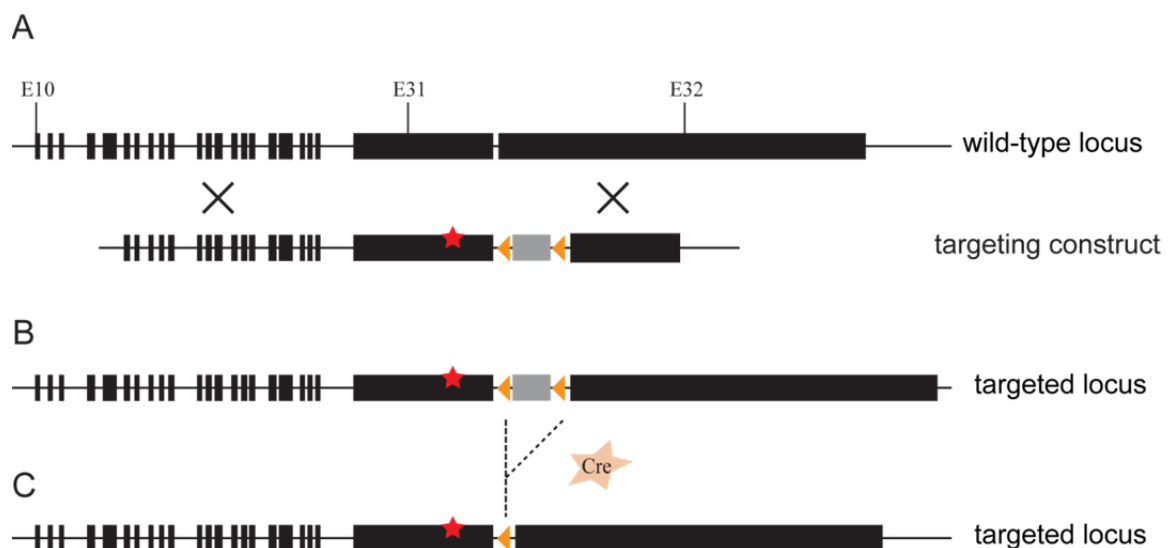


**Figure 10. Schematic representation of the Ogna plectin gene knock-in strategy.** (A) The wild-type plectin locus (upper scheme) and the targeting construct (lower scheme) containing the neomycin-resistance ( $neo^R$ ) cassette (gray box) flanked by two loxP sites (orange triangles) and the site of the Ogna mutation (red star) in exon 31 are shown. (B) The targeted plectin locus in the knock-in allele before  $neo^R$  elimination is shown. (C) The targeted plectin locus in the knock-in allele upon  $neo^R$  removal is shown. Solid boxes represent exons, full lines symbolize introns. E10, E31, and E32, denote exons 10, 31 and 32 of the mouse plectin gene. Dashed lines indicate  $neo^R$  elimination after Cre recombinase (Cre) activation.

crossing mice carrying the targeted plectin locus with transgenic mice ubiquitously expressing Cre recombinase (Cre deleter mice). Eventually neo<sup>R</sup> was removed, leaving one *loxP* site at the targeted locus of the genome (Fig. 10C). Since this *loxP* site was located in intron sequences, it was expected not to interfere with normal gene expression.

### Construction of the targeting vector

The targeting construct contained the EBS-Ogna mutation introduced into exon 31 of the plectin gene, and *loxP* sites flanking the neo<sup>R</sup> cassette, with the two *loxP* sites in the same orientation (Fig. 10A). To facilitate homologous recombination (usually a quite rare event), the targeting vector included a total of 15 kb recombination target, starting at exon 15 and finishing in exon 32 of the plectin gene. The neo<sup>R</sup> cassette, required for selection of cells that have undergone recombination, was flanked by target sites (*loxP* sites) for Cre recombinase to enable later removal of the selection cassette from the modified genome. *LoxP*, a site with an asymmetric 8 bp sequence in between two sets of palindromic, 13 bp sequences (**ATAACTTCGTATA-GCATACAT-TATACGAAGTTAT**) is conventionally used in site-specific (Cre-Lox) recombination. When exposed to the Cre recombinase, the *loxP* sites undergo reciprocal recombination, resulting in the deletion of the intervening DNA. The targeting construct was created in several cloning steps (see Appendix, p122-125).

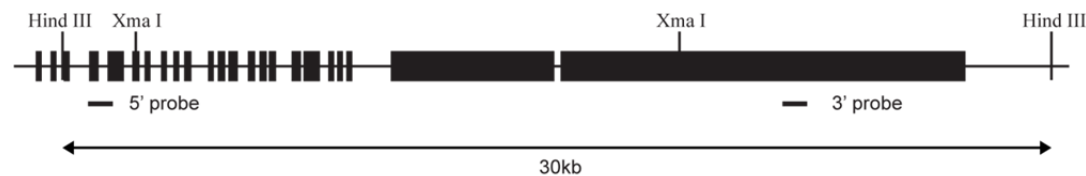
### Gene targeting in mouse embryonic stem cells

The targeting vector was linearized by digestion with *SacI* and electroporated into E14.1 embryonic stem (ES) cells. ES cells were subjected to G418 selection followed by picking of neomycin (G418) resistant clones. About 100 neo resistant ES clones were successfully expanded in each round of electroporation and the integration of the targeting construct at the correct locus was first assessed by Southern blot analysis. For that purpose genomic DNA was digested with *HindIII*, and the size of the resulting fragments (30 kb for the wild-type; 12 and 18 kb for the targeted allele) is presented in Fig. 11A. For the hybridization two external probes (outside the targeting construct) were used. The 5' probe (0.6 kb), was obtained from plasmid pKA9 (M&M, Table 8, p93) by *BamHI/HindIII* double digestion. The 3' probe (0.8 kb) was isolated from plasmid pPF26 (M&M, Table 8, p93) with restriction enzymes *SacII* and *XmaI*. When genomic DNA *HindIII* digests were hybridized with the 5' probe, bands of 30 kb or 12 kb derived from

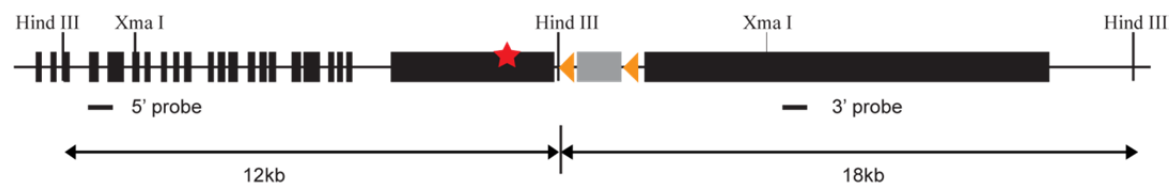
the wild-type or Oga allele, respectively, were recognized; whereas the 3' probe recognized corresponding bands of 30kb or 18kb. ES clones that were positive by Southern blotting (Fig. 11B) were further analyzed by sequencing.

**A**

Wild-type allele - 5' and 3' probe



Oga allele - 5' and 3' probe



**B**

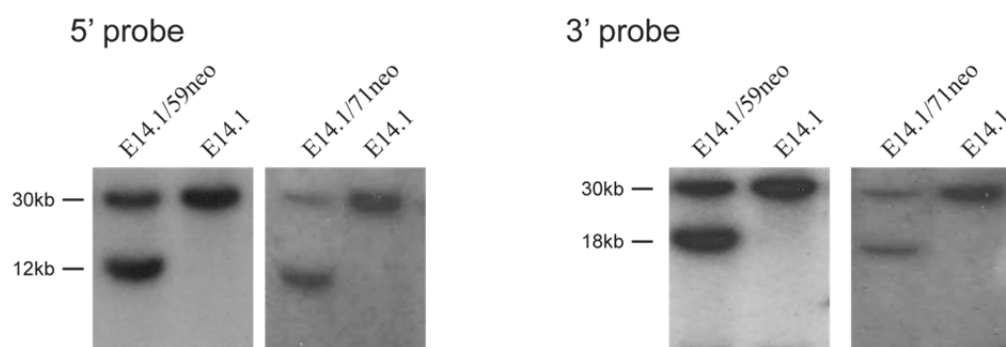


**Figure 11. Southern blot analysis of targeted ES clones.** (A) Schematic representation of the genomic locus of the wild-type allele (top) and the targeted allele (bottom), containing the neo<sup>R</sup> cassette (gray box) flanked by two loxP sites (orange triangles). Red star, Oga mutation. Relevant exons (solid boxes), restriction sites (*Hind*III, *Xma*I) and positions of the 5' and 3' external probes used in Southern blot analysis are indicated. Sizes of fragments obtained by *Hind*III digestion of genomic DNA is 30kb for the wild-type allele, versus 12kb and 18kb for the Oga allele. (B) Southern blot analysis of *Hind*III-digested genomic DNA from two successfully targeted ES clones (E14.1/59neo and E14.1/71neo); E14.1, parental ES clone.

In total, six independent electroporation series were performed using different ES cell stocks. E14.1 stocks for the first three electroporations were obtained from E. Wagner (IMP, Vienna), those for the following two from M. Busslinger (IMP, Vienna). As a back up, one electroporation was done outside our laboratory, at the Gene Targeting Unit (Stem Cell Center/Austrian Network for Functional Mouse Genomics, IMBA, Vienna).

The analysis of the ES cell clones resulting from this last (sixth) electroporation was never completed because two different Ogn<sup>a</sup> mouse lines had meanwhile successfully been generated using ES clones produced in the fourth and fifth electroporation series (see below). The targeting efficiency achieved in the five analyzed electroporations was high, homologous recombination occurred in 20% of ES cell clones, and 50% of them carried the Ogn<sup>a</sup> mutation (Table 3).

**Table 3. Homologous recombination efficiency**

Electroporation	ES clones analyzed by Southern blotting	Correctly targeted ES clones	ES clones carrying the Ogn <sup>a</sup> mutation
I	35	1	0
II	89	12	5
III	94	19	9
IV	87	20	12
V	105	29	13
total	410	81	39

Two of the ES clones carrying the Ogn<sup>a</sup> mutation (E14.1/59neo and E14.1/71neo) were eventually used to generate two independent mouse lines. In both cases Southern blotting revealed bands of 30 and 12 kb when hybridized with the 5' end probe, and of 30 and 18 kb (3' end probe), corresponding to wild-type and targeted alleles (Fig. 11B). This confirmed the presence of the Ogn<sup>a</sup> allele in the ES cells. Validation was completed by sequencing (Fig. 12). The double signal at the position of the Ogn<sup>a</sup> mutation again confirmed the heterogeneity of the ES cells, with cytosine (blue) derived from the wild-type allele and thymine (red) from the targeted allele.

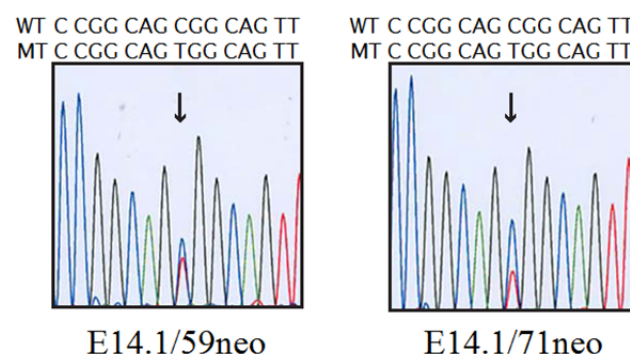


**Figure 12. DNA sequencing of targeted ES clones E14.1/59neo and E14.1/71neo.** Note the presence of a double signal at the position of the Ogn<sup>a</sup> mutation (arrow). Cytosine (blue) is derived from the wild-type and thymine (red) from the Ogn<sup>a</sup> allele.



### Generation of mice with a targeted plectin locus

Targeted ES cell clones carrying the EBS-Ogna mutation were expanded and used for blastocyst injections to generate chimeric animals. In numerous blastocyst injections performed over several months using many different ES clones, most mice showed a very low percentage of chimerism and the few that were highly chimeric were infertile. I assumed this was due to a decrease in the totipotency of the targeted ES cells during expansion and maintenance. In order to improve results, the electroporation and selection of ES clones was repeated using ES cell-pretested serum all along the process (electroporation III). The new ES cell clones were injected into blastocysts of C57BL/6 mice. Even though an increased number of highly chimeric animals was produced (paradoxically exclusively females) and many of them after mating with C57BL/6 males gave rise to offspring, no germ line transmission occurred. Consequently, another round of electroporation/selection was performed, using E14.1 cells and serum from a different source. In this case, germ line transmission was obtained from chimeras of two independent ES clones, E14.1/59neo and E14.1/71neo. Chimeric animals, derived from these ES cell clones, are listed in Table 4.

**Table 4. Generation of chimeras and germ line transmission from 2 targeted ES clones**

ES clone	chimeric animal	percentage of chimerism	sex	fertility	offspring coat color	germ-line transmission
E14.1/59neo	289/2/2	100	F	yes	black	no
	289/4	100	M	yes	black	no
	292/2	90	M	yes	black	no
	302/4/1	100	M	yes	black	no
	302/4/2	100	M	no	-	-
	302/4/3	100	M	no	-	-
	304/1/2	100	M	yes	black	no
	304/1/3	100	M	yes	black	no
	304/2	90	F	yes	black/brown	yes
	308/1/1	100	F	yes	black/brown	yes
	309/2/1	100	F	yes	black	no
	309/2/2	100	F	yes	black/brown	yes
	309/2/3	60	F	yes	black/brown	yes
	309/3	100	M	yes	black	no
E14.1/71neo	307/1	100	M	yes	black	no
	311/1/1	80	F	yes	black/brown	yes
	311/4	90	F	yes	black	no
	311/5	100	F	yes	black	no

Note, that positive germ line transmission was obtained only from female chimeric animals.

Clone E14.1/59neo gave rise to chimeric animals of 60% to 100% chimerism (Fig. 13A). Tail DNA samples were analyzed by Southern blot analysis in the same fashion as the ES clones (see p25) to show that the chimeras were heterozygotes. These heterozygous mice

were mated to C57BL/6 males and brown offspring pups were analyzed for germ line transmission (Fig. 13B). Due to the heterozygosity of the chimeras, only ~50% of brown pups were expected to have received the targeted gene. Sequencing analysis showed that indeed 60% of the brown pups carried the *Ogna* mutation and two *loxP* sites in one allele at the plectin locus. To sum up, two independent mouse lines were generated, *Plec*<sup>+/Ogna-neo</sup> #59 and #71, derived from ES cell clones E14.1/59neo and E14.1/71neo. These mice were heterozygous, carrying the *Ogna* mutation and the neo<sup>R</sup> cassette in only one allele.

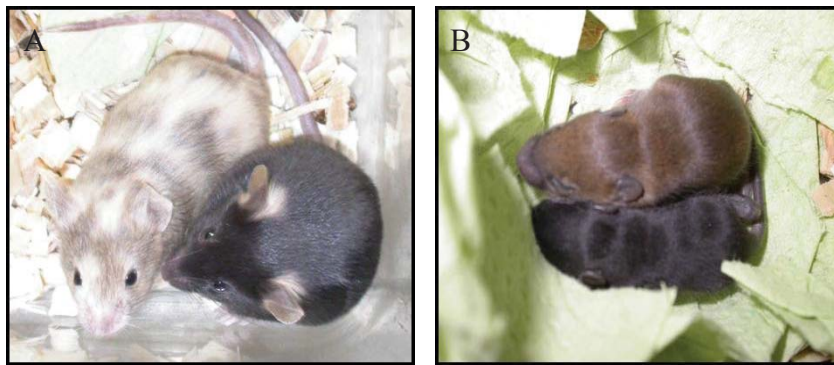


**Figure 13. Different phases in generation of knock-in mice using coat color as a marker. (A)** Chimeric animals obtained after blastocyst injection with targeted ES cells. One mouse showed 100% chimerism, next to a litter-mate with black fur indicating very low chimerism. **(B)** Germ line transmission. Coat color of brown pups indicates animals derived from injected cells.

### Removal of the neomycin resistance cassette

In order to remove the neo<sup>R</sup> cassette from the targeted plectin locus and to obtain mice of the *Plec*<sup>+/Ogna</sup> genotype, heterozygous mice with one targeted allele (*Plec*<sup>+/Ogna-neo</sup>) were crossed to transgenic mice ubiquitously expressing Cre recombinase (Cre deleter mice). To confirm the correct targeting of the plectin locus, genomic DNAs from the transgenic mouse lines before and after Cre-mediated deletion of the neo<sup>R</sup> cassette, were digested with the restriction enzyme *HindIII*, and subjected to Southern blot analysis using the 5' and 3' probes already described for the ES cells analysis. Additionally a neo-specific probe which detected a 18 kb fragment that was generated only if the *flox-neo* allele was present was also included (Fig. 14A). Thus the successful deletion of the neo<sup>R</sup> cassette from the targeted allele was indicated by the absence of the 18 kb signal from the targeted allele after Cre recombination (Fig. 14B, central panel). Of paramount importance was also the absence of other hybridization signals, demonstrating that the targeting vector had not been integrated into the genome anywhere else in the course of the gene targeting

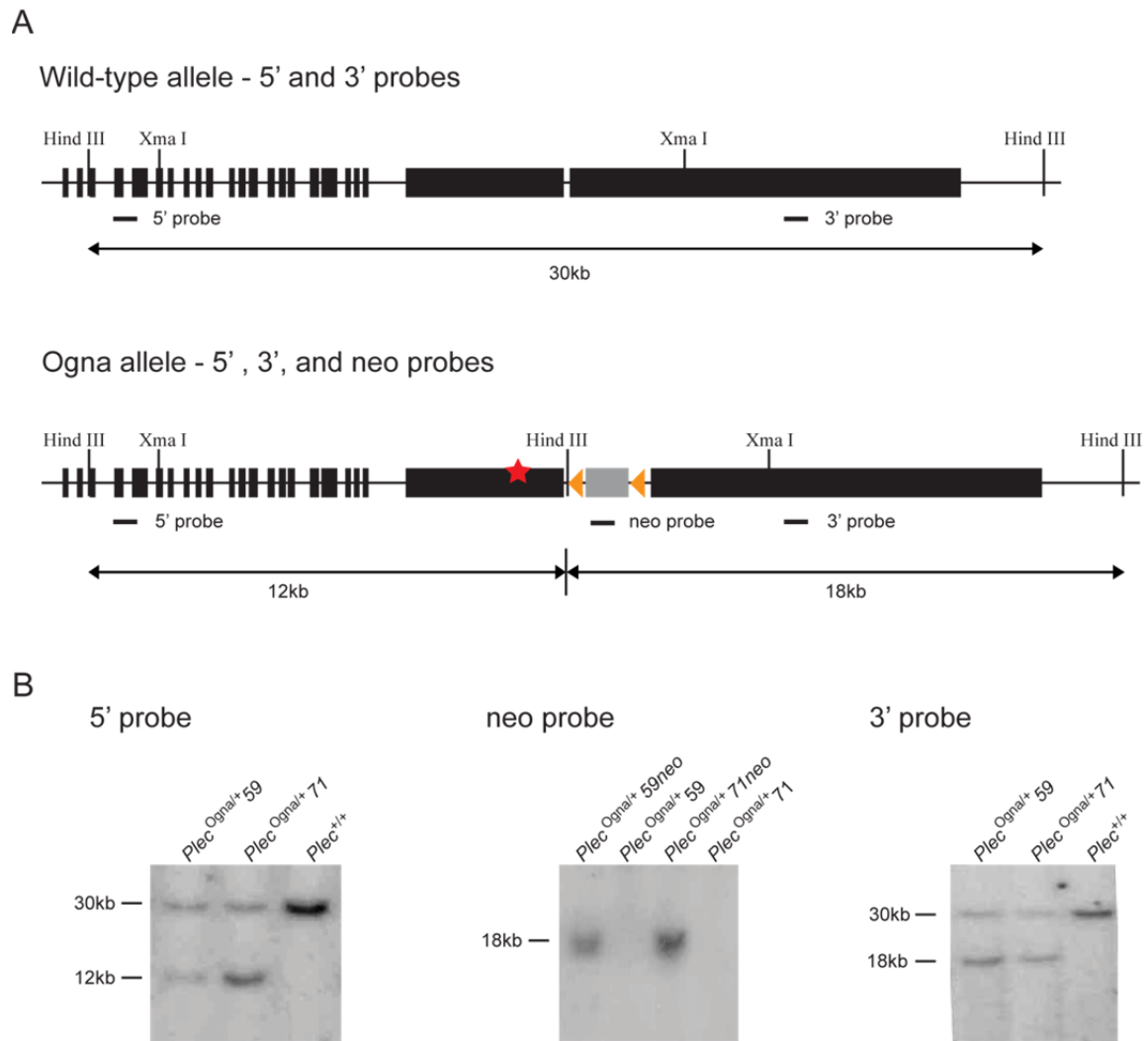


**Figure 14. Southern blot analysis of knock-in Ogn mice.** (A) Schematic representation of the genomic locus of the wild-type (top) and targeted alleles (bottom) with neo<sup>R</sup> cassette (gray box) flanked by two loxP sites (orange triangles) and the Ogn mutation (red star) in exon 31. Relevant exons (solid boxes), significant restriction sites, and positions of 5', 3' and neo probes used in Southern blot analysis are indicated. Size of fragments obtained by *Hind*III digestion of genomic DNA is 30kb for the wild-type allele and 12kb and 18kb for the Ogn allele. (B) Southern blot analysis of tail DNAs before and after neo<sup>R</sup> removal. Note the absence of hybridization signal in *Plec*<sup>Ogn+/59</sup> and *Plec*<sup>Ogn+/71</sup> versus *Plec*<sup>Ogn+/59neo</sup> and *Plec*<sup>Ogn+/71neo</sup> mouse DNA (central panel).

experiments. As expected, the 5' probe detected two clearly distinguishable fragments of 30 kb or 12 kb corresponding to one wild-type and one targeted allele (Fig. 14B left panel), while the 3' probe detected the same 30 kb fragment corresponding to the wild-type allele and a 18 kb fragment corresponding to the targeted allele (Fig. 14B right panel). Thus, the hybridization pattern with the external probes remained unchanged before and after removal of the neo<sup>R</sup> cassette, confirming the accuracy of the genomic integration and demonstrating that no rearrangements had occurred in the targeted region.

Additional steps to confirm that i) the targeting vector was integrated only once and in the correct position, ii) the  $\text{neo}^R$  cassette had been removed, and iii) the Ogn $\mu$  mutation was indeed present, were carried out by PCR and sequencing analysis. The PCR strategy for genotyping Ogn $\mu$  mice with primers specific for the mouse plectin gene and the targeting event is presented in Fig. 15. Amplification of genomic DNA with primers Ple31/U7314 and Ple32/L7384 resulted in a 204 bp fragment from the wild-type allele, and 745 bp or 270 bp fragments from the targeted allele still containing (Fig. 15A), or not containing anymore the  $\text{neo}^R$  cassette (Fig 15B). This analysis confirmed a correct targeting event (Fig 15A) and the successful removal of the  $\text{neo}^R$  cassette (Fig 15B). The presence of the Ogn $\mu$  mutation in *Plec*<sup>Ogn $\mu$ /+</sup> mice was demonstrated by sequencing of the amplified PCR product (Fig.15C).

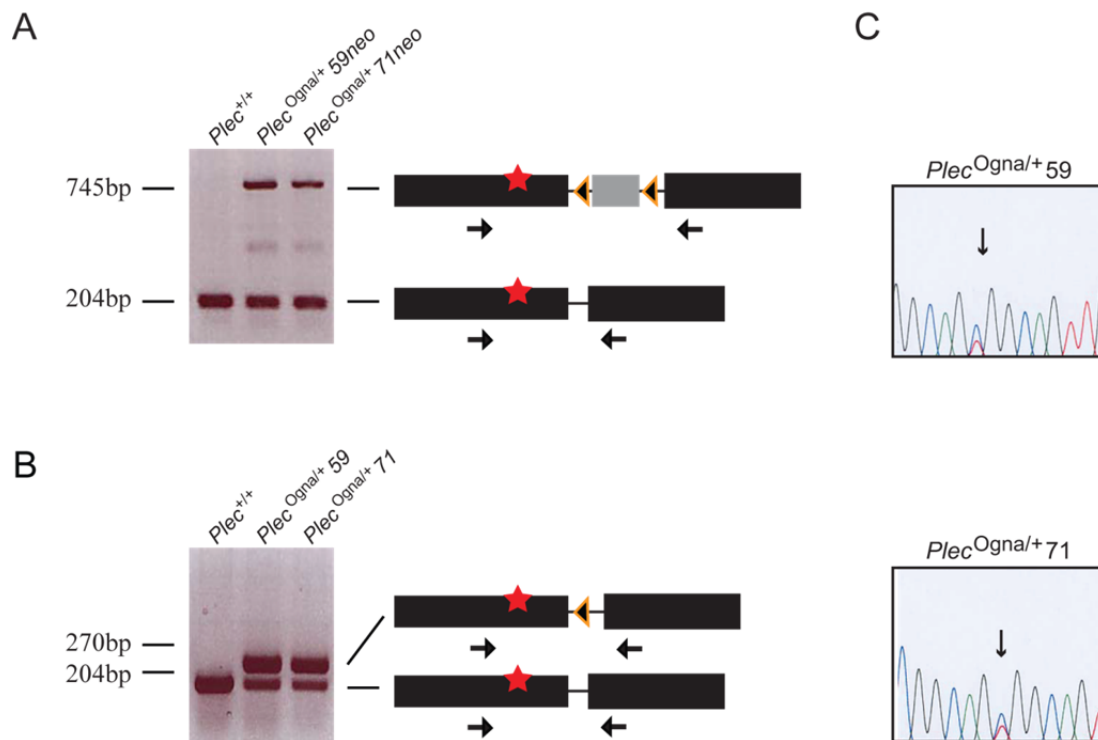


**Figure 15. Verification of the *Plec*<sup>Ogn $\mu$ /+</sup> mouse genotype by PCR analysis and sequencing.** (A) PCR analysis of two independent mouse lines (59 and 71) prior to removal of the  $\text{neo}^R$  cassette. Schematic representation of the genomic locus showing the wild-type and the targeted allele. Orientation and position of primers used for the analysis is indicated. (B) PCR analysis of mouse lines 59 and 71 after removal of the  $\text{neo}^R$  cassette. Schematic representation of the genomic locus as in A. (C) DNA sequence analysis of amplified PCR products. Note the presence of a double signal at the position of the Ogn $\mu$  mutation (arrow). Cytosine (blue) was derived from the wild-type and thymine (red) from the Ogn $\mu$  allele.

### Generation of a homozygous Ogn plectin knock-in mouse line

To study gene dosage effects homozygous mice harboring the Ogn mutation on both alleles ( $Plec^{Ogn/Ogn}$ ) were generated by intercrossing heterozygous ( $Plec^{Ogn/+}$ ) mice. Two independent mouse lines, with Ogn mutation on both alleles, derived from E14.1/59 and E14.1/71 ES clones, were created. By amplifying genomic tail DNA isolated from Ogn homozygous mice with primers Ple31/U7314 and Ple32/L7384 a 270 bp fragment, derived from the targeted plectin locus after  $neo^R$  removal was obtained (Fig. 16). The absence of the wild-type allele in these mice was demonstrated by the lack of the 204bp band (representative of the wild-type alleles) upon agarose gel electrophoresis.

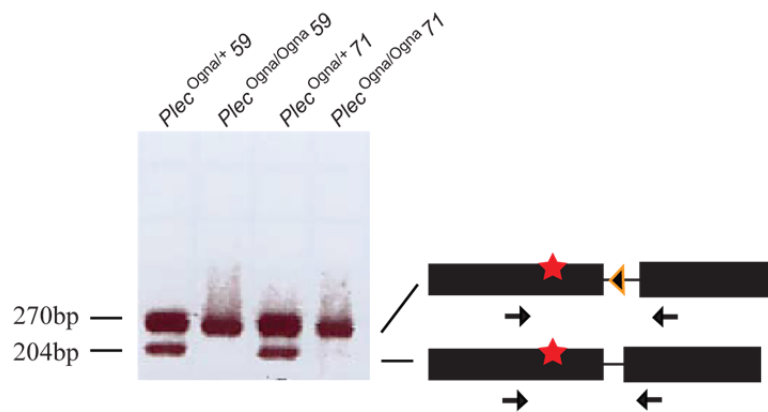


**Figure 16. Verification of the plectin<sup>Ogn/Ogn</sup> mouse genotype by PCR analysis.** PCR analysis of two independent mouse lines heterozygous or homozygous for the Ogn mutation is shown. Two PCR products were obtained from heterozygous mice corresponding to the wild-type (204 bp) and the targeted allele (270 bp); while homozygous mice delivered a single 270 bp product. Schematic representation shows the wild-type and the targeted locus with position and orientation of the primers used.

## II. Expression of Ogn plectin mRNA in mouse tissues and primary keratinocytes

After the Ogn knock-in mouse had been generated and sequencing confirmed the presence of the mutation in one of the plectin alleles, the obvious next goal was to demonstrate that the transgenic allele was transcribed. To this end, total plectin RNA, isolated from skin, muscle, heart, kidney, brain, and primary keratinocytes, was subjected to reverse transcription and the generated cDNA samples were amplified using one primer located upstream the Ogn mutation in exon 31, and another one in either the intron preceding exon 32, or exon 32 (Fig. 17A). PCR products were then analyzed by agarose gel electrophoresis (Fig. 17B) and directly sequenced. Fig. 17C shows the sequences of the two areas of interest. One is the region that confirmed the presence of the Ogn mutation in the cDNA (upper panel) and consequently in the mRNA. The other

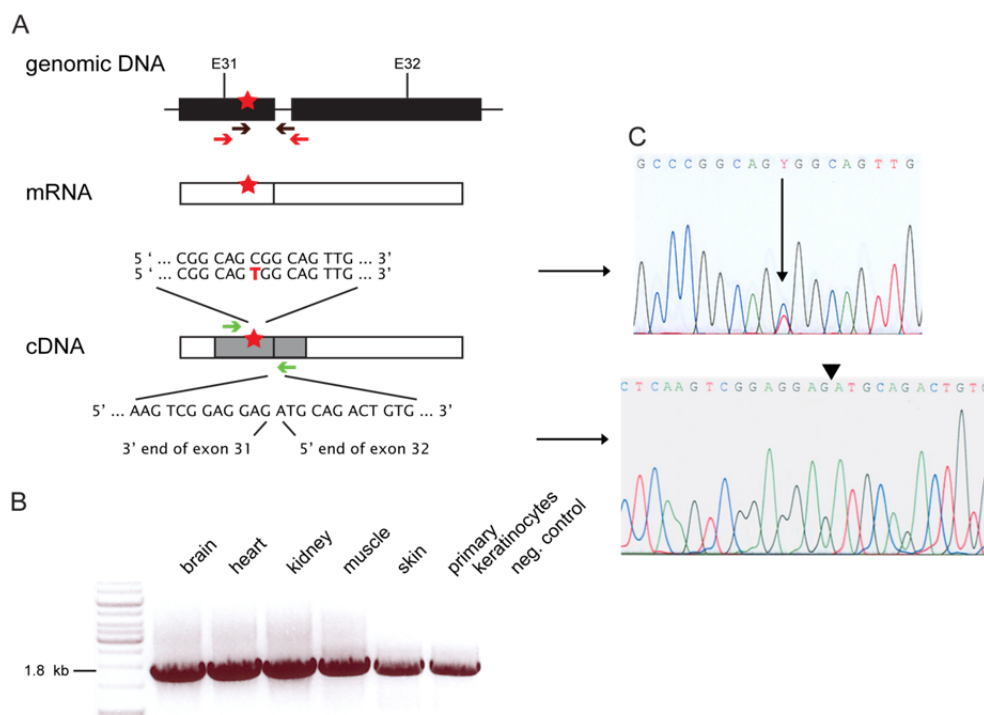


**Figure 17. Expression of Ogn plectin mRNA in various tissues and in epithelial cells. (A)** Schematic representation of genomic DNA, mRNA, and cDNA of mouse plectin exons 31 and 32. Arrows below the genomic DNA graph represent the two primers used for the RT-PCR shown in B (black), and the ones used for obtaining larger fragments for sequencing (red). Green arrows above and below the cDNA graph correspond to the positions of the primers used for sequencing the amplified RT-PCR products (gray shadowing). Nucleotide sequences flanking the Ogn mutation (mutated residue in red) are shown above the cDNA graph; sequences at the 3' end of exon 31 and the 5' end of exon 32, are shown below the cDNA graph. **(B)** Electrophoresis of RT-PCR products amplified from different tissue and primary keratinocyte cDNAs on 0.5 % agarose gels. **(C)** Sequencing results showing the presence of the Ogn mutation in skin (upper panel) and the absence of the intron (lower panel). Arrow in C points to C/T heterozygosity; arrowhead, exons 31/32 transition.

was the exon 31/32 border (lower panel) where the absence of intron sequences provided evidence for the absence of genomic DNA contamination in the analyzed specimen. Data shown in Fig 17C correspond to skin; muscle and primary keratinocytes yielded similar results.

### **Transcript levels of plectin isoforms in mouse epidermis and primary keratinocytes**

As no, or hardly any plectin is detected in the epidermis of Ogn patients, I asked the question whether the lack of plectin could be due to downregulation at the transcriptional level. To monitor changes, at the transcript levels, RNA collected from the epidermis of wild-type, and mutant mice were analyzed by quantitative real-time PCR (qRT-PCR). For comparative purposes qRT-PCR was also performed with muscle samples and primary keratinocytes derived from these mice. Total plectin as well as isoforms 1, 1a, 1c, and 1f were included in the analysis as these are the predominant isoforms expressed in skin (Fuchs et al. 1999, Andrä et al. 2003). The first exons corresponding to the different isoforms were chosen as target for the amplification. Results of absolute (determines the absolute amount of target, expressed as copy number or concentration, in the sample) and relative (change in expression of a target in a test sample relative to the same target in a control sample, e.g. wild-type alleles versus mutated alleles) quantification are given in Fig. 18. A calibration curve consisting of serial dilutions of the different exon sequences cloned into plasmids (Reznicek et al. 2003) was used for absolute quantification. Relative quantification was done by the method of Pfaffl (Pfaffl 2001) using the house keeping gene hypoxanthine guanine phosphoribosyl transferase (HRTPI) for normalization. The results of this analysis revealed no significant differences in transcript levels between mutant and wild-type samples (Fig. 18A,B), indicating that the mutation does not alter plectin transcript levels. Unexpectedly, the expression level of plectin isoform P1a was about three times higher in primary keratinocytes than in epidermis, while that of P1c was about 4 times higher in epidermis than in primary keratinocytes, although in both cases P1a and P1c were the main isoforms. Similar results have been reported for the dominant expression of P1a over P1c in primary human and mouse keratinocytes (Gostyńska et al. 2015). A plausible explanation for these findings is that cultured primary keratinocytes grown as monolayers are rich in HD-like structures where P1a is accumulated, whereas the epidermis contains all the suprabasal cell layers in which predominantly P1c is expressed (Gostyńska et al. 2015).

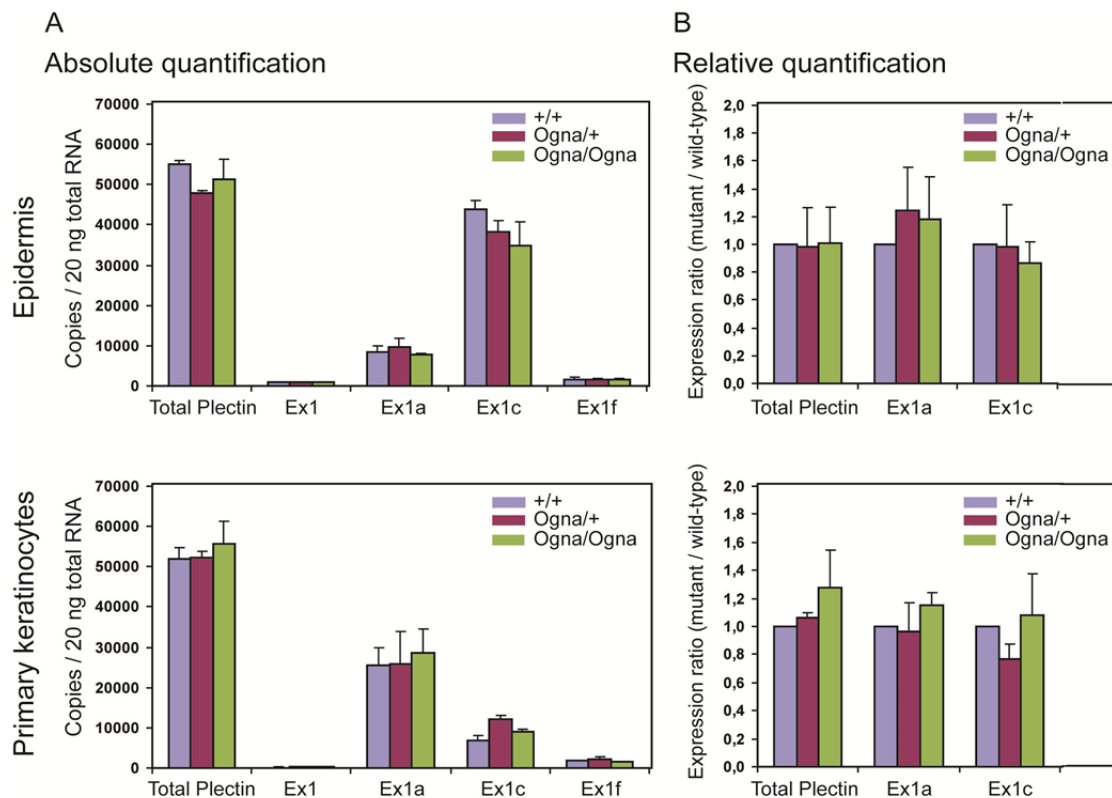


**Figure 18. Expression pattern of plectin isoform transcripts in wild-type and mutant mouse epidermis and in primary keratinocytes.** Transcript levels were quantified by qRT-PCR as described in Materials and Methods. **(A)** Absolute quantification. Estimated absolute copy numbers of plectin isoforms were calculated from standard curves obtained by serial dilutions of plasmids harboring the different exons. **(B)** Relative quantification. Values represent fold changes relative to wild-type levels. A ratio of 1 indicates no different in expression between mutant and wild-type.

A comparison of plectin isoform expression patterns in epidermis and skeletal muscle tissue is shown in Fig. 19. While total plectin levels were found to be much higher in skeletal muscle compared to epidermis, a relatively high expression level of exon 1c (Ex1c), followed by Ex1a, was observed in epidermis, but not in muscle; whereas Ex1f expression was prominent in muscle, but not in epidermis.

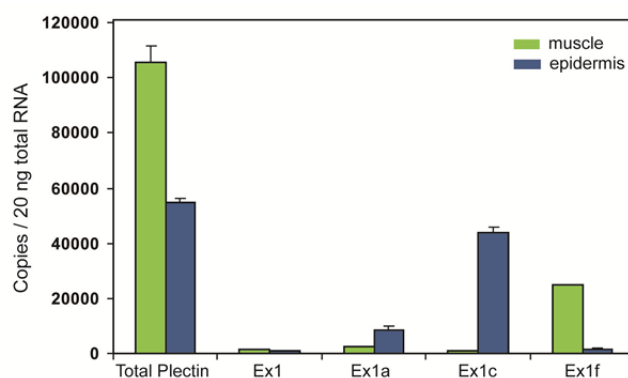


**Figure 19. Quantification of mRNA expression levels of plectin isoforms in skeletal muscle versus epidermis.** Transcript levels were quantified by qRT-PCR. Absolute quantification as in Fig.18A. Note that exons 1c and 1a are preferentially expressed in the epidermis.



### III. Phenotypic analysis of Ogn mice

Having no overt phenotype, Ogn heterozygous mice were viable, fertile, and showed no difference in size, milk intake, postnatal development, reproduction rates, or life span when compared to the wild-type littermates (Fig. 20A,B). Newborn homozygous mice looked similar to the heterozygous mice (Fig. 20C), but developed a severe skin phenotype later (see below).

#### 1. Skin Phenotype

As the most characteristic phenotype of Ogn patients is their skin fragility with recurrent blister formation upon exposure to the slightest friction, special emphasis was placed on studying the skin phenotype of the Ogn mice.

#### **Macroscopic analysis**

Neither in heterozygous ( $Plec^{Ogn/+}$ ) nor in homozygous ( $Plec^{Ogn/Ogn}$ ) newborn mutant mice were visible blisters, skin lesions, or hemorrhages observed, including fore- and hindlimbs, the most affected areas in plectin knock out mice (Andrä et al. 1997). Thus, at the gross morphological level, Ogn newborns had no obvious skin phenotype (Fig. 20A-C). A few days after birth, pups of all genotypes developed fur that served as a natural protection of the skin, with no pathological alterations becoming noticeable thereafter (Fig. 20D), except for a fraction of  $Plec^{Ogn/Ogn}$  mice (~39%, n=23) that developed severe skin lesions within ~18 months (Fig 20E-F). These lesions developed not only in hairless zones but also on fur-covered skin, and were localized on the head, particularly around ears, mouth and nasal cavities, and on the frontal body side reachable by the hind legs. Irrespectively of their genotype, many mice develop changes in behavior including repeated cleaning movements probably due to cage life conditions (restricted area, movement limitations). In most cases this kind of behavior results in loss of hair, but without skin damage. Thus, it was assumed that the lesions observed in some of the  $Plec^{Ogn/Ogn}$  mice were self-inflicted by means of repeated cleaning and scratching, eventually leading to the detachment of the epidermis. Although the wounds triggered a self-healing process, the ensuing recovery process could not set off resulting in chronic inflammation. Actually, glands in the underlying dermis were swollen by up to ~5-times their normal size. Mice were usually culled after unsuccessful recovery and deterioration of their general condition. Similar, although milder abnormalities have been reported for a

subset of mice (16%) carrying a skin-restricted conditional ablation of integrin  $\beta 4$  (Raymond et al. 2005).

#### Newborn mice



#### Adult mice



**Figure 20. Gross appearance of wild-type and *Ogna* mutant mice at various stages.** A-C, newborn wild-type (A), and heterozygous *Ogna* (B), and homozygous *Ogna* (C) mice. D-F, adult heterozygous (D), and homozygous (E,F) *Ogna* mice. Note severe lesions (removed epidermis) in regions exposed to repeated mechanical trauma in E-F.

#### **Skin integrity**

Although *Plec*<sup>*Ogna*/+</sup> and *Plec*<sup>*Ogna*/*Ogna*</sup> mice were born without apparent skin defects, thorough inspection of their skin under a stereo microscope revealed the presence of small epidermal lesions. To visualize the lesions I used an assay based on the percuta-

neous absorption of toluidine blue, a dye that does not penetrate the barrier of unlesioned skin. It detects however areas where the skin barrier is defective by staining ruptures and allowing the visualization of micro-lesions, while undamaged skin remains unstained. Examination of neonatal (1-day-old) mice revealed multiple localized dark blue spots in the epidermis (particularly on the head, legs, and back skin) of both heterozygous and homozygous *Ogna* mutant mice, but not in wild-type mice, (Fig. 21).

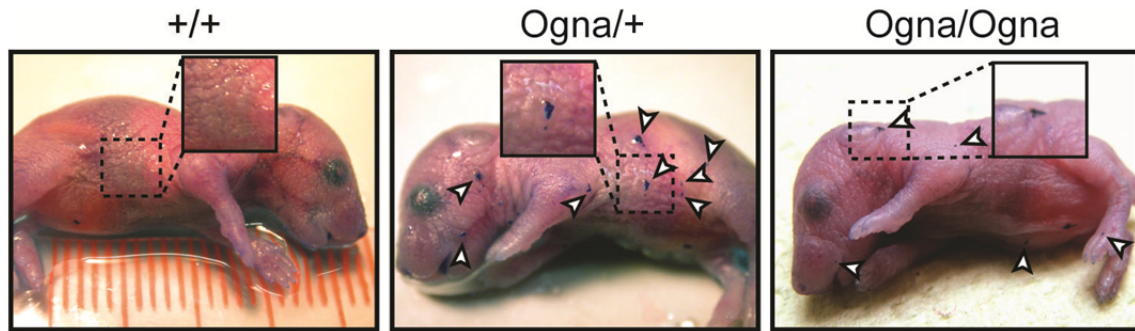


**Figure 21. Barrier-dependent assay.** A typical toluidine blue dye exclusion assay was performed on wild-type and mutant neonates. Note localized breaches (arrowheads) of the skin barrier in mutant mice. (Modified from Walko et al. 2011, Fig. 1A)

To test the resistance of the skin towards mild mechanical stress, newborn mice were subjected to tape stripping followed by the quantitative analysis of transepidermal water loss (TEWL). TEWL measurements are based on changes in the rate of passive evaporation through the skin and are expressed as g/m<sup>2</sup>/h. These values are considered to be a measure of the integrity of the skin barrier function. Tape stripping was performed on the back skin of newborn mice using D-squame discs. TEWL measurements were taken immediately after each tape stripping. Wild-type newborn mice did not develop any noteworthy skin detachment after six consecutive tape strippings, whereas six tape strippings were enough to induce the formation of a large epidermal exfoliation in *Plec*<sup>*Ogna*/+</sup> mice (Fig. 22A). In the case of *Plec*<sup>*Ogna*/*Ogna*</sup> mice, 2-3 tape strippings were sufficient to remove the entire epidermis of the stripped area (Fig. 22A) and the experiment had to be discontinued at this point. Values for TEWL measurements are as shown in Fig. 22B. No substantial differences in TEWL values were observed between control and *Plec*<sup>*Ogna*/+</sup> mice, before or after 4 tape strippings, although the values increased with successive strippings. There was a significant difference, 4-fold increase, however, in TEWL values, roughly a after the 6th stripping, coinciding with the removal of the epidermis and disruption of the skin barrier. These experiments clearly demonstrated that the skin of mutant mice was more sensitive to mechanical stress.

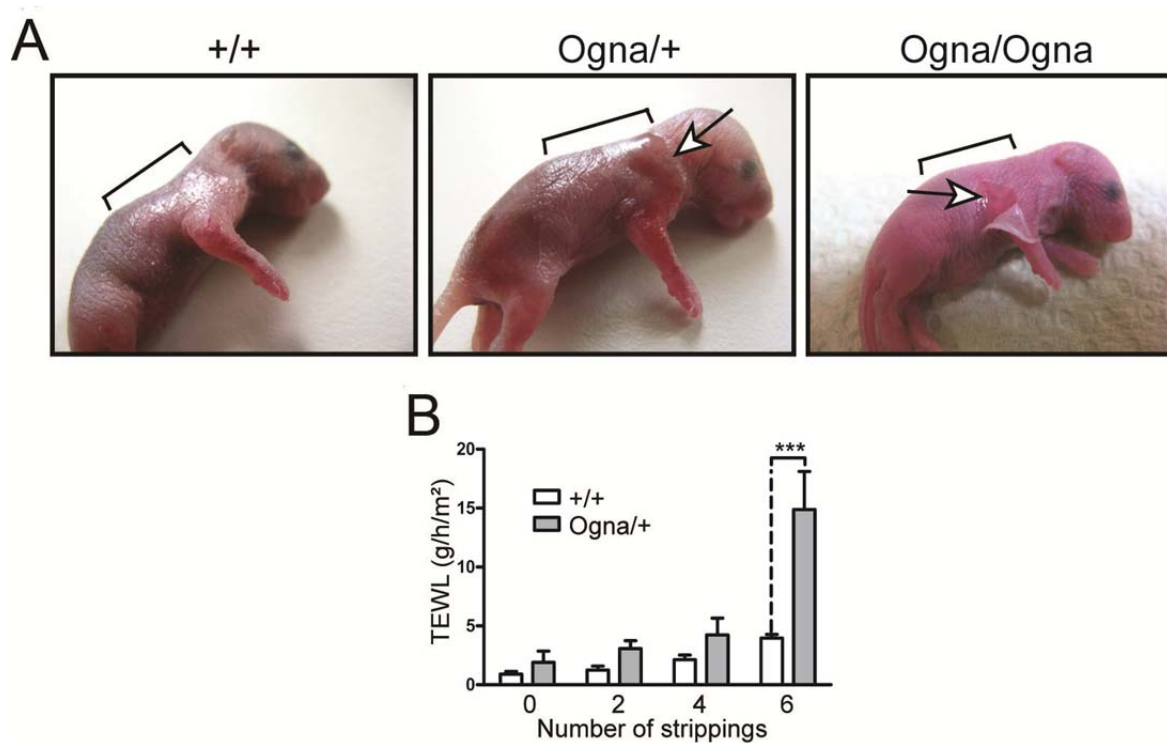


**Figure 22. Mechanical resistance of the epidermis.** (A) Note epidermal exfoliation after 6 consecutive tape strippings of 1-day-old *Plec*<sup>Ogn/+</sup> mice (arrow), and complete epidermal detachment (arrow) for *Plec*<sup>Ogn/Ogn</sup> mice after only 2–3 tape strippings. Brackets mark areas to which tape stripping was applied. (B) Bar diagram showing transepidermal water loss (TEWL). Note, the sharp rise in TEWL after 6 consecutive tape strippings in 1-day-old *Plec*<sup>Ogn/+</sup> mice, compared to their *Plec*<sup>+/+</sup> littermates. Data are shown as mean values  $\pm$  SD; (n=6). \*\*\* P < 0.001 (two-way ANOVA with Bonferroni post test). (Modified from Walko et al. 2011, Fig. 1B,C)

### Histological analysis of the skin

For histological evaluation, skin biopsies were taken from different parts of the body, including apparently healthy as well as blistered areas, and sections were embedded in epoxy resin, stained with 1% toluidine blue and examined by light microscopy. Specimens from wild-type (Fig. 23A) and undamaged areas of mutant mouse skin (Fig. 23B,C), revealed an undisturbed structure of the epidermis, with no epidermal-dermal detachment, and a continuous basal keratinocyte cell layer. In contrast, skin sections of lesion biopsies taken from *Plec*<sup>Ogn/+</sup> as well as *Plec*<sup>Ogn/Ogn</sup> Ogn mice (Fig. 23D,E), showed a normal pattern of epidermal cell layers but typical signs of epidermal-dermal separation at the level of basal keratinocytes (Fig. 23D,E).



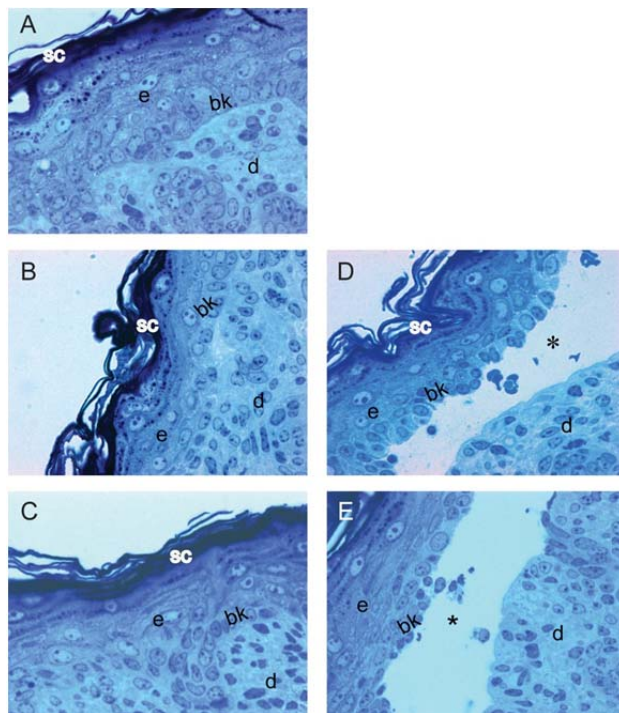


**Figure 23. Histological analysis of skin from newborn mice.** Epoxy resin-embedded and toluidine blue-stained skin sections from wild-type and Ogn<sup>a</sup> mutant mice are shown. (A-C) In unlesional skin, no differences in the organization of mutant and wild-type skin were visible. (D,E) In lesional skin, note the separation of the dermis from the epidermis between the stratum basale and the dermis. sc, stratum corneum; e, epidermis; bk, basal keratinocyte cell layer; d, dermis. Asterisk, blister cavity. Bar, 20  $\mu$ m. (Modified from Walko et al. 2011, Fig. 2A).

### Ultrastructural analysis of skin lesions

To characterize skin lesions in more detail, specimens from Ogn<sup>a</sup> mutant mice were examined by electron microscopy. Micrographs shown in Fig. 24 illustrate that the epidermal-dermal separation occurred within basal keratinocytes. Parts of broken basal keratinocytes including plasma membrane and HD remnants that remained attached to the dermis lesion floor were clearly identifiable, while the upper remnants underwent lysis. In contrast, a regular attachment of intact HDs to the basal lamina was seen in wild-type skin. Cytolysis at the level just above the dermo-epidermal is the hallmark of EBS due to plectin deficiency (Andrä et al. 1997, Smith et al. 1996, Chiaverini et al. 2010).

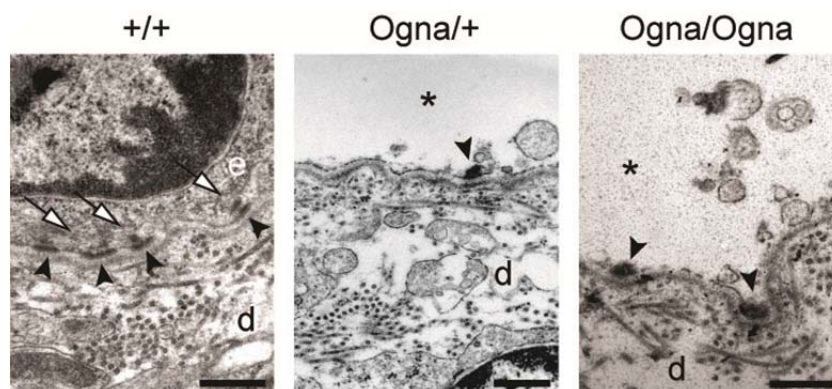


**Figure 24. Ultrastructural analysis of newborn mouse skin.** Arrowheads indicate either intact HDs with attached keratin filament bundles (arrows) aligned along the basal cell surface of basal keratinocytes (wild-type), or remnants of HDs lacking keratin filaments at blister (\*) floors in mutant skin. Bars, 500 nm. (Modified from Walko et al. 2011, Fig. 2B).

### Ultrastructural and morphometric analyses of hemidesmosomes

As it has been reported that HDs are not fully functional in OgnA patients (Koss-Harnes *et al.* 2002), I next focused on the analysis of hemidesmosomal parameters such as number, morphological appearance, and competence to anchor keratin filaments. This analysis was first done in newborns and later extended to adults. In specimens of neonatal wild-type skin, densely packed HDs were observed all along the basal membrane, whereas in skin samples isolated from OgnA mutant mice more sparsely distributed HDs were visible (Fig. 25A). Additionally, the basal membrane itself appeared to be less sinuous. Close ups at higher magnification showed that the HDs located at the basal surface of basal mutant keratinocytes exhibited well-defined inner and outer plaques (Fig. 25B). Keratin filaments appeared well and profusely inserted into the HDs of wild-type skin (Fig. 25A), but loosely and scantily inserted into OgnA HDs, demonstrating a flawed connection of the keratin filaments to these structures (Fig. 25B).

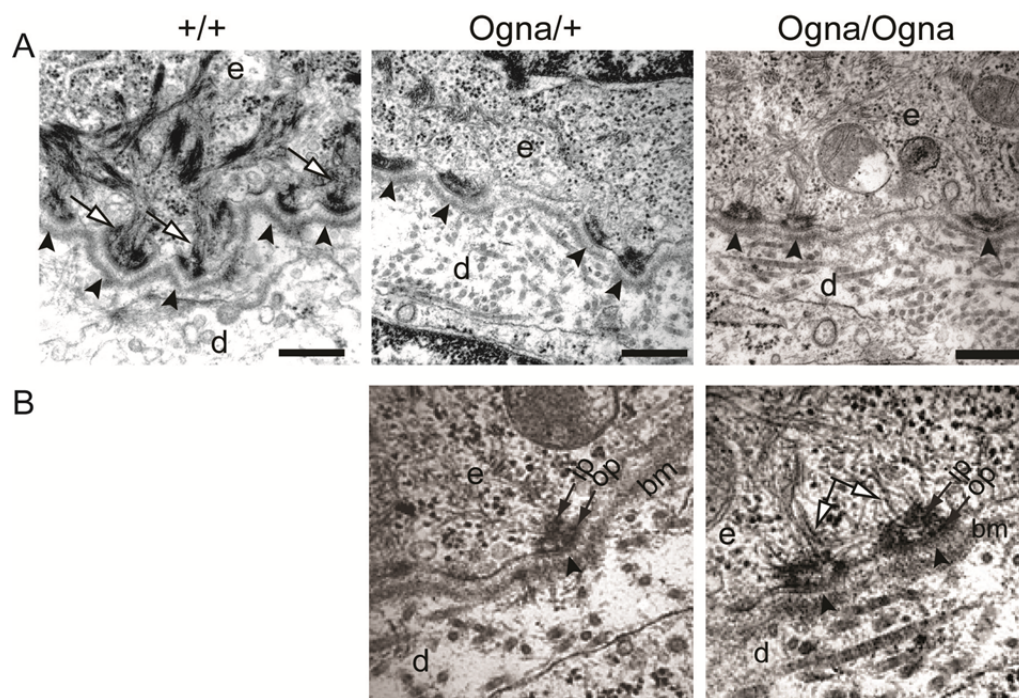


**Figure 25. Ultrastructural analysis of hemidesmosomes in newborn mouse skin.** (A) Representative micrographs of HDs. Note the distantly spaced location of HDs (arrowheads) along the basal membrane in mutant compared to wild-type skin. Arrows point to keratin filaments attached to the HDs. Bars, 500 nm. (B) HDs at higher magnifications. Note reduced or absent keratin filaments connected to HDs in specimens from heterozygous and homozygous mice revealed at higher magnification. e, epidermis; d, dermis; bm, basal membrane; k, keratin network; ip, inner plate; op, outer plate. (Modified from Walko *et al.* 2011, Fig. 2C).

Electron microscopy of wild-type, heterozygous, and homozygous skin samples from adult mice (Fig. 26) revealed hemidesmosomal features that were similar to the ones

observed for newborn mice. Structurally, the HDs of mutant mice looked normal, with well-defined inner and outer plaques. However they showed a reduction in numbers and attachment of keratin filaments, compared to wild-type specimens (Fig. 26).

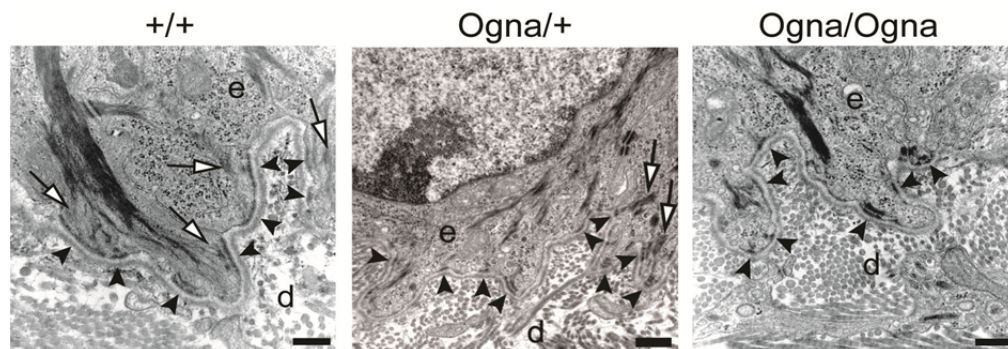


**Figure 26. Ultrastructural analysis of hemidesmosomes in adult mouse skin.** Skin specimens from paws are shown. Arrowheads, HDs; arrows, keratin filaments attached to HDs. Note decrease in numbers, size, and keratin filament attachment in *Plec*<sup>Ogna/+</sup> and *Plec*<sup>Ogna/Ogna</sup> samples; also, HDs have clearly discernable outer and inner plates. e, epidermis; d, dermis. Bars, 500 nm. (Modified from Walko et al. 2011, Fig. 2D).

As the size of HDs, their number, and their morphology are highly relevant for their function, these features were assessed by quantitative morphometry of electron micrographs.

**Size.** Hemidesmosomal size estimations turned out to be a demanding task due to the variability of the positions where the cut across the HDs occurred. To obtain representative figures more than 1000 hemidesmosomal cuts were measured in samples from tongue and footpad skin. The analysis of newborn mice showed that HDs in mutant specimens were significantly smaller than in wild-type specimens (110-105 vs ~150 nm). While in adult mice this difference was even more pronounced (114-139 vs ~248) (Table 5).

**Table 5. Average hemidesmosome size in mice epithelia**

	Geometric mean of measured hemidesmosomal cuts (nm)		
	Wild-type	Ogna/+	Ogna/Ogna
Newborns	149,89	110,32	104,92
Adults	247,67	114,28	138,93

The size distribution of HDs in wild-type and mutant mice is presented as area plots in Fig. 27 A,B. The trend to form larger HDs in wild-type mice is clearly visualized in the area plots. Furthermore, hemidesmosomal cuts larger than 300 nm or 600 nm in newborn and adult mice, respectively, were never found in samples of mutant mice.



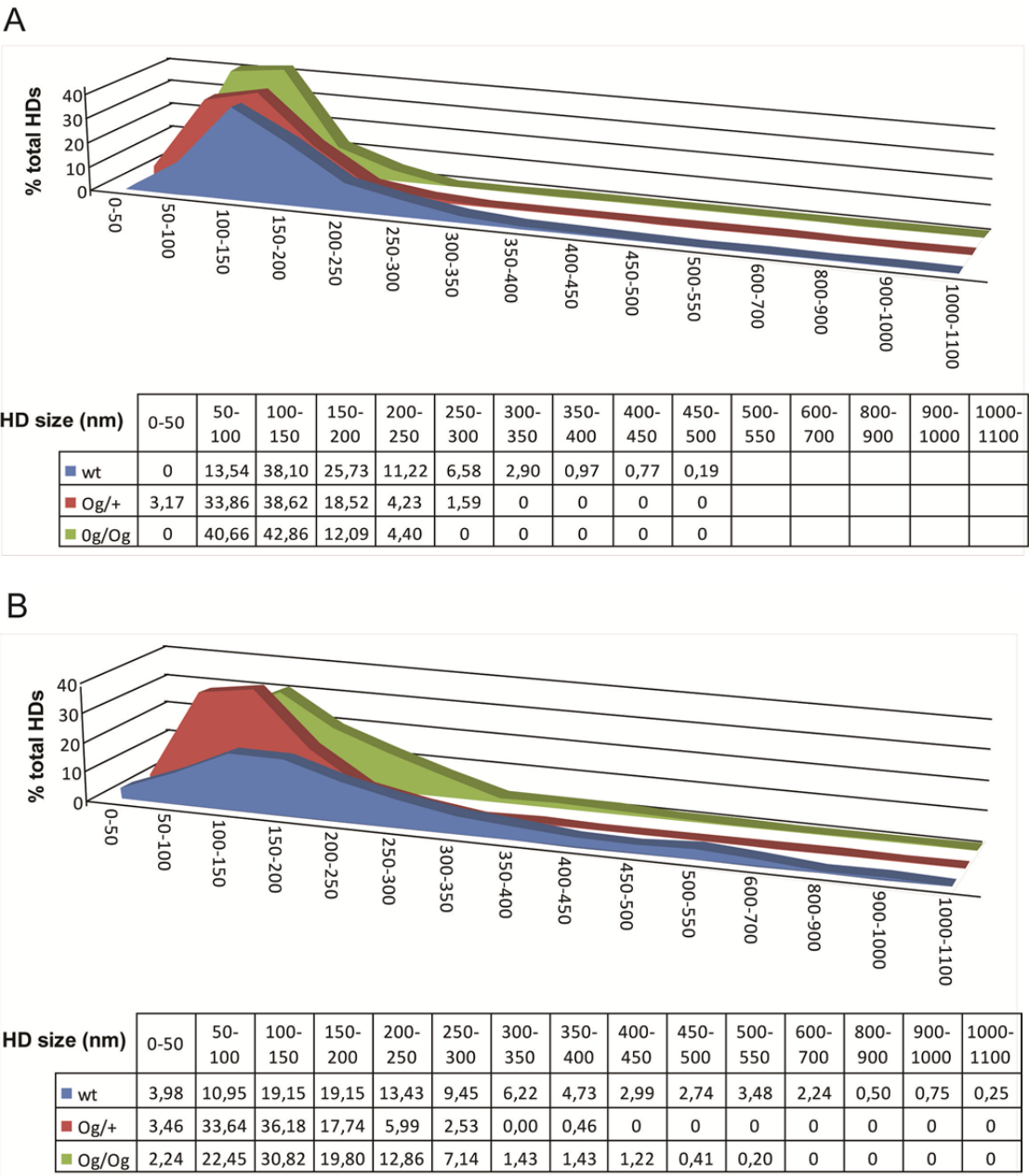


**Figure 27. Hemidesmosome size distribution in wild-type and mutant mice. (A)** Newborns. **(B)** Adult mice. Length of individual hemidesmosomal cuts were measured in electron micrographs of ultrathin sections from tongue and foot pad of wild-type and mutant littermates (numbers of HDs scored  $\geq 400$  per genotype). The lengths were sorted into 15 groups and the size distribution represented as percentage of the total number of HDs counted.

**Numbers.** Instead of counting the number of HDs per micrometer of basal cell membrane I measured the length of basal cell membrane containing HDs and expressed it as percentage of the total length. As shown in Fig. 28A the percentage of basal membrane containing HDs in adult mutant mice (19-22%) was well below that in wild-type mice (45%). There were not significant differences in HD density between hetero- and homozygous skin. In newborns, the same trend was observed although HD density along



the basal membrane was somehow lower (39% for wild-type skin, but a merely in 11% for mutant skin).

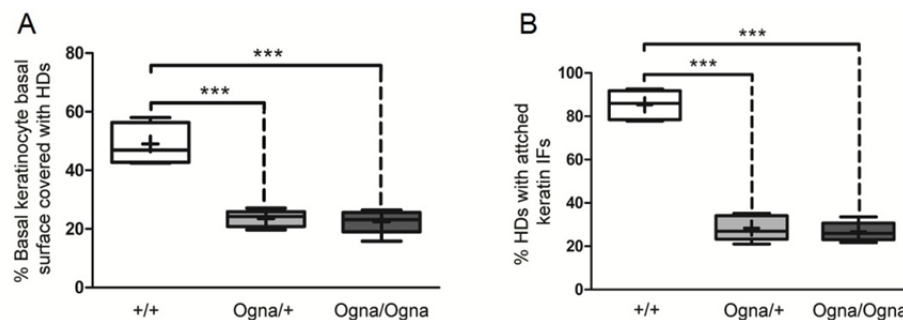


**Figure 28. Morphometric analysis of hemidesmosomes from adult mouse skin. (A)** Numerical density of HDs in the basal membrane. A total length of 50–60  $\mu\text{m}$  of basal membrane of basal keratinocytes was analyzed as described in the text in electron micrographs of foot pad skin section from wild-type and mutant littermates ( $n=5$ ; total numbers of HDs scored  $\geq 590$  per genotype). **(B)** Keratin filament attachment. Values are expressed as percentage of the total number of HDs counted (same as in A). Box and whisker plots indicating the median (middle line) and mean (small crosses), 25<sup>th</sup> and 75<sup>th</sup> percentiles (bottom and top line of the box, respectively), and 2.5<sup>th</sup> and 97.5<sup>th</sup> percentiles (whiskers) are shown. \*\*\*  $P < 0.001$  (one-way ANOVA with Tukey post test for multiple comparisons). (Modified from Walko et al. 2011, Fig. 2F,G).

**Keratin filament attachment.** While the vast majority of the HDs in wild-type skin showed properly inserted keratin filaments into the HDs attachment plates, two thirds of the mutant HDs lack keratin filament association with the inner plate (Fig 28B). Data for mutant newborn mice showed a similar strong decrease in the number of HDs associated with keratin filament.

**Presence of an inner plate.** Most HDs in control and mutant skin possessed well-formed inner plates. Accordingly, there were no significant differences in the percentage of HDs with inner plates between the three genotypes (Fig. 29).

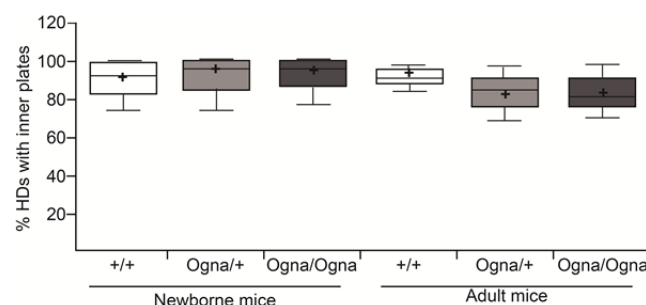


**Figure 29. Quantification of hemidesmosomes with inner plates.** HDs in electron micrographs of foot pad skin were scored for the presence or absence of an inner plate. Values are expressed as percentage of the total number of HDs counted ( $n=3$ , total numbers of HDs scored  $\sim 400$  per genotype). Box and whisker plots as in Fig. 28.

In conclusion, no important alterations were observed in the structure of Ogna HDs, but their numbers and association to keratin were critically reduced. Furthermore, these both traits, were similarly affected irrespective of the allelic state of the mutation.

### **Ultrastructural analysis of desmosomes**

Besides HDs, desmosomes have a significant function in establishing the epithelial sheet (Jamora and Fuchs, 2002). Desmosomes are organized as highly symmetrical plasma membrane multiprotein complexes associated with IFs. Although plectin has been shown to form part of desmosomes (Wiche et al. 1983), no obvious abnormalities in desmosomal morphology or in their association with intermediate filaments were observed in the epidermis of hetero- or homozygous Ogn mice (Fig. 30).

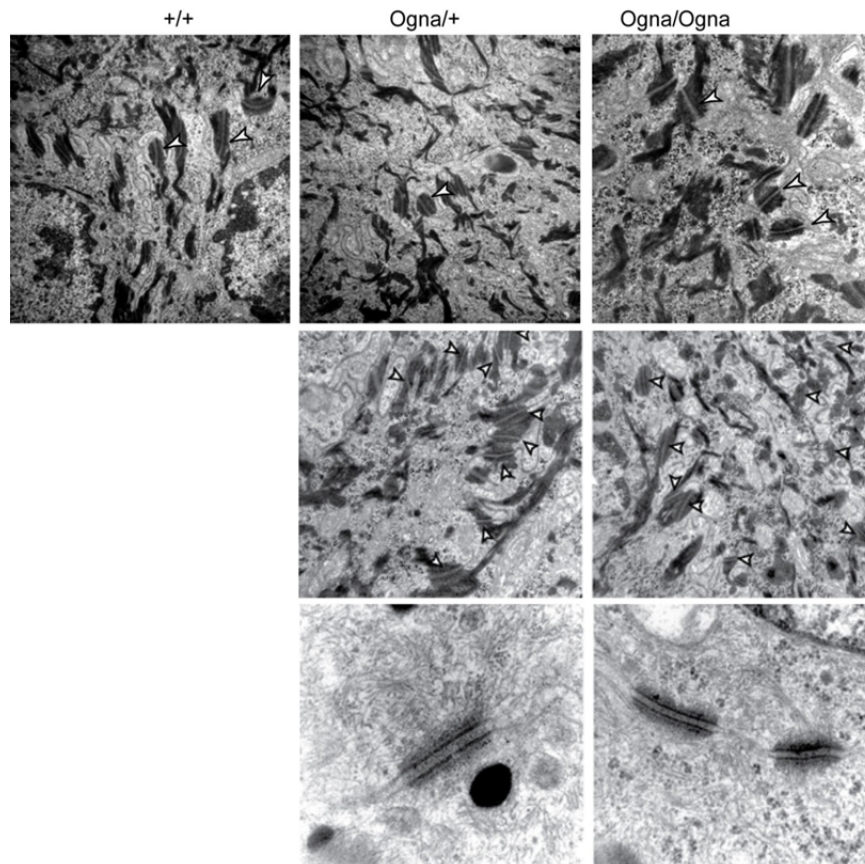


**Figure 30. Ultrastructural analysis of desmosomes in mouse skin.** Upper panels, newborn skin. Central panels, adult footpad skin. Lower panels, detail of desmosomes in stratum spinosum. Note, the normal morphology, similar size and number of desmosomes as well as filament attachment in all panels. Arrows point to desmosomal structures and arrowheads to the IFs.

### **Expression of hemidesmosomal components**

The expression of major HD proteins was examined by immunofluorescence microscopy of frozen skin section from 1-day-old and adult mice.

**Plectin.** First, I used antibodies to plectin that have been employed in the diagnosis of cases identified as EBS-associated plectin, as well as EBS-Ogna (Gache et al. 1996; Shimizu et al. 1999; Koss-Harnes et al. 1997, 2002). These included two monoclonal antibodies (mAb), 10F6 (Foisner et al. 1991) and HD121 (Hieda et al. 1992), that have a

rod based epitope, and an antiserum #46 bearing epitopes in the rod and preceding sequences (Wiche and Baker 1982; Andrä et al. 2003). All three recognize all plectin isoforms. Unfortunately, none of the 12 mAbs available (Foisner et al. 1991) allows discrimination between wild-type and Ogn<sup>a</sup> plectin. Two of them, that were shown to map to a region of 132 amino acids flanking the Ogn<sup>a</sup> mutation (J. Breitenbach, Diploma Thesis, 2006) and could have given a different staining pattern, did not work for immunocytochemistry. Additionally, two isoform-specific antibodies, against P1c and P1a, were used in the analysis. P1c is the isoform most abundantly expressed in epidermis (Fuchs et al. 1999 and this work p33), while P1a is the isoform found in HDs (Rezniczek et al. 2003, Andrä et al. 2003).

In *Plec*<sup>+/+</sup> epidermis of newborn mice, mAb 10F6 prominently stained the basal membrane, while staining of the suprabasal layers and the stratum corneum was less intense. In mutant mice, however, plectin immunoreactivity was strongly reduced along the basal membrane of basal keratinocytes; in contrast, plectin immunoreactivity was only slightly diminished in the suprabasal cell layers (Fig 31, upper panels, see also Walko et al. 2011). Labeling the skin samples with mAb HD121 produced a staining pattern where the basal cell membrane of basal keratinocytes was strongly outlined in wild-type, but drastically reduced in mutant skin (Fig 31 central panels). Antiserum #46 showed strong plectin expression at the dermo-epidermal borderline and membrane and weak cytoplasmic staining of all epidermal keratinocytes, in wild-type skin. In *Plec*<sup>Ogn<sup>a</sup>/+</sup> mice, the borderline separating the epidermis from the dermis was discontinuously stained, with interruptions where plectin staining was totally absent, whereas in *Plec*<sup>Ogn<sup>a</sup>/Ogn<sup>a</sup></sup> mice, the discontinuous effect was more pronounced with only occasional patches of plectin positive staining found in this area (Fig. 31 lower panels).

Although the staining patterns obtained with the 3 different pan-plectin antibodies differed slightly, they all showed a drastic reduction of plectin expression along the basement membrane of basal keratinocytes. Several publications have documented that different anti-plectin antibodies (both monoclonal and polyclonal), stain the suprabasal and basal keratinocyte cell layers of the epidermis with different intensities giving rise to overall distinct staining patterns (Koss-Harnes et al. 1997; Ortonne Gache et al. 1996; Shimizu et al. 1999; Andrä et al. 2003). The reason for these differences is still unknown, but likely involves differential epitope accessibility.

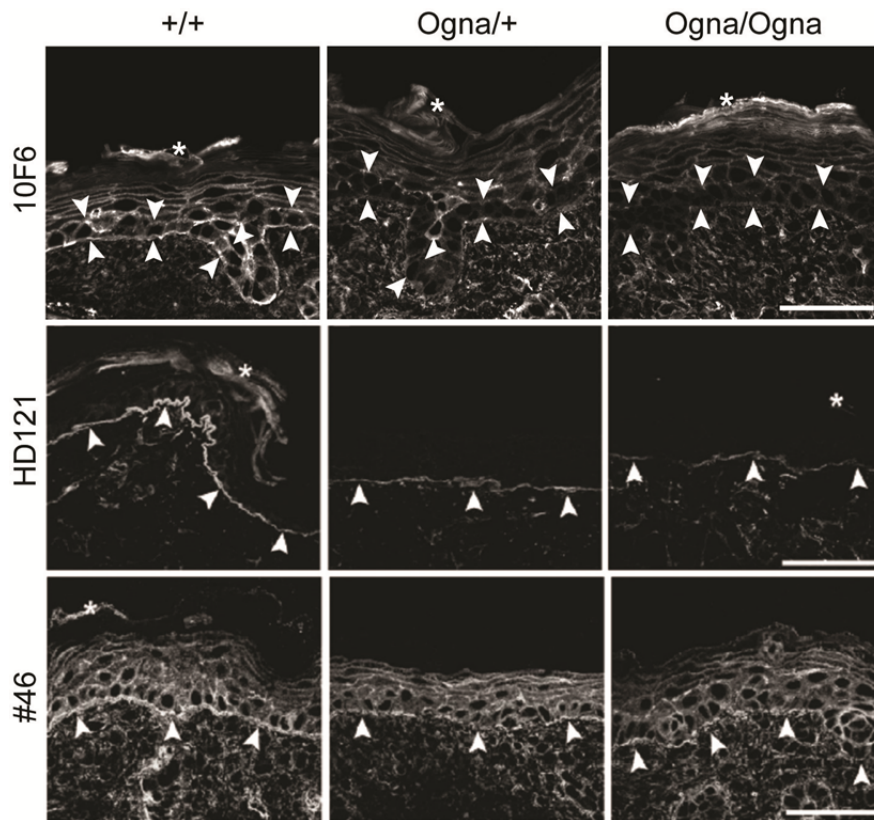


**Figure 31. Immunolocalization of plectin on frozen sections of leg skin from 1-day-old wild-type and mutant mice.** Note, that mAbs 10F6 and HD121 as well as serum #46 recognize all plectin isoforms. Note, the reduction of plectin staining at the basal cell membrane of basal keratinocytes (arrowheads), but not in suprabasal keratinocytes in mutant skin. Bars, 50  $\mu$ m. (Modified from Walko et al. 2011, Fig. 3A-C).

Using isoform-specific antibodies against P1c and P1a, I found no differences in P1c expression among the three skin genotypes (Fig 32, upper panels). In contrast, no expression of P1a was detected in the epidermis of mutant mice except for a few positive patches in *Plec*<sup>Ogn<sup>+/+</sup></sup> epidermis (Fig 32, lower panels; see also Walko et al. 2011), while expression of P1c was unchanged

Analysis of footpad skin samples from 2 month-old adult mice using the same panel of antibodies to plectin yielded similar observations to those obtained for newborns. Most significant results are shown below. When using mAb 10F6, mutant mice showed complete lack of cytoplasmic staining in the basal layer including the underlying basal membrane, whereas the upper suprabasal epidermal zone appeared unaffected (Fig. 33, upper panels). P1c-specific staining was comparable for all three genotypes (Fig. 33, central panels). In contrast, a remarkable reduction of P1a-specific staining along the basal membrane was observed in *Plec*<sup>Ogn<sup>+/+</sup></sup> and *Plec*<sup>Ogn/Ogn</sup> skin sections (Fig. 33, lower panels).



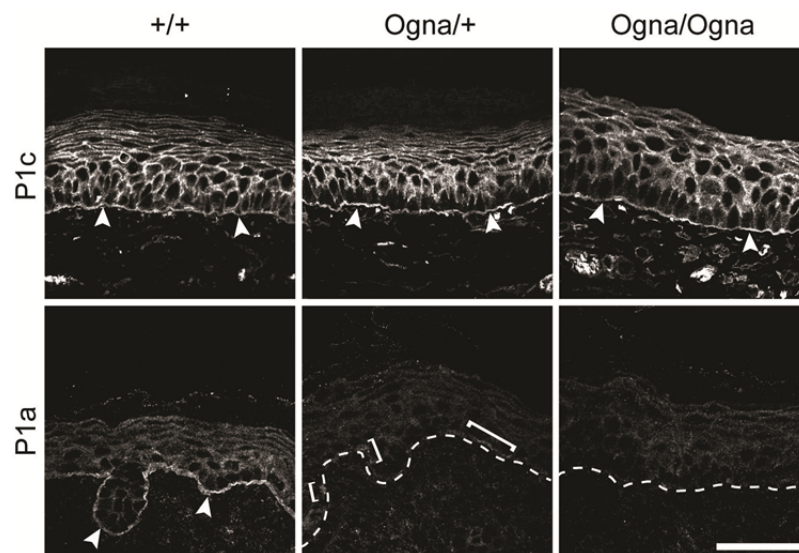


**Figure 32. Immunolocalization of plectin isoforms P1c and P1a on frozen sections of leg skin from 1-day-old wild-type and mutant mice.** Upper panels. Expression levels and localization of P1c are about the same in the three genotypes. Lower panels. Expression of P1a at the basal cell membrane of basal keratinocytes is clearly detected in *Plec*<sup>+/+</sup> skin, but is clearly absent in mutant epidermis, except for a few positive patches (brackets) in *Plec*<sup>Ogna/+</sup> skin. Dashed lines, dermo-epidermal border. Bar, 50  $\mu$ m. (Modified from Walko et al. 2011, Fig.3D-I).

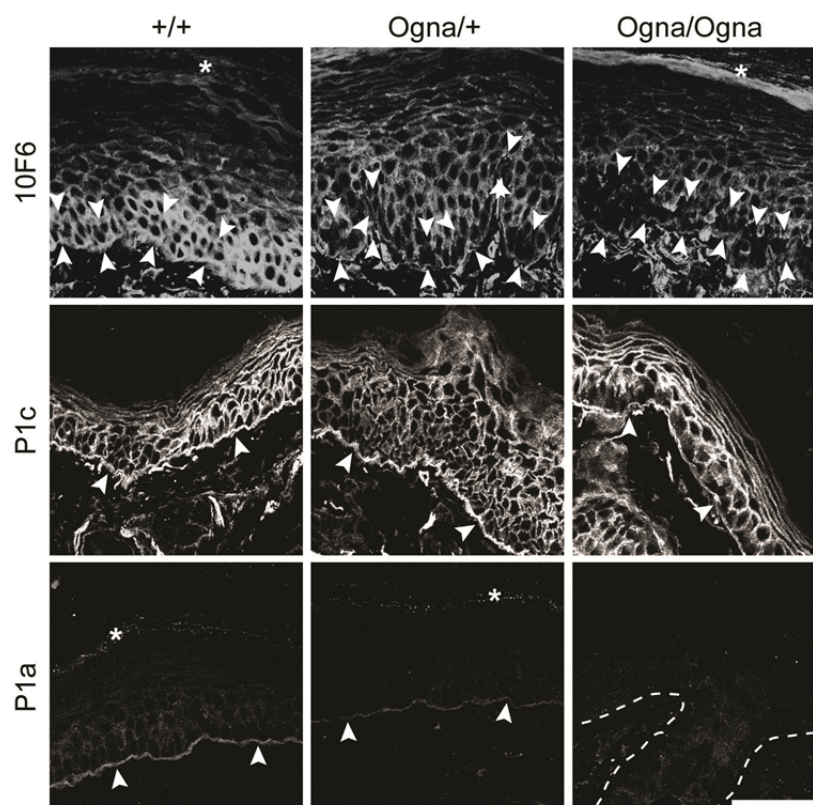


**Figure 33. Immunolocalization of plectin on frozen sections of foot pad skin from 2-month-old mice.** Upper panels, total plectin stained with mAb 10F6. Central and lower panels, plectin isoforms P1c and P1a. Note, the reduction of total plectin, but most particularly isoform P1a, staining in mutant skin; while expression of P1c remains unchanged. Arrowheads point to basal-membrane line. Opposite double arrowheads indicate unstained basal membrane and basal keratinocytes. Dashed line outlines the dermo-epidermal border. Bars, 50  $\mu$ m.

**Other hemidesmosomal proteins.** To assess whether Ogn1 plectin had an effect on the expression or localization pattern of other hemidesmosomal structural proteins, skin sections from mutant and control mice, were stained using antibodies against integrin  $\beta 4$  (ITG $\beta 4$ ), BPAG1, and the basal keratinocytes IF protein, keratin 5. The immunofluorescence analysis was performed in back skin biopsies from both, newborn and adult mice. The integrin  $\beta 4$  signal was confined to the basal membrane of basal keratinocytes (Fig. 34 and 35, upper panels). No alteration or disruption of the basal membrane was observed, but the intensity of the signal appeared to be slightly reduced in *Plec*<sup>Ogn1/Ogn1</sup> epidermis (see also Walko et al. 2011). Similar observations were made for BPAG1, although in this case, the reduction of the signal in mutant mice epidermis was more pronounced (Fig. 34 and 35, central panels). Keratin 5 was located in the layer of basal keratinocytes and transit amplifying cells, with similar fluorescence intensities in wild-type and Ogn1 specimens (Fig. 34 and 35, lower panels). Arrowheads point to basal membrane. Bars, 50  $\mu$ m.

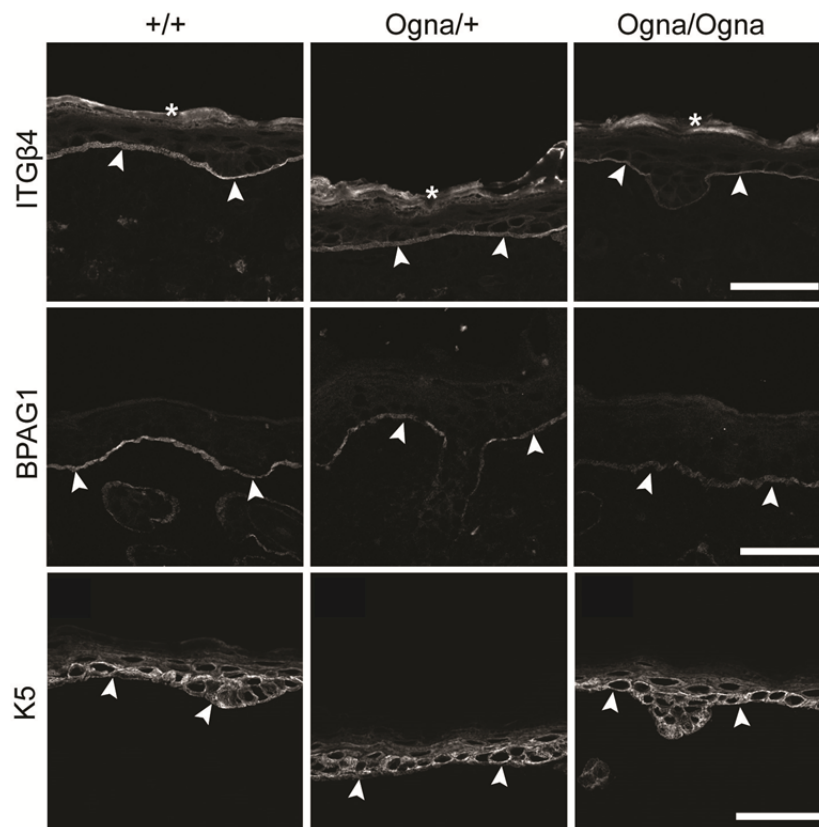


**Figure 34. Immunolocalization of hemidesmosomal proteins on frozen sections of leg skin from 1-day-old mice.** Note, staining of ITG $\beta 4$  at the basal membrane of basal keratinocytes is unaltered in *Plec*<sup>Ogn1/+</sup> skin, but slightly decreased in *Plec*<sup>Ogn1/Ogn1</sup> skin (upper panels). The BPAG1 signal is more discontinuous and weak in mutant mice than in *Plec*<sup>+/+</sup> skin (central panels). While staining of K5 is unchanged in mutant mice (lower panels). Arrowheads point to basal membrane. Bars, 50  $\mu$ m. (Modified from Walko et al. 2011, Fig. 3J-O).

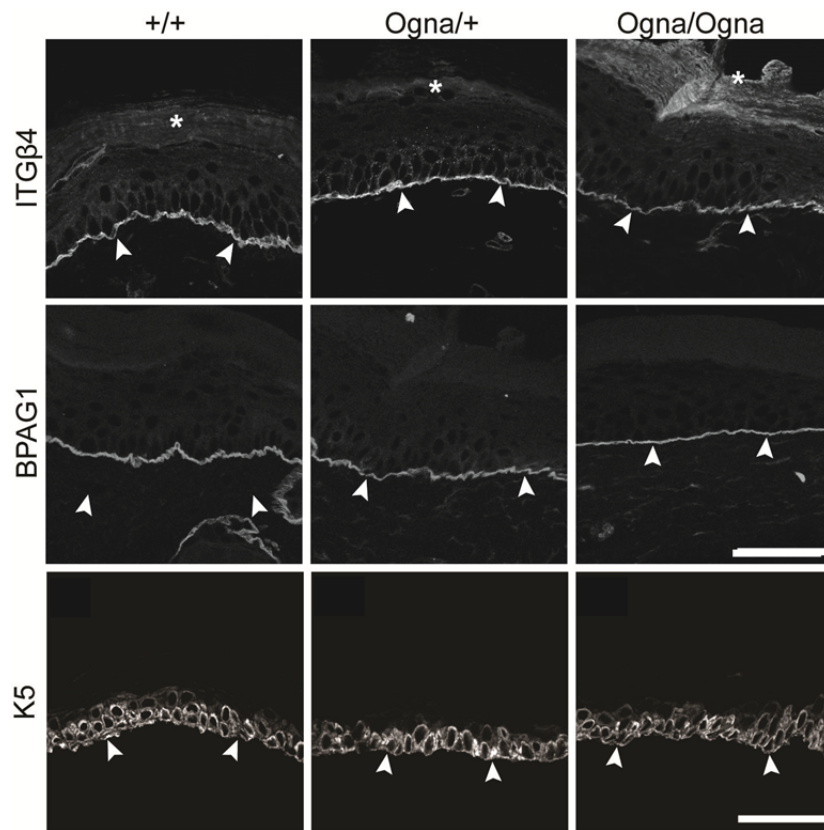


**Figure 35. Immunolocalization of hemidesmosomal proteins on frozen sections of footpad skin from 2-month-old mice.** Note, staining of ITGβ4 is slightly reduced in *Plec*<sup>Ogna/Ogna</sup> cells (upper panels); whereas BPAG1 staining decays progressively with the number of mutant alleles, *Plec*<sup>+/+</sup> > *Plec*<sup>Ogna/+</sup> > *Plec*<sup>Ogna/Ogna</sup> (central panels). Staining of K5 is unchanged in mutant mice (lower panels). Arrowheads point to basal membrane. Bars, 50 μm.

**Expression under mechanical stress.** As tape stripping mimics mechanical injury I investigated the subcellular distribution of hemidesmosomal proteins in the lesions inflicted in the skin of newborn mice after 4 times tape stripping. For this purpose, mice were first examined under a stereo microscope to precisely localize the microlesion and take skin biopsies. Biopsy specimens were then processed and examined by standard immunohistochemical methods. In all skin samples, but particularly in those from *Plec*<sup>Ogna/+</sup> mice, dermal-epidermal separation within the basal keratinocytes was prominent throughout the lesion area (Fig. 36). Integrin β4 was confined to the lesion floor. The fluorescence signal intensity in the lesion was similar to the one in the intact region. Keratin 5, the cytoskeletal binding partner of hemidesmosomal plectin, was faithfully located at the lesion roof in the basal keratinocyte cell layer as well as in transit amplifying cells. Plectin staining was positive in all layers of epidermis and underlying dermis, with pronounced but partially discontinuous staining of the dermo-epidermal borderline. Merged panels on the right (Fig. 36) show colocalization of plectin with

integrin  $\beta 4$  in the basal membrane and with keratin 5 in basal keratinocytes. Thus, the interaction of plectin with these binding partners appeared to be unaffected.

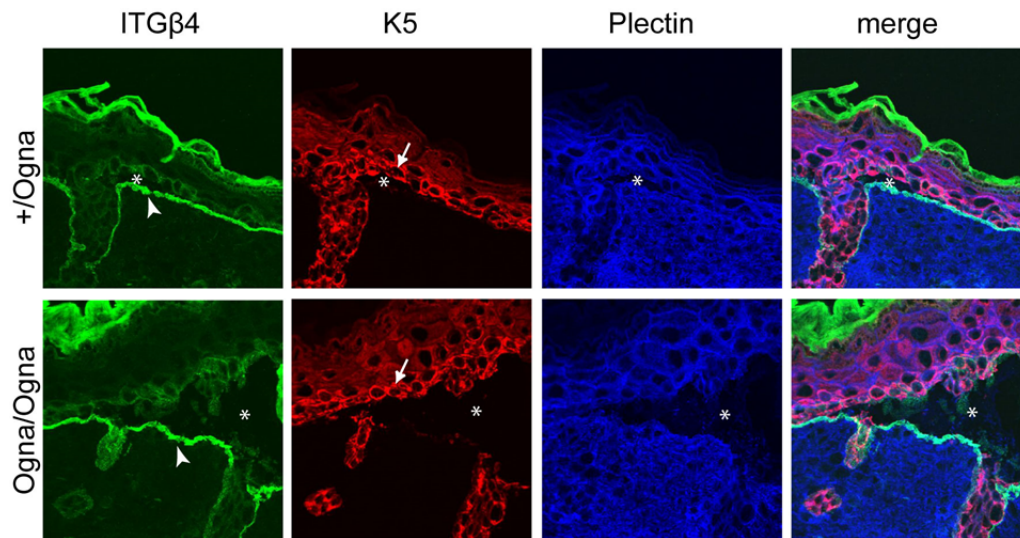


**Figure 36. Detection of integrin  $\beta 4$ , keratin 5, and plectin in skin lesions inflicted by mechanical injury.** Note, separation of the dermal-epidermal layer in micro-lesions (asterisks), restriction of ITG $\beta 4$  to the lesion floor (arrowheads), and location of K5 signal in basal keratinocyte layer at the lesion roof (arrows). Notice colocalization of plectin with ITG $\beta 4$  in the basal membrane and with K5 in basal keratinocytes (merged panels). Bars, 50  $\mu$ m.

### **Expression of epidermal stratification markers**

Keratins 5 and 14 are typically expressed in the mitotically active layer of basal keratinocytes. As these cells exit from the basal layer and enter terminal differentiation, becoming postmitotic and suprabasal, expression of K5 and K14 is replaced by expression of K1 and K10. In order to test whether epidermal stratification was affected by the presence of the Ogna mutation, I assessed the expression of K5 and K10 in normal and mutant mouse epidermis by double immunofluorescence microscopy. The simultaneous use of antibodies to these two proteins facilitated distinction between differentiating and non-differentiating regions of the epidermis. I observed that K5 was expressed in the basal cells, whereas K10 was confined to the suprabasal layers (results not shown). Thus, no abnormalities in epidermal stratification and differentiation were revealed by immunofluorescence microscopy of skin from knock-in mice when compared to control animals.



## 2. Muscle phenotype

EBS-Ogna phenotype in humans is supposed to be restricted to skin without any obvious effect on other tissues (Koss-Harnes, 1977, 2002). However, plectin is expressed in almost all mammalian tissues (Wiche et al. 1983; Wiche 1989) and lack of plectin results in EBS with muscular dystrophy (Pfundner et al. 2005, Winter and Wiche 2013). Furthermore, a skeletal muscle conditional KO mouse of plectin has shown how important plectin is for preserving the functional integrity of skeletal muscle fibers and cardiomyocytes (Konieczny et al. 2008). Thus, although no muscular phenotype has been reported for Ogna patients, I considered it important to test for signs of a mild muscular defect that could have gone undetected in patients. Furthermore, since very few biopsies from tissues other than skin are available from Ogna patients I deemed it important to conduct an immunofluorescence analysis of striated and cardiac muscle in the Ogna mice.

### **Voluntary wheel running**

I first monitored the mice for signs of muscle weakness while engaged in voluntary exercise. In this context, voluntary wheel running performance is considered an indirect indicator of muscle's structural integrity (Smythe and White 2012). Young mice aged 2 months were housed in single cages equipped with a running wheel that was connected to a computer recording. Voluntary wheel running activity was monitored during 3 weeks by measuring the distances travelled daily. On average, mice ran 9.32 km/24 h (Fig. 37) and no significant differences in the overall running performance were found between wild-type and mutant mice. Thus, it was concluded that the Ogna mutation has no overt signs of muscular dysfunction.

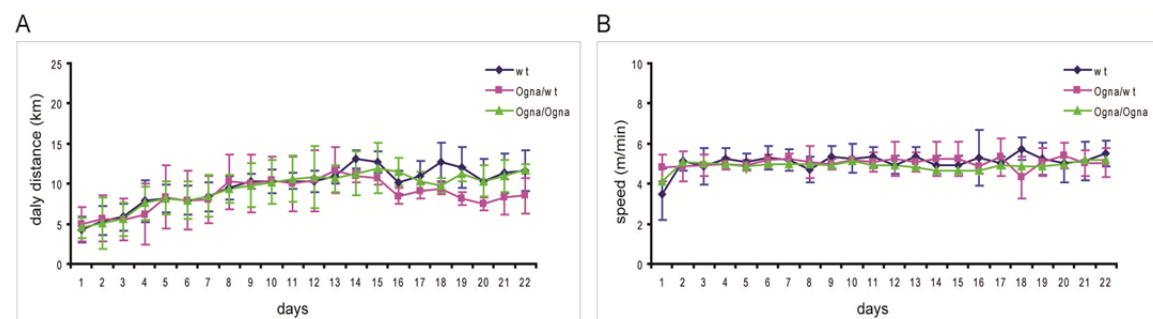


**Figure 37. Voluntary wheel-running of 2-month-old mice. (A)** Daily running distance of individual mice. **(B)** Daily average speed. Values shown are the mean  $\pm$  SD. ( $n \leq 3$  per genotype).

**Expression of plectin, desmin, and  $\alpha$ -actinin in skeletal and cardiac muscle**

To assess the subcellular localization of plectin and intermediate filament constituent protein, desmin, cryosections of soleus muscle, EDL muscle, and heart were double immunolabeled with anti-plectin antiserum #46 and an anti-desmin antiserum, and examined by laser confocal microscopy. This analysis revealed the characteristic staining pattern of plectin along Z-disks and at the sarcolemma in longitudinal (Fig. 38, upper panels) as well as cross-sections (Fig. 38, central panels) of skeletal muscle, and at in the Z and the intercalated disks of cardiomyocytes (Fig. 38, lower panels). No noticeable differences in plectin localization or staining intensity between wild-type and Ogn mutant mice were observed.

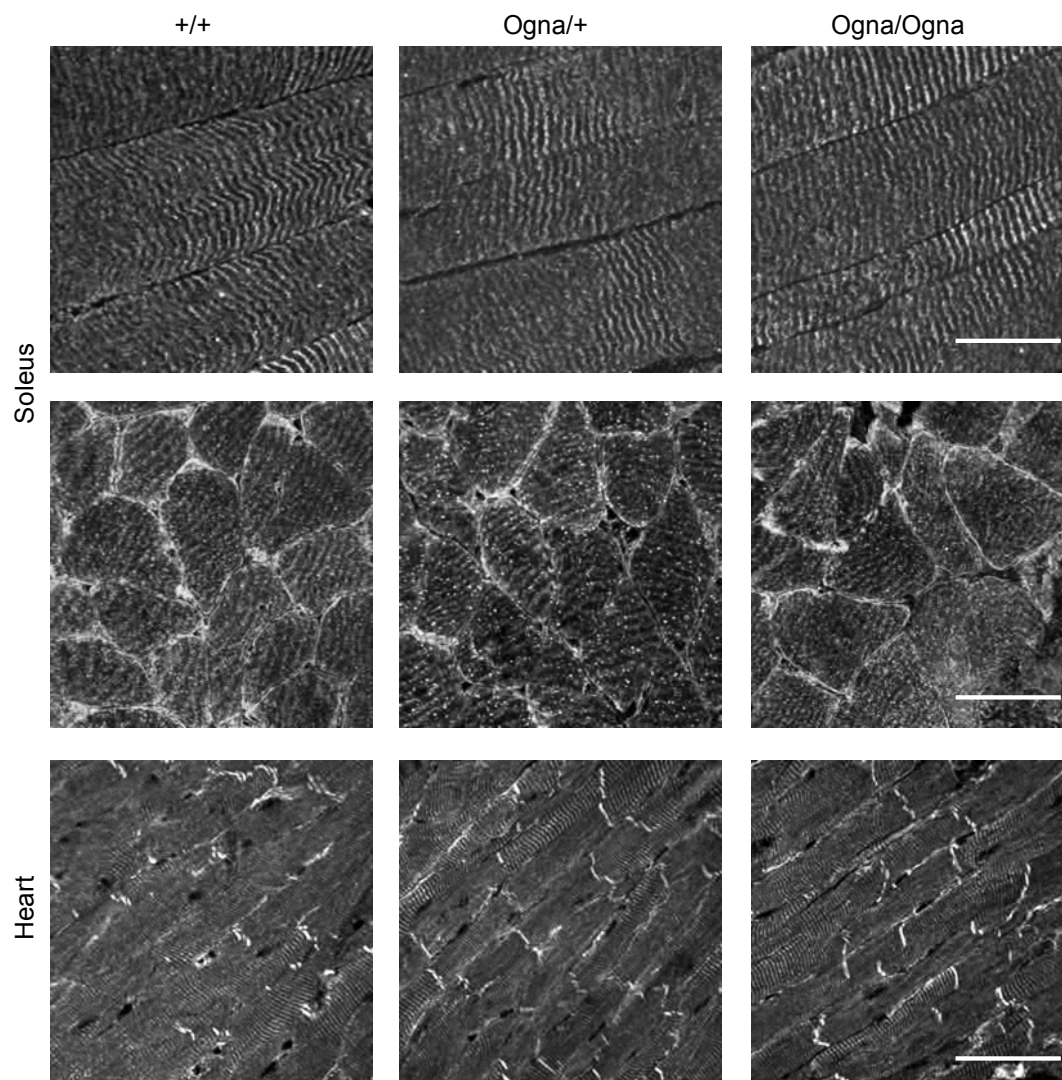


**Figure 38. Immunolocalization of plectin in skeletal and cardiac muscle.** Longitudinal (upper panels) and transversal sections (central panels) of soleus muscle and cross-sections of heart (lower panels) were immunolabeled with anti-plectin antiserum #46. Note, characteristic staining patterns of plectin in all samples. Bars, 50  $\mu$ m. (Modified from Walko et al. 2011, Fig. 4 plectin staining).

Similar results were obtained for desmin. No alterations in the subcellular distribution of desmin were observed neither in *Plec*<sup>Ogna/+</sup> nor *Plec*<sup>Ogna/Ogna</sup> mice. Desmin intermediate filaments were typically located at the level of Z-disks and underneath the sarcolemma (Fig. 39). Furthermore, the desmin content appeared to be unaltered at the sarcolemma and in the interior of fibers. Desmin aggregates in the sarcoplasm and in the sub-sarcolemmal region, typical for plectin-deficient fibers, were not observed.

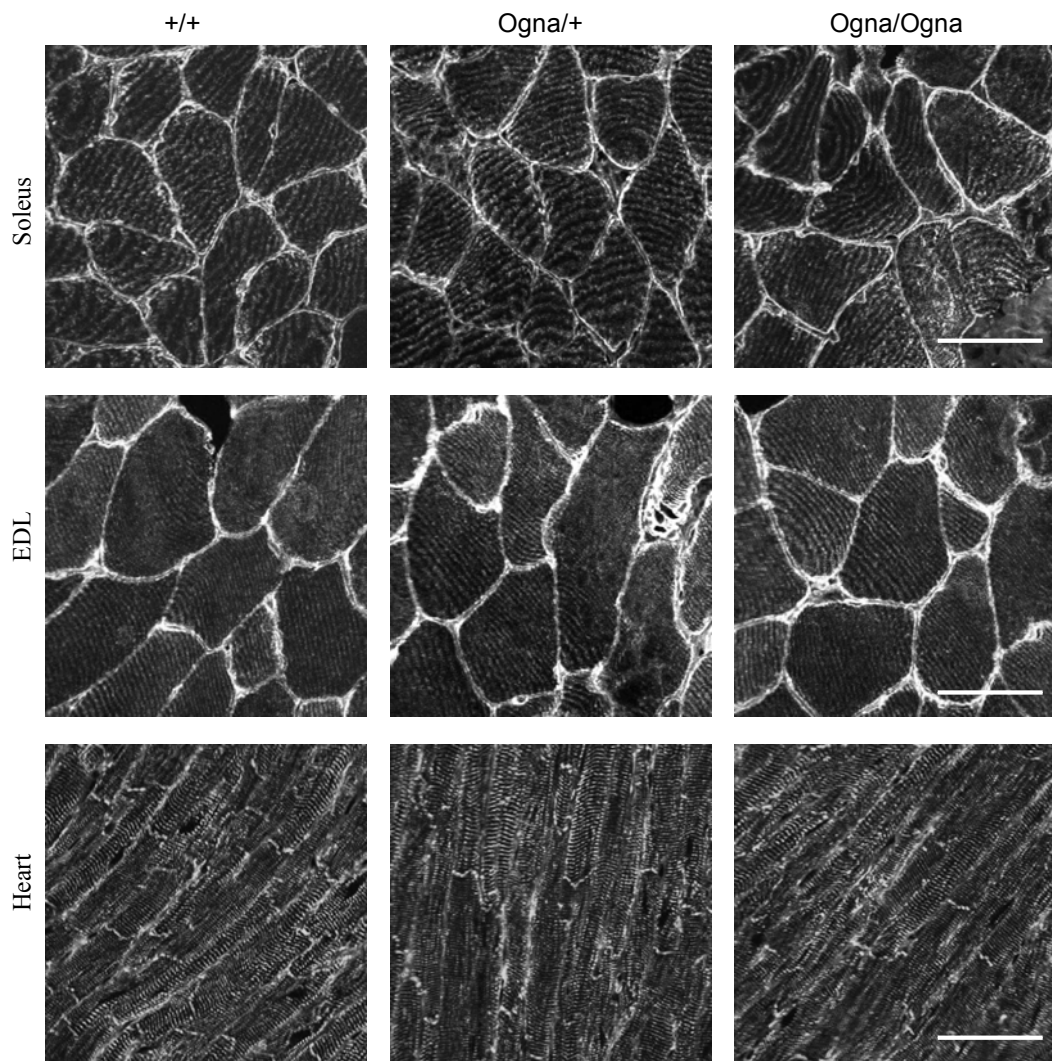


**Figure 39. Immunolocalization of desmin in skeletal and cardiac muscle.** Transversal cryosections of soleus and EDL muscles, and longitudinal heart sections were stained with anti-desmin antibodies. Bars, 50  $\mu$ m. (Modified from Walko et al. 2011 Fig.4, desmin staining)

The merged images of plectin and desmin are shown in Fig. 40. The color code is red for plectin and green for desmin, colocalization of both proteins appearing in yellow. In skeletal muscle, plectin and desmin staining signals overlapped extensively along Z-disks and underneath the sarcolemma, and again, no differences were observed between samples from wild-type and mutant mice (Fig. 40, upper and central panels). Plectin and



desmin also overlapped at the intercalated disk structures of cardiomyocytes, where the typical cross-striated pattern was well visible (Fig. 40, lower panels). In magnified areas the proper alignment of Z- disks consisting of desmin and plectin was evident (insets).

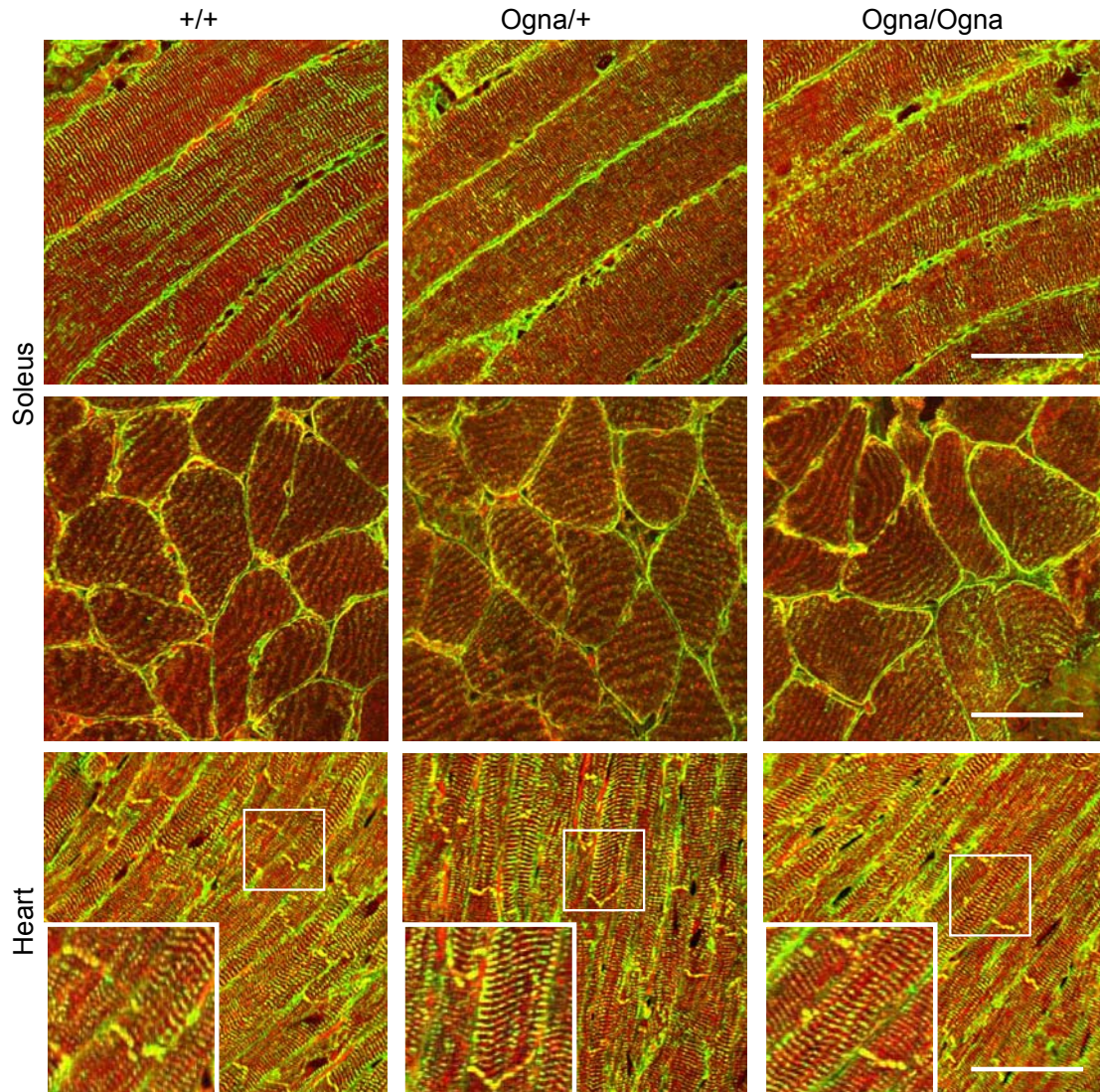


**Figure 40. Colocalization of plectin and desmin in skeletal and cardiac muscle.** Longitudinal and transversal sections of soleus, and cross-sections of heart were immunolabeled for plectin (red) and desmin (green). Frames indicate areas shown magnified in insets. Note, unaltered plectin/desmin localization at Z-disks and intercalated disks in all tissues. Bars, 50  $\mu$ m.

To complete this analysis the distribution of  $\alpha$ -actinin and desmoplakin was examined in skeletal muscle and heart sections. Skeletal and cardiac  $\alpha$ -actinins, are actin-binding proteins localized at the Z-disk, where they anchor the myofibrillar actin filaments. Using a muscle-specific anti- $\alpha$ -actinin antibody I verified the proper alignment of the protein along Z-disks in skeletal muscle (Fig. 41, upper panels), and cardiomyocytes (Fig. 41, lower panels), and found no difference between Ogna and control mice.



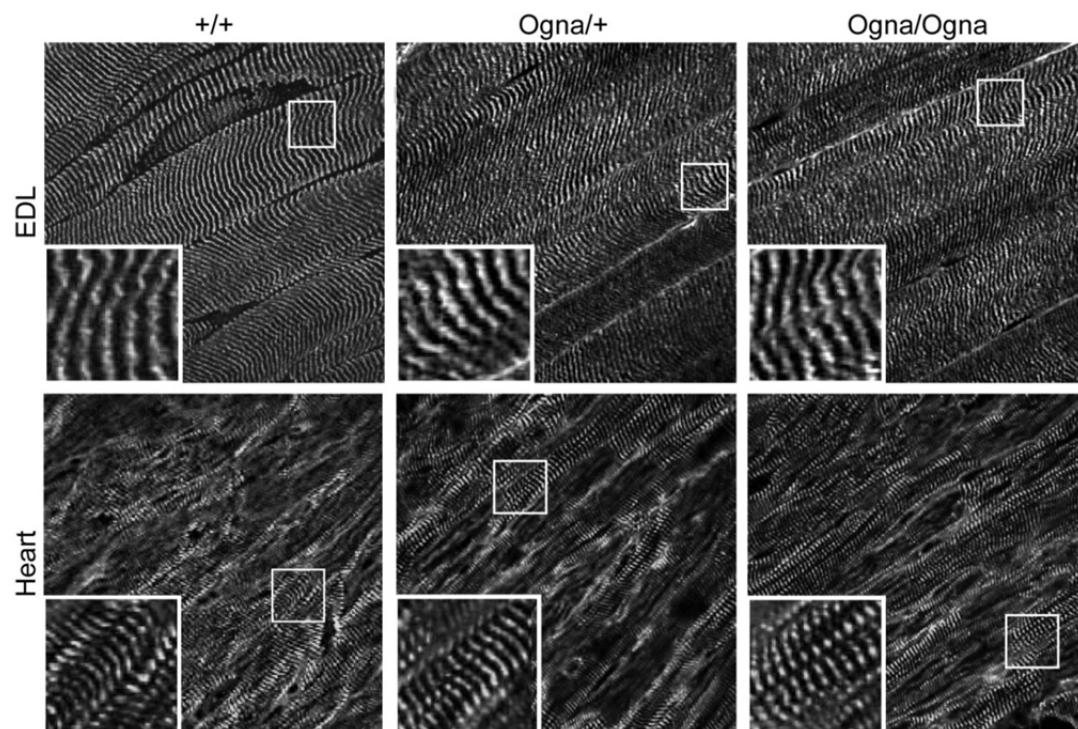


**Figure 41. Detection of  $\alpha$ -actinin in EDL and heart using immunofluorescence microscopy.** Frames indicate areas shown magnified in insets. Note, the regularity of the Z-disks at high magnification. Bars, 50  $\mu$ m.

### ***Expression of plectin and desmoplakin in cardiac muscle***

Desmosomes play a key role in maintaining the integrity not only of skin, but also of heart. Because desmoplakin is the principal protein of desmosomes I examined whether the localization of desmoplakin at intercalated disks might be altered in the Ogna mouse. This appeared not to be the case since no abnormalities in the cytoarchitecture of myocardiocytes were detected and the intercalated disk structures appeared to be intact, with normal desmoplakin staining patterns overlapping with plectin (Fig. 42).

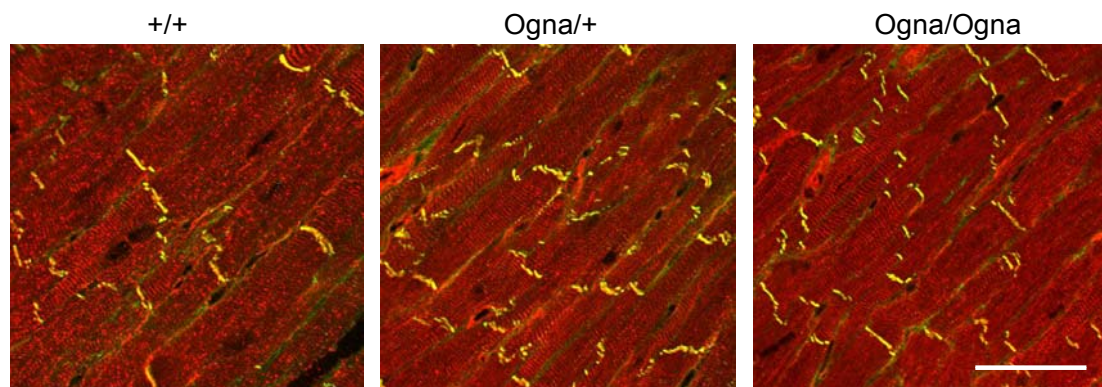


**Figure 42. Immunolocalization of desmoplakin and plectin in cardiac muscle.** Color code: red plectin, green desmoplakin, yellow intercalated disks. Note well preserved intercalated disks structures in cardiac muscle of mutant mice. Bars, 50  $\mu$ m. (Modified from Walko et al. 2011, Fig. 4F).

## IV. Ex vivo analysis of primary keratinocytes

### Expression of hemidesmosomal proteins in primary keratinocytes

Cultured keratinocytes form HD-like protein complexes (HPCs, Geuijen et al. 2002, Ozawa et al. 2010), whose assembly requires the binding of laminin322 to integrin  $\alpha 4\beta 6$ , and their association with plectin and keratin 5/14 (Koster et al. 2003). To investigate HPC formation in Ogn<sup>a</sup> versus wild-type keratinocytes, primary keratinocytes were isolated from newborn mice, cultured at low density in keratinocyte growth medium (supplemented with 0.3 mM Ca to stimulate HPC formation) and the distribution of plectin and integrin  $\alpha 6$  was examined by confocal immunofluorescence microscopy as described in Walko et al. 2011. In wild-type keratinocytes, plectin and integrin  $\alpha 6$  colocalized and were found at sites of cell-substrate contacts, appearing in discrete bow-like patches (Fig. 43A). This punctuated pattern is no longer identifiable in keratinocytes isolated from *Plec*<sup>Ogn<sup>a</sup>/+</sup> and *Plec*<sup>Ogn<sup>a</sup>/Ogn<sup>a</sup></sup> mice. Plectin appeared diffusely distributed in the cytoplasm of mutant cells and integrin clustering was suppressed (Fig. 43A).

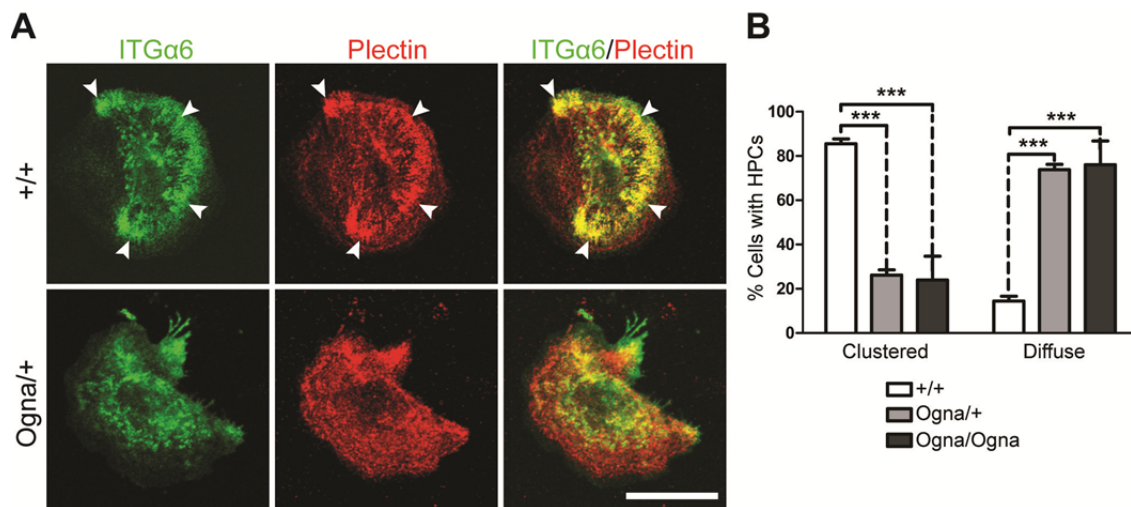


**Figure 43. Immunolocalization of plectin and integrin  $\alpha 6$  in primary keratinocytes and quantification of integrin clustering.** (A) Immunolocalization (double labeling) of ITG $\alpha 6$  and plectin in primary keratinocytes isolated from newborn mice. Primary keratinocytes—were immunolabeled with antibodies to plectin (antiserum #46) and ITG $\alpha 6$  (mAB 5A). In wild-type (+/+) keratinocytes ITG $\alpha 6$  and plectin show codistribution in densely clustered HPCs (arrowheads) contrasting with the more diffuse distribution in Ogn<sup>a</sup> keratinocytes. Bar, 20  $\mu$ m. (B) Column diagram showing the percentage of wild-type (+/+) and mutant keratinocytes that had formed HPCs (clustered), or were lacking them (diffuse). Data are shown as mean values  $\pm$  SD from cell counts (>100/genotype) in randomly chosen optical fields from three independent experiments. \*\*\* $P < 0.001$  (two-way ANOVA with Bonferroni post test). (Modified from Walko et al. 2011, Fig. 5A,B).

This observation prompted us to count the number of cells showing either, a clustered or diffuse integrin-specific staining pattern. Data quantification revealed that the vast major-

ity (>80%) of wild-type keratinocytes had formed integrin  $\alpha 6$ /plectin-positive HPCs, while only a minor population (<20%) showed a diffuse integrin  $\alpha 6$ /plectin distribution. In contrast, in *Plec*<sup>Ogna/+</sup> and *Plec*<sup>Ogna/Ogna</sup> keratinocytes, the situation was reversed (Fig. 43B). No differences were observed with regard to this parameter between hetero- or homozygous mutant keratinocytes. These data can be interpreted as implying that Ogna plectin is able to interact with integrin  $\alpha 6$ , but has lost the capacity to induce proper integrin clustering.

### Keratin network organization

Since plectin, together with BPAG1, mediates the attachment of the keratin filament network to HDs, next I examined whether the keratin network was altered in mutant keratinocytes. For this purpose primary keratinocyte cultures were subjected to immunofluorescence microscopy analysis. However, mutant and wild-type cells revealed no differences in keratin filament organization. In both cases the keratin filament network was densely packed around the cell center with extensions reaching the inner part of the clustered ring-shaped zone. Furthermore, in contrast to plectin-null keratinocytes which exhibited keratin networks of enlarged mesh size and increased bundling (Osmanagic-Myers et al. 2006), the filaments retained their delicate network structure without undergoing bundle formation (Fig. 44).

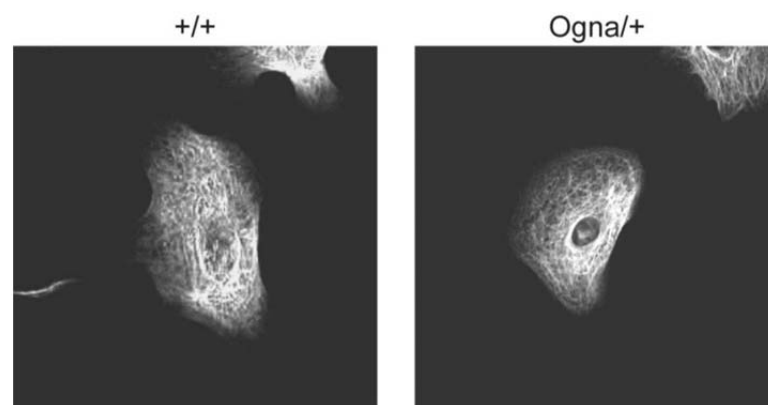


**Figure 44. Keratin network organization in primary keratinocytes.** Primary keratinocytes were immunostained using antibodies to K5. Note the typical cage-like envelope structure of the keratin network surrounding the nucleus, and filament extension from the nucleus towards the cell periphery.

The cells shown in Fig. 43A were not only immunolabeled for integrin  $\alpha 6$  (ITG $\alpha 6$ ) and plectin, but also for keratin K5. Images of triple-immunostained specimens (ITG $\alpha 6$ /Plectin/K5) are shown in Fig. 45. As demonstrated in the figure, the merged image of wild-type keratinocytes is radically different from that of mutant keratinocytes. Most striking is the lack of anchorage of the keratin network, which appears as freely floating in the cytoplasm.

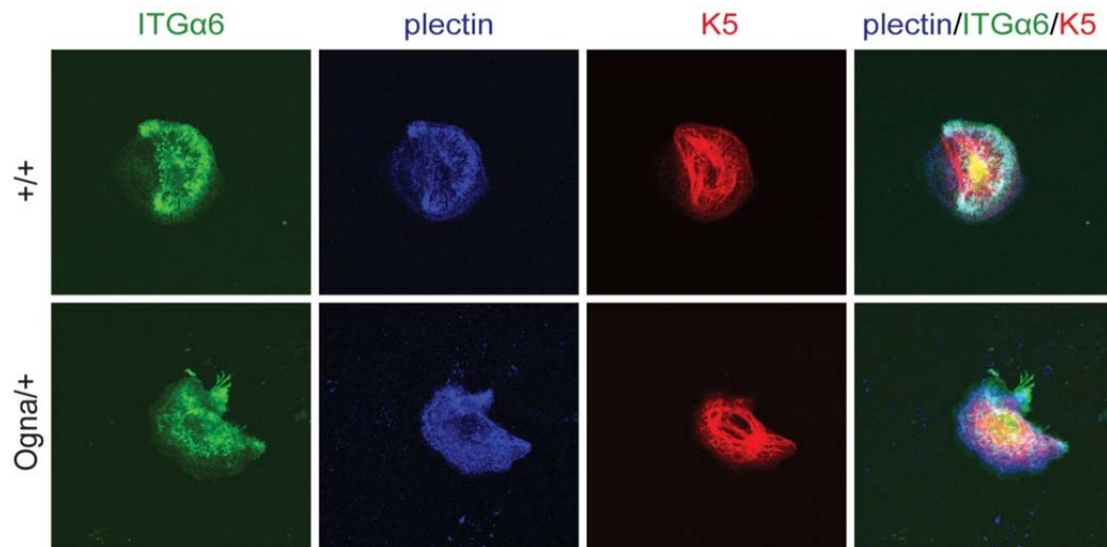


**Figure 45. Colocalization of K5 with ITGa6 and plectin in primary mouse keratinocytes.** Note, the intact keratin network organization in wild-type and mutant keratinocytes, but the lack of ITGa6 and K5 colocalization in *Ogna* keratinocytes. Note, also that the color code of the channels is different to that of Fig. 43.

### Attempted rescue of the abnormal HPC phenotype

To demonstrate that the observed phenotype of reduced HPCs was a direct outcome of the *Ogna* mutation, I planned to perform rescue experiments. However, attempts to rescue the phenotype with full-length plectin failed due to a combination of factors, such as low transfection efficiency of primary keratinocytes, the extremely large size of full-length plectin, and difficulties to incorporate plectin in already assembled HPCs. First, primary *Ogna*<sup>+/−</sup> keratinocytes were transiently transfected with GFP- tagged wild-type full-length P1a (pNV29), the plectin variant that is recruited into HDs (Andrä et al. 2003). This approach failed because of the low transfection efficiency (< 3%). In a second approach, I changed the strategy and sought to transfect immortalized plectin-deficient keratinocytes (*Plec*<sup>−/−</sup>) with expression plasmids encoding either wild-type or *Ogna* (pNV29 and pNV30, see Appendix p126) versions of GFP-tagged full-length P1a, to examine whether both or only wild-type P1a could restore proper HPC formation. In this case, transfection efficiency was very high, but exogenous GFP-plectin did not incorporate into the HPCs. Instead, it was found bound to keratin filaments. I then aimed at improving conditions for the integration of overexpressed plectin into HPCs, by splitting cells shortly after transfection to facilitate disassembly of the HPCs and de novo formation of the complex. This approach again failed because as in the case before, overexpressed plectin bound preferentially to the keratin network, without causing it to collapse. What we observed,



nevertheless, was that P1a alone could rescue the aberrant keratin network cytoarchitecture of plectin-null keratinocytes, which changed from a network with greatly increased mesh sizes and bundled keratin filaments to a dense network of delicate filaments typical for *Plec*<sup>+/+</sup> keratinocytes (Fig. 46).

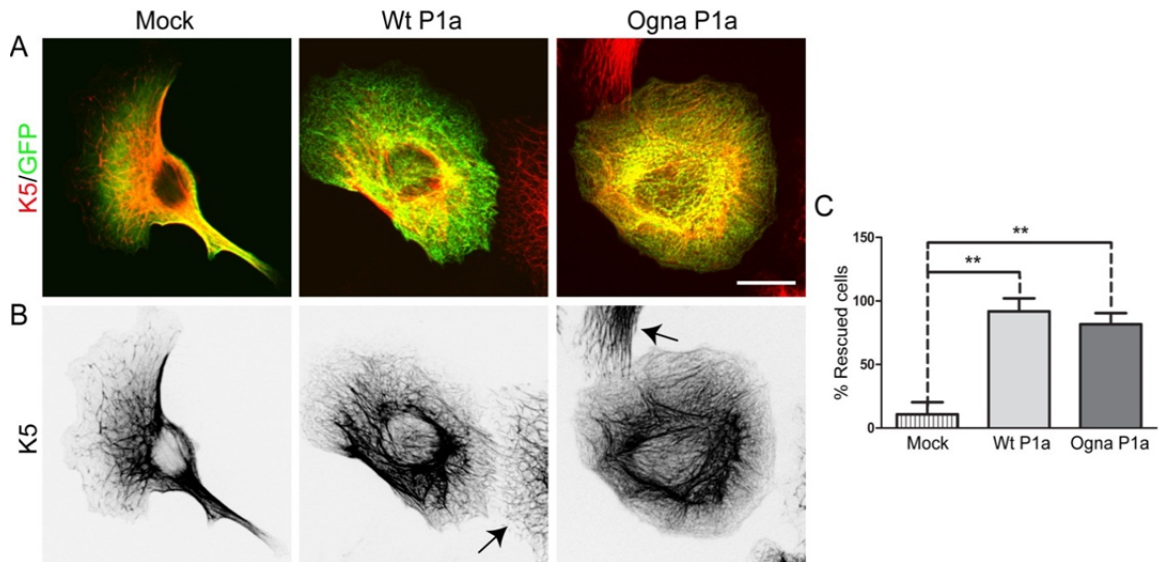


**Figure 46. Wild-type and Ogna plectin P1a restores normal keratin network cytoarchitecture in plectin-null keratinocytes.** (A-B) *Plec*<sup>-/-</sup> keratinocytes transfected with expression plasmids encoding GFP-tagged full-length P1a (either wild-type or Ogna), or GFP (mock), were fixed and immunolabeled for K5 and GFP. K5 immunofluorescence images were contrast-enhanced by conversion to grey scale and inversion of contrast. Note more delicate (filamentous) K5 IF networks upon forced expression of either wild-type or Ogna P1a, compared to untransfected cells (arrows) or cells expressing GFP alone. (C) Column diagram showing the average percentage of rescued cells. Rescue efficiency was determined by analysis of >100 plectin-null keratinocytes transiently expressing wild-type P1a, Ogna-P1a, or GFP (mock). Keratinocytes with average filament-filament distances of below 1.5 nm were considered rescued. Data of three independent experiments are presented as mean  $\pm$  SD. \*\*  $P < 0.01$  (one-way ANOVA with Tukey post test for multiple comparisons). Bar, 20  $\mu$ m. (Modified from Walko et al. 2011, Fig. S5).

### Response to hypo-osmotic shock

Hypo-osmotic shock is a common physiological stress that causes the transient reorganization of the cytoskeleton. Hypo-osmotic shock has been used to assess the severity of keratin mutations (D'Alessandro et al. 2002). Thus, I addressed the question whether this type of stress elicit the same extent of response in wild-type as in mutant keratinocytes. For this purpose, primary keratinocytes isolated from newborn animals were exposed to 150 mM urea. Following 2 min incubation, cells were fixed and monitored by immunofluorescence microscopy to assess integrin clustering and the status of the keratin network. As previously documented (D'Alessandro et al. 2002) changes in cell shape

were detected upon urea treatment, but integrin remained clustered in wild-type keratinocytes (Fig. 47). In contrast *Plec*<sup>+/*Ogna*</sup> keratinocytes were not capable of preserving the partially clustered integrin  $\alpha 6$  observed in untreated cells and the pattern of integrin  $\alpha 6$  staining became rather diffuse (Fig. 47).

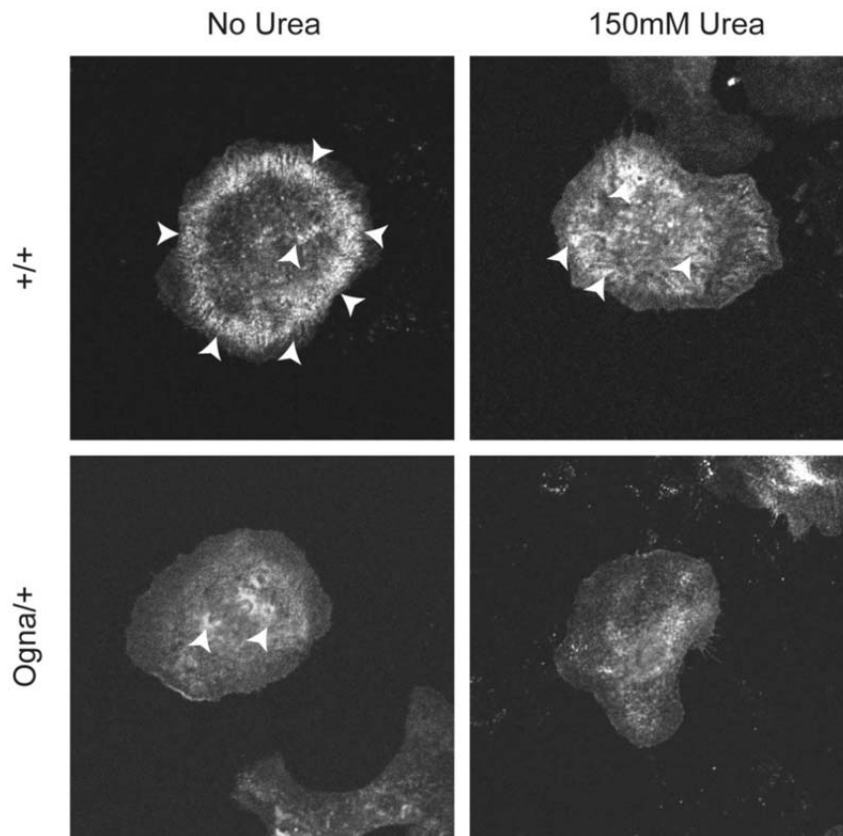


**Figure 47. Effect of hypo-osmotic shock on integrin clustering.** Subconfluent cultures of primary keratinocytes before and after exposure to 150 mM urea were immunostained with antibodies to integrin  $\alpha 6$ . Arrowheads depict integrin clusters. Note the absence of integrin clustering in the case of *Ogna* keratinocytes upon urea treatment.

I then performed a similar experiment, following the changes in the keratin network as read out. In wild-type cells exposed to hypo-osmotic shock (150 mM urea) the keratin network appeared to be more bundled, but still distributed all over the cell, exhibiting numerous fine and short filaments filling the space between the filament bundles and extending further to the cell periphery (Fig. 48A,B). By contrast, keratin filaments of *Plec*<sup>*Ogna*/+</sup> cells appeared to be retracted from the cell periphery with prominent lateral bundling in the central part of the cytoplasm sometimes followed by a complete lateral collapse in form of a massive filamentous bundle (Fig. 48A,B). A quantitative analysis revealed that about 70% of *Plec*<sup>*Ogna*/+</sup> keratinocytes, but only 13% wild-type keratinocytes showed a collapsed keratin network after urea exposure (Fig. 48C) (Walko et al. 2011).

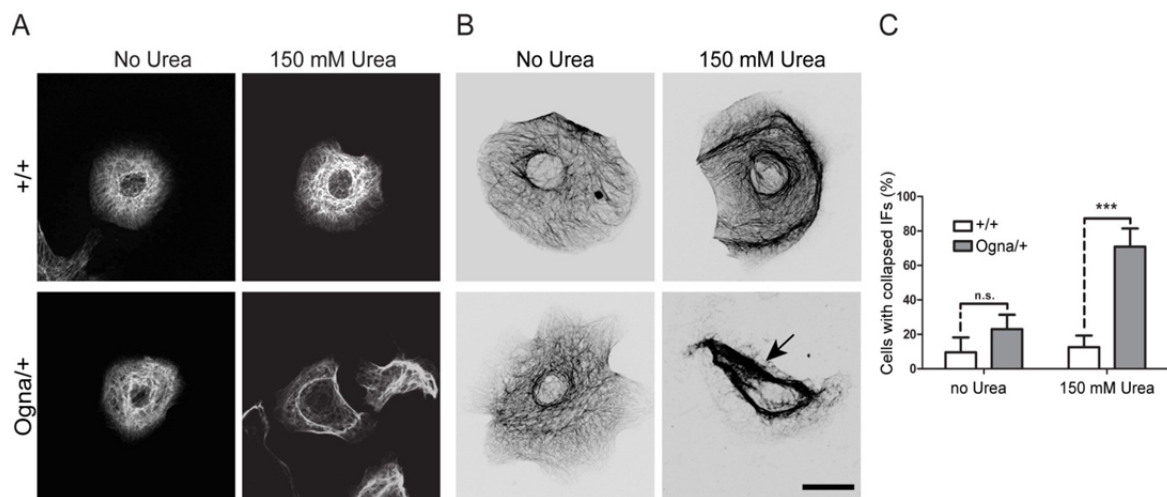


**Figure 48. Effect of hypo-osmotic shock on the keratin network.** (A) Subconfluent primary keratinocyte cultures, before and after 2 minutes exposure to 150 mM urea, immunostained with antibodies to keratin K5. (B) Contrast-enhanced (by conversion to grey scale and inversion of contrast) micrographs of keratin networks. Note collapse of keratin network in Ogna keratinocytes upon urea treatment. (C) Column diagram showing percentage of cells with collapsed K5 networks. Data shown represent mean values  $\pm$  SD from cell counts ( $>120$ /genotype). \*\*\*  $P < 0,001$  (two-way ANOVA with Bonferroni post test). (Modified from Walko et al. 2011, Fig. 5C and S6).

### Migration behavior

Plectin involvement in the attachment of the keratin cytoskeleton to integrin  $\alpha 6 \beta 4$  through HDs is known to stabilize the adhesion of keratinocytes to the extracellular matrix, and in that way inhibit cell migration (Geuijen and Sonnenberg 2002). Since I had thus far observed that Ogna plectin by failing to induce integrin clustering does not quite fulfill this function, I decided to test whether this impairment is also reflected in the migratory behaviour of *Plec*<sup>Ogna/+</sup> keratinocytes. To address this issue the classical scratch wound closure assay was performed on keratinocyte monolayers. Freshly isolated basal keratinocytes were cultivated on collagen I matrix until confluence was reached. The monolayer was then scratched with a sterile yellow tip to create a cell-free strip area, and gently rinsed with PBS to remove floating cells. Photographs of phase contrast microscope fields were taken at the same positions with the help of a line marker after incubation for 16 and 24 h. Results of a typical scratch assay are shown in Fig. 49. These results demonstrated that *Plec*<sup>Ogna/+</sup> keratinocytes migrated into the wound area faster than *Plec*<sup>+/+</sup> cells (Fig. 49A). Counting the cells that repopulated the scratch area confirmed this observation (Fig. 49B).

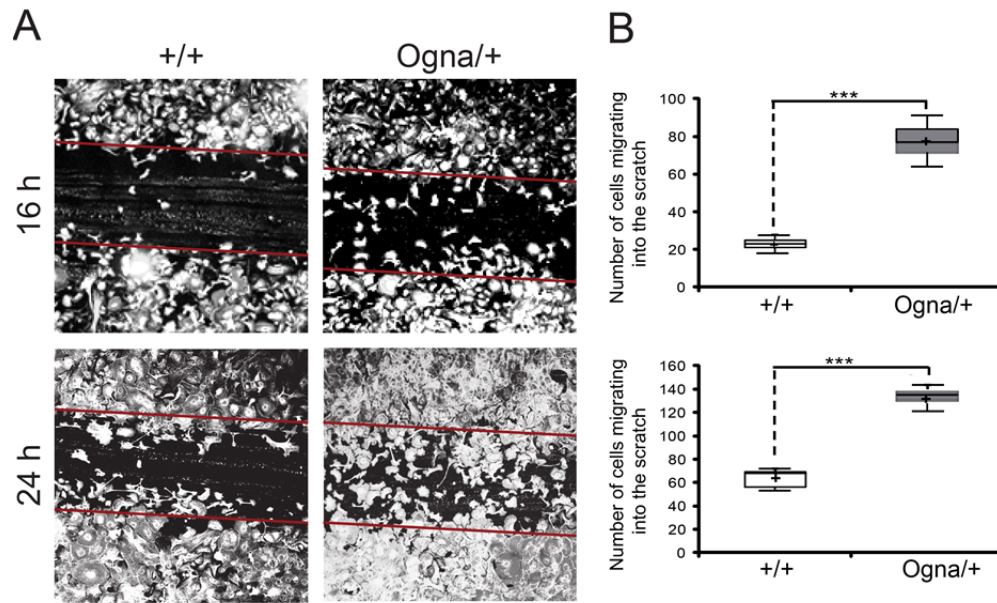


**Figure 49. Migration of primary keratinocytes in response to scratch wounding.** (A) Confluent keratinocyte monolayers were scratch wounded and incubated for additional times. Photographs of representative areas 16 and 24 h after wounding are shown. The lines indicate the position of the initial artificial wound. (B) Quantification of the scratch closure. The number of cells migrating into the scratch were counted at 16 and 24 h post-wounding. Data derived from 3 independent experiments ( $n = 15$ ). Box and whisker plots as in Fig. 28. \*\*\*  $P < 0,001$  (unpaired, two-tailed t-test). (Modified from Walko et al. 2011, Fig. 5D).

In addition, experiments were done to quantify the migration velocity of individual keratinocytes using time-lapse video microscopy combined with computer-assisted cell tracking. In this case, cultures were grown to low density on collagen I matrix. Within 1 h after seeding cells started to spread irrespectively of genotype. Spreading was characterized by flattening of cells, followed by extension of lamellipodia. Migration speed was calculated from the traced distance travelled over 24 h. The computed average speed of the cells was  $0.85 \mu\text{m}/\text{min}$  for wild-type cells and  $1.62 \mu\text{m}/\text{min}$  for *Plec*<sup>Ogna/+</sup> keratinocytes (Fig. 50A). Thus Ogna keratinocytes migrated 2 times faster than wild-type cells. These results are in agreement with the increased migration observed in the scratch assays.

In a complementary approach, immortalized wild-type (*Plec*<sup>+/+</sup>) and plectin deficient (*Plec*<sup>-/-</sup>) keratinocytes were transiently transfected with expression plasmids encoding GFP fusions of full-length plectin P1a with or without the Ogna mutation (pNV29 and pNV30, respectively). Twenty four h after transfection the cells were replated and their migration patterns monitored for additional 24 h by time-lapse video microscopy. Consistent with the previous observations, *Plec*<sup>+/+</sup> keratinocytes transfected with P1a-Ogna

migrated two times faster (0.88  $\mu\text{m}/\text{min}$ ) than the ones transfected with wild-type plectin P1a that showed an average migration speed of 0.47  $\mu\text{m}/\text{min}$  (Fig. 50B). This speed is very similar to that of mock-transfected control cells (0.48  $\mu\text{m}/\text{min}$ ) (Fig. 50B) (Walko et al. 2011). Thus, overexpression of wild-type P1a did not further delay migration of *Plec*<sup>+/+</sup> keratinocytes, but overexpression of Ogn P1a significantly increased their migration.

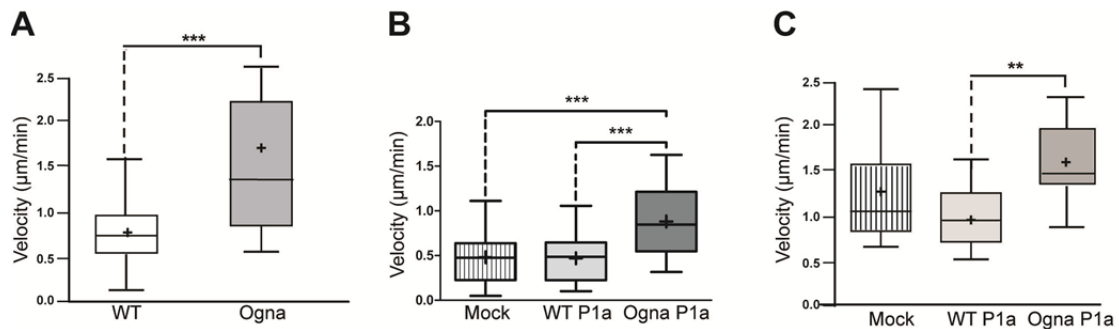


**Figure 50. Migration velocities of mouse keratinocytes expressing wild-type or Ogn P1a.** (A) Primary keratinocytes isolated from wild-type or Ogn knock-in mice. (B) and (C) Immortalized *Plec*<sup>+/+</sup> keratinocytes (B) or *Plec*<sup>-/-</sup> keratinocytes (C), transfected with full-length wild-type (WT) P1a, Ogn P1a, or empty vector (mock). Note, *Plec*<sup>-/-</sup> keratinocytes migrated faster than *Plec*<sup>+/+</sup> keratinocytes, and expression of Ogn P1a led to a significant increase in the migration velocity of *Plec*<sup>+/+</sup> keratinocytes and a further small, but statistically significant, increase in *Plec*<sup>-/-</sup> keratinocytes. Box and whisker plots as in Fig. 28. \*\*\*  $P < 0,001$ ; \*\*  $P < 0,01$  (one-way ANOVA with Tukey post test for multiple comparisons). (Modified from Walko et al. 2011, Fig. 5E).

Plectin-deficient keratinocytes (*Plec*<sup>-/-</sup>) moving at a speed of 1.03  $\mu\text{m}/\text{min}$ , migrate two times faster than their wild-type counterparts (Fig. 50B,C); an outcome that was expected based on previous experiments (Osmanagic-Myers et al. 2006). However, their migration was reduced to 0.87  $\mu\text{m}/\text{min}$  by the expression of wild-type P1a (Fig. 50C). Yet, the most interesting result, was that expression of Ogn P1a could not reverse the phenotype of plectin-deficient keratinocytes, rather, the migration velocity was further increased to 1,27  $\mu\text{m}/\text{min}$  (Fig. 50C). Collectively these results showed that expression of Ogn P1a, leads to an increase in cell migration, probably reflecting a defective and loosely assembled HD.

## V. The plectin rod: structure and interactions

In the final part of my thesis I studied the impact of the Ogn mutation on the stability, dimerization and oligomerization of the rod domain of plectin. Due to its central position within the plectin molecule (see Fig. 7), its length (~ 190 nm), secondary structure (long stretches of heptad repeat regions predicted to form a coiled coil), and ability to form dimers or even oligomers, the plectin rod domain is supposed to confer structural stability to the molecule. As a dominant negative mutation, the Ogn may compromise the stability of the rod, and thus its ability to interact with itself and/or other proteins. To study how the rod of plectin interacts with itself and other proteins by a biochemical approach, several versions of the plectin rod domain were expressed in baculovirus. This expression system was selected because of the large size of the recombinant proteins to be expressed (130-190 kDa) and concerns about their solubility if produced in bacteria. An additional advantage of this system is that proteins are expressed in insect cell lines which allow folding and post-translational modification of proteins in a manner similar to that of mammalian cells.

Recombinant baculovirus encoding tagged fusion proteins of plectin's rod domain, were already available both as wild-type and Ogn mutant versions. For this purpose each plectin cDNA fragment had been subcloned into pFASTBAC HT vector (Invitrogen) or into a modified derivative in which the HIS tag was replaced by the GST tag (excised from pGEX-2T, Pharmacia Biotech), and introduced into the baculovirus genome by *in vitro* recombination (M. Castañón, personal communication). The resulting recombinant bacmids (baculovirus shuttle vectors) were transfected into Sf9 cells and the virus-containing supernatants used to generate a viral stock that after titration was routinely used to infect insect cells for protein production. Fig. 51 shows a scheme of the expressed plectin domains. Also shown are the names of the constructs used to generate the recombinant baculoviruses and resulting viral stocks, the names assigned to the expressed proteins, and the molecular masses of the proteins.



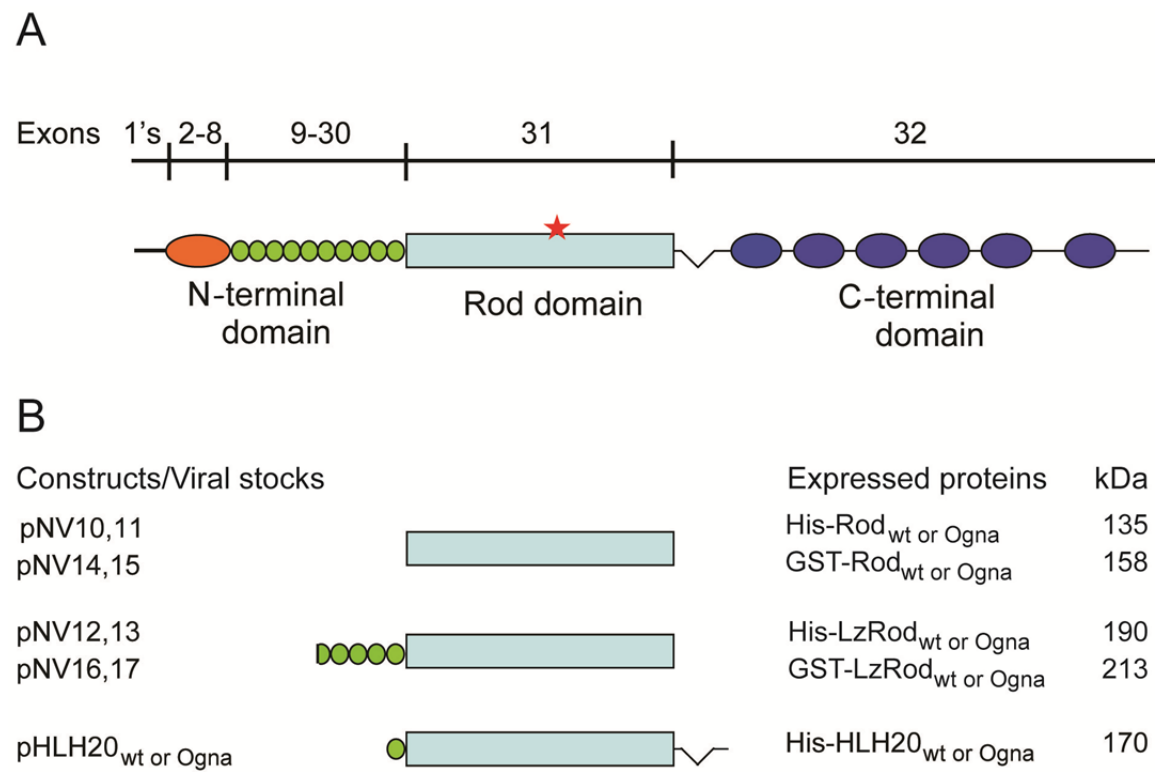


**Figure 51. Schematic presentation of plectin rod variants expressed in insect cells. (A)** Main structural features of the plectin molecule and its corresponding coding exons. 1's stands for 11 first exons alternatively spliced into exon 2. The N-terminal domain is subdivided into an actin binding domain (orange), and a plakin domain formed by 9 spectrin repeats (green), the central  $\alpha$ -helical rod domain (light blue) is a coiled-coil structure that spans ~190 nm, and the C-terminal domain comprises 6 plectin repeats (dark blue). Red star, position of the Ogn<sub>a</sub> mutation. **(B)** Expressed plectin domains. Constructs used to produce the recombinant baculoviruses (left), encoded domains (center), and names assigned to the expressed proteins (right). pNV10 and pNV11, recombinant His-tagged wild-type and Ogn<sub>a</sub> versions of plectin's rod domain (135 kDa); pNV14 and pNV15, corresponding GST-tagged versions (158 kDa); pNV12 and pNV13, recombinant His-tagged wild-type and Ogn<sub>a</sub> plectin rod domain preceded by 5 spectrin repeats (190 kDa); pNV16 and pNV17, corresponding GST-tagged versions (213 kDa); pHLH20/wt and pHLH20/Ogn<sub>a</sub>, recombinant His-tagged wild-type and Ogn<sub>a</sub> versions of the rod domain flanked by the 9th spectrin repeat and the linker region between plectin's rod and the C-terminal region (170 kDa).(Modified from Walko et al. 2011, Fig.6A).

The rod domain, corresponding to a polypeptide of 1127 amino acid residues, is encoded by a single exon (exon 31). For this work, four variants of it were expressed as His- or GST-tagged proteins as wild-type or mutant versions. One was the rod alone, a second one was the rod preceded by the last four and a half spectrin repeats of the nine spectrin repeats that make up the plakin domain of plectin (Sonnenberg et al. 2007; Ortega et al. 2011). The N terminus of this polypeptide starts with four leucines spaced every seven amino acid residues (LEAQHQALVTLWHQLHVDKMSLLAWQSL), thus containing a putative leucine zipper motif. Sequences of this kind have been suggested to help align  $\alpha$ -helical rod domains of molecules and promoting coiled-coil formation (Kammerer et al.

1998, Chiravuri et al. 2000). In a third variant, the rod was flanked by the last spectrin repeat and the linker region preceding the C-terminal domain. A fourth (minimal) version of the rod comprising a fragment surrounding the Ogn mutation will be discussed later (see p72).

### Expression and purification of the rod domain

To optimize the yield of recombinant proteins the following expression parameters were tested: cell density, infection rate, and harvesting time. For that purpose Sf9 cells were infected with different amounts of viral stock, and harvested sequentially at different post-infection times. In small scale tests (6-well plates), infection of  $1 \times 10^6$  Sf9 cells with 30  $\mu$ l of viral stock to be harvested 72 h post-infection, was found to be optimal (results not shown). An additional test was carried out to extrapolate these conditions to higher cell concentrations. In this case T175 cell culture flasks were seeded with  $2 \times 10^7$  or  $4 \times 10^7$  Sf9 cells and infected with 1 ml, or 0.5 ml of viral stock ( $\sim 1.2 \times 10^8$  pfu/ml), resulting in an estimated multiplicity of infection (MOI) of 6, 1.5 and 3, respectively (Fig. 52A). Although no larger differences in protein yields were observed, a MOI of 3 was considered as optimal. Immunoblotting using mAbs 10F6 confirmed the identity of the recombinant protein as plectin (Fig. 52B).

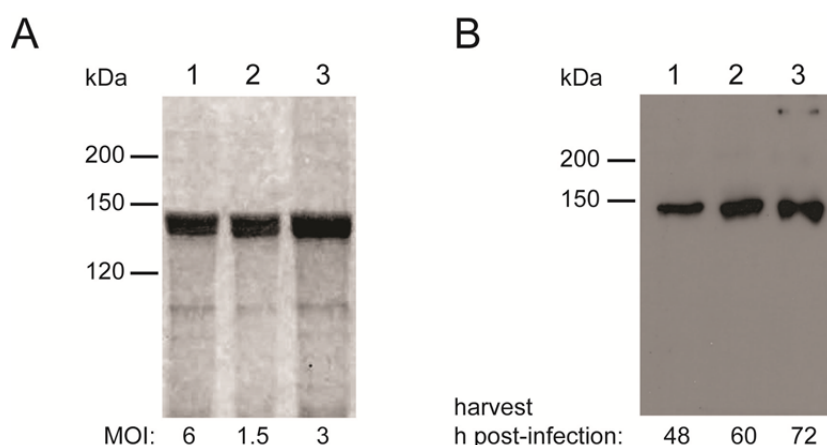


**Figure 52. Optimization of recombinant His-tagged protein expression.** (A) Infection rate. T175 flasks were seeded with  $2 \times 10^7$  (lane 1),  $4 \times 10^7$  (lane 2), and  $4 \times 10^7$  (lane 3) Sf9 cells and infected with 1ml, 0.5ml, or 1ml, respectively, of recombinant pNV10 viral stock (MOI 6, 1.5 and 3, respectively). Three days post-infection, cells were lysed in sample buffer and analyzed by SDS-6% PAGE. (B) Time course.  $1 \times 10^6$  Sf9 cells in one well of a 6-well plate infected with 30  $\mu$ l of viral stock (MOI 3), were harvested at 48, 60, and 72 h post-infection, lysed and the proteins resolved by SDS-6% PAGE. The gel was transblotted to a nitrocellulose membrane and incubated with mouse anti-plectin (1:2) mAbs 10F6, followed by HRP-conjugated goat anti-mouse secondary antibodies (1:10000). Molecular mass standards (in kDa) are indicated on the left.

For protein production, recombinant baculovirus encoding the rod variants described above (Fig. 51) were used to infect Sf9 cells in stationary cultures. Routinely, T175 cell culture flasks were seeded with  $4 \times 10^7$  cells, infected with 1 ml of viral stock, and harvested 72 h post-infection. Harvested cells were lysed and proteins in the soluble lysates were purified via their HIS or GST tags using either spin columns or FPLC (for details see Materials and Methods). Representative examples of the His-tagged rod domain (His-Rod<sub>wt</sub> and His-Rod<sub>Ogna</sub>) purified in such ways are shown in Fig. 53. In both cases proteins were purified to a satisfactory level, migrating as a major band of the expected size on SDS-polyacrylamide gels. Similar results were obtained for the GST-tagged rod (GST-Rod<sub>wt</sub> and GST-Rod<sub>Ogna</sub>) purified over glutathione (GSH) Sepharose (results not shown).

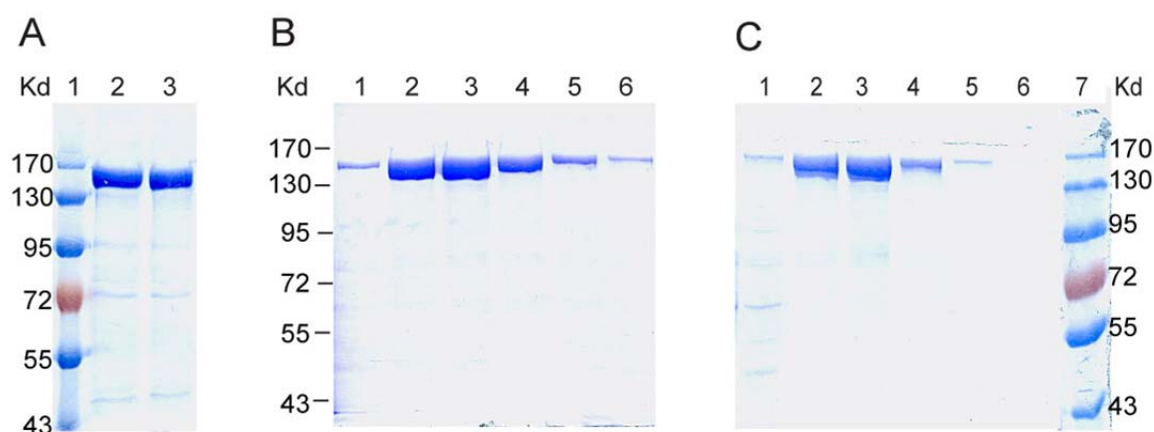


**Figure 53. SDS-PAGE of fractions obtained during the purification of HIS-tagged rod fusion proteins.** Cell lysates derived from Sf9 cells infected with viral stocks of either pNV10 or pNV11 (encoding His-Rod<sub>wt</sub> or His-Rod<sub>Ogna</sub> respectively) were subjected to affinity chromatography using spin columns or FPLC. Aliquots of eluted fractions (10  $\mu$ l) were analyzed by SDS-8% PAGE. **(A)** 1-step spin column purification. Lanes 1, size markers; 2, His-Rod<sub>wt</sub>; and 3, His-Rod<sub>Ogna</sub>. Total volume of each eluted fraction: 150  $\mu$ l. **(B)** FPLC purification of His-Rod<sub>wt</sub>. Lanes 1-6, eluted fractions A6-A11, respectively; volume of each eluted fraction: 750  $\mu$ l. **(C)** FPLC purification of His-Rod<sub>Ogna</sub>. Lanes 1-6, as in (B). Lane 7, size markers.

### Oligomeric state of the plectin rod

The long alpha-helical rod domain of plectin has the potential as all proteins of this type to form coiled-coils. Foisner et al. (1987) has shown that plectins molecule self-associate into various oligomeric states. To determine the oligomeric state of the recombinant rod domain of plectin three different experimental approaches were taken, chemical cross-linking, blue native gel electrophoresis (BN-PAGE), and gel filtration. HIS-tagged plectin rod domains expressed from constructs pNV10 and pNV11 were used for these set of experiments because of the small-sized tag that is unlikely to interfere with protein folding.

Chemical cross-linking was carried out using dimethyl suberimidate (DMS), a homo-bifunctional bis-imidoester, which reacts with primary amines. Because the cross-linker forms covalent bonds among protein subunits, the oligomeric forms can be analyzed by SDS-PAGE. As shown in Fig. 54A, prior to cross-linking, purified rod proteins run as a major band of ~140 kDa; while after cross-linking, a predominant cross-linked product migrating above the position of full-length plectin (~500 kDa), appeared. Additional bands of even higher molecular mass were generated but could not be resolved because they did not enter the running gel, remaining in the stacking gel (Fig. 54B). Note as well that a fraction of the proteins could not be cross-linked and was detected as a monomer. No assembly intermediates were detected when low concentrations of DMS were used for cross-linking (data not shown) (Walko et al. 2011). In conclusion, the major cross-linked product had an apparent molecular mass well above the estimated mass of a dimer (~ 280 kDa), suggesting that it corresponded to a tetramer (predicted size of the tetramer ~ 560 kDa).

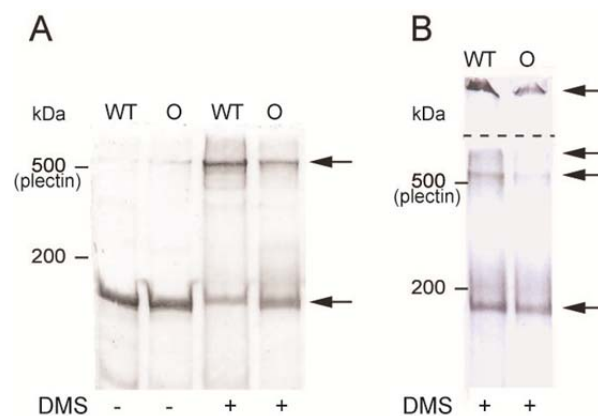


**Figure 54. Chemical cross-linking of the plectin's rod domain. (A)** SDS-5% PAGE of purified His-Rod<sub>wt</sub> (WT) and His-Rod<sub>O<sub>gna</sub></sub> (O) before and after cross-linking with DMS. **(B)** Same as A but including the stacking gel (4% polyacrylamide). The position of the molecular weight standards is indicated. Arrows point to the monomer and the cross-linked species. The border between the stacking and separating gels is marked by a dash line. Note that a fraction of the protein could not be cross-linked, the major cross-linked species migrated in the range of full-length plectin, and a prominent fraction of cross-linked large proteins did just enter the stacking gel. (Modified from Walko et al. 2011, Fig. 6C).

BN-PAGE can be used to determine the molecular mass of proteins in their native oligomeric state. The method, relying on binding of the negatively charged dye Coomassie blue G250 to the surface of proteins without dissociating them, enables the proteins to migrate towards the anode. Under these conditions the electrophoretic mobility of proteins is proportional to their molecular size, allowing a reasonable accurate molecular mass determination, although tertiary structure (shape) also plays a role. In BN-PAGE

plectin His-Rod<sub>wt</sub> and His-Rod<sub>Ogna</sub> migrated as a single major molecular species with an apparent molecular mass of ~ 500-600 kDa, as estimated from its position between the 880- and 440 kDa ferritin bands (Fig. 55 A,B) using two different BN-PAGE systems, the Bistris-tricine gel system (Schägger et al. 1994), and the Tris-histidine gel system (Niepmann and Zheng, 2006). This was consistent with plectin rod domain forming tetramers in solution (Walko et al. 2011). To get a more accurate estimate, thyroglobulin was included in the BN-PAGE analysis. In this case, the rod domain of plectin was running slightly above the 670 kDa thyroglobulin band (Fig. 55C). Faint bands of a molecular mass higher than 880 kDa could also be seen in the gels, which probably corresponded to higher oligomers. Protein bands with apparent molecular masses corresponding to monomers and dimers were never detected, despite the application of different electrophoretic conditions (Walko et al. 2011). The versions of the rod domain preceded by spectrin repeats expressed from pNV12, pNV13 and pHLH20 migrated as a single major band of > 880 kDa (results not shown).

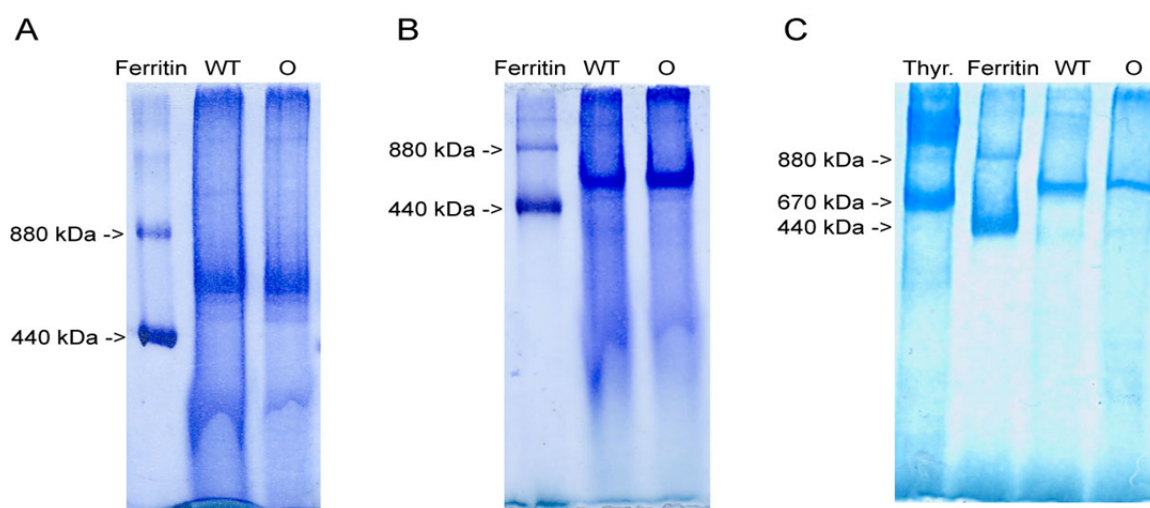


**Figure 55. BN-PAGE analysis of the oligomeric state of the plectin rod.** Purified HIS-tagged aliquots of His-Rod<sub>wt</sub> and His-Rod<sub>Ogna</sub>, were separated in 4-10% polyacrylamide gradient gels by BN-PAGE. **(A)** Bistris-tricine gel system. **(B, C)** Tris-histidine gel system. Ferritin (880 and 440 kDa) and thyroglobulin (670 kDa) were used as molecular mass markers. Note, the position of the major plectin band between the two major bands of ferritin and close to the band of thyroglobulin. (Modified from Walko et al. 2011, Fig. 6B).

Gel filtration chromatography is widely used to determine the quaternary structure of proteins. The method relies on the assumption that proteins elute from an inert matrix in a time inversely proportional to their size. Thus, separation takes place on the basis of size, although both molecular weight and three-dimensional shape contribute to the

degree of retention. Following FPLC purification, the recombinant proteins were applied to a Superose 6 column which was previously calibrated under the same chromatographic conditions using a high molecular mass calibration kit. The elution profile of His-Rod<sub>wt</sub> determined by immunoblotting of protein-containing fractions (shadowed in grey) is shown in Fig. 56. The rod domain eluted as a broad peak ahead of, and partially overlapping, with the thyroglobulin (670 kDa) peak. The broadness of the peak points towards the heterogeneity of the sample, and thus the presence of oligomers of various sizes.

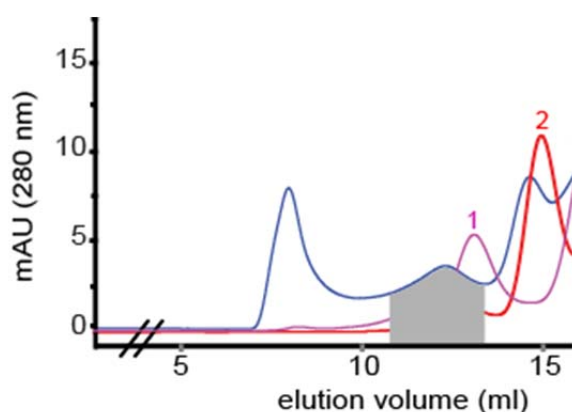


**Figure 56. Elution profile of plectin's rod domain on a Superose-6 column.** The elution profiles of His-Rod<sub>wt</sub> (grey area) and of the molecular mass standards (1, thyroglobulin, 670 kDa; 2, ferritin, 440 kDa) are shown. All eluted fractions were analyzed by immunoblotting using anti-plectin mAbs 10F6 to identify and validate the presence of plectin in the eluates. The grey area indicated fractions containing plectin; no plectin was detected in fractions eluted later (not shown).

Although the molecular mass of plectin's rod domain could not be estimated unequivocally and considering that the plectin rod is not a globular protein, but rather highly asymmetric, the data gathered by the three methods suggested that the native state of the plectin rod domain is a tetramer, which still can self associate into octamers and higher-order oligomers.

To solve the question of the oligomeric state of the native protein more exactly, colleagues in our group used size exclusion chromatography coupled to multiangle laser scattering (SEC-MALS). This method can directly determine the absolute molecular mass of a protein, and is independent of the elution volume and of the shape of the protein. Using this technology they established that plectin rod domain is actually a dimer, with a calculated and experimentally determined molecular mass of 270 kDa (Walko et al. 2011). The aberrant migration behavior of the rod dimer upon electrophoresis on SDS-PA-gels, BN-PG-gels, and gel filtrations columns, making us believe that it was a tetramer, is not uncommon for extended proteins composed almost entirely of  $\alpha$ -helical structure (Kaufmann et al. 1984; Yang et al. 2004). Whether the native state of the rod is a dimer or a tetramer is irrelevant for its capacity to oligomerize (Walko et al. 2011).



### Differential stability of the RD oligomers

As the O<sub>gna</sub> mutation causes a local disruption of the coiled-coil (see Discussion p82) this may result in a decreased stability of the oligomers formed by the mutant rod. Thus, to compare their stability, oligomers of wild-type and mutant rod domains formed in solution were exposed to increasing temperature and urea concentrations prior to chemical cross-linking with DMS (Walko et al. 2011). The samples were then resolved by SDS-PAGE and the dry Coomassie Blue-stained gels analyzed by densitometric scanning using the program Quantiscan (Biosoft, Cambridge, UK). This analysis revealed that even without denaturing treatment, the fraction of the rod domain found in oligomeric form was higher for wild-type (~75%) than for O<sub>gna</sub> (~40%) (Fig. 57 A,B). This trend persisted as oligomers dissociated into monomers with either increasing temperature (Fig. 57A) or urea concentrations (Fig. 57B) (Walko et al. 2011). Midpoints calculated on the basis of their apparent linear dissociation kinetics were 44°C and 4.45 M urea for His-Rod<sub>wt</sub>, compared to 41°C and 4.21 M urea for His-Rod<sub>O<sub>gna</sub></sub> (Walko et al. 2011). This small difference in biochemical parameters, in this case midpoints of dissociation kinetics, is

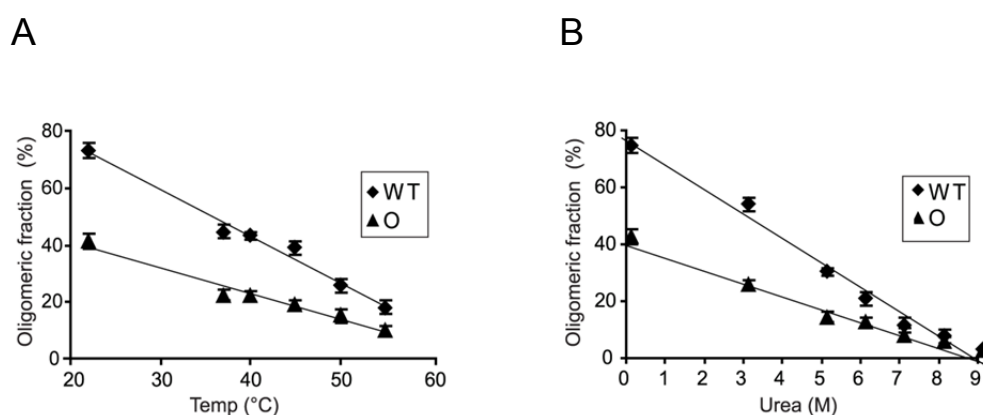


**Figure 57. Dissociation of plectin rod domain oligomers as a function of temperature and urea concentration.** Samples of His-Rod<sub>wt</sub> (WT) and His-Rod<sub>O<sub>gna</sub></sub> (O) were preincubated at increasing temperatures or concentrations of urea, cross-linked with DMS, and resolved by SDS-PAGE. The relative percentages of oligomers in each sample, determined by densitometric analysis of the gel lanes, were plotted as a function of temperature (A) or added urea (B). Data represent the mean  $\pm$ SD of three independent experiments performed in duplicates. The solid line denotes the lineal regression fit of the data ( $r^2$  0.9689). (Modified from Walko et al. Fig. 6E,F).

not uncommon for mutants in long coiled coils where only 1 amino acid is substituted by another one, often resulting in a disease phenotype (Armel and Leiwand 2009). The above results suggested that the O<sub>gna</sub> mutation impairs the efficiency of chemical cross linking and slightly decreases the global stability of the rod dimer. Furthermore, the

difference in crosslinking efficiencies between wild-type and Ogn<sub>a</sub> rod domains most likely reflected local unfolding of the coiled coil structure. In fact wild-type and Ogn<sub>a</sub> rod domains show similar migration behavior in BN-PAGE, arguing against a gross effect of the mutation on the global structure of the rod domain.

### Binding affinity

After having shown that the stability of rod domain oligomers differs depending on the mutation status, we tried to set up a method for measuring the binding affinity of plectin Rod<sub>wt</sub> and Rod<sub>Ogn<sub>a</sub></sub> for themselves and for each other. The method of choice was developed by Konrat and coworkers (Ludwiczek et al., 2004) and required that one binding partner is tagged with a ligand binding domain, and that the binding of the other partner causes a detectable increase in the molecular weight of the complex. Then, the protein-protein interaction is monitored via changes in the NMR relaxation of a reporter ligand.

To perform the assay, a small fragment of the plectin rod domain was fused to the SH2 domain of PLC $\gamma$ 1 (phospholipase C, generous gift from R. Konrat, MFPL, Vienna). This section of the rod domain, thereafter referred to as minirod, consisted of a stretch of 134 amino acid residues forming a continuous alpha helical domain containing the region of the Ogn<sub>a</sub> mutation (Fig. 58). The SH2-minirod fusion protein was successfully expressed and purified. However, neither the minirod nor the full-length rod could be prepared in monomeric form, except under denaturing conditions, as they readily oligomerized as soon they were synthesized. Furthermore, no interaction of the minirod with the full-length rod could be demonstrated by pull-down assays under conditions where the full-length rod/minirod heterodimer would have been formed in vivo (J. Breitenbach, Diploma Thesis, 2007). This result was interpreted in terms that the minirod cannot compete with the full-length rod to form a short hybrid coiled-coil (see below, hetero-oligomer formation). Unfortunately, this experimental approach had to be discontinued.

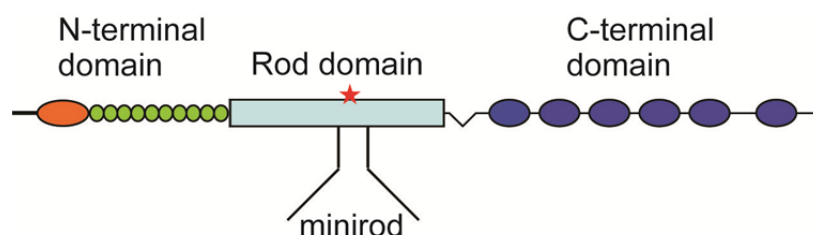


**Figure 58. Schematic representation of minirod.** Main structural features of the plectin molecule as in Fig. 51. The position of the rod domain segment corresponding to the minirod (amino acid residues 601-732) relative to the full-length 1127 residues long rod domain is indicated.

### Hetero-oligomer formation

Having shown that the wild-type plectin rod domain and the O<sub>gna</sub> mutant self-associate forming homo-oligomeric structures, as a next step I set out to determine whether the two rod species could associate with each other, forming hetero-oligomers. For this, we took an *in vivo* as well as an *in vitro* approach. In both cases wild-type and mutant rod domains fused to different tags were used.

For the *in vivo* approach, Sf9 cells were coinfecting with baculovirus expressing HIS-tagged wild-type and GST-tagged O<sub>gna</sub> rod domains (GST-Rod<sub>wt</sub> and His-Rod<sub>O<sub>gna</sub></sub>) or vice versa. By pulling down the oligomeric products via the GST tag and detection of the pull-down partner with antibodies to the His tag, hetero-oligomer formation could be assessed (Fig. 59A). As shown in Fig. 59B both proteins were expressed and could be detected in the total cell lysate prior to the pull-down (I, input). After the pull-down, an enrichment of the GST-Rod<sub>O<sub>gna</sub></sub> species together with a smaller amount of the His-Rod<sub>wt</sub> protein was observed (E, eluate). Immunoblotting with antibodies to the His tag was used to validate the presence of His-Rod<sub>wt</sub> in the eluate.

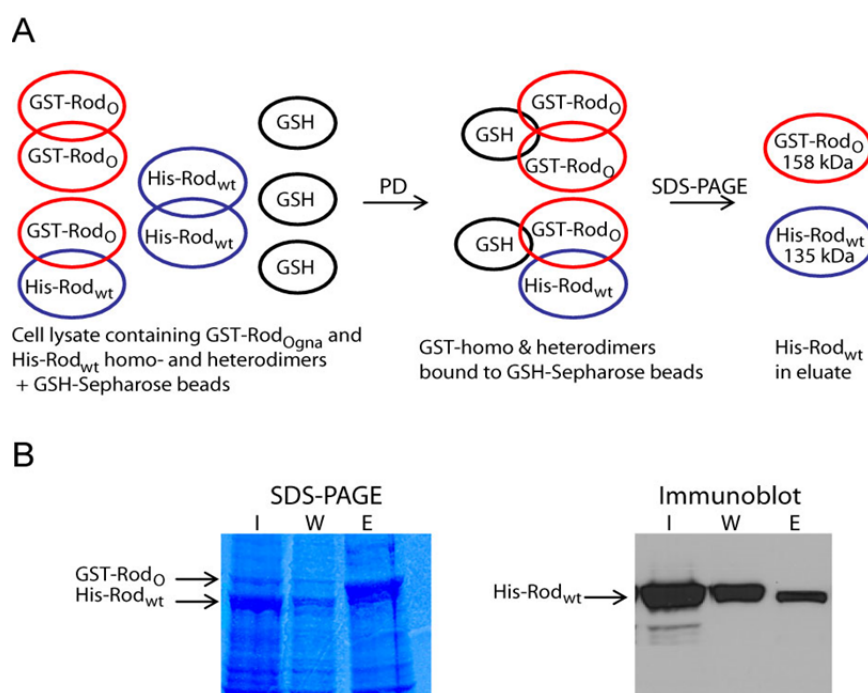


**Figure 59. Formation and detection of plectin rod hetero-oligomers.** (A) Experimental strategy for the isolation and identification of hetero-oligomeric complexes by coexpression of differently tagged wild-type and O<sub>gna</sub> RDs. (B) GST-pull-down. Total cell lysates of Sf9 cells coexpressing HIS-Rod<sub>wt</sub> and GST-Rod<sub>O<sub>gna</sub></sub> were incubated with glutathione sepharose beads. After extensive washing the Sepharose-bound GST-Rod<sub>O<sub>gna</sub></sub> and its associated proteins were eluted with 5x-SDS sample buffer. Eluates were resolved by SDS-PAGE and analyzed by immunoblotting using anti HIS-tag antibodies. I, input; W, wash fractions; E, pull-down eluate. Note, that unbound HIS-Rod<sub>wt</sub> homo-oligomers are removed during the washes, while GST-Rod<sub>O<sub>gna</sub></sub>-bound HIS-Rod<sub>wt</sub> was detected in the eluate. (Modified from Walko et al. 2011, Fig. S7A,B).

For the *in vitro* approach, purified GST-Rod<sub>Ogna</sub> and His-Rod<sub>wt</sub> were first combined in 9 M urea in a 1:1 molar ratio to allow monomer formation. The urea was dialyzed away in several steps to allow oligomerization. Subsequently, hetero-oligomerization was analyzed by pull-down assays as described above. As shown in Fig. 60 both proteins were present in the dialyzed material (I, input) and after selectively eluting the homo- and heterodimerization complexes (E, eluate). Since in this case the pull-down was performed via the His-Rod<sub>wt</sub>, immunodetection of the Ogna partner (GST-Rod<sub>Ogna</sub>) was done using anti-GST antibodies. The results again demonstrated that wild-type and Ogna rod domains can form hetero-oligomers (Fig. 60).

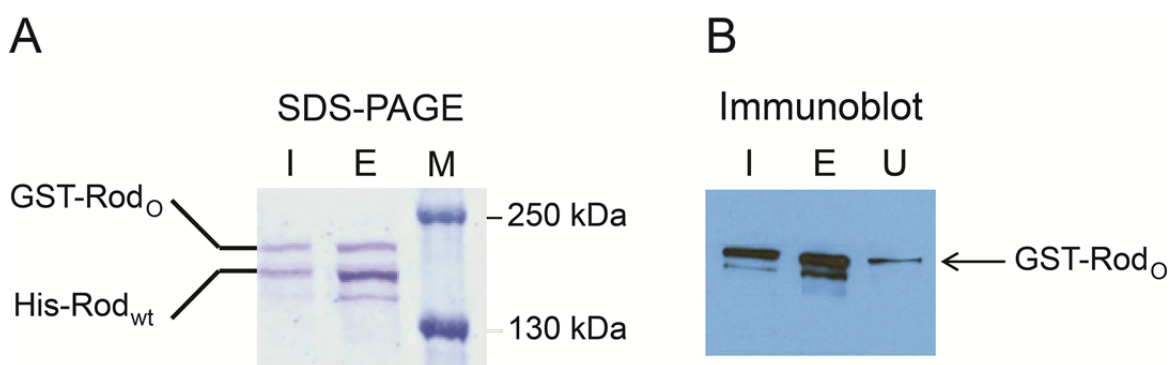


**Figure 60. Pull-down analysis of oligomer complexes formed *in vitro* upon mixing wild-type and Ogna rod domains.** Purified HIS-Rod<sub>wt</sub> and GST-Rod<sub>Ogna</sub> in 9M urea/20 mM Hepes, pH 7.4, were mixed in a 1:1 ratio and incubated overnight at 4°C. Subsequently the urea was removed by sequential dialysis against 5M, 3M, 1M, 0M urea/20 mM Hepes, pH 7.4. For the pull-down, cobalt-charged His-Bind resin was used. After binding and extensive washing, the complexes were eluted with 5x-SDS sample buffer. Eluates were resolved by SDS-PAGE and analyzed by immunoblotting using anti GST-tag antibodies. **(A)** Coomassie blue staining. **(B)** Immunoblot of a gel similar to that shown in A. I, input; E, pull-down eluate; U, unbound material representing GST-Rod<sub>Ogna</sub> homodimers; M, molecular mass markers. Note, that unbound GST-rod<sub>Ogna</sub> homo-oligomers are removed during the washes, while GST-Rod<sub>Ogna</sub>-bound HIS-Rod<sub>wt</sub> was detected in the eluate.

These data clearly indicated that hetero-oligomer formation was indeed possible. However the rate of hetero-oligomer formation *in vivo*, and thus its biological significance, remained obscure. Attempts to quantify the ratio of homo- to hetero-oligomers in the co-expression assay failed because the aberrant migration of the dimers (see Figs. 54, 55) precluded the separation by size of otherwise discernible species (theoretical size of His- and GST-homodimers: 270 and 316 kDa, respectively; His-GST-heterodimer: 293 kDa). Furthermore, His-Rod<sub>wt</sub> as well as His-Rod<sub>Ogna</sub>, were expressed at higher levels in Sf9 cells than the GST-tagged counterparts. However, when the much smaller minirod constructs were expressed in Sf9 cells and hetero-oligomerization was quantified, homo-oligomerization could be shown to be favored over hetero-oligomerization (Fig. 61).

coexpression:

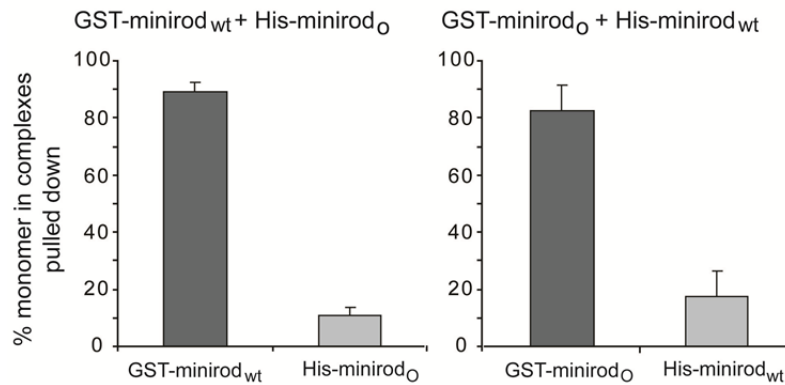


**Figure 61. Quantification of pulled-down oligomeric complexes formed upon coexpression of wild-type and OgnA miniroads.** Total cell lysates of Sf9 cells co-expressing GST-miniroad<sub>wt</sub> and HIS-miniroad<sub>OgnA</sub>, or GST-miniroad<sub>OgnA</sub> and HIS-miniroad<sub>wt</sub>, were incubated with glutathione-Sepharose beads. After extensive

washing, the Sepharose-bound GST-miniroad<sub>wt</sub> (left) or GST-miniroad<sub>OgnA</sub> (right) complexes were eluted with 5x-SDS sample buffer. Eluates were resolved by SDS-PAGE and quantified by scanning gel densitometry of Coomassie blue-stained bands.

Collectively, the data indicated that wild-type/OgnA heterodimers could be formed, but the amounts of heterodimer formed are much lower than that of the respective homodimers. According to stoichiometry the relative ratio of GST-tagged to His-tagged monomers should be 3:1. Taking also into consideration that the full-length rod domain could not associate with the miniroad, and viceversa (see p72), we speculate that wild-type and mutant rod domains form preferentially homodimers. Furthermore, due to the intrinsic tendency of the polypeptide chains to form coiled-coils, oligomer formation most likely takes place while their synthesis is still ongoing.

### Identification of novel binding partners

To identify proteins expressed in keratinocytes that associated with OgnA plectin but not wild-type plectin, I pursued a pull-down strategy using as bait either wild-type or OgnA rod domains and as prey primary mouse keratinocyte lysates derived from plectin<sup>+/+</sup> and plectin<sup>-/-</sup> mice. For the pull-downs, purified GST-Rod<sub>wt</sub> and GST-Rod<sub>OgnA</sub> were immobilized onto glutathione-Sepharose beads and incubated with keratinocyte lysates; glutathione-Sepharose beads alone or with bound GST were used as negative controls. After binding, washing, and elution, the pull-down eluate was fractionated by SDS-PAGE and proteins were detected by silver staining. Results of the pull-down performed with plectin-deficient (plectin<sup>-/-</sup>) keratinocytes are presented in Fig. 62A. Of the several proteins associating with both types of GST-fusion proteins, one with an apparent mass between 60 and 50 kDa showed a difference in band intensity between the GST-rod<sub>OgnA</sub> and GST-rod<sub>wt</sub> samples (lane 3). Several antibodies recognizing proteins of this size, cytokeratins among them, were used to probe protein complexes derived from the pull-

down. Probing the blot with antibodies recognizing K5, K6, and K18, two bands corresponding to K5 and K6 were detected (results not shown). The band corresponding to K6 was also recognized by antibodies specific to K6 (Fig. 62B). In agreement with the silver-stained gel, the intensity of the band on the immunoblot was higher for the Ogn<sub>a</sub> rod sample. However, this result was observed only once and needs to be verified.

The interaction of the plectin rod with K6 was further tested in a blot overlay assay. To this end, keratin-enriched insoluble fractions from mouse keratinocytes were separated by SDS-PAGE, transferred to nitrocellulose filters, and overlaid with purified His-Rod<sub>wt</sub> and His-Rod<sub>Ogn<sub>a</sub></sub>. Bound proteins were detected with anti-plectin antibodies. Both the wild-type and the Ogn<sub>a</sub> version of the rod, bound to a band corresponding to K5 and K6, with the mutant (Ogn<sub>a</sub>) showing a stronger signal (Fig. 62C). This result confirmed that the plectin rod domain bound to K6. Whether the mutant rod domain has indeed a higher affinity for K6 than the wild-type awaits confirmation by an alternative assay. Pull-downs

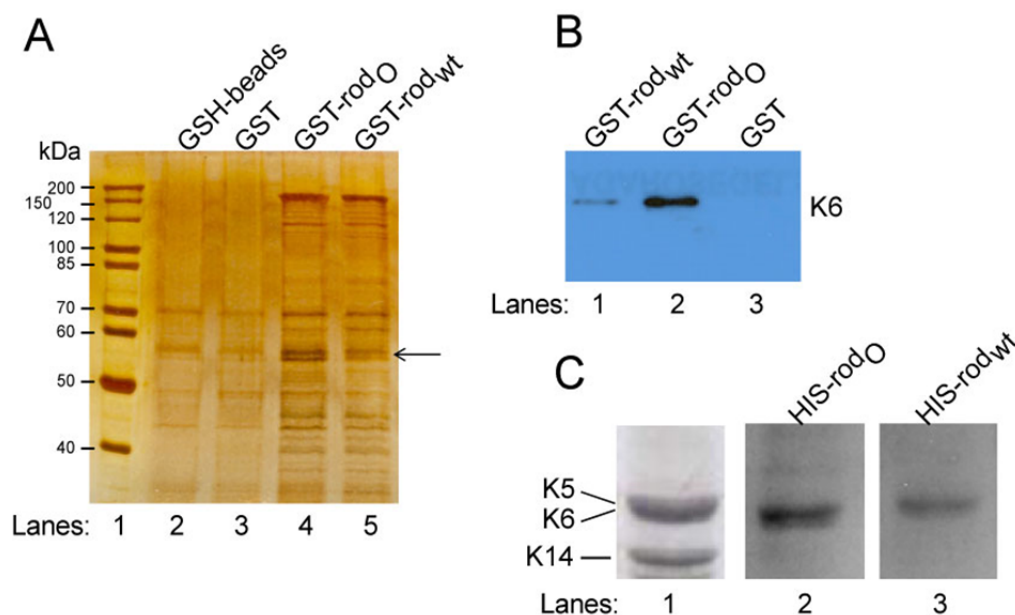


**Figure 62. Analysis of pull-down complexes and protein overlay assay.** (A) SDS-PAGE of proteins pulled down by GST-rod fusion proteins from plectin-deficient keratinocytes. Following coupling to the glutathione–Sepharose beads and extensive washing, the beads were incubated with a keratinocyte cell lysate and washed. The beads were then boiled in equal parts of lysis and sample buffer and an aliquot of each sample analyzed by silver staining. Lanes: 1, molecular weight markers (masses shown at left in kDa); 2, Sepharose-GSH beads only; 3-5, beads with bound GST, GST-Rod<sub>WT</sub>, or GST-Rod<sub>Ogn<sub>a</sub></sub>, respectively. (B) Immunoblotting analysis of proteins derived from the pull-down using antibodies specific to K6. Samples as in A. (C) Blot overlay assay of keratins with His-Rod<sub>Ogn<sub>a</sub></sub>, or His-Rod<sub>Ogn<sub>a</sub></sub>. Proteins in keratin-enriched detergent-resistant fraction were resolved by SDS-PAGE, transferred to a membrane and overlaid with purified His-Rod fusion proteins. Lane 1, Coomassie-blue stained gel showing epidermal keratins. Lanes 2-3, detection of bound proteins with antibodies to plectin (10F6). Note the stronger signal of His-Rod<sub>Ogn<sub>a</sub></sub> at the position of keratins 5 and 6 compared to His-Rod<sub>wt</sub>.



are not inherently quantitative and it cannot be excluded that the observed differences in staining intensity may have been due to the experimental variability of the method.

Additional binding partners of the rod domain were identified by mass spectrometry. For this, pull-down complexes were resolved by SDS-PAGE and protein bands, identified as unique to the O<sub>gna</sub> sample, were isolated and analyzed. For this approach the keratinocyte lysates were preincubated with an excess of GST-Rod<sub>wt</sub> beads to remove proteins that bind to the wild-type rod domain, and the lysates depleted of wild-type rod-bound proteins were then incubated with GST-Rod<sub>O<sub>gna</sub></sub> beads. One aliquot of the pull-down eluate was analyzed by SDS-PAGE (Fig. 63) and another one by MALDI-TOF mass spectrometry (MS) after excision of the protein bands from the gel and in-gel digestion with trypsin. Several proteins were identified, among them K6, a number of serine proteases, and eukaryotic translation elongation factor 1 gamma (eEF1- $\gamma$ ). eEF1- $\gamma$  was the protein with the highest (and highly significant) Mascot score, and also the most abundant protein in the mixture (exponentially modified protein abundance index, emPAI) (Table 6).

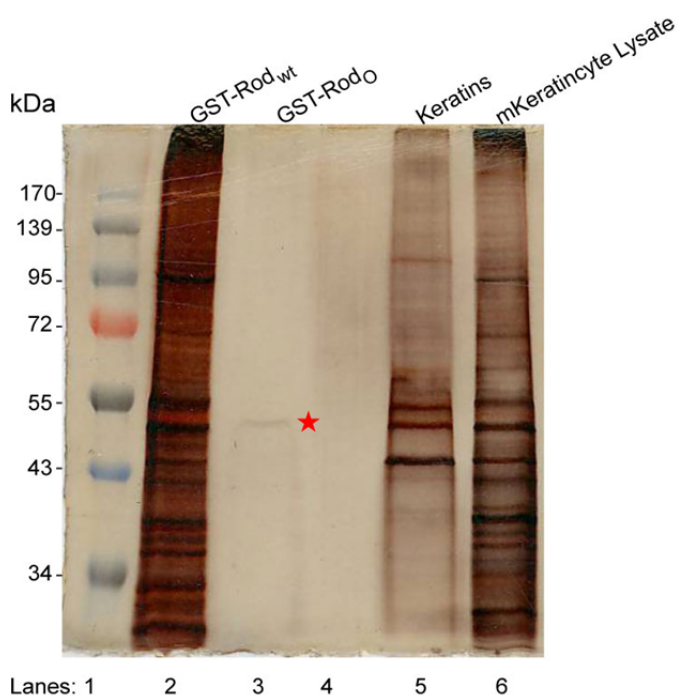


**Figure 63. SDS-PAGE analysis of proteins pulled down by GST-Rod<sub>O<sub>gna</sub></sub> after subtraction of GST-Rod<sub>wt</sub>-bound proteins from the keratinocyte lysate.** Purified GST-Rod<sub>wt</sub> proteins were prebound to glutathione-Sepharose beads and incubated with a lysate prepared from plectin-deficient keratinocytes. The lysate depleted of GST-Rod<sub>wt</sub>-bound proteins was recovered by centrifugation and incubated again with bead-bound GST-Rod<sub>O<sub>gna</sub></sub>. The beads were then washed, and proteins on the beads as well as input controls were electrophoresed and visualized by silver staining. The lanes show: 1, molecular weight markers (masses shown at left in kDa); 2-3, proteins bound on GST-Rod<sub>wt</sub> or GST-Rod<sub>O<sub>gna</sub></sub> beads, respectively; 4, void; 5-6, proteins in keratin-enriched detergent resistant fractions or mouse keratinocyte lysate (input), respectively. The red star marks the position of the proteins that were analyzed by MS.

**Table 6. Mascot Search Results for eEF1- $\gamma$** 

Protein summary										
1.	gi   110625979 eukaryotic translation elongation factor 1 gamma [Mus musculus]									
	Mass: 50371		Score: 494		Queries matched: 40		emPAI: 4.44			
Query Table										
Query	Query	Observed	Mr(expt)	Mr(calc)	Delta	Miss	Score	Expect	Rank	Peptide
	360	729.40	728.40	728.44	-0.05	0	24	9.3	1	R.AILGEVK.L
	405	806.47	805.47	805.40	0.07	0	33	3.1	1	K.FAESQPK.K
411	409	810.33	809.32	809.37	-0.05	0	35	0.61	1	K.MAQFDAK.K
	420	821.49	820.49	820.44	0.04	0	33	0.33	1	R.TFLVGER.V
502	505	463.07	924.13	923.49	0.64	0	36	0.45	1	K.DPFAHLPK.S
515	517	468.19	934.36	933.49	0.87	1	46	0.052	1	K.KFAESQPK.K
533, 534, 538	536	474.56	947.10	946.46	0.64	0	45	0.069	1	R.QAFPNTNR.W
560	557	488.36	974.70	974.52	0.18	0	44	0.011	1	K.QVLEPSFR.Q
676	680	543.64	1085.26	1084.54	0.72	0	48	0.036	1	K.STFVLDEFK.R
698, 700	699	562.19	1122.36	1121.68	0.68	0	69	0.00025	1	R.ILGLLDTHLK.T
697, 701	703	562.68	1123.34	1122.62	0.72	1	47	0.035	1	K.AKDPFAHLPK.S
844, 847	848	621.67	1241.33	1240.65	0.69	1	59	0.0027	1	K.STFVLDEFKR.K
	853	624.08	1246.14	1245.62	0.52	1	52	0.012	1	K.QATENAKEEVK.R
948, 949, 953	950	674.61	1347.20	1346.73	0.47	0	84	8.6e-06	1	K.ALIAAQYSGAQVR.V
1044	1043	702.21	1401.72	1402.42	0.69	2	64	0.00075	1	K.QATENAKEEVKR.I
	1082	723.71	1445.41	1443.72	1.69	0	83	9.2e-06	1	K.LDPGSEETQTLVR.E
1210, 1212	1208	787.02	1572.02	1571.82	0.20	1	79	2.7e-05	1	R.KLDPGSEETQTLVR.E 1
1301, 1304	1303	854.78	1707.54	1706.86	0.67	0	70	0.00019	1	R.VLSAPPHFHFGQTNR.T

**Protein Summary.** 1, Rank order and accession number of the identified protein. Mass, expected molecular mass of the protein. Protein score reflects the combined scores of all observed mass spectra that can be matched to amino acid sequences within that protein. The higher the score, the more confident the match. Queries matched, number of MS/MS spectra matched to the protein. [MS/MS spectra are obtained by tandem MS (two or more sequentially linked mass spectrometer analyzers in a single instrument). Tandem MS delivers structural information about a compound by fragmenting specific sample ions inside the mass spectrometer and identifying the resulting fragment ions]. emPAI, exponentially modified Protein Abundance Index. **Query Table.** Query, numbers for peptide MS/MS spectrum. Observed, Mr(expt), Mr(calc), Delta, observed and predicted peptide masses, and theoretical observed differences. Miss, number of missed trypsin cleavage sites. Score (ion score) measures how well the observed MS/MS spectrum matches the stated peptide. Proteins identified by two or more peptides with a combined score of higher than 50 or by one single peptide with a score higher than 60 are considered significant. Expect, probability that the observed match would occur by chance; confident matches have expect values <0.1.

To validate the MS result, we used immunoblotting and silver staining to document the presence of eEF1- $\gamma$  in the keratinocyte lysates and pull-down eluates. As in the case of K6, we could confirm that eEF1- $\gamma$  bound to plectin's rod domain, albeit we could not show that this was specific for the Ogn mutant (Fig. 64). eEF1- $\gamma$ , also known as eEF1B $\gamma$ , is part of the eukaryotic translation elongation factor-1 (eEF1) complex which

plays a central role in polypeptide chain elongation during protein synthesis. eEF1 consists of two distinct units, a G-protein named eEF1A and a nucleotide exchange factor, eEF1B, which in turn is composed of at least two subunits, alpha (eEF1A $\alpha$ ) and gamma (eEF1B $\beta$ ). The eEF1B $\alpha$  subunit is the nucleotide-exchange factor, and the eEF1B $\gamma$  is the structural protein that mediates dimerization of the eEF1 complex (Le Sourd et al. 2006). The identification of eEF1B $\gamma$  as a keratin binding protein in epithelial cells (Kim et al. 2007) suggests that intermediate filaments also participate in the spatial organization of translation (Kim and Coulombe 2010). As plectin is known to bind to keratins and one of its isoforms, plectin 1, is targeted to the outer nuclear/ER membrane (Rezniczek et al. 2003; Konieczny et al. 2008), the finding that eEF1B $\gamma$  binds to plectin rod domain is in line with previous findings.

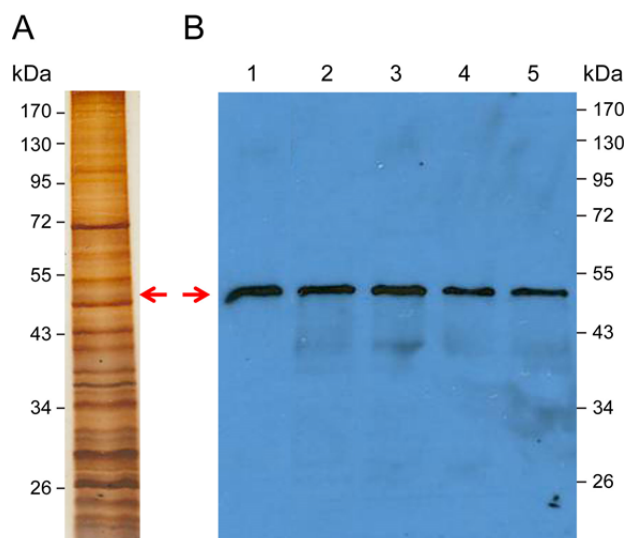


**Figure 64. Detection of eEF1B $\gamma$  protein in mouse keratinocytes and proteins pulled-down by plectin's rod domain.** (A) SDS-PAGE of proteins present in the plectin-deficient keratinocyte lysates used for the pull-downs described in the text. (B) Immunoblot of eEF1B protein in plectin-deficient keratinocyte lysates (lane 1) and in the eluate from His-Rod<sub>wt</sub> beads (lane 2), His-Rod<sub>Ogna</sub> beads (lane 3), GST-Rod<sub>wt</sub> beads (lane 4), GST-Rod<sub>Ogna</sub> beads (lane 5) after SDS-PAGE separation. Arrows indicate the immunoreactive band detected with anti-eEF1B $\gamma$  antibodies (Sigma, clone 3F11-1A10; cat number WH0001937M1).

## DISCUSSION

In this study I generated a knock-in mouse line that faithfully replicates the main features of the human disease EBS-Ogna, namely intraepidermal skin fragility and absence of muscular dystrophy. Mechanistically I could show that the restricted skin phenotype of the *Plec*<sup>Ogna/+</sup> mouse line (Ogna mice) is due to the absence of plectin isoform 1a in basal keratinocytes and defective HD formation.

Plectin is known to play an important role in strengthening cells against mechanical stress and to perform this task by connecting intermediate filaments to different cellular junctions and membrane attachment sites, such as HDs, focal adhesions, Z-lines, etc (Wiche et al. 2014). In accordance with these properties, mutations in the plectin gene result in multisystemic diseases that primarily affect skin and skeletal muscle. Rarely, mutations have been found that affect muscle or skin only (Winter and Wiche 2013). One such mutation is the autosomal dominant one that leads to EBS-Ogna and affects only the skin. The generation of a mouse line carrying the Ogna mutation opened the possibility to study functions of plectin that are specific for skin but not for other tissues, such as muscle. As the different plectin isoforms are expressed in a tissue-specific way and their unique N termini target the protein to different cellular sites, the Ogna mouse also opened the way to discern the functions of the two major isoforms expressed in skin, P1a and P1c.

### **The Ogna mouse mimics the human disease**

In addition to the original description of the clinical symptoms and pedigree analysis of families carrying the Ogna mutation done by Gedde-Dahl (1971), and the mapping of the mutation to exon 31 of the plectin gene (Koss Harnes et al. 2002), 7 other unrelated cases of EBS-Ogna have been resported in the literature (Kiritsi et al. 2013, Bolling et al.2014). As is the case for patients with EBS-Ogna, the Ogna mouse showed impaired skin integrity manifesting in poor resistance to mechanical stress and the presence of blisters and erosions. However, since the possession of a fur coat protects mice from developing mechanically induced blisters, erosions, and hemorrhagic blebs as seen in the patients, skin fragility in mice had to be evaluated by different means (e.g. tape stripping and dye penetration assays). Histologically and structurally, Ogna mice and Ogna patients presented similar phenotypes including separation of the dermis from the epidermis

between the stratum basale and the dermis, with the split occurring above the hemidesmosomal plaque and clear signs of basal cell cytolysis. Another shared hallmark was the presence of hypoplastic HDs and their reduced numbers. Plectin expression along the basal membrane of basal keratinocytes ranged from strongly reduced to absent in skin biopsies of Ogn mice as well as in Ogn patients.

### **P1a but not P1c is the isoform missing in the basal cell layer of the Ogn epidermis**

Immunofluorescence microscopy of skin biopsies using anti-pan plectin mAbs 10F6 showed reduced to absent plectin expression along the basal cell layer, but unchanged expression levels in the suprabasal epidermal layers. By applying isoform-specific antibodies I could show that the isoform expressed in the basal cell layer is P1a and that this isoform is missing in the skin of Ogn mice. This result, although expected, could not be verified for Ogn patients since thus far expression of P1a has not been tested in their skin biopsies. However, immunofluorescence staining with anti-P1c antibodies revealed that P1c, the most abundant isoform expressed in the epidermis, is predominantly found in suprabasal cell layers. These results were consistent with the data obtained for RNA expression levels in cultured primary keratinocytes and total epidermis: These data, too, showed that P1a is the isoform predominantly expressed in basal keratinocytes while P1c is the dominant isoform of total epidermis. Thus, as cultured keratinocytes lack suprabasal layers, their dominantly expressed isoform is P1a, while in whole epidermis where the basal cell layer coexists with several suprabasal layers, P1c prevails.

### **Absence of P1a correlates with rudimentary HDs at the dermo-epidermal junction**

Plectin, together with integrin  $\alpha 6\beta 4$  and BPAG1e, is required for HD assembly. The three proteins form a backbone that facilitates the incorporation of the transmembrane proteins that form the outer HD plaque and provides the link to cytoplasmic keratins (Koster et al. 2003; Koster et al. 2004; Walko et al. 2014). Studies in this thesis refine this model by showing that P1a is the plectin isoform relevant for HD formation. This is further substantiated by (i) the smaller size and reduced numbers of HDs, associated with a flawed attachment of keratins to the inner plate found in the skin of Ogn mice; and (ii) the faster migration of *Plec*<sup>Ogn/+</sup> keratinocytes and their lesser resistance to hypo-osmotic shock.

### Impact of the Ogn1 mutation on the plectin rod

Plectin's rod domain is made up of a long polypeptide (1127 amino acid residues) with an almost entirely  $\alpha$ -helical structure that mediates dimerization. Although my data seemed to indicate that the native state of the RD was a tetramer, it has later been shown to be a dimer (Walko et al. 2011). I demonstrated in this thesis that the dimers formed by the Ogn1 rod are less stable than the ones formed by the wild-type rod. A computational model of a small moiety of the RD surrounding the Ogn1 mutation (Fig. 65) suggests that the mutation causes a local unfolding of the coiled-coil, thereby decreasing its stability (Walko et al. 2011). This confirms the biochemical data presented in this thesis.

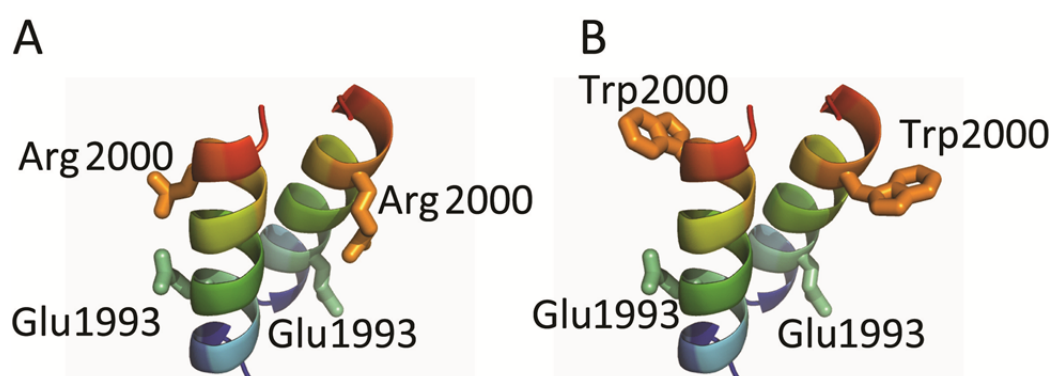


**Figure 65. Molecular modeling of RD fragments harboring the p.Arg2000Trp mutation.** Ribbon views of three-dimensional models of fragments of wild-type coiled-coil dimers (A), and of its p.Arg2000Trp mutant version (B) in which the participating  $\alpha$ -helices are arranged in parallel. Each fragment contains two copies of the segment 1988–2003. Chains are colored according to blue-to-red (N to C terminus) scheme. Note that arginine 2000 can form an intrahelical salt bridge with glutamine 1993, which is disrupted by the p.Arg2000Trp mutation and concomitantly exposes the hydrophobic side chain of tryptophan to the solvent. This situation is energetically unfavorable and leads to the hypothesis that the Trp 2000 side chain enters into the apolar inter-helical interface, leading to a local unfolding of the helix. (Modified from Walko et al. 2011).

The arrangement of two plectin molecules parallel to one another and in registry has long been predicted as well as their capacity to form higher order structures (Wiche et al. 1991, Green et al. 1992). A detailed analysis of the amino acid sequence in the rod region revealed a highly repetitive pattern in the distribution of positive and negative charges along the helical arrays. The periodicities in acidic and basic residues ( $\sim 10.4$  residues) are out of phase by  $\sim 180^\circ$  suggesting that they could promote lateral association, and thus facilitate the assemble of the protein into higher order oligomers. Indeed, polymeric tube-like structures have been visualized by electron microscopy after negative staining (Walko et al. 2011, Fig 5). The local disruption of the coiled-coil through the mutation did not prevent the mutant rod to oligomerize and form highly ordered structures that



were similar to the ones formed by the wild-type rod specimens although smaller in size (Walko et al. 2011, Fig S7B). In sum, although the Arg2000Trp substitution, by reducing the stability of plectin's secondary and probably higher order structures, would explain the generation of less stable HDs, it does not explain the total absence of P1a in the skin of mutant mice.

Another consequence of the Arg2000Trp substitution could be the creation of new interfaces for molecular interactions or the disruption of existing ones due to changes in charge or local conformation introduced into the rod domain. The pull-down and mass spectrometry approaches, that I took to identify binding partners of the mutated rod and potentially provide a link between the mutation and the observed phenotype, did not yield conclusive results. The analysis, however, uncovered the presence of serine proteases associated with plectin's rod. This is of interest in light of zymographic analyses (conducted by colleagues in the lab) that confirmed the presence of calpain and serine proteases in epidermal protein extracts (Walko et al. 2011).

### **Spatiotemporal regulation of P1a degradation**

The depletion of mutant P1a protein found in Ogn mice can not be due to low expression of the mutant protein since no changes in mRNA expression levels were observed when compared to wild-type. Rather, the absence of mutant P1a is presumably due to proteolytic degradation. Walko et al. 20(2011) have shown that the plectin rod, which otherwise is a very stable protein, can be rapidly cleaved under conditions resembling those prevailing during basal keratinocyte differentiation. Their experimental approach and conclusions included the cleavage of the rod by the active form of calpain-1 present in epidermal cell lysates or by purified calpain; the prominent localization of calpain at the basal cell membrane of basal keratinocytes; the progressive degradation of plectin with concomitant loss of HPCs upon calpain activation; and the observation that the degradation can be blocked by calpain inhibitors.

As aberrant calpain activation can result in uncontrolled protein degradation and irreversible cell damage, its activation must be tightly regulated. The currently working model is that calpain, and probably other proteases, targets and degrades HD-anchored P1a. Thus, the spatiotemporal regulation of P1a degradation, provided by its localization at the HD and calpain activation, conveys the required specificity. This spatiotemporal regulation explains why P1c as well as other plectin isoforms are not degraded despite sharing the mutated Ogn rod.

### Impact of the mutated rod on hemidesmosome formation

In wild-type epidermis, formation of stable (mature) HDs is mediated by multimerization of full-length P1a molecules via their rod domain, as the self-association of plectin molecules creates extraordinary stable protein arrays which are then able to resist shear forces exerted on the epidermis (Fig. 66) (Walko et al. 2014). In Onga skin, however, neither the stabilization of HDs via the plectin rod nor adequate formation of HDs can occur, as the protein is being degraded in the basal cells. The reduced level of P1a becomes then insufficient to promote formation of HDs in sufficient numbers and with optimal stability for keratin IF network anchorage. Sonnenberg and coworkers have postulated that the formation of HDs is a sequential process started by the backbone formed by laminin-322, integrin  $\alpha 6\beta 4$ , plectin and that plectin is required for the subsequent incorporation of BPAG2 and BPAG1e (formerly BP180 and BP230, respectively) (Koster et al. 2004).

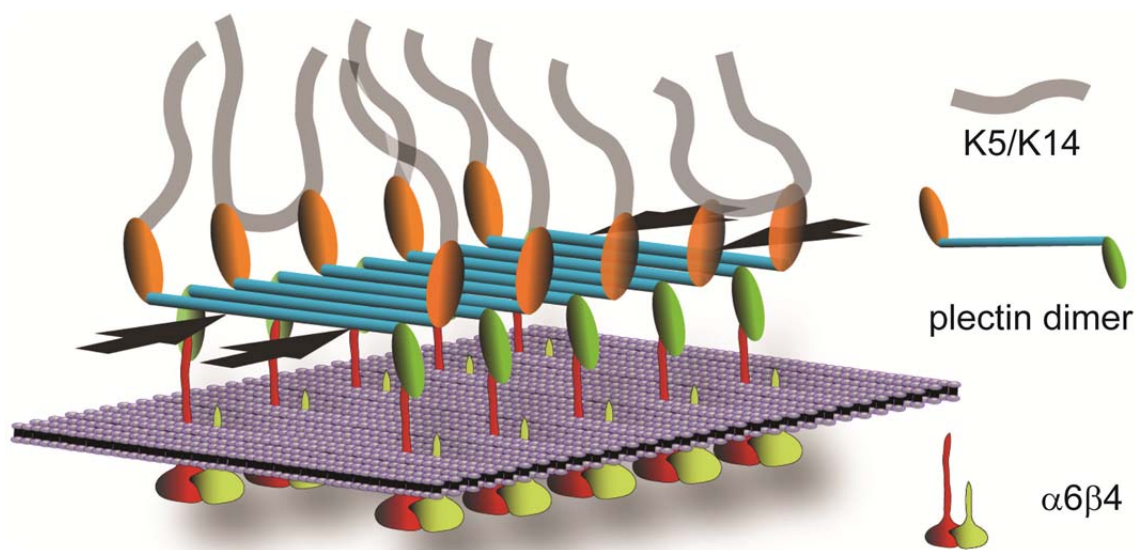


**Figure 66. Model of HD stabilization through plectin multimerization.** Schematic model depicting the major protein-protein interactions that provide the mechanical stability of HDs. Interaction of P1a dimers with integrin  $\beta 4$  and K5/K14 provides a vertical force component, whereas the integrin  $\beta 4$ -induced lateral association of multiple dimeric P1a molecules (in an anti-parallel fashion via their rod domains) could generate an additional horizontal force component (arrows), parallel to the plasma membrane (violet sheet). Note that individual proteins are not drawn to scale and BPAG1e and BPAG2 are not depicted. In contrast to classical models of HD protein organization, the sheet-like association of plectin molecules in our model is better suited to incorporate the dimensions of plectin molecules (>230 nm) within the 50-60 nm thick HD inner plate (from Walko et al. 2011, Fig. 8D).

### **Ethiopathogenesis/molecular basis of EBS-Ogna**

Genetically, EBS-Ogna is transmitted as an autosomal dominant disease caused by a C to T transition in the PLEC gene (c.5998C>T) that results in the substitution of arginin at position 2000 by tryptophan (p.Arg2000Trp) in the central rod domain of plectin. The immense functional importance of the arginine residue at position 2000 is suggested by the fact that it is conserved among all vertebrate species for which the sequence of plectin is known. To date 78 mutations have been found within the plectin gene (Winter and Wiche 2013, Natsuga 2014), among which the Ogna c.5998C>T mutation is the most frequently reported one, as individuals from 9 apparently unrelated families of Norwegian, German, Dutch, and Turkish descent have been identified as carriers (Gede-Dahl 1971, Koss-Harnes et al. 2002, Kiritsi et al. 2013, Bolling et al. 2014). Thus, the mutation accounts for nearly 12% of all known plectin mutations, indicating that it might be a mutational hotspot. Mutation hotspots can originate from a phenotypic preference for a particular amino acid substitution or by intrinsic mutational bias due to structural features of the DNA sequence. In any case, the location of a hotspot is thought to denote a functionally critical amino acid residue.

Structurally, the mutation brings about a local disruption in the rod domain of plectin which results in a moderate decrease in stability of the oligomeric complex. Additionally, the conformational changes at the site of the mutation expose the rod domain to proteolytic degradation, preventing HD assembly and keratin anchorage. Consequently, the epithelium is only loosely anchored to the connective tissue allowing its separation with ensuing blister formation. In contrast to the epidermis, mutated plectin isoforms expressed in skeletal muscle are not at the proper location for degradations by calpains and in addition calpains in muscle extracts are in their inactive form (Walko et al. 2011). This explains the lack of muscular dystrophy symptoms in EBS-Ogna patients and mice. Recently, patients specifically deficient in isoform P1a due to a mutation in exon 1a, and with a phenotype similar to EBS-Ogna patients, have been reported (Gotynska et al. 2015).

### **Conclusions**

For this PhD thesis I have generated an Ogna knock-in mouse line that opened the door for studies of the pathomechanism of the disease EBS-Ogna. Based on the phenotypic characterization of these mice and a combination of ex vivo and in vitro approaches, I

could identify P1a as the plectin isoform which is essential for HD integrity. Furthermore, the successful expression of the plectin rod with and without flanking domains (up to 190 kDa) in baculovirus-infected insect cells has been instrumental to establish the mechanism of P1a degradation in subsequent studies. Finally, the fact that the Oga mice live to adulthood makes them a reliable genetic model to study pharmacological and genetic therapies to correct EBS diseases.

## MATERIALS & METHODS

### Materials

#### 1. Buffers and Solutions

##### • *Isolation of genomic DNA from cells and mouse tails*

###### Lysis buffer

Tris-HCl pH 8.0	50 mM
EDTA	100 mM
NaCl	100 mM
SDS	1%
Proteinase K	0.5 mg/ml

##### • *DNA solubilization and precipitation*

TE buffer		3 M Na-Acetate	
Tris-HCl, pH 8.0	10 mM	Na acetate	3.0 M
EDTA	1 mM	adjust to pH 5.2	with acetic acid

##### • *DNA gel electrophoresis*

50x TAE buffer		6x DNA loading buffer	
Tris-base	2 M	Ficoll 4000	15%
Acetic acid	1 M	Bromphenol blue	0.25%
EDTA	50 mM	EDTA	120 mM

##### • *RNA gel electrophoresis*

10x MOPS		Loading buffer	
MOPS, pH 7.0	0.4 M	5xMOPS pH 7.0	400
μl			
Na acetate	0.1 M	37% formaldehyde	700
μl			
EDTA	0.01 M	deionized formamide	2000
μl			
		50% glycerol-bromophenol blue	400 μl

###### 50% glycerol-bromophenol blue

bromophenol blue	0.25 g
H <sub>2</sub> O	10 ml, when dissolved add 10 ml glycerol

##### • *Southern blot analysis*

Denaturation solution		Saline-sodium citrate (SSC) buffer	
NaOH	0,5 N	NaCl	150 mM
NaCl	1,5 M	Na citrate pH 7.0	15 mM
<b>Church buffer</b>		<b>Church wash buffer</b>	
NaP <sub>i</sub> , pH 7.2	0.5 M	NaP <sub>i</sub> , pH 7.2	12 mM
SDS	7%	SDS	1%
EDTA	1 mM		

### • Preparation of competent cells

Transformation storage solution (TSS)		5x KCM buffer	
PEG 3350	10%	KCl	0.5 M
DMSO	5%	CaCl <sub>2</sub>	0.15 M
MgCl <sub>2</sub>	10 mM	MgCl <sub>2</sub>	0.25 M
MgSO <sub>4</sub>	10 mM	sterilize by filtration through a 0.2 $\mu$ m	
in LB medium; adjust to pH 6.5		filter, store at 4°C	
sterilize by filtration (0.2 $\mu$ m filter)			

### • Plasmid preparations

Solution E1 (Cell Resuspending)		Solution E4 (Column Equilibration)	
Tris-HCl pH 8.0	50 mM	NaCl	600 mM
EDTA	10 mM	Na acetate	100 mM
add RNase A to a final concentration of 100 $\mu$ g/ml		TritonX-100	0.15 %
		acetic acid ad pH 5.0	
Solution E2 (Cell Lysis)		Solution E5 (Column Washing)	
NaOH	200 mM	NaCl	800 mM
SDS	1.0 % (w/v)	Na acetate	100 mM
		acetic acid ad pH 5.0	
Solution E3 (Neutralization)		Solution E6 (DNA Elution)	
K acetate	3.1 M	NaCl	1250 mM
acetic acid ad pH 5.5		Tris-HCl pH 8.5	100 mM

### • Protein expression

in <i>E. coli</i> : Lysis buffer in insect cells: Lysis buffer			
Tris-HCl	50 mM pH 7.9	Hepes	20 mM pH 7.4
Imidazole	20 mM	Triton X-100	1%
Glycerol	5%	Glycerol	1%
Triton X-100	0.5 M	PMSF	1 mM
EDTA	0.5 M	prepared freshly	

### • Purification of recombinant proteins

#### Spin column purification

His-tagged proteins		GST-tagged proteins	
Binding buffer		Binding buffer	
Hepes pH7.4	20mM	PBS	1x
Triton X-100	1%	Triton X-100	1%
Glycerol	1%	glycerol	1%
PMSF	1mM	PMSF	1mM
Washing buffer		Washing buffer	
Binding buffer	1x	PBS	1x
Imidazole	20 mM	PMSF	1mM



**Elution buffer**

Hepes pH 7.4	20 mM
Triton X-100	1%1%
Imidazole	250 mM
PMSF	1mM

**Elution buffer**

Tris-HCl pH 8.0	50 mM
Glutathione	10 mM

**FPLC purification****HIS-tagged proteins****Binding & Washing buffer**

Na Phosphate buffer pH 7.4 50 mM

Na Cl 300 mM

PMSF 1mM

**Elution buffer**

Na Phosphate buffer pH 7.4 50 mM

Na Cl 300 mM

PMSF 1 mM

Imidazole 0-500 mM

**GST-tagged proteins****Binding & Washing buffer**

PBS

PMSF 1mM

**Elution buffer**

Tris-HCl pH 8.0 50 mM

NaCl 50 mM

Glutathion 10 mM

**● Protein determination****Bradford solution**

Coomassie G-250 100 mg  
95% ethanol 50 ml  
85% phosphoric acid 100 ml  
ad 1000 ml with dH<sub>2</sub>O  
filter (Whatman paper #1), store at 4°C

**Bicinchoninic Acid (BCA)**

bought from Pierce

**● SDS-PAGE electrophoresis****Acrylamide mix**

Acrylamide 29 g  
N,N'-metylenbisacrylamide 1 g

**Separating gel mix**

	5%	6%	8%	10%	12%	15%
dd water	2.8 ml	2.6 ml	2.3 ml	1.9 ml	1.6 ml	1.1 ml
30% acrylamide mix	0.85 ml	1.0 ml	1.3 ml	1.7 ml	2.0 ml	2.5 ml
1.5 M Tris pH 8.8	1.3 ml	1.3 ml	1.3 ml	1.3 ml	1.3 ml	1.3 ml
10% SDS	50 µl	50 µl	50 µl	50 µl	50 µl	50 µl
10% APS	50 µl	50 µl	50 µl	50 µl	50 µl	50 µl
TEMED	2 µl	4 µl	3 µl	2 µl	2 µl	2 µl

TEMED, N, N, N', N'-tetramethyl ethylenediamine

APS, ammonium persulfate

**Stacking gel mix**

0.5 M Tris-HCl pH 6.8	750 µl
30% acrylamide mix	390 µl
10% SDS	30 µl
10% APS	30 µl
H <sub>2</sub> O	1830 µl
TEMED	3 µl

**Running buffer**

Tris-HCl	25 mM
Glycine	200 mM
SDS	1%

**2x SDS-PAGE sample buffer**

Tris-HCl, pH 6.8	160 mM
SDS	4%
Glycerol	20%
DTT	200 mM
Bromphenolblue	0.05%

**5x SDS-PAGE sample buffer**

Tris-HCl pH 6.8	0.4 M
SDS	10%
Glycerol	50%
DTT	0.5 M
Bromphenolblue	0.1%

**Coomassie staining solution**

Coomassie R-250	0.4%
Methanol	45%
Acetic acid	10%
at least 20 min shaking at RT	

**Coomassie destaining solution**

Methanol	30%
Acetic acid	10%

**• Silver staining of proteins in PAGE gels****Fixing solution**

Methanol	50%
Acetic acid	12%
Formaldehyde	0.5 ml/l of 37%

**Sensitizing solution**

Na <sub>2</sub> S <sub>2</sub> O <sub>3</sub> *5H <sub>2</sub> O	0.2 g/l
--	---------

**Staining solution**

AgNO <sub>3</sub>	2 g/l
Formaldehyde	0.75 ml/l of 37%

**Developing solution**

Na <sub>2</sub> CO <sub>3</sub>	60 g/l
Na <sub>2</sub> S <sub>2</sub> O <sub>3</sub> *5H <sub>2</sub> O	4 mg/l
Formaldehyde	0.5 ml/l of 37%

**Stop solution**

Methanol	50%
Acetic acid	12%

**• Western Blotting****Transfer buffer (wet blotting)**

Tris-HCl	48 mM pH 8.6
Glycine	40 mM

**Ponceau S staining solution**

Ponceau S	0.5%
Acetic acid	1%

**PBS (phosphate buffered saline)**

KH <sub>2</sub> PO <sub>4</sub> /Na <sub>2</sub> HPO <sub>4</sub> ,	10 mM pH 7.5
NaCl	150 mM

**Blocking buffer**

5% dried milk in PBS-T

**PBS-T**

PBS containing 0.1% Tween-20

**Strip buffer**

Glycine	200 mM pH 2.5
NaCl	200 mM

**Chemiluminescent detection (horseradish peroxidase (HRP))**

SuperSignal West Pico Stable Peroxide Solution (Thermo Scientific)

SuperSignal West Pico Luminol/Enhancer Solution (Thermo Scientific)

mix equal volumes of each solution prior to incubation.

**Colorimetric detection****Alkaline phosphatase buffer (AP-buffer)**

Tris-HCl 100 mM

NaCl 100 mM

MgCl<sub>2</sub> 5 mM

adjust to pH 9.5 with 5 M NaOH

**AP substrate solution**

NBT\* 66 µl

BCIP\*\* 33 µl

AP- buffer 10 ml

mix components prior to incubation

\* Nitro blue tetrazolium (prepare 5% NBT in 70% dimethyl formamide)

\*\* 5-bromo-4-chloro-3-indolyl phosphate

**● Preparation of cell and tissue extracts****Lysis buffer****Buffer A**

Hepes/HCl, pH 7.0 50mM

MgCl<sub>2</sub> 1mM

EGTA 1mM

NaCl 100mM

**Lysis buffer**

Buffer A 1x

Triton X-100 0.5%

DTT 0.1mM

DNase I 0.5mg/ml

RNase A/ddH<sub>2</sub>O 0.2 mg/ml

PMSF 1mM

Benzamidin/ddH<sub>2</sub>O 10mMApprotinin/ddH<sub>2</sub>O 10 µg/ml

Pepstatin/DMSO 10µg/ml

Leupeptin/ DMSO 10µg/ml

**Keratin preparation****Solution A**

PBS

EDTA 10 mM

PMSF 1 mM

NP-40 1%

¼ tablet of proteinase inhibitor

**Solution B**

PBS

EDTA 10 mM

PMSF 1mM

Empigen 1%

¼ tablet of proteinase inhibitor

**● Bacterial growth media****LB-medium (Luria-Bertani-Medium)**

Trypton 10 g

Yeast extract 5 g

NaCl 10g

per 1000 ml, pH 7.5

**LB<sub>amp</sub> and LB<sub>kan</sub>**

ampicillin 100 µg/ml

kanamycin 50 µg/ml

added to LB after cooling at 55°C

**LB-plates LB + Agar** 15.0 g/l**LB<sub>amp</sub> and LB<sub>kan</sub>-plates LB<sub>amp</sub> and LB<sub>kan</sub> + Agar** 15.0 g/l

**TB (Terrific broth)****TB-basic**

Tryptone	12.0 g
Yeast extract	24.0 g
Glycerol	4.0 ml
ddH <sub>2</sub> O ad	900 ml
autoclave, cool to 60°C	

**K-phosphate for TB**

KH <sub>2</sub> PO <sub>4</sub>	2.31 g
K <sub>2</sub> HPO <sub>4</sub>	12.5 g
ddH <sub>2</sub> O ad	100 ml
autoclave, cool to 60°C, and add TB-basic	

**• Cell culture media****Sf9 medium**

Insect Express (Lonza)

FCS	10%
Pen/Strep	1%
L-Glutamine	1%

**ES cells medium**

DMEM (Life Technologies)	
FCS	18.5%
L-Glutamine	2mM
Na pyruvate	1 mM
Non essential amino acids	1%
Pen/Strep	1%
2-βME	0.1 mM
LIF	0.25%

**MEF medium**

DMEM (Life Technologies)	
FCS	10%
L-Glutamine	2mM
Na pyruvate	1 mM
Non essential amino acids	1%
Pen/Strep	1%
2-βME	0.1 mM

**Keratinocyte growth medium****KGM solution**

KCM (Clonetics Bullet Kit)	
FCS	8%
ITS	1%

**Primary basal keratinocytes isolation medium**

KGM (Lonza)	
FCS (chelex-treated)	8%
CaCl <sub>2</sub>	0.05 mM

**2. Bacterial strains****Cloning**

**XL1-Blue** *recA1 endA1 gyrA96 thi<sup>-1</sup> hsdR17 supE44 relA1 lac [F' proAB lacIqZΔM15 Tn10 (Tet<sup>r</sup>)]*

**Expression**

**BL21-CodonPlus (DE3)-RIL** *F<sup>-</sup> ompT hsdS(r<sub>B</sub><sup>-</sup> m<sub>B</sub><sup>-</sup>) dcm<sup>+</sup> Tet<sup>r</sup> gal l (DE3) endA Hte [argU ileY leuW Cam<sup>r</sup>]*

### 3. Baculoviruses

**Table 7.**

Name	Description: encoded plectin domain	Source
NV10	His-tagged rod <sub>wt</sub> domain	M. Castañón <sup>1</sup>
NV11	His-tagged rod <sub>Og</sub> domain	M. Castañón <sup>1</sup>
NV12	His-tagged SR5-9+rod <sub>wt</sub> domain	M. Castañón <sup>1</sup>
NV13	His-tagged SR5-9+rod <sub>Og</sub> domain	M. Castañón <sup>1</sup>
NV14	GST-tagged rod <sub>wt</sub> domain	M. Castañón <sup>1</sup>
NV15	GST-tagged rod <sub>Og</sub> domain	M. Castañón <sup>1</sup>
NV16	GST-tagged SR5-9+rod <sub>wt</sub> domain	M. Castañón <sup>1</sup>
NV17	GST-tagged SR5-9+rod <sub>Og</sub> domain	M. Castañón <sup>1</sup>
JB3	His-tagged rod <sub>wt</sub> mini	J. Breitenbach <sup>2</sup>
JB4	GST-tagged rod <sub>wt</sub> mini	J. Breitenbach <sup>2</sup>
JB5	His-tagged rod <sub>Og</sub> mini	J. Breitenbach <sup>2</sup>
JB6	GST-tagged rod <sub>Og</sub> domain	J. Breitenbach <sup>2</sup>

<sup>1</sup> generated for this work.

<sup>2</sup> Diploma Thesis University of Vienna, 2007.

### 4. Plasmids, cloning and expression vectors used for preparation of new constructs

**Table 8**

Name	Vector	Description	Source
pBSII KS		Cloning vector	Stratagene
pCR2.1		Cloning vector for PCR products	Invitrogen
pNeo-flox8		Neomycin cassette flanked by <i>loxP</i> sites	M. Kraus <sup>1</sup>
pKA9	pBSII KS	Mouse genomic DNA including plectin exons 11-32	K. Andrä
pPF26	pBSII KS	548 bp fragment encoding exon 31 ( <i>SacII</i> to <i>NotI</i> )	V. Proll <sup>2</sup>
pDL1-1	pBSII KS	1080 bp fragment from exon 31 ( <i>NotI</i> to end)	D. Mezricky
pET42-SH	pET42	GST tag of pET42 exchanged by SH2 domain of PLC $\gamma$ 1	B. Baminger <sup>3</sup>
pEGFP-N2		Mammalian expression vector	Clontech
		<b>pEGFP derived constructs encoding:</b>	
pVP37	pPFmyc57 <sup>4</sup>	Full-length P1a Ogna	V. Proll <sup>2</sup>
pVP40	pPFmyc57 <sup>4</sup>	Full-length P1a wild-type	V. Proll <sup>2</sup>
pVP42	pPFmyc57 <sup>4</sup>	Plectin rod domain wild-type	V. Proll <sup>2</sup>
pVP43	pPFmyc57 <sup>4</sup>	Plectin rod domain Ogna	V. Proll <sup>2</sup>
pVP44	pPFmyc57 <sup>4</sup>	Plectin rod domain wild-type + C terminus	V. Proll <sup>2</sup>
pVP45	pPFmyc57 <sup>4</sup>	Plectin rod domain Ogna + C terminus	V. Proll <sup>2</sup>

<sup>1</sup> Kraus et al. 2001

<sup>2</sup> Diploma Thesis, University of Vienna, 2002

<sup>3</sup> Ludwiczek et al. 2004

<sup>4</sup> derived from pEGFP-N2 by exchanging EGFP for the myc tag

## 5. Primers

**Table 9**

Primers used for generation of the targeting construct	Sequence 5→3'
MCS ogna 1 sense	GTACCACTAGTCCCAAGCTTGAT
MCS ogna 1 antisense	ATCAAGCTTGGGACTAGTG
MCS ogna 2 sense	ATCGGGGCGGCCGCTCGAGCCCGAATCCCCG
MCS ogna 2 antisense	GGGAATTCGGGCTCGAGGCGGCCGCCCGAT
<b>Primers used for genotyping</b>	
Cre sense	CCAATTTACTGACCGTACACC
Cre antisense	TAATCGCCATCTTCCAGCAGG
Neo-3086	TCGGCAGGAGCAAGGTGAGATG
mPle31/U7314	GCTCAAGCAGGAGGCGAAGTTACTG
mPle32/L7384	GTATCTGCTCCTGCTGCACAGTCTG
mPle31/L5866 Oгна	CCTCTGCCGCCAACTGCCACTGCCG
mPle31/L5866 wt	CCTCTGCCGCCAACTGCCGCTGCCG
<b>Primers used for cDNA synthesis &amp; RT-PCR (Reverse Transcriptase PCR)</b>	
mPle32 8029/L	TCATTGGTGGGCTTCAGTAACAG
mPle31/U5464	GCCACACGGCTCAAGACGGAGGCAG
mPle32/L7714	GCAGCCGCTGGTTTTCTCCGCCAG
MC-13575/U (at 5581)	GCGGCACTGCACAAGGCTGACATC
mPle32/L7384	GTATCTGCTCCTGCTGCACAGTCTG
mPle32/ L7378)	GCTCCTGTTGAACAGTCTGCATCTC
13253/U (at 5184)	GCGGGCCGAGACAGAGCAAGGTGA
pHLH20 L4m (at 7857)	GAATTCCTCGGGTTCAGCCTCCACGGACGGG
mPleEx31/32 L (over junction)	GCTCCTGTTGAACAGTCTGCATCTC
<b>Primers used for sequencing PCR products &amp; constructs</b>	
mPle31/U5701	GAGGAGGAGATCATGGCGCTGAAGG
MC-13575/U (at 5581)	GCGGCACTGCACAAGGCTGACATC
MC-13574/L (at 6174)	CTCCGCAGCCGATCCAGCATGTTT
mPle31/L5918	CTGCCAGGCTCCTCTGCACGCGCTC
<b>Primers used for qRT-PCR (quantitative Real Time PCR)</b>	
HPRT1/F	CAGGCCAGACTTTGTTGGAT
HPRT1/R	TTGCGCTCATCTTAGGCTTT
Ex1a/F	GGTAGCAAGAGAACCAGCTCA
Ex1b/F	TGGTAGTCGTGGGTCATGTTGTC
Ex1c/F	AAGTGGAGGTGGTTCTGTGG
Ex1d/F	GAAGATCGTGCCCGATGAA
Ex2/R	AGGTGTTTGTGACCCACTTG
Ex26/F (at 3204)	CAGCTTGGTGATTTCGAGTA
Ex27/R (over junction at 3340)	CCCGCAGCTTCTTTAGTGAG
<b>Primers used for generation of HLH20 and rod mini constructs</b>	
HLH20/U	CTGAGCGCCTGGCTGCAGGATGCCA
HLH20/L	GAATTCCTCGGGTTAGCCTCCACGGACGGG
Rod mini/U	CCATGGAATTCGGGAGGATTCTGAGCAACGCGGAGGACACA
Rod mini/L	AAGCTTAGAATTCGCCGAGCCGATCCAGCATGTTCTG

Numbers in plectin primers indicate the position of the 5' end of the primer in the cDNA sequence of mouse plectin starting with exon 2 (see Appendix)



## 6. Antibodies and enzyme conjugates

### Primary Antibodies

**Table 10**

Directed against	Type & Host	Epitope	Dilution	Reference
$\alpha$ -Actinin	monoclonal, mouse	n.d.	1:1000 (WB); 1:500 (IF)	Sigma-Aldrich
BPAG1	monoclonal, mouse	n.d.	1:100 (IF)	Hashimoto et al. 1993
Desmin	polyclonal, rabbit	n.d.	1:80 (IF)	Sigma-Aldrich
Desmoplakin	monoclonal, mouse	n.d.	1:10 (IF)	Progen Biotechnik
Integrin $\alpha 6$	monoclonal, rat	n.d.	1:100 (IF)	BD Bioscience
Integrin $\beta 4$	monoclonal, rat	C-term.	1:300 (WB); 1:100 (IF)	S. J. Kennel et al. 1989
Keratin 10	monoclonal, mouse	n.d.	1:400 (IF)	Chemicon IHC/Millipore
Keratin 5	rabbit	C-term.	1:2000 (WB); 1:1000 (IF)	BAbCO/Covance
Keratin 6	rabbit	C-term.	1:2500 (WB); 1:1000 (IF)	BAbCO/Covance
Keratine 5, 6, 18	monoclonal, mouse	n.d.	1:100 (IF)	Dako, Denmark
plectin #46	polyclonal, rabbit	rod	1:100 (WB; IF)	Åndra et al. 2003
plectin #9	polyclonal, rabbit	exon 9-12	1:3000 (WB)	Åndra et al. 2003
plectin 10F6	monoclonal	rod	1:2 (WB)	Foisner et al. 1994
plectin 1a	polyclonal, rabbit	exon 1a	1:500 (WB); 1:1000 (IF)	Fuchs et al. 2009
plectin 1c	polyclonal, rabbit	exon 1c	1:1000 (WB)	Åndra et al. 2003
plectin 6B8	monoclonal	rod	1:2 (WB)	Foisner et al. 1994
plectin 7A8	monoclonal	rod	1:2 (WB)	Foisner et al. 1994

IF, immunofluorescence microscopy; WB, Western blot analysis.

### Secondary antibodies

**Table 11**

Directed against	Enzyme conjugate	Host	Dilution	Source
rabbit	Texas red	Goat	1:200 (IF)	Jackson ImmunoResearch Lab.
rabbit	Alexa FluorTM 488	Goat	1:800 (IF)	Molecular Probes
mouse-IgG	Texas red	Goat	1:200 (IF)	Jackson ImmunoResearch Lab.
mouse-IgG	Alexa FluorTM 488	Goat	1:800 (IF)	Molecular Probes
rabbit	Texas red	Donkey	1:200 (IF)	Jackson ImmunoResearch Lab.
???	Alexa FluorTM 488	Donkey	1:3000 (IF)	Molecular Probes
mouse-IgG	Cy5	Donkey	1:400 (IF)	Jackson ImmunoResearch Lab.
rabbit	Cy-5	Goat	1:400 (IF)	Jackson ImmunoResearch Lab.
rat-IgG	Cy2	Goat	1:100 (IF)	Jackson ImmunoResearch Lab.
rabbit-AP	AP	Goat	1:5000 (WB)	Jackson ImmunoResearch Lab.
rabbit-HRPO	HRPO	Goat	1:10000 (WB)	Jackson ImmunoResearch Lab.
mouse-IgG	AP	Goat	1:5000 (WB)	Jackson ImmunoResearch Lab.
mouse-IgG	HRPO	Goat	1:10000 (WB)	Jackson ImmunoResearch Lab.

IF, immunofluorescence microscopy; WB, Western blot analysis; AP, alkaline phosphatase; HRPO, horseradish peroxidase.

## Methods

### 1. Molecular Biology: DNA and RNA

#### ***Isolation of genomic DNA from cells and mouse tails***

ES cell clones were incubated in 750 µl of lysis buffer at 55°C overnight on an eppendorf thermomixer with gentle agitation. For removal of proteins, 50 µl 6 M NaCl were added, mixed vigorously and centrifuged at 14000 rpm for 10 minutes at RT in an eppendorf centrifuge. 750 µl of the supernatant was transferred to a fresh tube and the genomic DNA was precipitated by addition of 500 µl isopropanol, incubation at -20°C for 30 min, and centrifugation at 14000 rpm for 10 minutes at RT. The pellet was washed with 70% EtOH, briefly centrifuged again, air-dried, dissolved in 100 µl dH<sub>2</sub>O and incubated at 37°C for several hours.

For isolation of genomic DNA from mouse tails, a piece (0.5 cm) of tail was cut and incubated in 750 µl of lysis buffer. All steps were performed as described above.

#### ***Phenol-purification and precipitation of DNA***

Extraction of DNA with phenol-chloroform-isoamyl alcohol (PCI 25:24:1, Saturated with 10 mM Tris, pH 8.0, 1 mM EDTA, Sigma-Aldrich) was performed by adding an equal volume of PCI to the DNA solution, mixing by vortexing for 15 seconds and centrifuging at 14000 rpm for 1 minute (Eppendorf centrifuge). The aqueous phase was transferred to a new tube and extracted with chloroform twice.

Precipitation of DNA was done by adding 1/10 volume of 3 M NaOAc, pH 5.2 and 2.5 volumes of ice-cold EtOH. The mixture was incubated at -20°C for 30 minutes and centrifuged at 14000 rpm, for 20 minutes, at room temperature (Eppendorf centrifuge). TE buffer, pH 8.0.

#### ***Quantification of DNA and RNA***

Determination of the DNA concentration was performed using UV spectrophotometry. OD<sub>260</sub>=1.0 corresponds to 50 µg/ml of DNA or 40 µg/ml RNA. °

#### ***Polymerase chain reaction***

For genotyping of transgenic mice polymerase chain reactions (PCR) were performed in a total volume of 25 µl [2.5 µl 10x PCR buffer, 0.75 µl 50 mM MgCl<sub>2</sub>, 0.5 µl dNTPs (10 mM each), 0.5 µl of each primer (10 pmol/µl), 0.5 µl Taq-polymerase (5 U/µl) and 1 µl template DNA] according to the recommendations of the manufacturer (Invitrogen). The The Gene Amp<sup>®</sup> PCR System 2400 (Perkin Elmer)/9700 (Applied Biosystems) was used

as the thermal cycler. Amplification conditions are given below:

Cycles	Denaturation		Annealing		Extension	
1x	94°C	5 min				
35x	94°C	30 sec	62°C	30 sec	72°C	90 sec
1x					72°C	7 min
1x					4°C	∞

PCR products were analyzed on a 0.8-1.8% agarose gel.

For cloning and expression constructs amplification of DNA was done using ELONGase (Life Technologies), a high fidelity polymerase mix. The PCR reaction mixture consisted of 4 µl 2.5 mM dNTPs (200 µM each), 2 µl forward and 2 µl reverse primer both at 10 µM (400 nM each), 25 ng template DNA, 2 µl elongase buffer A, 8 µl elongase buffer B, 1 µl elongase enzyme, and water to a final volume of 50 µl. The conditions of amplification were 94°C for 30 sec, followed by 25 cycles of 60 sec at 94°C, 30 sec at 55°C, and 90 sec at 68°C, and a final extension of 7 min at 68°C. To facilitate cloning of the PCR products into a vector carrying 3' T-overhangs (pCR2.1, Invitrogen), 3' A-overhangs were attached after amplification by adding 1 unit of Taq polymerase to each reaction and incubating at 72°C for 10 minutes.

### ***Preparation of plasmid DNA***

Small scale preparation of plasmid DNA from bacteria was carried out according to the method of Birboim (1983). Large scale preparation of plasmid DNA was performed using JetStar columns according the manufacturer's protocol (Genomed). Plasmid DNA of sequencing quality was prepared using a spin miniprep kit (Qiagen).

### ***Digestion of DNA with restriction enzymes***

For analytical purposes plasmid DNA (0.5-1.0 µg) was digested with 2-5 units of restriction enzyme in a volume of 20 µl according to the instructions of the manufacturer. Incubation time ranged from 1 hour to overnight.

For preparative digestions 5 µg of DNA were digested in a total volume of 50 µl with a 2-fold excess enzyme (2 units/µg DNA/number of cuts. The reaction was incubated for 2-3 hours, the DNA dephosphorylated, if required, and loaded onto an agarose gel.

### ***Dephosphorylation of vector DNA***

Dephosphorylation of 5'-ends of digested DNA was performed by calf intestine phosphatase (CIP, Promega). The DNA mixture from previous step was treated with 7 µl of 10x CIP buffer and 2 sequential additions of 0.5 µl CIP (1 unit/µl). The reaction was incubated at 37 C for 15 min and subsequently loaded onto an agarose gel.

**Separation of DNA by agarose gel electrophoresis**

Agarose was suspended in 1x TAE and heated in the microwave. After cooling down of the solution, ethidium bromide was added to a final concentration of (0.1 µg/ml), and the gel poured into a casting tray. The DNA samples were mixed with 1/10 of 10x DNA loading buffer and loaded into the gel slots, which were previously covered with 1x TAE. Gels were run at 80-120 V. After electrophoresis, the DNA was visualized by placing the gel on a UV light source and photographed (BioRad GelDoc XR+) for further analyses.

**Recovery of DNA from agarose gels.**

Under UV light, the DNA band was excised from the agarose gel and placed in an eppendorf tube. The DNA was purified using the QIAEX Gel Extraction Kit (Qiagen) according to the instructions of the manufacturer.

**Ligation**

Ligations were carried out in a total volume of 10 µl. A typical reaction contained vector and insert in a molar ratio of 1:3 to 1:4, 1x ligation buffer and 1-5 units of T4-DNA ligase. The reactions were incubated overnight at 16°C.

**Preparation of competent bacteria and transformation**

Competent bacteria for electroporation were prepared by inoculation of 1000 ml LB-medium with an overnight culture of bacteria (1/100 volume). Bacterial cells were grown at 37°C to an OD<sub>600</sub> of 0.5 then, cooled on ice for 15 minutes. Cells were pelleted at 3500 rpm, for 20 minutes at 4°C. The pellet was washed twice with ice-cold autoclaved dH<sub>2</sub>O (1000 and 500 ml respectively) and one time in 40 ml ice-cold, sterile 10% glycerol. The glycerol-washed pellet was centrifuged at 4100 rpm for 10 minutes at 4°C, and the harvested cells resuspended in 4 ml ice-cold, sterile 10% glycerol. Aliquots of the electro-competent bacterial cells were either used immediately or frozen in liquid nitrogen and stored at -80°C.

Alternatively, the TSB method (Chung et al. 1989) for preparation of competent bacteria was used. Bacterial cultures were grown overnight in LB medium, diluted 1/100 into 50ml of LB and grown at 37°C to and OD<sub>600</sub> of 0.5. After incubation on ice for 10 min, harvesting and centrifugation (4000 rpm, 10 min, 4°C), cells were pelleted, resuspended in 2 ml of ice-cold TSS solution and incubated on ice for 60 min. Cells were aliquoted, shock-frozen in liquid nitrogen, and kept at -80°C for long-term storage.

For transformation by electroporation, electrocompetent cells (100 µl aliquots) were thawed on ice and the DNA added. The cell/DNA mixtures were transferred to pre-chilled cuvettes (BioRad) and immediately electroporated using a BioRad Gene Pulser set at 25µF, 600Ω. After addition of 1 ml pre-warmed LB-medium to each cuvette, the cells were transferred to 2 ml eppis, incubated at 37°C for 30-60 minutes with shaking, and plated onto LB-agar plates containing the appropriate antibiotics.

For transformation by the TSB method, the DNA was mixed with 5x KCM, brought to a total volume of 100 µl with sterile H<sub>2</sub>O, and added to 100 µl of thawed competent cells. The cell/DNA mix was incubated on ice for 20 minutes and kept for 20 min at RT. After the addition of 200 µl of LB, the cells were incubated at 37 °C for 20-30 min, and plated on the LB-agar plates with the required antibiotic selection.

### ***Preparation of bacterial stocks***

1 ml of cultured bacteria were pelleted by centrifugation, resuspended in 0.5 ml of fresh LB medium or LB medium with the appropriate selection, and mixed with 0.25 ml of sterile 60% glycerol in a cryo-tube, making sure that the glycerol was evenly dispersed. The cultures were shock-frozen in liquid nitrogen and stored at -80°C.

### ***DNA sequencing***

The nucleotide sequence was determined by the dideoxynucleotide chain termination method using fluorescence methodology and an automated capillary DNA sequencer (ABI Prism 3100, Applied Biosystems). Sequencing reactions were done in a total volume of 10 µl containing 0.3 µg dsDNA, 2.5 µM primer and 4 µl sequence mix (Big-Dye v. 3.1 Terminator Cycle Sequencing Kit, Applied Biosystems). PCR amplification was performed using a Gene Amp PCR system 9700 (Perkin Elmer) and the following conditions: 96°C for 30 sec, followed by 25 cycles of 10 sec at 96°C, 5 sec at 50°C, and 4 min at 60°C.

Sequencing of PCR products. After amplification, PCR products were loaded onto an agarose gel, visualized and purified as described above (Recovery of DNA from agarose gels, p98). Depending on the size of the product 40-100 ng of DNA were taken for sequencing. The amplicons were sequenced with primers different from the ones used for their generation.

Sequence data were edited and analyzed by the programs "EditSeq" and "SeqMan" (DNA Star Inc., Madison, USA).

### ***Southern blot analysis***

10 µg of genomic DNA were digested with 30-40 units of a restriction enzyme in a total volume of 300 µl. The digested DNA was precipitated with NaOAc/EtOH, redissolved in 40 µl TE, pH 8.0 and separated by agarose gel electrophoresis (0.8% gel). Depurination of the DNA was done by soaking the gel once for 15 minutes in 500 ml of 0.25 M HCl and denatured twice for 15 minutes in 500 ml of denaturation solution. Semi-dry electrophoretic transfer of the DNA fragments to a nylon membrane (PALL Biodyne<sup>®</sup>B, pore size 0.45 µm) was carried out overnight. Following transfer, the membrane was neutralized for 1 minute in 0.2 M Tris/HCl pH 7.5, 1x SSC, baked for 30 minutes at 80°C and crosslinked using UV light (120 mJ/cm<sup>2</sup>, Stratalinker 2400, Stratagene). Hybridization probes were labeled with  $\alpha$ -<sup>32</sup>P dCTP using the Prime-it II random labeling kit (Stratagene). Labeled probes were purified with ProbeQuant<sup>™</sup> G-50 Micro columns (Amersham Pharmacia Biotech), and their activity measured by Cerenkov counting (Liquid Scintillation Analyzer, Packard). Prehybridization was carried out in Church buffer for 2-3 hours at 65°C in sealable glass tubes. Before hybridization, the labeled probe was denatured at 95°C for 5 minutes, cool on ice for 3 min and added to Church buffer. Hybridization was done overnight at 65°C. Unbound probe was removed by washing the membrane three times for 20 minutes at 65°C with Church wash buffer. The membrane was wrapped in a thin plastic foil and exposed to an X-ray sensitive film (Fuji medical X-ray film HR-E30) at -80°C using an intensifying screen.

### ***Isolation of RNA***

Total RNA was isolated from mouse tissues and primary cells using TRIzol (Life Technologies). RNA preparations were quantified in a NanoDrop (ND-2000, Thermo Scientific).

### ***RNA electrophoresis***

Electrophoresis of RNA was performed under denaturing conditions in 2.2 M formaldehyde (Lehrach et al. 1977). Agarose (1%) was suspended in 1x MOPS, heated, and formaldehyde added to a final concentration of 2.2 M (8 ml 37% formaldehyde for a 45 ml gel). The gel was run at 60 V in the cold room until the dye has migrated 2/3 of the gel. The 18S and 28S rRNA bands should be visible in an intact RNA sample.



### **Reverse Transcription and RT-PCR**

RNA (1 µg) was reverse transcribed into cDNA using the SuperScript III reverse transcriptase (Invitrogen), random hexamer primers (Fermentas) and RNasin plus (Promega) following the instructions of the manufacturers. RNA was also transcribed using a plectin specific primer, mPle 8029/L located on exon 32. The resulting cDNAs were diluted 1:5 and amplified using Advantage cDNA polymerase (Clontech, BD), a touch-down protocol and a nested PCR approach. For the first round, primers mPle31/U5464 and mPle32/L7714 located within exons 31 and 32 were chosen to amplify a 2251 bp product that included the site of the Ogn mutation and the exons 31/32 border. The reaction was loaded onto an agarose gel and the 2251 bp DNA fragment eluted by centrifugal filtration through a polyester plug (Glenn and Glenn 1994). For the nested PCR, 1/10 of the previous PCR product was amplified with primers 13575 and mPle32/L7384 also located within exons 31 and 32. PCR conditions were:

Cycles	Denaturation		Annealing		Extension	
1x	94°C	45 sec				
5x	94°C	7 sec	72°C	45 sec	68°C	3 min
5x	94°C	7 sec	70°C	45 sec	68°C	3 min
30x	94°C	9 sec	68°C	45 sec	68°C	3 min
1x					68°C	7 min
1x					4°C	∞

The nested PCR product, 1803 bp in length, was isolated from an agarose gel, purified using QIAEX (Qiagen), and sequenced.

For an independent confirmation a second set of cDNAs were amplified using GoTaq polymerase (Invitrogen) and primers 13253 and pHLH20 L4m located within exons 31 and 32. The 2760 bp product generated was then used for a nested amplification with internal primers 13575 and mPleEx31/32 L (its 3' end goes over the exon 31/32 splicing site). Amplification conditions were: 3 min at 94°C and 40 cycles of 94°C for 30 sec, 63°C for 30 sec and 72°C for 3.5 or 2 min, followed by 5 min extension at 72°C. Also in this case the nested PCR product was recovered and sequenced.

### **Real Time quantitative PCR (RT-qPCR)**

RT-qPCR was done as described in Walko et al. (2011). RNA (1 µg) was reverse transcribed, the resulting cDNAs diluted 1:5 with TE buffer pH 8.0 and stored in aliquots at -80°C until used. Primer pairs were designed using Primer3 (<http://frodo.wi.mit.edu/primer3>). The amplicons ranged from 100 to 120 base pairs and spanned an intron. RT-qPCR was performed in duplicates in 96-well plates on

Lightcycler 480 (Roche Diagnostics). Reactions were carried out in 20 µl final volume using SYBR detection (SYBR Green I Master Mix, Roche Diagnostics). Crossing point values (Cp) values were obtained by the second derivative maximum method, all calculations were done by the software supplied with the instrument. In absolute quantification transcript copy numbers were calculated using a standard curve based on serial dilutions of the same exons cloned into plasmids. Relative quantification was done by the method of Pfaffl. The housekeeping gene hypoxanthine guanine phosphoribosyl transferase 1 (HPRT1) was used for normalization.

## **2. Biochemistry: protein expression, purification, and interactions**

### ***Expression of recombinant proteins in insect cells***

Insect cells Sf9 were cultured in T-175 flasks. At an 80% confluence the culture was infected with 1 ml of viral stock and incubated at 27°C for 72 hours. Cells were collected by centrifugation at 2500 rpm for 5 minutes, washed once with PBS, and either resuspended in lysis buffer or frozen for later use.

### ***Purification of recombinant proteins***

#### ***Lysis of the cells***

Harvested Sf9 cells were resuspended in lysis buffer (1.5 ml per T-175 culture) and incubated on ice for 15 min with occasional vortexing. The disrupted cells were centrifuged at 14000 rpm, for 15 min at 4 C, and the supernatants collected.

#### ***Spin Column Purification***

His-tagged proteins were purified by affinity chromatography using TALONspin™ Columns (BD Biosciences). GST-tagged proteins were purified using MicroSpin™ GST Purification columns (Amersham Biosciences). All procedures were done according to the instructions of the manufacturer. Briefly, columns were equilibrated with lysis buffer and the cell lysate applied to the top of the column. After a brief spin (3000 rpm) the columns were washed twice with wash buffer and bound proteins eluted with 200 µl of elution buffer. The elution step was repeated once, the eluates combined and analyzed by SDS-PAGE. Purified proteins were stored at -20°C after addition of 10% glycerol.

#### ***FPLC Purification***

High scale purification was performed on Äkta FPLC system (GE Healthcare) using HiTrap chelating HP or GSTrap 5 ml columns. His-tagged fusion proteins were bound to

Co<sup>2+</sup>-charged columns in either Hepes buffer or NaPhosphate buffer and eluted with a linear gradient of 0–500 mM imidazole in Hepes buffer or NaPhosphate buffer, respectively. GST-tagged proteins were bound in PBS and eluted with 50 mM Tris-HCl, pH 8.0, 10 mM glutathione. Collected fractions were analysed on SDS-PAGE. Fractions containing purified proteins were pooled, and their protein content quantified (Bradford reagent, BioRad), before being stored at 4°C, -20°C and -80°C.

### ***Preparation of cell and tissue extracts***

For the preparation of total cell lysates confluent cells were washed once with PBS and scraped off using a rubber policeman in the presence of 2x SDS-PAGE sample buffer.

Preparation of soluble cell lysates. Cells grown to confluence on 10 cm tissue culture plates were washed twice with cold PBS prior to the addition of 1 ml of cold lysis buffer. The cells were then scraped off using a rubber policeman, transferred to an eppendorf tube, and incubated for 10 min at RT. At this point Triton X-100 was added to reach a final concentration of 1%, and the cells were incubated for other 5 min at RT. Insoluble matter was pelleted by centrifugation (14000 rpm, 20 min, 4°C) in a microfuge. The supernatant, soluble cell lysate, was transferred to a new eppendorf tube, and the pellet resuspended in 2x SDS-PAGE sample buffer.

Keratin preparation from immortalized keratinocytes. Cells were washed in PBS, scraped off with a rubber policeman, transferred to an eppendorf tube, and incubated with solution A for 1 hour at 4°C. Following centrifugation (14000 rpm, 20 min, 4°C), the supernatant was removed and the pellet homogenized in solution B. After incubation for 60 min, at 4°C, the homogenate was spun down (14000 rpm, 20 min, 4°C) and the pellet (insoluble fraction rich in keratins) resuspended in 30 µl 2x SDS-PAGE sample buffer. Supernatants were stored at -20°C after addition of 6x sample buffer.

Mouse tissues were excised, shock frozen and pulverized in liquid nitrogen. Lysis buffer was added (1 µl/mg of tissue), and tissues homogenized using a Polytron PT 3000 Kinematic homogenizer and centrifuged at 12000 rpm, at 4°C. Samples were incubated for 5 min at RT in an equal volume of 2x SDS-PAGE sample buffer. Insoluble material was removed by centrifugation (14000 rpm, 2 min, RT). Samples were heated to 95°C before SDS-PAGE.

### ***Protein quantification***

The concentration of protein was measured according to Bradford (1976) using bovine serum albumin as standard. Protein samples were diluted with 150 mM NaCl. 5–20 µl of

diluted samples were added to 1 ml of Bradford solution, mixed and incubated for 5 minutes at RT. The absorbance at 595 nm was measured in a spectrophotometer. For higher accuracy the bicinchoninic Acid (BCA) Protein Assay kit (Pierce) was also used to determine protein concentration.

### ***SDS-polyacrylamide gel electrophoresis (PAGE)***

SDS-PAGE was performed according to Laemmli (1970) using the Mini-Protean system from Biorad. Typical polyacrylamide concentrations ranged from 5 to 12% depending upon the molecular weight of the proteins of interest. Prior to loading the protein samples on the gel, they were denatured by boiling for 5 min at 95°C in sample buffer. Running conditions were 20 mA (constant current) per minigel in a 1x running buffer. After electrophoresis, the gel was rinsed with dH<sub>2</sub>O, incubated in Coomassie G-250 staining solution for ~20 minutes at RT, and destained by several changes of destaining solution.

### ***Native and blue native (BN) – PAGE***

Preparation of native PAGE gels was as described for SDS-PAGE but in the absence of SDS in all buffers. BN-PAGE was carried using the bistris-tricine system (Wittig et al. 2006) and the discontinuous tris-histidine system (Niepmann and Zheng 2006). Samples were resolved in 4–10% polyacrylamide gradient gels. Gels were run at constant voltage (100 V) in the cold room (4°C).

### ***Size exclusion chromatography (SEC) – gel filtration***

Size exclusion chromatography was performed on a Superose-6 10/300 GL column by FPLC (GE Healthcare UK Ltd. Buckinghamshire, UK). FPLC purified proteins were applied to the column that was ran at a flow rate of 0.5 ml/min. To determine molecular weight, the same column was run in identical conditions with molecular weight standards thyroglobulin (669 kDa), ferritin (440 kDa), catalase (232 kDa), aldolase (158 kDa), albumin (67 kDa) and ovoalbumin (45 kDa). Collected fractions were analyzed by SDS-PAGE analysis immediately after separation and probed by immunoblot analyses with anti-plectin antibodies.

### ***Buffer exchange and microdialysis***

NAP-25 (GE Healthcare) and Bio-Spin 6 (BioRad) desalting column were used for buffer exchange according to the instructions of the manufacturer. Microdialysis was performed in microfuge tubes with a dialysis membrane covering the open end of the tube as described in Current Protocols in Immunology (1997; A.3H.2-A.3H.3).

**Cross-linking experiments**

Dimethyl suberimidate (DMS) (Pierce), a bisimidoester which reacts with primary amino groups on protein molecules was used as the cross-linker. Purified recombinant proteins (5-15 $\mu$ g) were incubated with 20mg/ml DMS in 20mM Hepes pH 7.4 for 1 hour at room temperature. Reaction was stopped by adding 6x sample buffer containing 18% SDS (final concentration 3%). Cross-linked proteins were separated on 5 or 6% SDS-PAGE.

**Immunoblotting**

After SDS-PAGE proteins were transferred onto a nitrocellulose membrane (Schleicher & Schuell) using a Mini Protean II wetblotting chamber (BioRad). The electrophoretic transfer was performed in transfer buffer at constant current (40 mA/12 hours or 400 mA/2hours) and at 4°C. After the transfer, the nitrocellulose membranes were washed with H<sub>2</sub>O, stained with Ponceau-S staining solution, examined to evaluate the efficiency of the transfer, and destained by washing with H<sub>2</sub>O. Blocking was done either for 1 hour at RT or overnight at 4°C, in a solution containing 5% milk powder in PBST or 3% BSA in PBS. The membrane was washed with PBST, and incubated with the primary antibody (previously diluted in PBST) for 1 hour at RT. Unbound primary antibody was washed away with three changes of PBST and the membrane incubated with the secondary antibody for 1 hour at RT. After another three washes with PBST the secondary antibody was detected by enhanced chemiluminescence (ECL, Super Signal West Pico System, Pierce). X-Ray film (Fuji medical X-ray film HR-E30) was exposed to the membranes and developed. Alternatively, membranes were incubated in AP (alkaline phosphatase) buffer. The AP-reaction was ended by addition of H<sub>2</sub>O/20 mM EDTA (pH 8.0).

**Quantification of protein bands in gels and immunoblots**

Quantiscan software (Biosoft) was used to quantify protein bands after electrophoresis in polyacrylamide gels and immunoblots.

**Pull-downs**

To demonstrate protein interactions Co<sup>2+</sup>-charged beads and glutathione Sepharose beads pull-downs were performed after Sf9 cells were infected with baculovirus encoding GST-fusion proteins of interaction partner 1 (e.g. Rod<sub>wt</sub>) and HIS-fusion proteins of interaction partner 2 (e.g. Rod<sub>O<sub>gna</sub></sub>). Typically 1x10<sup>6</sup> Sf9 cells in 6-well plates were infected with 100  $\mu$ l of each viral stock. Infected cells were collected after 72 hours, lysed and the soluble cell lysate bound to beads. After extensive washing the bound proteins, and its associated

partners, were eluted with sample buffer and analyzed by SDS-PAGE and detected by immunoblotting with the indicated antibodies.

To search for new binding partners of the Ogn<sub>a</sub>-Rod, 200 µl of Sf9 infected cell lysate or 3.5 µg of purified GST-Rod<sub>Ogn<sub>a</sub></sub> protein in PBS were added to 200 µl (bed volume) Glutathione Sepharose beads 4B (Pharmacia) and incubated for 1 hour at 4°C with head-to tail rotation. After extensive washing with PBS and removal of traces of supernatant with a 27G needle, 1 ml of mouse keratinocytes cell lysate prepared under native conditions (see below) was added to the beads and the mixture incubated overnight at 4°C with head-to-tail rotation. Next day, the keratinocyte lysate was removed by centrifugation (3500 rpm, 5 min, RT) and the beads were washed three times with keratinocyte lysis buffer. The beads were then resuspended in 40 µl keratinocyte lysis buffer + 40 µl 5x SDS-sample buffer, boiled for 5 min and 10 µl supernatant resolved in a 10% SDS-PAGE. Sf9 cell lysate, purified GST-Rod<sub>wt</sub> and GST proteins treated in a similar way were used as controls. Subtraction pull-downs were done by sequential incubation of the mouse keratinocyte lysate with GST-Rod<sub>wt</sub>-coupled glutathione Sepharose beads first, and with GST-Rod<sub>wt</sub>-coupled beads afterwards

For detection by silver staining, the gel was incubated for at least one hour to overnight in fixing solution, then washed three times (20 min each) in 50% ethanol. The gel was immersed for 1 minute in sensitizing solution, rinsed three times (20 sec) in H<sub>2</sub>O and incubated in staining solution for 20 minutes in the dark. After washing twice (20 sec) in H<sub>2</sub>O, the gel was placed in developing solution until bands appeared. The gel was washed twice (2 min) in water, and the reaction stopped by incubation (10 min) in stopping solution. The gel was rinsed in 20% methanol with a drop of glycerol.

### **Overlay binding assay**

A mouse keratin prep was blotted onto a nitrocellulose membrane. The membrane was blocked with 4% BSA in 0.1% PBST (overnight at 4°C), and afterwards overlaid with full-length plectin rod, either wild-type or mutant Ogn<sub>a</sub> HIS-Rod<sub>wt</sub> and HIS-Rod<sub>Ogn<sub>a</sub></sub>, (both at a final concentration of 10µg/ml) in 20mM Hepes pH 7.4). After 3 hours incubation, membranes were thoroughly washed with 0.05% PBST. For detection of bound proteins, membranes were incubated with plectin mAb 10F6 (1:1000 in 0.05% PBST) for 1 hour, followed by HRP-coupled goat anti-mouse antisera (1:10000 in 0.05% PBST). Membranes were washed three times with PBST five minutes and detection was done by ECL (Super Signal West Pico kit, Pierce).



### 3. Cell Culture

#### ***Insect cell culture***

Fall Armyworm *Spodoptera frugiperda* (Sf9) cells were grown at 27°C in Insect Express medium (Lonza) supplemented with 10% FCS, 2 mM glutamine (Invitrogen) and antibiotics (50 units/ml penicillin and 50 µg/ml streptomycin). For routine maintenance cells were split 1:10 to 1:20 two times per week. Cell viability of Sf9 cells was checked by mixing equal volumes of cell suspension and Trypan Blue (0.4% in PBS), and counting viable and dead (stained) cells under an inverted microscope.

Freezing and thawing. Cells from 80% confluent flasks were resuspended in pre-chilled cryopreservation medium (Insect Express containing 10% FCS and 7.5% DMSO) at a density of  $1-2 \times 10^7$  Sf9 cells/ml. Frozen cells were thawed in a 37°C water bath, transferred to a Falcon tube, washed with 3 ml of fresh medium and spun down at 1200 rpm for 5 min. The cell pellet was resuspended in 3 ml fresh medium, and used to seed a T75 flask.

#### ***Mammalian cell culture***

##### ***Maintenance of mouse cell lines***

Frozen cells were thawed in a 37°C water bath, washed in growth medium, and pelleted by centrifugation (1000 rpm, 3 min). The cell pellet was resuspended in fresh growth medium, seeded into an appropriate cell culture dish and incubated at 37°C in a humidified atmosphere containing 5% CO<sub>2</sub>. For splitting of cells, the cell monolayer was washed with PBS and incubated with trypsin (0.05% trypsin, 0.2% EDTA) for 5 minutes at 37°C. The reaction was stopped by addition of 3 volumes of fresh medium. Detached cells were transferred to a tube, spun down (Heraeus Megafuge, 1000 rpm, 3 minutes), resuspended in medium and split at the desired ratio into new culture dishes. For freezing, the cells were trypsinized, resuspended in freezing medium (growth medium with 12.5% DMSO), aliquoted into cryotubes, stored at -80°C for 24 hours and then transferred to a liquid nitrogen tank.

##### ***Isolation of primary basal keratinocytes***

Newborn mice (1-2 day after birth) were sacrificed, limbs and tail were amputated, and the skin was detached making a longitudinal incision from neck to tail. The skin patch was placed in a Petri dish with the dermis side down and then floated on Dispase II for 30 minutes at 37°C. Afterwards, the dermis was separated from the epidermis using forceps. The epidermis was then minced using sterile razorblades and incubated in trypsin/EDTA

(0.05% trypsin, 0.2% EDTA) for 10 minutes at 37°C, to obtain single cells. The cell suspension was filtered through a 70 µm cell strainer to remove cornified sheets, washed in KGM (keratinocyte growth medium) and pelleted by centrifuging at 800 rpm for 5 min. Keratinocytes were resuspended in fresh KGM solution, and seeded on collagen I pre-coated cell culture plates. [3 or 5 ml of collagen I solution (Sigma-Aldrich) 1:10 in PBS were used to coat 6 or 10 cm plates, respectively; the plate were incubated for 2 hours at 37°C and washed with PBS prior to use]. Cells from one mouse skin were seeded in two cell culture dishes (5.5 cm Ø) and incubated at 37°C, 5% CO<sub>2</sub>. After keratinocyte attachment, cells were washed with PBS to remove unattached cells. Medium was changed every other day.

#### ***Transient transfection of mouse keratinocytes***

FuGENE 6 reagent (Roche) was used for transfections according to the manufacturer's instructions. Cells were seeded at low densities onto glass coverslips or cell culture dishes 3-24 hours prior to transfection. For transfection of cells in one 5.5 cm dish, 8 µl FuGENE 6 were diluted into 200 µl serum-free medium, mixed gently, and 5 µg of plasmid DNA added. After the mixture was incubated for 30 minutes at RT, 300 µl of serum-free medium were added, mixed again, and the suspension added drop wise to the culture dish. 18 hours post-transfection, the transfection mix was removed from the cells, and the cells washed with growth medium, incubated in freshly added medium overnight, and analyzed by different techniques.

#### ***Maintenance of embryonic stem (ES) cells***

ES cells of low passage number were maintained on a layer of inactivated murine embryonic fibroblasts (MEFs) that have to be seeded one day before splitting the ES cells. ES cells were grown in ES medium (high glucose DMEM medium with 18,5% fetal calf serum [FCS], 2 mM glutamine, 1 mM sodium pyruvate, 1% non essential amino acids, 1% penicillin/streptomycin, 0.1 mM 2-mercaptoethanol and 0,25% leukemia inhibitory factor [LIF]). ES cells were split in a ratio 1:3 to 1:8 after a short trypsinization (2 min at 37°C).

MEF were grown in MEF medium and split 1:3 to 1:5 when confluent. For inactivation, cells were treated with mitomycin C (Sigma Aldrich) at a concentration of 10 µg/ml for 2-3 hours. The drug was removed by two washes with PBS and the cells resuspended in fresh MEF medium. LIF was obtained from supernatants of cultured cos-7 cells grown for 48 hours in high glucose DMEM with 18.5% FCS, 2 mM glutamine, 1 mM sodium pyruvate 1% non essential amino acids, 1% 0.1 mM 2-mercaptoethanol. The

supernatant was cleared by centrifugation at 4000 rpm for 20 minutes, aliquoted and frozen at -20°C.

### ***Electroporation of ES cells with targeting vector***

One day prior to electroporation ES cells were split 1:2 to 1:3. On the day of electroporation ES cells were washed with PBS, trypsinized, resuspended in fresh medium and counted. An aliquot containing  $8 \times 10^6$  cells was taken, washed twice with PBS, and resuspended in 700  $\mu$ l PBS; then 30  $\mu$ g *SacI* linearized DNA diluted in 100  $\mu$ l PBS were added to the cell suspension. The electroporation was performed in a BioRad Gene Pulser, with the following setting: 800 V field strength, 3  $\mu$ F capacitance. After zapping, the electroporated cell suspension was transferred to a 15 ml tube containing 10 ml of ES medium and seeded at different densities on separated cell culture dishes coated with MEFs. Selection with geneticin (G418, Life Technologies) at a concentration of 500  $\mu$ g/ml was started 24 hours after electroporation. Medium was changed daily. ES cell clones were grown until colonies were visible (8-10 days); at this point 80-120 clones were picked for expansion and analysis. Picked ES cell clones were transferred to a 96-well microtiter plate, treated with 100  $\mu$ l trypsin for 3-4 min at 37 C, and the resulting single cell suspension was transferred to a 24-well plate coated with inactivated MEFs, and grown in fresh growth medium for 2-4 days. Half of ES cells from each clone were frozen (freezing medium is growth medium plus 25% DMSO) and the other half was further grown for several days and used for preparation of genomic DNA and genotypic analysis.

## **4. Histology**

### ***Preparation of tissue sections***

Tissues were surgically removed and shock frozen in liquid nitrogen-cooled isopentane. Sections of 2  $\mu$ m were prepared on a cryomicrotome (Cryostat HM 500 OM), fixed with acetone at -20°C and stored at -80°C for further processing. Alternatively, adult mice were fixed in situ by perfusion with 2.5% paraformaldehyde, 0.5% glutaraldehyde in PBS, pH 7.5, at 37°C via intercardiac puncture (Spazierer et al. 2006). For transmission electron microscopy sections were fixed in 3% glutaraldehyde in Sorensens buffer, pH 7.5 overnight at 4°C, then treated with 1.5% OsO<sub>4</sub>, dehydrated in ascending concentrations of ethanol, and embedded in epoxy resin. Semithin (~1  $\mu$ m) and ultrathin (70 nm) sections for structural analysis were cut with an ultramicrotome (Ultracut S, Leica

Microsystems) and stored at -80°C. Sections were prepared in collaboration with I. Fischer.

### ***Staining of tissue sections***

Semithin sections embedded with epoxy-resin were heated at 80°C for 2 min and stained with filtered toluidine blue solution (Unicryl, staining kit) for 1 min. Samples were washed with water, briefly rinsed with dH<sub>2</sub>O and dried at 80°C for 2 minutes. Mounting was done with Histofluid.

## **5. Immunofluorescence and cell assays**

### ***Immunofluorescence and phase contrast microscopy of tissue sections and cells***

Frozen tissue sections, were thawed, air-dried for 30 minutes. Samples were blocked in 2% BSA in PBS, incubated with primary antibodies (60 min, RT), washed three times with PBS, incubated with fluorescence-labeled secondary antibodies (60 min, RT), washed again three times with PBS and once with dH<sub>2</sub>O, and mounted in mowiol. Samples were examined using a Zeiss LSM 510 microscope equipped with Plan-Apochromat (40x/1.3NA, 63x/1.4NA and 100x/1.4NA) objective lenses. Digital images were processed using LSM 5 image browser and Adobe software package.

Cells were grown on glass coverslips or on cell culture dishes, washed with PBS, and fixed with 4% paraformaldehyde in PBS for 20 minutes at RT, or in pre-chilled (-20°C) methanol for 90 seconds. After washing with PBS, cells were permeabilized with 0.1% Triton X-100 in PBS for 5 minutes. Samples were blocked with 4% BSA in PBS (60 min, RT), and incubated with primary and secondary antibodies (as above). After mounting in mowiol, the samples were dried overnight at RT. Microscopy and processing as above.

### ***Electron microscopy***

Electron microscopy was performed by S. Reipert as described in Reipert et al. (2004). Thin sections for ultrastructural analysis were cut with an ultramicrotome (Ultracut S, Leica Microsystems), mounted on copper grids, counterstained with uranyl acetate and lead citrate, and examined at 80 kV in an electron microscope (JEOL JEM-1210, Jeol Ltd.). Images were acquired using a digital camera (Morada, Olympus SIS).

***Time-lapse video microscopy of single cells***

Keratinocytes were plated on collagen I pre-coated culture dishes at low density ( $2.5 \times 10^5$  cells/cm<sup>2</sup>) and kept in KGM/0.3 mM Ca<sup>2+</sup>. Migrating cells were monitored in parallel in a PM S1 incubator (Carl Zeiss MicroImaging) using the “mark and find” module of Axio Vision 4.8.1 image analysis software. Recordings were started 6 hours after plating and frames were taken in 10 min intervals over a period of 12 hours. Axio Vision 4.8.1 image analysis software was used to process the images. Migration speed was calculated from the total length of trajectories of the central nuclei over 12 hours. Statistics are based on the analysis of 30-40 cells per construct (GFP-tagged wild-type and Ogn1 mutant full-length P1a, or GFP alone) and three independent experiments.

***Scratch wound closure assay***

Primary keratinocytes were seeded at high density onto culture dishes pre-coated with collagen I and grown in KGM/0.05 M Ca<sup>2+</sup>. After reaching confluence, a scratch was made within the cell monolayer using a sterile p200 pipette tip. Remnants of scraped and detached cells were washed away with PBS and growth medium. Cell migration into the artificial wound was assessed at different times (16 or 24 hours). Images were made on a phase contrast microscope. Alternatively, 16 hr post-scratch, cells were fixed with methanol and processed for immunofluorescence microscopy using anti-actin and anti-keratin antibodies. Image acquisition was done using a fluorescent laser-scanning microscope (LSM 510, Carl Zeiss) equipped with a Plan-Apochromat 10x/0.45NA objective lens. The number of keratin positive cells migrating into the scratch was counted in randomly chosen fields along the scratch wound (Walko et al. 2011).

***Morphometric analysis of Hemidesmosomes***

This analysis was performed as described in Walko et al. (2011). Ultrathin sections of tongue and foot pad skin were examined by electron microscopy and electron micrographs of the dermal-epidermal junction were taken. Each micrograph was used to measure the total length of basal cell membrane of basal keratinocytes and the length of each individual HD. The software packages iTEM and analySIS FIVE (Olympus SIS) was used for this analysis. With these parameters we calculated for each electron micrograph the percentage of cross-sectioned basal cell membrane of basal keratinocytes containing HDs and the size of HDs. The average percentage of HDs with associated keratin IF bundles was analyzed by scoring similar numbers of HDs (~600) per genotype for keratin IF bundle attachment.

**Quantification of HPC formation in cultured keratinocytes**

HPC formation was induced by growing cells in KGM with the addition of 0.3 mM  $\text{Ca}^{2+}$ . Cells were fixed with methanol and immunostained using anti-integrin  $\alpha 6$  and anti-plectin antibodies as described in Walko et al. (2011). Colocalization of integrin  $\alpha 6$  and plectin in dense clusters at the basal cell surface was scored as HPC-positive. Cells that did not fulfill this criterion were scored as HPC-negative.

**Hypo-osmotic shock**

Primary keratinocytes isolated from newborns were seeded onto collagen I pre-coated culture dishes at very low density to allow single cell visualization and cultured for 24 hours. After removal of the medium, the cells washed with PBS and incubated in medium supplemented with 150 mM urea for 2 min. Then, the culture was briefly washed with PBS and fixed with methanol.

**6. Mice**

Experiments using mice were carried out in accordance with Austrian Federal Government laws.

**Generation of heterozygous and homozygous mice**

Correctly targeted ES cells were injected into blastocysts isolated from C57BL/6 at day 3.5 postcoitum and transferred into pseudopregnant C57BL/6XCBA females to generate chimeric offsprings that were distinguished by their agouti coat color. Female chimeras were mated with C57BL/6XCBA males and the F1 progeny genotyped for germline transmission. F1 mice heterozygous for the Ogn mutation were then crossed to Cre deleter mice (Schwenk et al. 1995) and their offspring screened for the removal neo<sup>r</sup> cassette by means of Southern blot analysis of tail DNA digested with *HindIII*. Wild-type, heterozygous and homozygous littermate mice used in experiments were obtained by mating heterozygous *Plec*<sup>Ogn<sup>+</sup>/+</sup> mice.

Mice were kept under standard housing conditions at the animal facility of the Institute of Biochemistry and Molecular Cell Biology at the Vienna Biocenter.

**Dye penetration assay**

Newborn mice were sacrificed by over-dose treatment of isofluoran (600  $\mu\text{l}$ ; Richter Pharma, Wells, Austria). The entire body of each animal was dehydrated through a series of 1-min incubations in increasing methanol concentrations (25%, 50%, 75% and 100%

in PBS) and rehydrated by 1-min incubations in decreasing methanol concentrations (75%, 50%, and 25%). Mice were washed in PBS and stained with 0.1% toluidine blue O (Sigma) in PBS for 1 minute. Destaining was performed in PBS. Areas where the dye had penetrated (skin barrier disruption areas) were photographed and analyzed.

### ***Tape stripping and transepidermal water loss (TEWL)***

Newborn mice were sacrificed as described above. Back skin was then repeatedly stripped with Tesa 3M cellophane tape. For each strip a fresh tape was lightly pressed over the skin area and pulled off with forceps. Transepidermal water loss (TEWL) was measured after every strip using an evaporimeter (ServoMed, Stockholm, Sweden) as described in Spazierer et al. (2006). TEWL values were registered in g/m<sup>2</sup>/h.

### ***Voluntary wheel-running***

Two months old mice were placed into separate cages of bigger dimensions than usual (140 mm x 207 mm x 367 mm), equipped with a metal hamster wheel (diameter 145 mm, Petsmart) attached to a bicycle computer (Sigma Sport, BC 800). Voluntary wheel running was monitored for 3 weeks, daily with recording values for running distance, running time, running speed and maximal speed (Konieczny et al. 2008).

## **7. Statistics**

Statistical data are presented as mean  $\pm$  SD. Comparisons between two groups were done by the Student's t test (data shown in Figure 49). Comparisons among multiple groups were done by one-way analysis of variance (ANOVA) with Tukey's post hoc test (data shown Figures 28, 46, 50) or by two-way ANOVA followed by Bonferroni post hoc test (data shown Figures 22, 43, 48). P values less than 0.05 with a 95% confidence interval were considered significant. The asterisks denote the significance levels. \*P < 0.05; \*\*P < 0.01; \*\*\*P < 0.001. Ute Jungwirth helped with the statistical analysis using GraphPad Prisma v5.



## REFERENCES

- Ackerl R, Walko G, Fuchs P, Fischer I, Schmuth M, Wiche G. (2007). Conditional targeting of plectin in prenatal and adult mouse stratified epithelia causes keratinocyte fragility and lesional epidermal barrier defects. *J Cell Sci.* 120:2435-2443.
- Andrä K, Lassmann H, Bittner R, Shorny S, Fassler R, Propst F, Wiche G. (1997). Targeted inactivation of plectin reveals essential function in maintaining the integrity of skin, muscle, and heart cytoarchitecture. *Genes Dev.* 11:3143-3156.
- Andrä K, Kornacker I, Jörgl A, Zörer M, Spazierer D, Fuchs P, Fischer I, Wiche G. (2003). Plectin-isoform-specific rescue of hemidesmosomal defects in plectin (-/-) keratinocytes. *J Invest Dermatol.* 20:189-197.
- Armel TZ, Leinwand LA. (2009). Mutations in the beta-myosin rod cause myosin storage myopathy via multiple mechanisms. *Proc Natl Acad Sci U S A.* 106:6291-6296.
- Astrin, K. H., Arredondo-Vega, F. X., Desnik, R. J. and Smith, M. (1982). Assignment of the gene for cytosolic alanine aminotransferase (AAT1) to human chromosome 8. *Ann Hum Genet.* 46:125-133.
- Banwell B L, Russel J, Fukudome T, Shen XM, Stilling G, Engel AG. (1999). Myopathy, myasthenic syndrome, and epidermolysis bullosa simplex due to plectin deficiency. *J Neuropathol Exp Neurol.* 58:832-846.
- Birnboim HC. (1983). A rapid alkaline extraction method for the isolation of plasmid DNA. *Methods Enzymol.* 100:243-255.
- Bolling MC, Jongbloed JD, Boven LG, Diercks GF, Smith FJ, McLean WH, Jonkman .F. (2014). Plectin mutations underlie epidermolysis bullosa simplex in 8% of patients. *J. Invest. Dermatol.* 134:273-276.
- Bouameur JE, Favre B, Borradori L. (2014). Plakins, a versatile family of cytolinkers: roles in skin integrity and in human diseases. *J Invest Dermatol.* 134:885-894.
- Boyer JG, Bernstein MA, Boudreau-Larivière C. (2010). Plakins in striated muscle. *Muscle Nerve* 41:299-308.
- Bradford MM. (1976). A rapid and sensitive method for the quantitation of microgram quantities of protein utilizing the principle of protein-dye binding. *Anal. Biochem.* 72:248-254.
- Breitenbach J. (2007). Studies Towards the Role of the Ogn Mutation in Plectin Dimerization. Diploma Thesis. University of Vienna.
- Burra S, Jiang, JX. (2011). Regulation of cellular function by connexion hemichannels, *Int J Biochem Mol Bio.* 2:119-128.
- Chiavérini C, Charlesworth A, Meneguzzi G, Lacour JP, Ortonne JP. (2010). Epidermolysis bullosa simplex with muscular dystrophy. *Dermatol Clin.* 28:245-255.
- Choi HJ, Park-Snyder S, Pascoe LT, Green KJ, Weis WI. (2002). Structures of two intermediate filament-binding fragments of desmoplakin reveal a unique repeat motif structure. *Nat Struct Biol.* 9:612-620.
- Chung HJ, Uitto J. (2010). Epidermolysis bullosa with pyloric atresia. *Dermatol Clin.* 28:43-54.
- Chung CT, Niemela SL, Miller RH. (1989). One-step preparation of competent *Escherichia coli*: transformation and storage of bacterial cells in the same solution. *Proc Natl Acad Sci U S A* 86:2172-2175.
- Clubb BH, Chou YH, Herrmann H, Svitkina TM, Borisy GG, Goldman RD. (2000). The 300-kDa intermediate filament-associated protein (IFAP300) is a hamster plectin ortholog. *Biochem Biophys Res Commun.* 273:183-187.

- Coulombe PA, Wong P. (2004). Cytoplasmic intermediate filaments revealed as dynamic and multipurpose scaffolds. *Nat Cell Biol.* 6:699-706.
- D'Alessandro M, Russell D, Morley SM, Davies AM, Lane EB. (2002). Keratin mutations of epidermolysis bullosa simplex alter the kinetics of stress response to osmotic shock. *J Cell Sci.* 115:4341-4351.
- de Pereda JM, Ortega E, Alonso-García N, Gómez-Hernández M, Sonnenberg A. (2009). Advances and perspectives of the architecture of hemidesmosomes. *Cell Adh Mig.* 3:361-364.
- Démarchez M. (2011). The dermal-epidermal junction. *Biology of Skin.*
- Eger A, Stockinger A, Wiche G, Foisner R. (1997). Polarisation-dependent association of plectin with desmoplakin and the lateral submembrane skeleton in MDCK cells. *J Cell Sci.* 110:1307-1316.
- Elliott, C. E., Becker, B., Oehler, S., Castanon, M. J., Hauptmann, R. and Wiche, G. (1997). Plectin transcript diversity: identification and tissue distribution of variants with distinct first coding exons and rodless isoforms. *Genomics*, 42, 115-25.
- Fine JD, Bruckner-Tuderman L, Eady RAJ, Bauer EA, Bauer JW, Has C, Heagerty A, Hintner H, Hovnanian A, Jonkman MF et al. (2014). Inherited epidermolysis bullosa: Updated recommendations on diagnosis and classification. *J. Am. Acad. Dermatol.* 70:1103-1126.
- Fletcher DA, Mullins RD. (2010). Cell mechanics and the cytoskeleton. *Nature* 28; 463:485-92.
- Foisner R, Wiche G. (1987). Structure and hydrodynamic properties of plectin molecules. *J Mol Biol.* 198:515-531.
- Foisner R, Feldman B, Sander L, Wiche G. (1991). Monoclonal antibody mapping of structural and functional plectin epitopes. *J Cell Biol.* 112:397-405.
- Foisner R, Malecz N, Dressel N, Stadler C, Wiche G. (1996). M-phase-specific phosphorylation and structural rearrangement of the cytoplasmic cross-linking protein plectin involve p34cdc2 kinase. *Mol. Biol. Cell* 7:273-288.
- Forrest K, Mellerio JE, Robb S, Dopping-Hepenstal P J, McGrath JA, Liu L, Buk S J, Al-Sarraj S, Wraige E, Jungbluth H. (2010). Congenital muscular dystrophy, myasthenic symptoms and epidermolysis bullosa simplex (EBS) associated with mutations in the PLEC1 gene encoding plectin. *Neuromuscul Disord.* 20:709-711.
- Fuchs E. (2008). Skin stem cells: rise to the surface. *J Cell Biol.* 80:273-284.
- Fuchs E, Cleveland DW. (1998). A structural scaffolding of intermediate filaments in health and disease. *Science* 279:514-519.
- Fuchs P, Zorer M, Rezniczek GA, Spazierer D, Oehler S, Castanon MJ, Hauptmann R, Wiche G. (1999). Unusual 5' transcript complexity of plectin isoforms: novel tissue-specific exons modulate actin binding activity. *Hum Mol Genet.* 8:2461-7242.
- Fuchs P, Zörer M, Reipert S, Rezniczek GA, Propst F, Walko G, Fischer I, Bauer J, Leschnik MW, Lüscher B, Thalhammer JG, Lassmann H, Wiche G. (2009). Targeted inactivation of a developmentally regulated neural plectin isoform (plectin 1c) in mice leads to reduced motor nerve conduction velocity. *J Biol Chem.* 284:26502-26509.
- Furuse, M. (2010). Molecular basis of the core structure of tight junction. *Cold Spring Harb Perspect Biol.* a002907.
- Gache Y, Chavanas S, Lacour JP, Wiche G, Owaribe K, Meneguzzi G, Ortonne JP. (1996). Defective expression of plectin/HD1 in epidermolysis bullosa simplex with muscular dystrophy. *J Clin Invest.* 97:2289-2298.
- García-Alvarez B, Bobkov A, Sonnenberg A, de Pereda JM. (2003). Structural and functional analysis of the actin binding domain of plectin suggests alternative mechanisms for binding to F-actin and integrin beta4. *Structure* 11:615-625.

- Gedde-Dahl T Jr. (1971). Epidermolysis bullosa. A clinical, genetic and epidemiological study. Universitetsforlaget Oslo. Johns Hopkins University Press, Baltimore.
- Geerts D, Fontao L, Nievers MG, Schaapveld RQ, Purkis PE, Wheeler GN, Lane EB, Leigh IM, Sonnenberg A. (1999). Binding of integrin  $\alpha 6 \beta 4$  to plectin prevents plectin association with F-actin but does not interfere with intermediate filament binding. *J Cell Biol.* 147, 417-434.
- Glenn TC, Glenn SJ. (1994). Rapid elution of DNA from agarose gels using polyester plug spin inserts (PEPSIs). *Trends Genet.* 10:344.
- Goodenough DA, Paul DL. (2009). Gap junctions. *Cold Spring Harb Perspect Biol.* 1:a002576. doi: 10.1101
- Gostyńska KB, Nijenhuis M, Lemmink H, Pas HH, Pasmooij AM, Lang KK, Castañón MJ, Wiche G, Jonkman MF. (2015). Mutation in exon 1a of PLEC, leading to disruption of plectin isoform 1a, causes autosomal-recessive skin-only epidermolysis bullosa simplex. *Hum Mol Genet.* Feb 24. pii: ddv066.
- Green KJ, Gaudry CA (2000). Are desmosomes more than tethers for intermediate filaments. *Nat Rev Mol Cell Bio.* 1:208-216.
- Green KJ, Virata ML, Elgart GW, Stanley JR, Parry DA. (1992). Comparative structural analysis of desmoplakin, bullous pemphigoid antigen and plectin: members of a new gene family involved in organization of intermediate filaments. *Int J Biol Macromol.* 14:145-153.
- Gundesli H, Talim B, Korkusuz P, Balci-Hayta B, Cirak S, Akarsu NA, Topaloglu H, Dincer P. (2010). Mutation in exon 1f of PLEC, leading to disruption of plectin isoform 1f, causes autosomal-recessive limb-girdle muscular dystrophy. *Am J Hum Genet.* 87:834-841.
- Hartsock A, Nelson WJ (2008). Adherens and tight junctions: structure, function and connections to the actin cytoskeleton. *Biochem Biophys Acta* 1778:660-669
- Hieda Y, Nishizawa Y, Uematsu J, Owaribe K. (1992). Identification of a new hemidesmosomal protein, HD1: a major, high molecular mass component of isolated hemidesmosomes. *J Cell Biol* 116:1497-1506.
- House C M, Frew IJ, Huang HL, Wiche G, Traficante N, Nice E, Catimel B, Bowtell DD. (2003). A binding motif for Shiah ubiquitin ligase. *Proc Natl Acad Sci U S A* 100:3101-3106.
- Janda L, Damborský J, Rezniczek GA, Wiche G. (2001). Plectin repeats and modules: strategic cysteines and their presumed impact on cytolinker functions. *Bioessays* 23:1064-1069.
- Jefferson JJ, Leung CL, Liem RK (2004). Plakins: goliaths that link cell junctions and the cytoskeleton. *Nature Reviews Molecular Cell Biology* 5:542-553.
- Kaufmann E, Geisler N, Weber K. (1984). SDS-PAGE strongly overestimates the molecular masses of the neurofilament proteins. *FEBS Lett.* 170:81-84.
- Ketema M, Sonnenberg A. (2011). Nesprin-3: a versatile connector between the nucleus and the cytoskeleton. *Biochem Soc Trans.* 39:1719-1724.
- Kielty CM, Povey S, Hopkins DA. (1982). Regulation of expression of liver-specific anzymes. II. Activation and chromosomal localization of soluble glutamate-pyruvate transaminase. *Ann Hum Genet.* 46:135-143.
- Kiritisi D, Pigors M, Tantcheva-Poor I, Wessel C, Arin MJ, Kohlhase J, Bruckner-Tuderman L, Has C. (2013). *J Invest Dermatol.* 133:270-273. Epidermolysis bullosa simplex ogna revisited.
- Konieczny P, Fuchs P, Reipert S, Kunz W S, Zeöld A, Fischer I, Paulin D, Schröder R, Wiche G. (2008). Myofiber integrity depends on desmin network targeting to Z-disks and costamers via distinct plectin isoforms. *J Cell Biol.* 181:667-681.

- Koss-Harnes D, Jahnsen FL, Wiche G, Soyland E, Brandtzaeg P, Gedde-Dahl T Jr. (1997). Plectin abnormality in epidermolysis bullosa simplex Ogna: non-responsiveness of basal keratinocytes to some anti-rat plectin antibodies. *Exp Dermatol.* 6:41-48.
- Koss-Harnes D, Høyheim B, Anton-Lamprecht I, Gjest A, Jørgensen RS, Jahnsen FL, Olaisen B, Wiche G, Gedde-Dahl T Jr. (2002). A site-specific plectin mutation causes dominant Epidermolysis bullosa simplex Ogna: Two identical *de novo* mutations. *J Invest Dermatol.* 118:87-93.
- Koss-Harnes, D. (2005). Epidermolysis bullosa due to plectin mutations. Role of plectin and its possible associations to skin diseases. Faculty of Medicine. University of Oslo.
- Koster J, Geerts D, Favre B, Borradori L, Sonnenberg A. (2003). Analysis of the interactions between BP180, BP230, plectin and the integrin alpha6beta4 important for hemidesmosome assembly. *J Cell Sci.* 116:387-399.
- Koster J, van Wilpe S, Kuikman I, Litjens SH, Sonnenberg A. (2004). Role of binding of plectin to the integrin beta4 subunit in the assembly of hemidesmosomes. *Mol Biol Cell* 15:1211-1223.
- Koszka C, Leichtfried FE, Wiche G. (1985). Identification and spatial arrangement of high molecular weight proteins (Mr 300 000-330 000) co-assembling with microtubules from a cultured cell line (rat glioma C6). *Eur J Cell Biol.* 38:149-156.
- Kim S, Kellner J, Lee CH, Coulombe PA. (2007). Interaction between the keratin cytoskeleton and eEF1Bgamma affects protein synthesis in epithelial cells. *Nat Struct Mol Biol.* 14:982-983.
- Kim S, Coulombe PA. (2010). Emerging role for the cytoskeleton as an organizer and regulator of translation. *Nat Rev Mol Cell Biol.* 11:75-81.
- Kraus M, Pao LI, Reichlin A, Hu Y, Canono B, Cambier JC, Nussenzweig MC, Rajewsky K. (2001). Interference with immunoglobulin (Ig)alpha immunoreceptor tyrosine-based activation motif (ITAM) phosphorylation modulates or blocks B cell development, depending on the availability of an Igbeta cytoplasmic tail. *J Exp Med.* 194:455-69.
- Kunz M, Rouan F, Pulkkinen L, Hamm H, Jeschke R, Bruckner-Tuderman L, Bröcker EB, Wiche G, Uitto J, Zillikens D. (2000). Mutation reports: epidermolysis bullosa simplex associated with severe mucous membrane involvement and novel mutations in the plectin gene. *J Invest Dermatol.* 114:376-380.
- Laemmli UK. (1970). Cleavage of Structural Proteins during the Assembly of the Head of Bacteriophage T4. *Nature* 227: 680 – 685.
- Lehrach H, Diamond D, Wozney JM, Boedtker H. (1977). RNA molecular weight determinations by gel electrophoresis under denaturing conditions, a critical reexamination. *Biochemistry* 16:4743-4751.
- Le Sourd F, Boulben S, Le Bouffant R, Cormier P, Morales J, Belle R, Mulner-Lorillon O. (2006). eEF1B: At the dawn of the 21st century. *Biochim Biophys Acta* 1759:13-31.
- Lieska N, Yang HY, Goldman RD. (1985). Purification of the 300K intermediate filament-associated protein and its in vitro recombination with intermediate filaments. *J Cell Biol.* 101:802-813.
- Litjens SH, de Pereda JM, Sonnenberg A. (2006). Current insights into the formation and breakdown of hemidesmosomes. *Trends Cell Biol.* 16:376-383.
- Liu CG, Maercker C, Castanon MJ, Hauptmann R, Wiche G. (1996). Human plectin: organization of the gene, sequence analysis, and chromosome localization (8q24). *Proc Natl Acad Sci U S A* 93:4278-4283.
- Lunter PC, Wiche G. (2002). Direct binding of plectin to Fer kinase and negative regulation of its catalytic activity. *Biochem Biophys Res Commun.* 296:904-910.

- Ludwiczek ML, Baminger B, Konrat R. (2004). NMR probing of protein-protein interactions using reporter ligands and affinity tags. *J Am Chem Soc.* 126:1636-1637.
- Maiweilidan Y1, Klauza I, Kordeli E. (2011). Novel interactions of ankyrins-G at the costameres: the muscle-specific Obscurin/Titin-Binding-related Domain (OTBD) binds plectin and filamin C. *Exp Cell Res.* 317:724-736.
- Malecz N, Foisner R, Stadler C, Wiche G. (1996). Identification of plectin as a substrate of p34cdc2 kinase and mapping of a single phosphorylation site. *J Biol Chem.* 271:8203-8208.
- Maselli R, Arredondo J, Cagney O, Mozaffar T, Skinner S, Yousif S, Davis R, Gregg J, Sivak M, Konia T, Thomas K, Wollmann RL. (2011). Congenital myasthenic syndrome associated with epidermolysis bullosa caused by homozygous mutations in PLEC1 and CHRNE. *Clin Genet.* 80:444-451.
- Mihailovska E, Raith M, Valencia RG, Fischer I, Al Banchaabouchi M, Herbst R, Wiche G. (2014). Neuromuscular synapse integrity requires linkage of acetylcholine receptors to postsynaptic intermediate filament networks via rapsyn-plectin 1f complexes. *Mol Biol Cell* 25:4130-4149.
- Natsuga K. (2014). Plectin-related skin diseases. *J Dermatol Sci.* doi:10.1016
- Niepmann M, Zheng J. (2006). Discontinuous native protein gel electrophoresis. *Electrophoresis* 27:3949-3951.
- Nikolic B., Mac Nulty E, Mir B, Wiche G. (1996). Basic amino acid residue cluster within nuclear targeting sequence motif is essential for cytoplasmic plectin-vimentin network junctions. *J. Cell Biol.* 134, 1455-1467.
- Okumura M, Uematsu J, Hirako Y, Nishizawa Y, Shimizu H, Kido N, Owaribe K (1999). Identification of the hemidesmosomal 500 kDa protein (HD1) as plectin. *J Biochem.* 126:1144-1150
- Olaisen B, Gedde-Dahl TJr. (1973). GTP-epidermolysis bullosa simplex (EBS Ogna) linkage in man. *Hum Hered.* 23:189-96.
- Ortega E, Buey R M, Sonnenberg A, de Pereda JM. (2011). The structure of the plakin domain of plectin reveals a non-canonical SH3 domain interacting with its fourth spectrin repeat. *J Biol Chem,* 286:12429-12438.
- Osmanagic-Myers S, Gregor M, Walko G, Burgstaller G, Reipert S, Wiche G. (2006). Plectin-controlled keratin cytoarchitecture affects MAP kinases involved in cellular stress response and migration. *J Cell Biol.* 174:557-568.
- Pfaffl MW. (2001). A new mathematical model for relative quantification in realtime RT-PCR. *Nucleic Acids Res* 29: 2002-2007.
- Pfendner E, Uitto J. (2005). Plectin gene mutations can cause epidermolysis bullosa with pyloric atresia. *J Invest Dermatol.* 124:111-115.
- Pytela R, Wiche G. (1980). High molecular weight polypeptides (270,000-340,000) from cultured cells are related to hog brain microtubule-associated proteins but copurify with intermediate filaments. *Proc Natl Acad Sci U S A* 77, 4808-4012.
- Raymond K1, Kreft M, Janssen H, Calafat J, Sonnenberg A. (2005). Keratinocytes display normal proliferation, survival and differentiation in conditional beta4-integrin knockout mice. *J Cell Sci.* 118:1045-1060.
- Reipert S, Fischer I, Wiche G. (2004). High-pressure cryoimmobilization of murine skin reveals novel structural features and prevents extraction artifacts. *Exp Dermatol.* 13:419-425.
- Rezniczek GA, de Pereda JM, Reipert S, Wiche G. (1998). Linking integrin alpha6beta4-based cell adhesion to the intermediate filament cytoskeleton: direct interaction between the beta4 subunit and plectin at multiple molecular sites. *J Cell Bio.* 141, 209-225.

- Rezniczek GA, Abrahamsberg C, Fuchs P, Spazierer D, Wiche G. (2003). Plectin 5'-transcript diversity: short alternative sequences determine stability of gene products, initiation of translation and subcellular localization of isoforms. *Hum Mol Genet.* 12, 3181-3194.
- Rezniczek GA, Walko G, Wiche G. (2010). Plectin gene defects lead to various forms of epidermolysis bullosa simplex. *Dermatol Clin.* 28:33-41
- Rocha J, Amorim A, Almeida V M, Oliveira JP, Leão M, Tavares MC, Pereira MS, Vidal-Pinheiro L. (1988). Gene dosage evidence for the regional assignment of GTP (glutamate-pyruvate transaminase; E. C> 2.6.1.2) locus to 8q24.2-8qter. *Hum Genet.* 80:299-300.
- Schägger H, Cramer WA, von Jagow G. (1994). Analysis of molecular masses and oligomeric states of protein complexes by blue native electrophoresis and isolation of membrane protein complexes by two-dimensional native electrophoresis. *Anal Biochem.* 217:220-230.
- Schara U1, Tücke J, Mortier W, Nüsslein T, Rouan F, Pfendner E, Zillikens D, Bruckner-Tuderman L, Uitto J, Wiche G, Schröder R. (2004). Severe mucous membrane involvement in epidermolysis bullosa simplex with muscular dystrophy due to a novel plectin gene mutation. *Eur J Pediatr.* 163:218-222.
- Schoenenberger CA, Mannherz HG, Jockusch BM. (2011). Actin: from structural plasticity to functional diversity. *Eur J Cell Biol.* 90:797-804.
- Schwenk F, Baron U, Rajewsky K. (1995). A cre-transgenic mouse strain for the ubiquitous deletion of loxP-flanked gene segments including deletion in germ cells. *Nucleic Acids Res.* 23:5080-5081.
- Selcen D, Juel V C, Hobson-Webb L D, Smith EC, Stickler DE, Bite AV, Ohno K, Engel AG. (2011). Myasthenic syndrome caused by plectinopathy. *Neurology* 6:327-336.
- Sevcík J, Urbániková L, Kostan J, Janda L, Wiche G. (2004). Actin-binding domain of mouse plectin. Crystal structure and binding to vimentin. *Eur J Biochem.* 271:1873-1884.
- Shimizu H, Masunaga T, Kurihara Y, Owaribe K, Wiche G, Pulkkinen L, Uitto J, Nishikawa T. (1999). Expression of plectin and HD1 epitopes in patients with epidermolysis bullosa simplex associated with muscular dystrophy. *Arch Dermatol Res.* 291:531-537.
- Smith FJ, Eady RA, Leigh IM, McMillan JR, Rugg EL, Kelsell DP, Bryant SP, Spurr NK, Geddes JF, Kirtschig G, Milana G, de Bono AG, Owaribe K, Wiche G, Pulkkinen L, Uitto J, McLean WH, Lane EB. (1996). Plectin deficiency results in muscular dystrophy with epidermolysis bullosa. *Nat Genet.* 13:450-457.
- Simpson CL, Patel DM, Green KJ. (2011). Deconstructing the skin: cytoarchitectural determinants of epidermal morphogenesis. *Nat Rev Mol Cell Biol.* 12:565-580.
- Smythe GM, White JD. (2012). Voluntary wheel running in dystrophin-deficient (mdx) mice: Relationships between exercise parameters and exacerbation of the dystrophic phenotype. *PLoS Curr.* doi:10.1371/currents. RRN1295.
- Sohocki MM, Sullivan LS, Harrison WR, Sodergren EJ, Elder FF, Weinstock G, Tanase S, Daiger SP. (1997). Human glutamate pyruvate transaminase (GTP): localization to 8q24.3, cDNA and genomic sequence, and polymorphic sites. *Genomics* 40:247-252.
- Sonnenberg, A. and Liem, R. K. (2007). Plakins in development and disease. *Experimental Cell Research*, 313: 2189-2203.
- Sonnenberg A, Rojas AM, de Pereda JM. (2007). The structure of a tandem pair of spectrin repeats of plectin reveals a modular organization of the plakin domain. *J Mol Biol.* 368:1379-1391.

- Spazierer D, Fuchs P, Reipert S, Fischer I, Schmuth M, Lassmann H, Wiche G. (2006). Epiplakin is dispensable for skin barrier function and for integrity of keratin network cytoarchitecture in simple and stratified epithelia. *Mol Cell Biol.* 26:559-568.
- Stegh AH., Herrmann H, Lampel S, Weisenberger D, Andrä K, Seper M, Wiche G, Krammer PH, Peter ME. (2000). Identification of the cytolinker plectin as a major early in vivo substrate for caspase 8 during CD95- and tumor necrosis factor receptor-mediated apoptosis. *Mol Cell Biol.* 20:5665-5679.
- Tsuruta D, Hashimoto T, Hamill KJ, Jones JC. (2011). Hemidesmosomes and focal contact proteins: functions and cross-talk in keratinocytes, bullous diseases and wound healing. *J Dermatol Sci.* 62:1-7.
- Wade RH. (2009). On and around microtubules: an overview. *Mol Biotechnol.* 43:177-191.
- Walko G, Vukasinovic N, Gross K, Fischer I, Sibitz S, Fuchs P, Reipert S, Jungwirth U, Berger W, Salzer U, Carugo O, Castañón MJ, Wiche G. (2011). Targeted proteolysis of plectin isoform 1a accounts for hemidesmosome dysfunction in mice mimicking the dominant skin blistering disease EBS-Ogna. *PLoS Genet.* 7:e1002396.
- Walko G, Castañón MJ, Wiche G. (2014). Molecular architecture and function of the hemidesmosome. *Cell Tissue Res.* [Epub ahead of print] PMID:25487405
- Wiche G. (1989). Plectin: general overview and appraisal of its potential role as a subunit protein of the cytomatrix. *Crit Rev Biochem Mol Biol.* 24:41-67.
- Wiche G. (1998). Role of plectin in cytoskeleton organization and dynamics. *J Cell Sci.* 111:2477-2486.
- Wiche G, Baker MA. (1982). Cytoplasmic network arrays demonstrated by immunolocalization using antibodies to a high molecular weight protein present in cytoskeletal preparations from cultured cells. *Exp Cell Res.* 138:15-29.
- Wiche G, Herrmann H, Leichtfried F, Pytela R. (1982). Plectin: a high molecular weight cytoskeletal polypeptide component that copurifies with intermediate filaments of the vimentin type. *Cold Spring Harbor Symp. Quant. Biol.* 46: 475-482.
- Wiche G, Krepler R, Artlieb U, Pytela R, Denk H. (1983). Occurrence and immunolocalization of plectin in tissues. *J Cell Biol.* 97:887-901.
- Wiche G, Krepler R, Artlieb U, Pytela R, Aberer W. (1984). Identification of plectin in different human cell types and immunolocalization at epithelial basal cell surface membranes. *Exp Cell Res.* 155:43-49.
- Wiche G, Becker B, Lubert K, Weitzer G, Castañón MJ, Hauptmann R, Stratowa C, Stewart M. (1991). Cloning and sequencing of rat plectin indicates a 466-kD polypeptide chain with a three-domain structure based on a central alpha-helical coiled coil. *J Cell Biol.* 114:83-99.
- Wiche G, Winter L. (2011). Plectin isoforms as organizers of intermediate filament cytoarchitecture. *Bioarchitecture* 1:14-20.
- Wiche G, Osmanagic-Myers S, Castañón MJ. (2014). Networking and anchoring through plectin: a key to IF functionality and mechanotransduction. *Curr Opin Cell Biol.* 32C:21-29.
- Wilhelmsen K, Litjens SH, Kuikman I, Tshimbalanga N, Janssen H, van den Bout I, Raymond K, Sonnenberg A. (2005). Nesprin-3, a novel outer nuclear membrane protein, associates with the cytoskeletal linker protein plectin. *J Cell Biol.* 171:799-810.
- Winter L, Wiche G. (2013). The many faces of plectin and plectinopathies: pathology and mechanisms. *Acta Neuropathol.* 125:77-93.
- Wittig I, Braun HP, Schagger H. (2006). Blue native PAGE. *Nat Protoc.* 1:418-428.



- Yang R, Bartle S, Otto R, Stassinopoulos A, Rogers M, Plamann L, Hartzell P. (2004). AglZ is a filament-forming coiled-coil protein required for adventurous gliding motility of *Myxococcus xanthus*. *J Bacteriol.* 186:6168-6178.

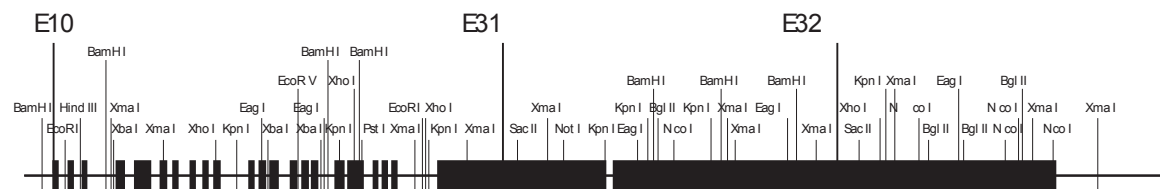
## APPENDIX

### Cloning of the targeting vector

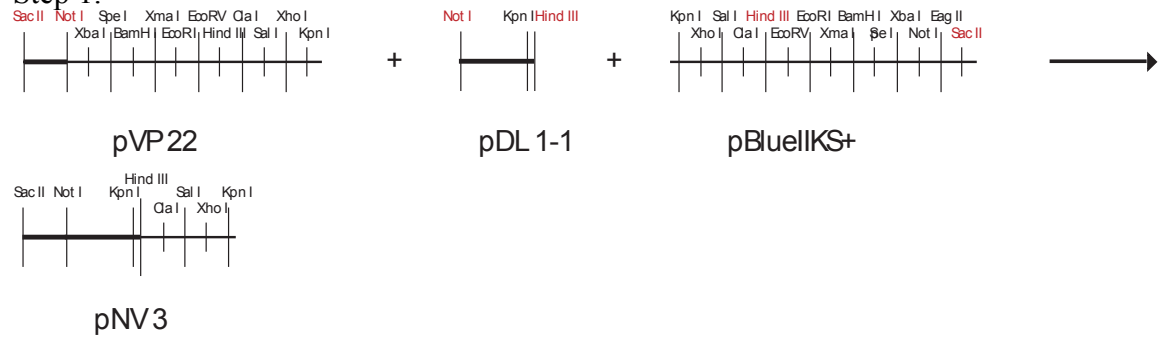
Construction of the targeting vector required nine cloning steps. First, the multicloning site of pBSIIKS<sup>+</sup> was modified to contain the restriction sites needed for later cloning steps. Thus, to generate pNV1 one pair of overlapping synthetic oligonucleotides, MCSogna1, were annealed and subcloned into *KpnI* and *EcoRV* sites of pBSIIKS<sup>+</sup>. Next, the oligonucleotide pair MCSogna2 were subcloned into *EcoRV* and *SacII* sites of pNV1, to generate pNV2.

Second, the left arm of the targeting vector was constructed in four steps. In first step, DNA fragments excised from pVP22 using *SacII* and *NotI* and from pDL1-1 using *NotI* and *HindIII*, were ligated into the *SacII* and *HindIII* sites of pBSIIKS<sup>+</sup>, to yield pNV3. To generate pNV4 a 3.1 kb-fragment spanning from exon 15 to 24 was excised from pKA9 with *XmaI*, *EcoRV* and inserted into the corresponding sites of pBSIIKS<sup>+</sup>. Next, pNV5 was generated by simultaneous ligation of three fragments,–an *EcoRV/SacII* 5.6 kb-fragment from KA9 spanning exon 24 to 31, the *SacII /HindIII* adapter excised from pNV3, and pBSIIKS<sup>+</sup> digested with *EcoRV* and *HindIII*.–Finally, plasmid pNV6 was created by subcloning the *SpeI/EcoRV* fragment excised from pNV4 into pNV5.

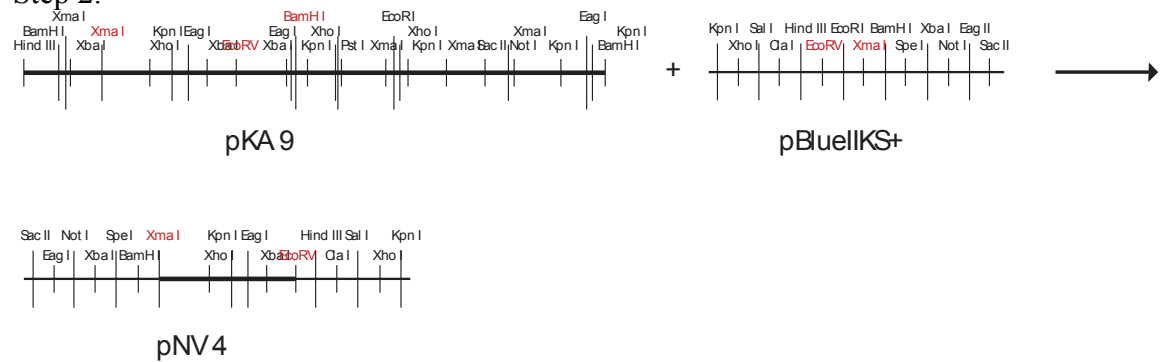
The main part of the targeting construct was made in three steps. In the first one, pNV7 was generated by excising with *XhoI/EcoRI* the 3'end of exon 32 from pRA intermediate C, and subcloning the fragment into pNV2. In the next step (pNV8) the neo cassette was excised from pneoflox8 and subcloned into pNV7 digested with *EcoRV* and *NotI*. This required to cut pneoflox8 with *XbaI*, convert the overhang to a blunt end, and digest the other end with *NotI*. In the last step the left arm was added to the main part of the targeting construct by subcloning the *SpeI/HindIII* fragment of pNV6 into pNV8. The targeting construct was designated pNV9 and was verified by partial sequencing and multiple restriction analyses.



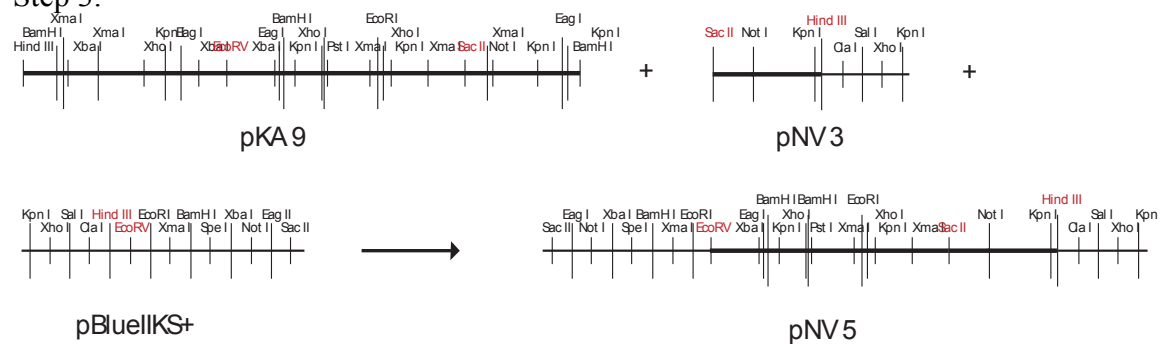
## Step 1.

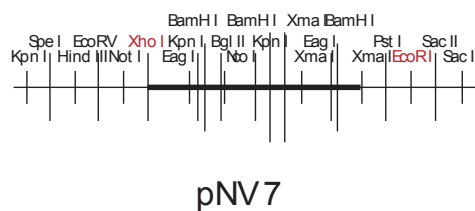


## Step 2.



## Step 3.





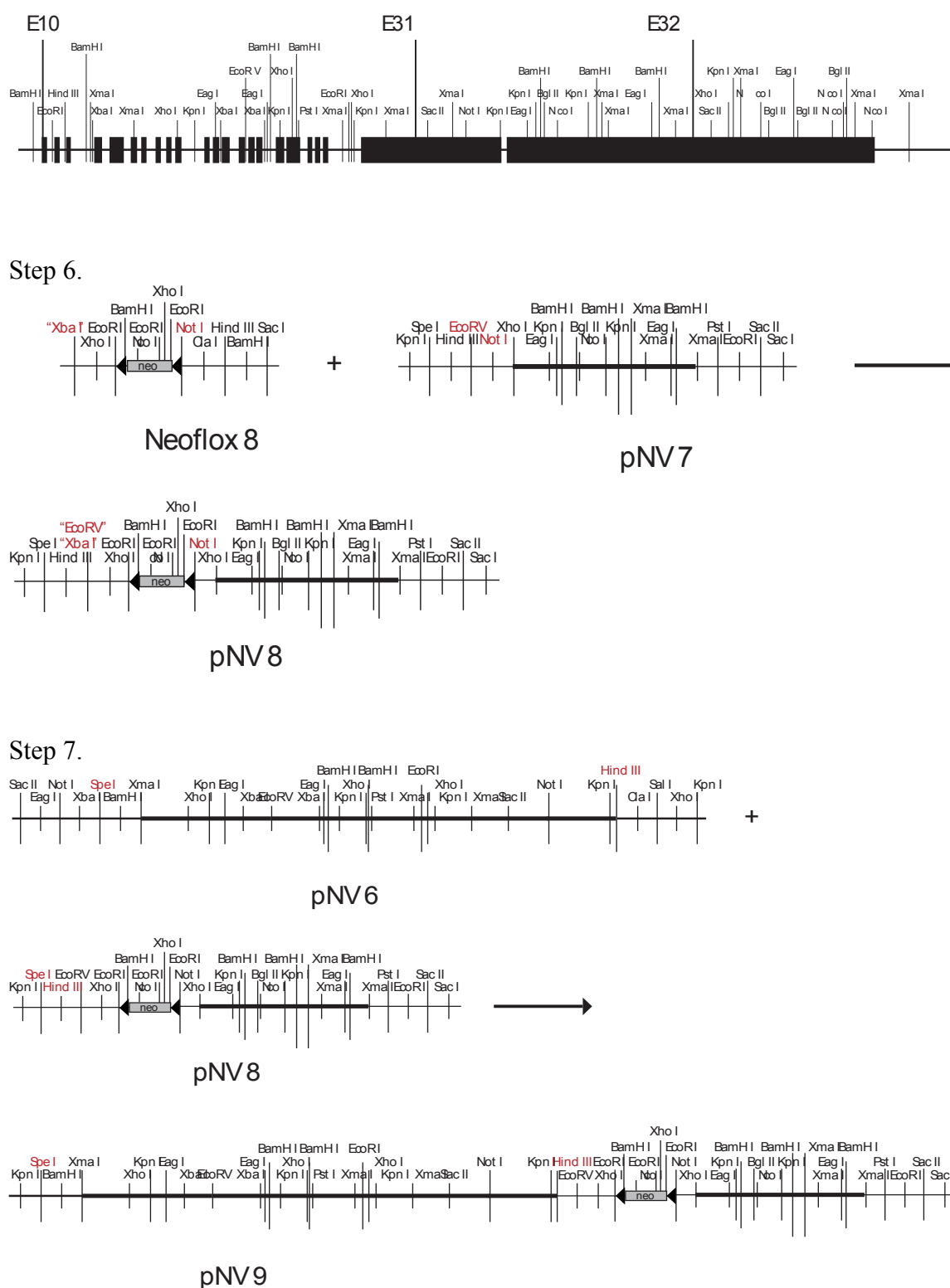


**Figure 67. Construction of the targeting vector.** Schematic representation of the mouse plectin gene from exon 10 (E10) to exon 32 (E32). Thick lines in the different plasmids indicate the fragments excised and ligated to generate the intermediate steps leading to the targeting vector (pNV9). The position of selected restriction sites is indicated; marked in red are the ones used for excision and flanking the resulting ligated fragment at every step.

## Plasmids generated in this work

Table 12

Purpose/Name	Description	Vector	Resistance
<b>for construction of the targeting vector</b>			
pNV1	MCSogna1 + pBSIIS+	pBSIIS+	Amp
pNV2	MCSogna2 + pBSIIS+	pBSIIS+	Amp
pNV3	pVP22 + pDL1-1 + pBSIIS+	pBSIIS+	Amp
pNV4	pKA9 + pBSIIS+	pBSIIS+	Amp
pNV5	pKA9 + pNV3 + pBSIIS+	pBSIIS+	Amp
pNV6	pNV4 + pNV5	pBSIIS+	Amp
pNV7	RA inter. C + pNV2	pBSIIS+	Amp
pNV8	Neoflox8 + pNV7	pBSIIS+	Amp
pNV9	pNV6 + pNV8	pBSIIS+	Amp
<b>for protein expression in baculovirus</b>			
pNV10	His + plectin rod <sub>wt</sub>	pFBHTa	Amp
pNV11	His + plectin rod <sub>Ogna</sub>	pFBHTa	Amp
pNV12	His + plectin SR5-9 + rod <sub>wt</sub>	pFBHTa	Amp
pNV13	His + plectin SR5-9 + rod <sub>Ogna</sub>	pFBHTa	Amp
pNV14	GST + plectin rod <sub>wt</sub>	pFBGST	Amp
pNV15	GST + plectin rod <sub>Ogna</sub>	pFBGST	Amp
pNV16	GST + plectin SR5-9 + rod <sub>wt</sub>	pFBGST	Amp
pNV17	GST + plectin SR5-9 + rod <sub>Ogna</sub>	pFBGST	Amp
<b>for transfection of mammalian cells</b>			
pNV25	plectin rod <sub>wt</sub> + EGFP	pEGFP-N2	kan
pNV26	plectin rod <sub>Ogna</sub> + GFP	pEGFP-N2	Kan
pNV27	plectin rod <sub>wt</sub> + C terminal domain + EGFP	pEGFP-N2	Kan
pNV28	plectin rod <sub>Ogna</sub> + C terminal domain + EGFP	pEGFP-N2	Kan
pNV29	full lenght isoform P1a <sub>wt</sub> + EGFP	pEGFP-N2	Kan
pNV30	full lenght isoform P1a <sub>Ogna</sub> + EGFP	pEGFP-N2	Kan

SR, spectrin repeats; see legend Fig. 51 (page 65)

## Sequence of mouse plectin Ex1a

```

1 cacaagaacttcagctctgagctgagcctctgctgagttacaagttactgtccagagcggcgggccggcagcctccagcagcctgtgtaccaccgcacgca 100
101 cgaggctgcctagactagacggagccagcactgagaactgagggacaggggtgaccaaggggcggggcagcacc ATG TCT CAG CAC CGG CTC 193
1 M S Q H R L 6
194 CGT GTG CCC GAG CCG GAA GGC CTG GGT AGC AAG AGA ACC AGC TCA GAG GAC AAC CTC TAC CTG GCT GTG CTC AGA 268
7 R V P E F E G L G S K R T S S E D N L Y CTG A V TG L R 31
269 GCC TCC GAG GGC AAG AAA G 287
32 A S E G K K 37

```

## Sequence of mouse plectin from exon 2 to end

```

1 *** *AT GAA CGA GAC CGT GTG CAG AAG AAA ACT TTC ACC AAG TGG GTC AAC AAA CAC CTT ATC AAG GCT CAG AGG 75
1 E R D R V Q K K T F T K W V N K H L I K A Q R 25
76 CAC ATC AGT GAC CTG TAC GAA GAC CTC CGT GAT GGC CAC AAC CTC ATC TCC CTG CTG GAA GTC CTC TCA GGA GAC 150
26 H I S D L Y E G D L R D G H N L I S L L E V L S TCA G G D 50
151 AGC CTG CCC CGC GAG AAA GGG AGG ATG CGC TTC CAC AAG CTC GAG AAT GTG CAG ATT GCC CTG GAC TAT CTC CGA 225
51 S L P R E K G R M R F H K L Q N V Q I A CTG D Y L R 75
226 CAT CGC CAG GTG AAG TTA GTG AAC ATC AGA AAT GAT GAC ATT GCT GAC GGC AAC CCC AAG CTG ACC CTC GGC CTC 300
76 H R Q V K L V N I R N D D I A D G N P K L T L G L 100
301 ATC TGG ACA ATC ATC CTG CAC TTC CAG ATC TCA GAC ATT CAG GTG AGC GGA CAG TCG GAG GAC ATG ACA GCA AAG 375
101 I W T I I L H F Q I S D I Q V S G Q S E D M T A K 125
376 GAG AAG CTG CTG CTG TGG TCA CAG CGT ATG GTA GAG GGC TAC CAA GGC CTG CGC TGT GAC AAC TTC ACC ACC AGT 450
126 E K L L L W S Q R M V E G Y Q G L R C D N F T T S 150
451 TGG CGC GAT GGC CGT CTC TTT AAT GCT ATC ATC CAC CGG CAC AAG CCC ATG CTC ATA GAT ATG AAA GTG TAT 525
151 W R D G R L F N A I I H R H C K P M L I D M N K V Y 175
526 CGA CAG ACC AAC CTG GAG AAC CTA GAC CAG GCA TTC TCG GTG GCA GAG CGG GAC CTG GGA GTT ACA CGG CTC CTG 600
176 R Q T N L E N L D Q A F S V A E R D L G V T R L L 200
601 GAC CCA GAT GTG GAC GTC CCT CAG P D E K S I I T Y V S S L Y TAC GAT GCT 675
201 D P E D V D V P Q P D E K S I I T Y V S S L Y TAC GAT GCT 225
676 ATG CCC CGC GTG CCT GGT GCA CAG GAC GGA GTG AGG GCC AAT GAG CTG CAG CTT CGT TGG CAG GAG TAC CGG GAG 750
226 M P R V P G A Q D G V R A N E L Q L R W Q E Y R E 250
751 CTT GTG TTG CTG CTG CAA TGG ATC CGG CAC CAC AAG TCC ATC ATC ACC TAT GTT TCA TCC CTG TAC GAT GCT 825
251 L V T L L L Q W I R H C H T A GCT A F F E E R K F P S S F 275
826 GAA GAG ATT GAG ATC CTA TGG TGC CAG TTT TTG AAG TTC AAG GAG ACA GAA CTT CCT GCC AAG GAG GCA GAC AAA 900
276 E E I E I L W C Q F L K F K E T E L P A K E A D K 300
901 AAC CGT TCC AAA GTT ATC TAC CAG TCT TTG GAG GGG GCA GTA CAA GCG GGC CAG CTC AAG ATT CCC CCT GGC TAC 975
301 N R S K V I Y Q S L E G G A V Q A G Q L K I P P G Y 325
976 CAC CCA CTA GAT GTG GAG AAG GAG TGG GGC AAG CTG CAT GTG GCC ATC CTG GAG CGG GAG AAG CAA CTG CGA AGC 1050
326 H P L D V E K E W G K L H V A I L E R E K Q L R S 350
1051 GAG TTT GAG AGG CTG GAG TGT CTT CAG CGC ATT GTG AGC AAG CTA CAG ATG GAG GCT GGG CTG TGT GAG GAG CAG 1125
351 E F E R L E C L Q R I V S K L Q M E A G L C E E Q 375
1126 CTG AAC CAG GCG GAC GCC CTA CTG CAG TCG GAT ATT CGG CTG CTG GCC TCA GGC AAG GTG GCT CAG CGA GCT GGG 1200
376 L N Q A D A L L Q S D I R L A S G K V A Q R A G 400
1201 GAA GTC GAG AGA GAC CTG GAC AAG GCT GAT GGT ATG ATC CGG CTG TTG TTC AAT GAT GTG CAG ACC CTT AAA GAT 1275
401 E V E R D L D K A D G M I R L L F N D V Q T L K D 425
1276 GGG CGG CAT CCA CAG GGT GAA CAG ATG TAC CGG AGG GTG TAT CGT CTG CAT GAG CGC CTG GTA GCC ATC CGC ACT 1350
426 G R H P Q G E G M Y R R Y Y L R L H E R L V A I R T 450
1351 GAG TAC AAC CTC CGG CTG AAG GCA GGA GTG GGT GCC CCT GTG ACC CAG GTG ACC CTG CAG AGT ACA CAG AGG CGC 1425
451 E Y N L R L K A G V G A P V T Q V T Q L Q S T Q R R 475
1426 CCA GAG CTA GAG GAC TCC ACA CTG CGC TAC CTG CAA GAC CTG CTG GCC TGG GTA GAG GAG AAC CAG CGT CGA ATA 1500
476 P E L E D S T L R Y L Q D L L A W V E E N Q R R I 500
1501 GAC AGT GCT GAG TGG GGC GTG AGT GTG GAG GCC CAG CTG GGC AGC CAC CGA GGC M H CAT CAG TCT 1575
501 D S A E W G V D L T P S V E A Q L G S H R G G M H Q T 525
1576 ATA GAG GAA TTT CGG GCC AAG ATC GAG CGG GCT CGG AAT GAT GAG AGC CAG CTC TCC CCT GCC ACC CGG GGT GCC 1650
526 I E E F F R A K I E R A G GCT R N D E S Q L S P A T R G G A 550
1651 TAC CGG GAC TGC CTA GGT CGC CTA GAC CTG CAG TAT GCA AAG CTG CTG AAC TCC TCC AAG GCC CGC CTC CGG TCC 1725
551 Y R D C L G R L D L Q Y A K L L N S S K A R L R S 575
1726 CTG GAG AGC TTG CAC GGG TTT GTG GCG GCA GCT ACC AAG GAG CTG ATG TGG CTG AAT GAG AAA GAA GAG GAG GAA 1800
576 L E S L H F V A A T K E L M W L N E G A A E E 600
1801 GTG GGC TTT GAT TGG AGT GAC CGC AAT ACC AAC ATG GCA GCC AAG AAA GAA AGT TAC TCG GCC CTG ATG CGA GAA 1875
601 V G F D W S D R N T N M A A K K E S Y S A L M R E 625
1876 CTG GAA ATG AAG GAA AAG AAA ATC AAG GAG ATC CAG AAC ACA GGG GAC AGG CTG CTG CGG GAA GAC CAT CCT GCC 1950
626 L E M K E K K I K E I Q N T G D R L R E T H P A 650
1951 CGG CCC ACG GTG GAG TCC TTC CAG GCT GCC TTG CAG ACA CAG TGG AGC TGG ATG CTG CAG CTG TGT TGC ATT 2025
651 R P T V E S F Q A L Q T Q W S W M L Q L C C C I 675
2026 GAA GCA CAC TTG AAA GAG AAT ACA GCC TAC TTC CAG TTC TCA GAT GTT CGG GAG GCG GAG GAA CAG TTG CAG 2100
676 E A H L K E N T A Y F S D V R E A E Q L Q 700
2101 AAG CTA CAG GAG ACG TTA CGC AGG AAG TAC AGC TGT GAC CGC ACC ATC ACC GTC ACC AGG CTC GAG GAT CTG CTG 2175
701 K L Q E T L R R K Y S C D R T I T V T R L E D L L 725
2176 CAG GAT GCC CAG GAT GAG AAG GAA CAA CTG AAT GAG TAC AAG GGG CAC CTC TCA GGC CTG GCC AAG CGG GCC AAG 2250
726 Q D A Q D E K E Q L N E Y K G H L S G L A K R A K 750
2251 GCT ATT GTG CAG TTG AAG CCA CGC AAC CCT GCC CAC CCG GTG CGG GGC CAC GTG CCC CTG ATA GCC GTG TGT GAC 2325
751 A I V Q L K P R N P A H P V R G H V P L I A V C D 775

```

2326	TAC	AAG	CAG	GTG	GAG	GTG	ACT	GTG	CAC	AAG	GGT	GAC	CAA	TGC	CAG	CTG	GTG	GGT	CCT	GCC	CAG	CCA	TCC	CAC	TGG	2400	
776	Y	K	Q	V	E	V	T	V	H	K	G	D	Q	C	Q	L	V	G	P	A	Q	P	S	H	W	800	
2401	AAG	GTG	CTC	AGT	GGT	TCC	AGC	AGC	GAG	GCC	GCT	GTG	CCT	TCT	GTG	TGC	TTT	CTT	GTG	CCG	CCG	CCC	AAC	CAG	GAG	2475	
801	K	V	L	S	G	T	S	S	S	E	A	A	V	P	S	V	C	F	L	V	P	P	N	Q	E	825	
Leucine zipper→																											
2476	GCC	CAG	GAA	GCT	GTC	GCT	AGA	CTG	GAG	GCG	CAG	CAT	CAG	GCC	CTG	GTC	ACA	CTG	TGG	CAC	CAG	CTT	CAC	GTG	GAC	2550	
826	A	Q	E	A	V	A	R	L	E	A	Q	H	Q	A	L	V	T	L	W	H	Q	L	H	V	D	850	
2551	ATG	AAG	AGC	CTT	CTG	GCG	TGG	CAG	AGC	CTC	AGT	CGG	GAC	ATA	CAG	CTC	ATC	CGG	TCC	TGG	TCC	CTA	GTC	ACG	TTC	2625	
851	M	K	S	L	A	S	F	Q	S	A	L	S	R	D	I	Q	L	I	R	S	W	S	L	V	T	F	875
2626	CGC	ACA	CTG	AAG	CCC	GAG	GAG	CAG	CGA	CAA	GCT	CTG	CGC	AAC	CTG	GAA	TTG	CAC	TAC	CAG	GCC	TTC	CTT	CGA	GAC	2700	
876	R	T	L	K	P	E	E	Q	R	Q	A	L	R	N	L	E	L	H	Y	Q	A	F	L	R	D	900	
2701	AGC	CAG	GAT	GCC	GGT	GGC	TTT	GGG	CCT	GAG	GAC	CGT	CTA	GTG	GCA	GAG	CGC	GAG	TAT	GGA	TCT	TGC	AGC	CGC	CAT	2775	
901	S	Q	D	A	G	G	F	G	P	E	D	R	L	V	A	E	R	E	Y	G	S	C	S	R	H	925	
2776	TAC	CAG	CAG	TTA	CTA	CAA	AGC	CTG	GAG	CAG	GGT	GAG	CAG	GAG	GAG	TCC	CGC	TGT	CAG	CGA	TGC	ATC	TCG	GAG	CTC	2850	
926	Y	Q	Q	L	L	Q	S	L	E	Q	G	E	Q	E	E	S	R	C	Q	R	C	I	S	E	L	950	
2851	AAG	GAT	ATC	CGG	CTG	CAG	CTG	GAG	GCC	TGT	GAG	ACT	CGG	ACT	GTG	CAC	CGT	CTG	CGG	CTG	CCA	CTG	GAT	AAG	GAC	2925	
951	K	D	I	R	L	A	E	A	C	E	D	R	L	V	H	R	L	R	L	P	L	V	T	F	975		
2926	CCC	GCA	CGG	GAG	TGC	GCC	CAG	CGC	ATC	GCT	E	GAG	CAA	CAG	AAA	GCG	CAG	GCT	GAG	GTG	GAG	GGG	CTG	GGC	AAG	GGA	3000
976	P	A	R	E	C	A	Q	R	I	A	E	Q	Q	K	A	Q	A	E	V	E	G	L	G	K	G	1000	
3001	GTT	GCC	CGG	CTG	TCT	GCT	GAG	GCT	GAG	AAA	GTT	CTA	GCC	TTG	CCA	GAG	CCG	TCA	CCT	GCT	GCA	CCC	ACT	CTG	CGC	3075	
1001	V	A	R	L	A	E	A	K	V	A	E	L	P	P	A	E	P	S	P	A	A	P	T	C	G	1025	
3076	TCG	GAG	TTG	GAA	CTG	ACC	CTG	GGC	AAG	CTG	GAA	CAG	GTC	CGA	AGC	CTG	TCT	GCC	ATC	TAC	CTG	GAG	AAA	CTC	AAG	3150	
1026	S	E	L	E	L	T	L	G	K	L	E	Q	V	R	S	L	S	A	I	Y	L	E	K	L	K	1050	
3151	ACC	ATC	AGC	TTG	GTG	ATT	CGC	AGT	ACC	CAG	GGG	GCT	E	GAG	GTG	CTT	AAA	ACC	CAT	GAG	GAG	CAG	CTG	AAG	GAG	3225	
1051	T	I	S	L	V	I	R	S	T	Q	E	A	E	V	L	K	T	H	E	E	Q	L	V	T	F	1075	
3226	GCC	CAG	GCT	GTG	CCT	GCC	ACT	CTC	CAA	GAG	CTT	GAA	GCC	ACC	AAG	GCC	TCA	CTA	AAG	AAG	CTG	CGG	GCC	CAG	GCC	3300	
1076	A	Q	A	V	P	A	T	L	Q	E	L	E	A	T	K	A	S	L	K	K	L	R	A	Q	A	1100	
3301	GAG	GCA	CAG	CAG	CCA	GTA	TTC	AAC	ACC	CTA	AGA	GAT	E	TTG	CGG	GGG	GCA	CAG	GAG	GTT	GGT	GAG	CGG	CTA	CAG	3375	
1101	E	A	Q	L	A	R	F	N	E	L	R	D	E	L	R	G	A	Q	E	V	G	E	R	L	Q	1125	
3376	CAG	CGG	CAT	GGT	GAG	CGG	GAC	GTA	GAA	GTT	GAG	CGC	TGG	CGA	GAA	CGT	GTC	ACT	CAG	TTG	CTG	GAG	CGC	TGG	CAG	3450	
1126	Q	R	H	G	E	R	D	V	E	V	E	R	W	R	E	R	V	T	Q	L	L	E	R	W	Q	1150	
3451	GCT	GTT	CTA	GCC	CAG	ACA	GAT	GTG	CGG	CAG	CGT	GAG	CTC	GAG	CAG	CTG	GGC	CGC	CAG	CTT	CGC	TAC	TAT	CGT	GAG	3525	
1151	A	V	L	A	Q	T	D	V	R	Q	R	E	L	E	Q	L	G	R	Q	L	R	Y	Y	R	E	1175	
pHLH20→																											
3526	AGC	GCG	GAT	CCT	CTG	AGC	GCC	TGG	CTG	CAG	GAT	GCC	AAG	AGG	CGG	CAA	GAG	CAG	ATC	CAG	GCC	GTG	CCA	ATA	GCC	3600	
1176	S	A	D	P	L	S	A	W	L	Q	D	A	K	R	R	Q	E	Q	I	Q	A	V	P	I	A	1200	
3601	AAC	TGT	CAG	GCT	GCG	CGA	GAA	CAG	CTG	CGC	CAG	GAG	AAG	GCC	CTG	CTG	GAG	GAG	ATT	GAG	CGT	CAT	GGT	GAG	AAG	3675	
1201	N	C	Q	A	A	R	E	A	C	L	R	E	K	A	L	L	E	E	I	E	R	H	G	E	K	1225	
3676	GTT	GAG	GAG	TGC	CAG	AAG	TTT	GCT	AAG	CAG	TAC	ATC	AAT	GCA	ATC	AAG	GAC	TAT	GAG	CTC	CAG	CTG	ATC	ACG	TAC	3750	
1226	V	E	E	C	Q	K	F	A	K	Q	Y	I	N	A	I	K	D	Y	E	L	Q	L	I	T	Y	1250	
3751	AAG	GCT	CAG	CTT	GAA	CCC	GTG	GCC	TCC	CCT	GCC	AAG	AAG	CCC	AAG	GTT	CAG	TCT	GGA	TCG	GAG	AGC	GTC	ATC	CAG	3825	
1251	K	A	Q	L	P	V	A	S	P	A	K	K	P	K	V	Q	S	G	E	S	V	I	Q	1275			
3826	GAG	TAC	GTG	GAT	CTG	CGC	ACG	CGC	TAC	AGC	GAG	CTG	ACC	ACG	CTC	ACG	AGC	CAG	TAT	ATC	AAG	TTC	ATC	AGT	GAG	3900	
1276	E	Y	V	D	L	R	T	R	Y	S	E	L	T	T	L	T	S	Q	Y	I	K	F	I	S	E	1300	
rod→																											
3901	ACC	CTT	CGC	CGC	ATG	GAA	GAG	GAG	GAG	CGG	CTG	GCT	GAG	CAA	CAG	CGG	GCA	GAG	GAG	CGG	GAG	CGA	CTG	GCC	GAG	3975	
1301	T	L	R	M	E	R	E	E	E	R	L	A	E	G	A	E	G	E	R	E	R	E	R	L	A	E	1325
3976	GTG	GAG	GCT	GCG	CTG	GAG	AAG	CAG	CGG	CAG	CTA	GCT	GAG	GCA	CAC	GCC	CAG	GCT	AAG	GCC	CAG	GCA	CAG	CTG	GAA	4050	
1326	V	E	A	A	L	E	K	Q	R	Q	L	A	E	A	H	A	Q	A	K	A	Q	A	E	L	E	1350	
4051	GCA	CAA	GAA	CTG	CAG	CGG	CGC	ATG	CAG	E	GAG	GTG	A	GCG	CGG	CGC	GAG	GAG	GCA	GCA	GTG	GAC	GCA	CAG	CAG	4125	
1351	A	Q	E	L	R	M	Q	R	E	G	E	V	R	R	E	R	E	A	V	D	A	Q	C	Q	Q	1375	
4126	AAG	CGC	AGC	ATC	CAA	GAG	GAG	CTG	CAG	CAC	CTG	AGG	CAG	AGC	TCG	GAG	GCA	GAG	ATC	CAG	GCC	AAG	GCC	CAG	CAG	4200	
1376	K	R	S	I	Q	E	E	L	Q	H	L	R	Q	S	S	E	A	E	I	Q	A	K	A	Q	Q	1400	
4201	GTG	GAG	GCT	GCA	GAA	CGC	AGC	CGG	ATG	CGC	ATT	E	GAG	GAA	E	ATC	CGT	GTA	GTA	CGT	CTG	CAG	CTG	GAG	ACA	ACT	4275
1401	V	E	A	A	E	R	S	R	M	R	I	E	E	I	R	V	V	R	L	R	L	Q	L	E	T	T	1425
4276	GAG	CGG	CAG	CGT	GGA	GGG	GCG	GAG	GGC	GAG	CTG	CAG	GCT	CTG	CGC	GCT	CGG	GCT	GAG	GAG	GCA	GAA	GCG	CAG	AAG	4350	
1426	E	R	Q	R	G	G	A	E	G	E	L	Q	A	L	R	A	R	A	E	E	A	E	A	Q	K	1450	
4351	CGG	CAG	GCT	CAG	GAG	GAA	GCT	GAA	CGC	TTG	CGA	AGG	CAG	GTG	CAG	GAT	GAG	AGC	CAG	CGC	AAA	CGG	CAG	GCA	GAG	4425	
1451	R	Q	A	Q	E	E	A	E	R	L	R	R	Q	V	Q	D	E	S	Q	R	K	R	Q	A	E	1475	
4426	GCA	GAG	CTG	GCC	CTG	CGT	GTG	AAG	GCT	GAA	GCT	GAG	GCA	GCG	CGA	GAG	AAG	CAG	AGG	GCC	CTG	CAG	GCC	CTG	GAT	4500	
1476	A	E	L	A	L	R	V	K	A	E	A	E	A	A	R	E	K	Q	R	A	L	Q	A	L	D	1500	
4501	GAG	CTG	AGA	CTG	CAG	GCC	GAG	GAG	GCC	GAG	CGG	CGG	CTG	CGC	CAA	GCC	GAG	GCA	GAG	CGG	GCA	CGC	CAA	GTG	CAG	4575	
1501	E	L	R	L	Q	A	E	E	A	E	R	R	L	R	Q	A	E	A	E	R	A	R	Q	V	Q	1525	
4576	GTG	GCC	CTG	GAG	ACG	GCA	CAG	CGC	AGT	GCG	GAA	GTG	GAG	CTG	CAG	AGC	AAG	CGG	GCA	TCC	TTT	GCA	GAG	AAG	ACC	4650	
1526	V	A	L	E	T	A	Q	R	S	A	E	V	E	L	Q	S	K	R	A	S	F	A	E	K	T	1550	
4651	GCA	CAA	TTG	GAG	CGC	ACT	CTG	CAG	GAG	GAG	CAT	GTA	ACA	GTG	GCC	CAG	CTG	CGG	GAG	GAG	GCC	CAG	CGA	CGG	GCA	4725	
1551	A	Q	L	E	R	T	L	Q	E	H	V	T	V	A	Q	L	R	E	E	A	E	R	R	A	E	1575	
4726	CAG	CAG	CAA	GCT	GAG	GCT	GAG	CGA	GCC	CGG	GAG	GAA	GCT	GAG	CGG	GAG	CTG	GAG	CGC	TGG	CAG	CTG	AAG	GCC	AAT	4800	
1576	Q	Q	Q	A	E	A	E	R	A	R	E	E	A	E	R	E	L	E	R	W	Q	L	K	A	N	1600	



5176	GAG	GTA	CTT	CTG	GCC	AGC	AAG	GCG	CGA	GCC	GAG	GAA	GAG	TCT	CGC	TCT	ACC	AGC	GAA	AAG	TCT	AAG	CAG	AGG	CTA	5250		
1726	E	V	L	L	A	S	K	A	R	A	E	E	E	S	R	S	T	S	E	K	S	K	Q	R	L	1750		
5251	GAG	GCT	GAG	GCA	GGC	CGC	TTT	CGG	GAA	CTG	GCC	GAG	GAG	GCT	GCC	CGG	CTG	CGT	GCT	CTG	GCG	GAG	GAG	GCC	AAG	5325		
1751	E	A	E	A	G	R	F	R	E	L	A	E	E	A	A	R	L	R	A	L	A	E	E	A	K	1775		
5326	AGG	CAG	AGG	CAG	TTG	GCA	GAG	GAG	GAT	GCC	GCC	CGC	CAG	CGG	GCC	GAG	GCA	GAG	CGG	GTG	CTT	ACT	GAG	AAG	CTG	5400		
1776	R	Q	R	E	L	A	E	E	D	E	A	F	R	Q	R	A	E	E	R	V	L	H	K	A	1800			
5401	GCT	GCC	ATC	AGT	GAG	GCC	ACA	CGG	CTC	AAG	ACG	GAG	GCA	GAG	ATT	GCA	CTC	AAA	GAG	AAG	GAG	GCC	GAG	AAT	GAG	5475		
1801	A	A	I	S	E	A	T	R	L	K	T	E	A	E	I	A	L	K	E	K	E	A	E	N	E	1825		
5476	CGC	CTG	AGG	CGC	CTG	GCA	GAA	GAC	GAG	GCC	TTC	CAG	CGG	CGG	CGT	CTG	GAG	GAG	CAG	GCG	GCA	CTG	CAC	AAG	GCT	5550		
1826	R	L	R	R	L	A	E	D	E	A	F	Q	R	R	R	L	E	E	Q	A	A	L	H	K	A	1850		
5551	GAC	ATC	GAG	GAG	CGC	CTG	GCC	CAG	CTG	CGC	AAG	GCA	TCA	GAG	AGC	GAG	CTG	GAG	CGG	CAG	AAG	GGC	TTG	GTG	GAG	5625		
1851	D	I	E	E	R	L	A	Q	L	R	K	A	S	E	S	E	L	E	R	Q	K	G	L	V	E	1875		
5626	GAC	ACC	CTG	CGA	CAG	CGG	CGG	CAG	GTG	GAG	GAG	GAG	ATC	ATG	GCG	CTG	AAG	GTG	AGC	TTT	GAG	AAA	GCC	GCC	GCG	5700		
1876	R	T	L	R	Q	R	E	E	E	E	E	E	I	M	A	L	K	V	S	F	E	A	A	A	A	1900		
5701	GGC	AAG	GCA	GAG	CTG	GAG	CTG	GAG	CTG	GAG	CTG	GGG	CGC	ATT	CGC	AGC	AAC	GCG	GAG	GAC	ACA	ATG	CGC	AGC	AAG	GAG	CAG	5775
1901	G	K	A	E	L	E	L	E	L	E	L	G	R	I	R	S	N	A	E	D	T	M	R	S	K	E	Q	1925
5776	GCG	GAA	CTG	GAG	GCG	GCC	CGG	CAG	CGG	CAG	TTG	GCG	GCA	GAG	GAG	GAG	CAG	AGG	CGC	CGG	GAG	GCC	GAG	GAG	CGC	5850		
1926	A	E	L	E	A	Q	R	Q	E	A	R	A	E	E	A	E	E	E	R	R	R	E	E	E	E	R	1950	
5851	GTG	CAG	AGG	AGC	CTG	GCA	GCG	GAG	GAG	GAA	GCC	GCT	CGG	CAG	CGC	AAG	GTG	GCA	CTG	GAG	GAG	GTC	GAG	CGA	CTC	5925		
1951	V	Q	R	S	L	A	A	E	E	E	A	A	R	Q	R	K	V	A	L	E	E	V	E	R	L	1975		
5926	AAG	GCC	AAG	GTT	GAA	GAA	GCA	CGG	CGC	CTG	CGA	GAG	CGG	GCA	GAG	CAG	GAG	TCG	GCC	AGG	CAG	CTG	CAG	CTG	GCC	6000		
1976	K	A	K	V	E	L	R	R	L	R	E	R	A	E	A	E	E	S	A	R	A	Q	L	A	A	2000		
6001	CAG	GAG	GCC	GCC	CAG	AAA	CGG	CTG	CAG	GCG	GAG	GAG	AAG	GCA	CAC	GCC	TTT	GTG	GTG	CAG	CAG	CGA	GAG	GAG	GAG	6075		
2001	Q	E	A	A	Q	K	R	L	Q	A	E	E	K	A	H	A	F	V	V	Q	Q	R	E	E	E	2025		
6076	CTG	CAG	CAG	ACG	CTT	CAG	CAA	GAG	CAG	AAC	ATG	CTG	GAT	CGG	CTG	CGG	AGT	GAG	GCA	GAG	GCA	GCG	AGG	CGA	GCC	6150		
2026	L	Q	Q	T	L	Q	E	Q	N	M	L	D	R	L	R	S	E	A	E	A	A	A	R	A	A	2050		
6151	GCC	GAG	GAG	GCG	GAG	GAG	GCC	CGG	GAG	CAG	GCG	GAG	CGC	GAG	GCA	GCG	CAG	TCT	CGG	AAA	CAA	GTG	GAA	GAG	GCC	6225		
2051	A	E	E	A	E	E	A	R	E	Q	A	E	R	E	A	A	Q	S	R	K	Q	V	E	E	A	2075		
6226	GAG	CGG	CTG	AAA	CAG	TCA	GCA	GAG	GAG	CAG	GCT	CAG	GCC	CAG	GCT	CAG	GCG	CAG	GCG	GCC	GCA	GAG	AAG	CTG	CGC	6300		
2076	E	R	L	K	Q	S	A	E	E	Q	A	Q	A	Q	A	Q	A	Q	A	A	A	E	K	L	R	2100		
6301	AAG	GAA	GCG	GAG	CAG	GAG	GCG	GCG	CGT	CGG	GCC	CAG	GCA	GAG	CAG	GCA	GCG	CTG	AAA	CAG	AAG	CAG	GCA	GCC	GAC	6375		
2101	K	E	A	E	Q	E	A	A	R	R	A	Q	A	E	Q	A	A	L	K	Q	K	Q	A	A	D	2125		
6376	GCG	GAG	ATG	GAG	AAG	CAT	AAA	AAG	TTT	GCA	GAG	CAG	ACA	CTC	CGG	CAG	AAG	GCC	CAG	GTA	GAG	CAG	GAG	CTG	ACC	6450		
2126	A	E	M	E	K	H	K	K	F	A	E	Q	T	L	R	Q	K	A	Q	V	E	E	L	T	2150			
6451	ACA	CTG	AGG	CTG	CAG	CTA	GAG	GAG	ACT	GAC	CAC	CAG	AAG	AGC	ATC	CTG	GAT	GAG	GAG	CTG	CAG	CGA	CTA	AAG	GCC	6525		
2151	T	L	R	L	Q	L	E	E	T	D	H	Q	K	S	I	L	D	E	E	L	Q	R	L	K	A	2175		
6526	GAG	GTA	ACA	GAG	GCA	GCC	CGG	CAG	CGC	AGC	CAG	GTA	GAG	GAG	CTC	TTC	TCT	GTC	CGT	GTG	CAG	ATG	GAG	GAG	6600			
2176	E	V	T	E	A	A	A	R	S	Q	V	E	E	E	E	S	V	R	V	Q	M	E	E	E	2200			
6601	CTG	GGC	AAG	CTC	AAG	GCT	CGC	ATT	GAA	GCT	GAA	AAC	CGG	GCC	CTC	ATC	CTT	CGT	GAC	AAG	GAC	AAC	ACA	CAG	CGC	6675		
2201	L	G	K	L	K	A	R	I	E	A	E	N	R	A	L	I	L	R	D	K	D	N	T	Q	R	2225		
6676	TTC	CTG	GAG	GAG	GAG	GCC	GAG	AAG	ATG	AAA	CAG	GTG	GCC	GAG	GAA	GCG	GCA	CGG	TTG	AGC	GTG	GCC	GCC	CAG	GAG	6750		
2226	F	L	E	E	A	E	K	M	K	Q	V	A	E	A	E	A	R	L	S	V	A	A	Q	E	2250			
6751	GCA	GCA	CGG	CTG	AGG	CAG	CTA	GCG	GAG	GAG	GAC	CTG	GCG	CAG	CAG	CGG	GCC	CTG	GCA	GAG	AAG	ATG	CTA	AAG	GAG	6825		
2251	A	A	R	L	R	Q	L	A	E	E	D	L	A	Q	Q	R	A	L	A	E	K	M	L	K	E	2275		
6826	AAG	ATG	CAG	GCG	GTG	CAG	GAA	GCC	ACG	AGG	CTC	AAG	GCC	GAG	GCT	GAG	CTG	CTG	CAG	CAG	CAG	AAG	GAG	CTT	GCC	6900		
2276	K	M	Q	A	V	A	T	R	L	K	A	E	A	E	A	E	Q	L	L	Q	K	E	L	A	2300			
6901	CAG	GAG	CAG	GCC	CGG	CGG	CTG	CAG	GAG	GAC	AAG	GAG	CAA	ATG	GCT	CAG	CAG	TTG	GTA	GAG	GAG	ACA	CAG	GGT	TTC	6975		
2301	Q	E	Q	A	R	R	L	Q	E	D	K	E	Q	M	A	Q	Q	L	V	E	E	T	Q	G	F	2325		
6976	CAG	AGG	ACT	CTG	GAG	GCC	GAG	CGG	CAG	CGG	CAG	CTG	GAG	ATG	AGC	GCG	GAG	GCC	GAG	CGC	CTC	AAG	CTG	CGC	ATG	7050		
2326	Q	R	T	L	E	A	Q	R	Q	Q	L	E	M	S	A	E	A	E	R	L	K	L	R	M	2350			
7051	GCT	GAG	ATG	AGC	CGG	GCT	CAG	GCC	CGC	GCG	GAG	GAC	GCC	CAG	CGC	TTC	CGG	AAG	CAG	GCT	GAA	GAG	ATC	GGC	7125			
2351	A	E	M	S	R	A	Q	A	R	A	E	E	D	A	Q	R	F	R	K	Q	A	E	E	I	G	2375		
7126	GAG	AAG	CTG	CAC	CGC	ACT	GAA	CTT	GCG	ACA	CAG	GAG	AAG	GTG	ACG	TTG	GTG	CAG	ACG	CTG	GAG	ATC	CAG	CGA	CAG	7200		
2376	E	K	L	H	R	T	E	L	A	T	Q	E	K	V	T	L	V	Q	T	L	E	I	Q	R	R	2400		
7201	CAG	AGT	GAC	CAC	GAT	GCT	GAG	CGT	CTG	AGG	GAG	GCC	ATT	GCG	GAG	CTG	GAG	CGT	GAG	AAG	GAG	AAC	CTC	AAG	CAG	7275		
2401	Q	S	D	H	D	A	E	R	L	R	E	A	I	A	E	L	E	R	E	K	E	K	L	K	Q	2425		
7276	GAG	GCG	AAG	TTA	CTG	CAG	CTC	AAG	TCG	GAG	GAG	ATG	CAG	ACT	GTG	CAG	CAG	GAG	CAG	ATA	CTG	CAG	GAG	ACC	CAG	7350		
2426	E	A	K	L	L	A	L	K	S	E	E	M	Q	T	V	Q	C	Q	E	I	L	G	E	T	Q	2450		
7351	GCC	CTG	CAG	AAG	AGC	TTC	CTC	TCT	GAG	AAG	GAC	ATG	CTG	CTG	CAG	CGC	GAG	CGC	TTC	ATC	GAG	CAG	GAG	AAG	GCC	7425		
2451	A	L	Q	K	S	F	L	S	E	K	D	S	L	L	Q	R	E	R	F	I	E	Q	E	K	A	2475		
7426	AAG	CTG	GAG	CAG	CTC	TTC	CAG	GAC	GAG	GTG	GCT	AAA	GCA	AAG	CAG	CTG	CGT	GAG	GAG	CAG	CAG	CGG	CAG	CAG	CAG	7500		
2476	K	L	E	Q	L	F	Q	D	E	V	A	K	A	K	Q	L	R	E	E	Q	Q	R	Q	Q	A	2500		
7501	CAG	ATG	GAA	CAG	GAA	AAG	CAG	GAG	CTG	ATG	GCC	ATG	GAG	GCC	AGG	AGG	CGG	CAG	CGC	GAG	GCT	GAG	GAG	GAG	7575			
2501	Q	M	E	Q	E	K	Q	E	L	M	A	S	M	E	E	A	R	R	R	Q	R	E	A	E	E	2525		
7576	GGC	GTG	AGG	CGC	AAG	CAA	GAG	GAA	CTG	CAG	CAT	CTG	GAG	CAG	CAG	CGG	CAG	CAG	CAG	GAG	AAG	CTC	CTG	GCG	GAG	7650		
2526	G	V	R	R	K	Q	E	E	L	Q	H	L	E	Q	Q	R	Q	Q	Q	E	K	L	L	A	E	2550		
7651	GAA	AAC	CAG	CGG	CTG	CGA	GAG	CGG	CTG	Q	R	C	G	G	GAG	GAA	GAG	CAC	CGC	GCT	GCC	TTG	GCT	CAC	TCT	GAG	ATC	7725
2551	E	N	Q	R	L	R	E	R	L	Q	R	C	L	E	E	E	H	R	A	A	L	A	H	S	E	I	2575	
7726	GCC	ACC	ACC	CAG	GCC	GCT	TCC	ACG	AAG	GCA	CTG	CCC	AAC	GGC	CGG	GAT	GCA	CCC	GAT	GGC	CGG	TCC	GTG	GAG	GCT	7800		
2576	A	T	T	Q	A	A	S	T	K	A	L	P	N	G	R	D	A	P	D	G	P	S	V	E	A	2600		
7801	GAA	CCC	GAG	TAC	ACC	TTT	GAG	GG	CTA	CGT	CAG	AAG	GTG	CCG	GCC	CAG	CTA	CAG	GAA	GCA	GGC	ATC	CTG	AGC	7875			
2601	E	P	E	Y	T	F	E	G	G	L	R	Q	K	V	T	A	Q	C	A	E	A	G	I	L	S	2625		
7876	CAG	GAG	GAA	CTG	CAG	CGT	TTG	GCA	CAG	GGT	CAC	ACC	ACG	GTG	GCT	GAG	CTC	ACG	CAG	CGG	GAA	GAT	GTG	TAC	CGG	7950		
2626	Q	E	E	L	Q	R	L	A	Q	G	H	T	T	T	V	A												

2676	L	Q	R	Q	L	L	S	P	G	T	A	L	I	L	L	E	A	Q	A	A	S	G	F	L	L	2700	
8101	GAT	CCT	GTG	CGG	AAT	CGG	CGG	CTG	ACA	GTC	AAT	GAG	GCT	GTG	AAG	GAG	GGT	GTC	GTG	GGT	CCT	GAG	CTG	CAC	CAC	8175	
2701	D	P	V	R	N	R	R	L	T	V	N	E	A	V	K	E	G	V	V	G	P	E	L	H	H	2725	
8176	AAA	CTG	CTG	TCA	GCT	GAG	CGT	GCC	GTC	ACC	GGC	TAC	AAG	GAC	CCC	TAT	ACA	GGG	GAA	CAG	ATC	TCG	CTC	TTC	CAG	8250	
2726	K	L	L	S	A	E	R	A	V	T	G	Y	K	D	P	Y	T	G	E	Q	I	S	L	F	Q	2750	
8251	GCC	ATG	AAG	AAG	GAC	CTT	ATT	GTC	AGG	GAC	CAT	GGC	GTC	CGC	CTG	CTG	GAG	GCC	CAG	ATC	GCC	ACC	GGT	GGC	ATC	8325	
2751	A	M	K	K	D	L	I	V	R	D	H	G	V	R	L	E	A	Q	I	A	T	G	F	I	I	2775	
8326	ATT	GAT	CCT	GTG	CAC	AGC	CAC	CGT	GTG	CCT	GTG	GAC	GTG	GCC	TAC	AAA	CGT	GGC	TAC	TTC	GAT	GAA	GAG	ATG	AAC	8400	
2776	I	D	P	V	H	S	H	R	V	P	V	D	V	A	Y	K	R	G	Y	F	D	E	E	M	N	2800	
8401	CGC	ATC	TTG	TCT	GAC	CCA	AGC	GAT	GAC	ACC	AAG	GGC	TTC	TTC	GAC	CCC	AAC	ACC	CAC	GAG	AAC	CTC	ACT	TAC	CTG	8475	
2801	R	I	L	S	D	P	S	D	D	T	K	G	F	F	D	P	N	T	H	E	N	L	T	Y	L	2825	
8476	CAG	CTG	CTG	GAG	CGC	TGT	GTG	GAG	GAC	CCC	GAG	ACC	GGC	CTG	CGC	CTC	CTG	CCA	CTC	ACA	GAT	AAG	GCT	GCC	AAG	8550	
2826	Q	L	L	E	R	C	V	E	D	P	E	T	G	L	R	L	L	P	L	T	D	K	A	A	K	2850	
8551	GGT	GGC	GAG	CTG	GTG	TAC	ACC	GAT	ACG	GAG	GCC	CGT	GAC	GTC	TTC	GAA	AAG	GCC	ACC	GTG	TCT	GCA	CCG	TTT	GGC	8625	
2851	G	E	L	S	D	Y	T	V	T	I	E	R	F	F	D	E	K	A	T	V	E	N	L	T	G	2875	
8626	AAG	TTC	CAG	GGC	AGG	ACC	GTG	ACC	ATC	TGG	GAG	ATC	ATC	AAC	TCG	GAG	TAC	TTC	ACG	GCG	GAA	CAG	CGA	CGG	GAC	8700	
2876	K	F	Q	G	R	T	V	T	I	W	E	I	I	N	S	E	Y	F	T	A	E	Q	R	R	D	2900	
8701	CTG	CTG	CAG	CAG	TTC	CGC	ACG	GGC	CAC	ATC	ACG	GTG	GAG	AAA	ATC	ATC	AAA	ATC	GTC	ATC	ACA	GTG	GTG	GAG	GAA	8775	
2901	L	I	L	S	D	P	T	T	T	I	T	V	E	I	K	I	V	I	T	V	I	L	T	Y	L	2925	
8776	CAC	GAG	CGG	AAG	GGC	CAG	CTC	TGC	TTT	GAG	GGC	CTC	CGT	GCC	CTC	GTG	CCC	GCC	GCA	GAG	CTG	CTG	GAC	AGT	GGG	8850	
2926	H	E	R	K	G	Q	L	C	F	E	G	L	R	A	L	V	P	A	A	E	L	L	D	S	G	2950	
8851	GTC	ATC	AGC	CAC	GAA	CTC	TAC	CAG	CAG	CTG	CAG	CGG	GGT	GAG	CGT	TCT	GTG	CGG	GAA	GTG	GCC	GAG	GCG	GAC	AGC	8925	
2951	V	I	S	H	E	L	Y	T	C	Q	L	R	S	V	R	E	V	A	E	A	E	A	D	S	S	2975	
8926	GTG	AGG	CAG	GCC	CTG	CGG	GGT	ACC	AAT	GTC	ATC	GCC	GGT	GTG	TGG	CTG	GAA	GAA	GCA	GGG	CAG	AAG	CTG	AGC	ATC	9000	
2976	V	R	Q	A	L	R	G	T	N	V	I	A	G	V	W	L	E	E	A	G	Q	K	L	S	I	3000	
9001	TAT	GAG	GCC	CTG	AAG	AAA	GAC	TTG	CTG	CAG	CCA	GAG	GTG	GCT	GTG	GCC	TTG	CTG	GAG	GCC	CAG	GCT	GGC	ACT	GGG	9075	
3001	Y	E	A	L	K	A	D	L	C	Q	A	V	A	V	A	L	L	E	A	Q	A	G	A	T	G	3025	
9076	CAT	ATC	ATC	GAC	CCT	GCC	ACC	AGC	GCC	AGG	CTG	ACT	GTG	GAC	GAG	GCG	GTG	CGT	GCT	GGC	CTG	GTG	GGG	CCT	GAG	9150	
3026	H	I	I	D	P	A	T	S	A	R	L	T	V	D	E	A	V	R	A	G	L	V	G	P	E	3050	
9151	CTG	CAC	GAG	AAG	CTG	CTG	TCA	GCC	AGG	AAG	GCC	GTG	ACA	GGC	TAC	AGG	GAT	CCC	TAC	TCA	GGA	CAG	AGT	GTC	TCA	9225	
3051	L	H	E	L	S	A	E	K	A	E	G	T	C	Y	R	D	P	Y	S	Q	S	Y	V	T	S	3075	
9226	CTG	TTC	CAG	GCC	TTG	AAG	AAG	GGT	CTC	ATC	CCC	CGA	GAA	CAG	GGC	CTG	CGC	CTG	CTG	GAT	GCC	CAG	TTA	TCC	ACT	9300	
3076	L	F	Q	A	L	K	K	G	L	I	P	R	E	Q	G	L	R	L	L	D	A	Q	L	S	T	3100	
9301	GGT	GGC	ATT	GTA	GAC	CCC	AGC	AAA	AGC	CAC	R	CGT	GTG	CCC	CTG	GAT	GTT	GCC	TAT	GCC	CGG	GGC	TAC	CTG	AAA	9375	
3101	G	I	V	I	D	P	S	K	A	C	H	R	V	P	L	D	V	A	Y	A	R	G	Y	L	D	K	3125
9376	GAG	ACT	AAC	AGG	GCC	CTG	ACG	TCA	CCC	AGA	GAT	GAT	GCC	AGA	GTC	TAC	CAT	GAC	CCC	AGC	ACC	CAG	GAG	CCA	GTC	9450	
3126	E	T	N	R	A	L	T	S	P	R	D	D	A	R	V	Y	H	D	P	S	T	Q	E	P	V	3150	
9451	ACC	TAC	AGC	CAG	CTC	CAA	CAG	CGG	TGC	CGG	TCT	GAC	CAG	CTG	ACC	GGC	TTG	AGC	CTA	CTG	CCA	CTC	TCA	GAG	AAG	9525	
3151	T	Y	S	Q	L	R	C	S	D	P	C	L	T	T	G	L	S	L	L	P	L	P	L	E	K	3175	
9526	GCC	GTC	CGG	GCC	CGG	CAG	GAG	GAG	GTC	TAC	TCT	GAG	CTC	CAG	GCC	CGG	GAG	ACA	CTG	GAG	CAG	GCC	AAG	GTT	GAG	9600	
3176	A	V	R	A	R	Q	E	E	V	Y	S	E	L	Q	A	R	E	T	L	E	Q	A	K	V	E	3200	
9601	GTT	CCT	GTG	GGC	AGC	TTT	AAG	GGC	AGG	GCG	ATG	ACT	GTG	TGG	GAG	CTC	ATC	AGC	TCT	GAA	TAC	TTT	ACT	GAG	GAG	9675	
3201	V	P	V	G	S	F	K	G	P	A	M	T	V	W	E	L	I	S	S	E	Y	F	T	E	E	3225	
9676	CAG	CGG	CAG	GAG	TTG	CTG	CGG	CAG	TTC	CGC	ACA	GGC	AAG	GTC	ACC	GTG	GAG	AAG	GTC	ATC	AAG	ATT	GTC	ATC	ACC	9750	
3226	Q	R	Q	E	L	L	R	Q	F	R	T	G	K	V	T	V	E	K	V	I	K	I	V	I	T	3250	
9751	ATC	GTG	GAG	GAG	GTG	GAG	ACT	CGG	CGG	CAG	GAG	AGA	CTG	TCC	TTT	AGT	GGC	CTC	CGT	GCC	CCT	GTG	PCG	GCC	AGT	9825	
3251	I	V	E	L	S	E	T	R	C	Q	A	R	L	S	F	G	L	R	A	P	V	P	G	D	S	3275	
9826	GAG	CTC	CTG	GAC	GCC	AAG	ATC	CTC	AGC	AGA	GCT	CAG	TTT	GAC	CAG	CTC	AAG	GAT	GGC	AAG	ACA	TCA	GTC	AAA	GAG	9900	
3276	E	L	L	D	A	K	I	L	S	R	A	Q	F	D	Q	L	K	D	G	K	T	S	V	K	E	3300	
9901	CTG	TCC	GAG	GTG	GGC	TCC	GTG	CGG	ACT	CTG	CTG	CAG	GGC	AGC	GGC	TGC	CTG	GCC	GGC	ATC	TAT	CTG	EAG	GAC	TCG	9975	
3301	L	S	E	V	R	S	V	R	T	L	L	Q	G	S	G	C	L	A	G	I	Y	L	G	D	S	3325	
9976	AAG	GAG	AAA	GTA	ACC	ATC	TAT	GAG	GCC	ATG	CGC	CGG	GSC	CTC	CTC	AGA	CCC	AGC	ACA	GCC	ACG	CTC	CTG	CTG	GAG	10050	
3326	K	E	K	V	T	I	Y	E	A	M	R	R	G	L	L	R	P	S	T	A	T	L	L	L	E	3350	
10051	GCC	CAG	GCA	GCC	ACT	GGT	TTT	CTG	GTG	GAC	CCT	GTG	CGG	AAC	CAA	CGT	CTG	TAT	GTC	CAT	GAG	GCT	GTC	AAG	GCG	10125	
3351	A	Q	A	A	T	G	F	L	V	D	P	V	R	N	Q	L	Y	V	H	E	A	G	V	K	A	3375	
10126	GSC	GTA	GTG	GGC	CCT	GAA	CTC	CAT	GAG	AAG	CTG	CTG	TCG	GCC	GAG	AAG	GCC	GTC	ACT	GGC	TAC	AAG	GAT	CCC	TAC	10200	
3376	G	V	V	G	P	E	L	H	E	K	L	L	S	A	E	K	A	V	T	G	Y	K	D	P	Y	3400	
10201	TCG	GGC	AAC	ACC	ATC	TSC	CTG	TTC	CAG	GCC	ATG	AAA	AAG	GGC	CTG	GTC	CTC	AGG	GAC	CAT	GCC	ATC	CGC	CTG	CTG	10275	
3401	S	G	N	A	I	C	L	T	F	Q	A	M	K	A	G	L	V	R	D	H	A	I	R	L	L	3425	
10276	GAG	GCC	CAG	GTC	GCC	ACG	GGT	GGC	ATC	ATC	GAC	CCG	GTG	CAC	AGC	CAC	CGC	CTG	CCT	GTG	GAC	GTG	GCC	TAC	CAG	10350	
3426	E	A	Q	V	A	T	G	G	I	I	D	P	V	H	S	H	R	L	P	V	D	V	A	Y	Q	3450	
10351	CGT	GGC	TAC	TTC	GAT	GAG	GAG	ATG	AAC	CGT	GTG	CTG	GCA	GAT	CCA	AGT	GAT	GAC	ACC	AAG	GCC	TTC	TTT	GAC	CCC	10425	
3451	R	G	Y	F	D	E	M	M	N	R	V	L	A	D	P	S	D	D	T	K	G	F	T	D	C	3475	
10426	AAC	ACC	CAC	GAG	AAC	CTC	ACC	TAC	CTG	CAG	CTG	CTG	GAG	CGC	TGT	GTG	GAG	GAC	CCC	GAG	ACC	GGC	CTG	CGC	CTC	10500	
3476	N	T	H	E	N	L	T	Y	L	Q	L	L	E	R	C	V	E	D	P	E	T	G	L	R	L	3500	
10501	CTG	CCA	CTC	AAA	GGG	GCA	GAG	AAG	ACC	GAG	GTG	GTA	GAA	ACC	ACA	CAG	GTG	TAT	ACT	GAG	GAG	GAG	ACT	CGG	AGG	10575	
3501	L	P	L	G	A	E	K	L	E	V	V	E	V	A	T	Q	V	Y	T	E	E	E	E	T	R	3525	
10576	GCG	TTC	GAG	GAG	ACG	CAG	ATT	GAC	ATC	CCG	GGT	GGT	GGC	AGC	CAC	GGT	GGC	TCC	TCC	ATG	TCT	CTG	TGG	GAG	GTG	10650	
3526	A	F	E	E	T	Q	I	D	I	P	G	G	G	S	H	G	G	S	S	M	S	L	W	E	V	3550	
10651	ATG	CAG	TCA	AAC	ATG	ATC	CCG	GAG	GAT	CAG	CGT	GCC	CGG	CTC	ATG	GCT	GAC	TTT	CAG	GCT	GGG	AGG	GTA	ACC	AAG	10725	
3551	M	Q	S	N	M	I	P	E	D	R	A	R	L	M	A	D	F	Q	A	G	R	V	T	T	K	3575	
10726	GAA	CGC	ATG	ATC	ATT	ATC	ATC	ATC	GAA	ATC	ATC	GAG	AAG	ACC	GAG	ATC	ATC	CGC	CAG	CAG	AAC	CTG	GCC	TCC	TAT	10800	
3576	E	R	M	I	I	I	I	I	E	I	I	E	K	T	E	I	I	R	Q	Q	N	L	A	S	Y	3600	
10801	GAC	TAC	GTG	CGC	CGC	CGC	CTC	ACT	GCC	GAA	GAC	CTG	TAC	GAG	GCC	CGG	ATC</										

11951	GCG	GTG	GCC	GGT	GTC	TAC	CTG	CCT	GGC	TCC	AGG	CAG	ACG	CTA	ACC	ATC	TAC	CAG	GCC	CTT	AAG	AAG	GGG	TTG	CTG	11025	
3651	A	V	A	G	V	Y	L	P	G	S	Q	T	L	T	I	Y	Q	Q	A	CTT	K	K	G	L	L	3675	
11026	AGT	GCC	GAG	GTG	GCC	CGC	TTA	TTG	CTG	GAA	GCA	CAG	GCA	ACC	ACG	GCG	TTC	CTG	CTG	GAC	CCA	GTG	AAG	GGG	GAG	11100	
3676	A	E	A	V	A	C	L	L	L	A	A	Q	A	A	T	G	F	L	L	D	P	V	K	G	E	3700	
11101	CGG	CTG	ACC	GTG	GAT	GAG	GCT	GTG	CGG	AAG	GGC	CTG	GTA	GGC	CCC	GAG	CTG	CAT	D	GAC	CGC	CTC	CTC	TCT	GCC	GAG	11175
3701	R	L	T	V	D	E	A	V	R	K	G	L	V	G	P	E	L	H	D	R	L	L	L	A	E	3725	
11176	CGA	GCT	GTA	ACT	GGT	TAC	CGA	D	CCC	TAC	ACG	GAA	CAG	ACC	ATC	TCA	CTC	TTC	CAG	GCC	ATG	AAG	AAG	GAG	CTG	11250	
3726	A	A	V	T	G	Y	R	D	P	Y	T	E	Q	T	I	S	L	F	Q	A	M	K	K	E	L	3750	
11251	ATC	CCT	GCT	GAG	GAG	GCG	CTG	AGG	CTG	CTG	GAT	ACG	CAG	CTA	GCC	ACA	GGA	GGC	ATT	GTG	GAC	CCC	CGC	CTG	GGT	11325	
3751	I	P	A	E	E	A	L	R	L	D	A	G	Q	L	A	T	G	I	V	D	P	R	G	C	G	3775	
11326	CTC	CAC	CTC	CCT	CTG	GAG	GTG	GCT	TAC	CAA	CGC	GGC	TAC	CTC	AAT	AAG	GAC	ACG	CAC	CAG	L	TCG	GAG	CCC	11400		
3776	T	H	L	P	L	E	V	A	Y	Q	R	G	Y	L	N	K	D	T	H	D	Q	L	S	E	P	3800	
11401	AGC	GAG	GTG	CGC	AGC	TAC	GTG	GAC	CCC	TCC	ACG	GAT	GAG	CGG	CTC	AGC	TAC	ACA	CAG	CTG	CTC	AAG	CGT	TGC	CGC	11475	
3801	S	E	V	R	S	Y	V	D	P	T	D	E	R	L	S	Y	T	Q	L	L	L	K	R	C	R	3825	
11476	CGT	GAT	GAC	CCC	AGC	GGC	CAG	ATG	CTG	CTG	CTC	CTC	TCT	GAT	GCC	CGC	AAG	CTG	ACC	TTC	CGC	GGT	CTC	CGC	AAG	11550	
3826	R	D	D	P	S	G	Q	M	L	L	L	L	S	D	A	R	K	L	T	F	R	G	L	R	K	3850	
11551	CAG	ATC	ACT	GTG	GAG	GAG	CTG	GTA	CGC	TCT	CAA	GTG	ATG	GAC	GAG	GCC	ACA	GCG	CTA	Q	CTA	CAA	GAA	GGC	CTG	11625	
3851	Q	I	T	V	E	E	L	V	R	T	Q	V	M	D	E	A	T	A	L	L	Q	Q	G	C	L	3875	
11626	ACC	TCC	ATC	GAG	GAG	GTC	ATC	AAG	AAC	CTG	CAG	AAG	TTC	CTC	GAG	GGT	ACC	AGC	TGC	ATT	GCC	GGA	GTC	TTT	GTT	11700	
3876	T	S	I	E	E	V	T	K	N	L	Q	K	F	L	E	G	T	S	C	I	A	G	V	F	V	3900	
11701	GAT	GCC	ACC	AAG	GAA	CGG	CTC	TCG	GTG	TAC	Q	GAT	ATG	AAG	AAG	GGC	ATC	ATC	CGC	CCC	GGG	ACA	GCC	TTT	GAG	11775	
3901	D	A	T	K	E	R	L	S	V	Q	A	M	K	A	K	G	I	I	I	P	T	A	F	E	E	3925	
11776	CTC	CTG	GAA	GCA	CAG	GCA	GCC	ACC	GGC	TAT	GTG	ATT	GAC	CCC	ATC	AAG	GGA	CTC	AAG	CTG	ACG	GTG	GAA	GAA	GCC	11850	
3926	L	L	E	A	Q	A	A	T	G	Y	V	I	D	P	I	K	G	L	K	L	T	V	E	E	A	3950	
11851	GTT	CGT	ATG	GGT	ATT	GTG	GGC	CCC	GAG	TTC	AAG	GAC	AAG	CTG	L	CTG	TCA	GCT	GAG	CGT	GCC	GTC	ACT	GGC	TAC	AAG	11925
3951	V	R	M	G	I	V	G	P	E	K	D	K	L	CTG	S	A	E	G	R	C	T	G	Y	K	K	3975	
11926	GAC	CCC	TAC	TCT	GGG	AAA	CTC	ATC	TCC	CTC	TTC	CAG	GCC	ATG	AAG	AAG	GGC	CTG	ATC	CTG	AAG	GAC	CAT	GGC	ATC	12000	
3976	D	P	Y	S	G	K	L	I	S	L	F	Q	A	M	K	K	G	L	I	L	K	D	H	G	I	4000	
12001	CGT	CTG	CTG	GAG	GCT	CAG	ATC	GCC	ACT	GGG	GGC	ATC	ATT	GAC	CCC	GAG	GAG	AGC	CAC	CGT	TTG	CCT	GTG	GAA	GTG	12075	
4001	R	L	L	E	A	I	A	T	G	G	I	I	D	P	E	E	S	H	C	R	L	P	V	E	V	4025	
12076	GCC	TAT	AAG	CGC	GGC	CTC	TTT	GAT	GAG	GAG	ATG	AAC	GAG	ATC	TTG	ACT	GAT	CCC	TCA	GAT	GAC	ACC	AAG	GGT	TTT	12150	
4026	A	Y	K	R	G	L	F	D	E	E	M	N	AC	E	I	L	T	D	P	S	D	T	K	G	F	4050	
12151	TTT	GAC	CCC	AAC	ACA	E	G	GAG	AAC	CTC	ACT	TAC	CTG	Q	L	CTG	ATM	GAG	CGC	TGC	ATC	ACT	GAC	CCC	CAG	12225	
4051	F	D	P	N	T	E	N	L	T	A	G	Y	L	L	G	E	R	C	I	T	D	P	Q	T	G	4075	
12226	CTG	TGT	CTC	CTG	CCC	CTG	AAG	GAG	AAG	AAG	CGG	GAA	CGG	AAG	ACA	TCC	TCC	AAG	TCC	TCA	GTG	CGC	AAG	CGC	CGC	12300	
4076	L	C	L	L	P	L	K	E	K	K	R	E	R	K	T	S	S	K	S	V	R	K	K	R	R	4100	
12301	GTG	GTG	ATT	GTG	GAC	CCA	GAG	ACG	GGC	AAG	GAG	ATG	TCT	GTG	TAC	GAG	GCC	TAC	CGC	AAG	GGT	CTC	ATT	GAC	CAC	12375	
4101	V	I	V	D	T	E	T	G	K	G	E	M	S	V	Y	E	A	Y	R	K	L	I	G	D	H	4125	
12376	CAG	ACG	TAC	CTG	GAG	TTG	TCG	GAG	CAG	GAG	TGT	GAG	TGG	GAG	ATC	ACC	ATC	TCC	TCC	TCA	GAT	GGC	GTC	GTC	12450		
4126	Q	T	Y	L	E	L	S	E	Q	E	C	E	W	E	E	I	T	I	S	S	D	G	V	V	4150		
12451	AAG	TCT	ATG	ATC	ATC	GAC	CGC	CGC	TCT	GGT	CGC	CAG	TAT	GAC	ATC	GAC	GAC	GCC	ATC	ACC	AAG	AAC	CTC	ATT	GAC	12525	
4151	K	S	M	I	I	D	R	S	R	S	G	Q	Y	D	I	D	A	I	T	G	N	L	C	I	D	4175	
12526	CGC	TCA	GCA	CTG	GAC	CAG	TAC	CGC	GCT	GGT	ACG	CTT	TCG	ATC	ACT	GAG	TTT	GCT	ACT	ATG	CTC	TCA	GGC	AAT	GCC	12600	
4176	R	S	A	L	D	Q	Y	R	A	G	T	L	S	I	T	E	F	A	D	M	L	S	G	N	A	4200	
12601	GGT	GGC	TTT	CGT	TCC	CGC	TCC	TCC	TCT	GTG	GGC	TCA	TCT	TCC	TCC	TAC	CCC	P	I	S	A	G	CCC	AGG	ACC	12675	
4201	G	F	R	S	S	S	S	S	S	V	S	S	S	S	S	S	P	I	S	A	G	P	R	T	4225		
12676	CAG	CTA	GCC	TCC	TGG	TCT	GAT	CCG	ACT	GAG	GAG	ACT	GGC	CCC	GTG	GCC	GGC	ATC	CTG	GAC	ACA	GAG	ACT	CTG	GAG	12750	
4226	Q	L	A	S	W	S	D	P	T	E	E	T	G	P	V	A	G	I	L	D	T	E	T	L	E	4250	
12751	AAG	GTG	TCC	ATC	ACT	GAG	GCC	ATG	CAC	CGC	AAC	CTG	GTA	GAC	NAC	ATC	ACC	GGC	Q	CGG	CTG	CTG	GAG	GCC	CAA	12825	
4251	K	V	S	I	T	C	E	A	M	H	R	N	L	V	D	I	T	G	C	R	L	L	E	A	Q	4275	
12826	GCC	TGC	ACC	GGG	GGC	ATC	ATT	GAC	CCC	AGC	ACT	GGT	GAG	CGC	TTC	CGT	GTC	ACT	GAA	GCT	GTC	AAC	AAG	GGC	CTG	12900	
4276	A	C	T	G	G	I	I	D	P	S	T	G	E	R	F	P	V	T	E	A	V	N	K	G	L	4300	
12901	GTG	GAC	AAG	ATC	ATG	GTA	GAC	CGT	ATC	AAT	CTG	GCC	CAG	AAG	GCC	TTC	TGT	GGG	TTT	GAG	GAC	CCA	CGT	ACC	AAG	12975	
4301	V	D	K	I	M	V	D	R	I	N	L	A	Q	K	A	F	C	G	F	E	D	P	R	T	K	4325	
12976	ACC	AAG	ATG	TCA	GCT	GCC	CAG	GCC	CTG	AAG	AAG	GGC	TGG	CTG	TAC	TAT	GAG	GCA	GGC	CAG	CGT	TTC	CTG	GAG	GTG	13050	
4326	T	K	M	S	A	A	Q	A	L	K	K	G	W	L	Y	Y	E	A	G	Q	R	F	L	E	V	4350	
13051	CAG	TAC	CTG	ACC	GGT	GGT	CTG	ATC	GAG	PCT	GAC	ACG	CCC	GGC	CGT	GTG	TCT	CTC	D	GAA	GCT	CTG	CAA	CGT	GGC	13125	
4351	Q	Y	L	T	G	L	I	E	P	D	T	P	G	T	V	S	L	L	G	A	L	L	R	G	G	4375	
13126	ACT	GTG	GAT	GCC	CGC	ACA	GCC	CAG	AAG	CTG	CGT	GAT	GTC	AGT	GCT	TAC	TCC	AAG	TAC	CTC	ACG	TGC	CCC	AAG	ACC	13200	
4376	T	V	D	A	R	T	A	Q	K	L	R	D	V	S	A	Y	S	K	Y	L	T	C	P	K	T	4400	
13201	AAG	CTC	AAG	ATC	TCC	TAC	AAG	GAC	GCT	CTG	GAC	CGT	AGC	ATG	GTG	GAG	GAG	GGC	ACG	GGG	CTG	AGG	CTG	CTG	GAG	13275	
4401	K	L	K	I	S	Y	K	D	A	L	D	R	S	M	V	E	E	G	T	G	L	R	L	L	E	4425	
13276	GCT	LGC	GCA	CAG	TCC	S	AG	GGC	TAC	TAC	AGC	CCG	TAC	ACG	GCT	AGT	GGC	TCT	GGC	TGC	ACC	GCC	GGC	TCA	CGC	13350	
4426	A	A	A	Q	S	K	G	Y	A	S	P	Y	S	T	S	V	G	S	S	T	A	G	G	S	R	4450	
13351	ACT	GGT	TCA	CGC	ACC	GGC	TCC	AGG	GCC	S	R	A	G	GGC	AGC	T	TTT	GAT	GCC	ACT	GGC	TCT	GGC	TTC	ATG	13425	
4451	T	G	S	R	T	C	R	A	G	S	R	R	R	R	G	F	D	A	A	T	G	S	G	F	S	M	4475
13426	ACC	TTT	TCT	TCT	TCC	TCC	TAC	TCT	TCC	TCA	GGC	TAT	GGC	CGC	CGC	TAT	GCC	TCA	GGG	CCT	TCA	GCC	TCT	CTT	GGG	13500	
4476	T	F	S	S	S	S	Y	S	S	S	G	Y	G	R	R	Y	A	S	G	P	S	A	S	L	G	4500	
13501	GGC	CCT	GAG	TCT	GCA	GTG	GCC	TGA																		13524	
4501	G	P	E	S	A	V	A	*																		4508	

## CURRICULUM VITAE

### Personal information

Name: Nevena Jaksic (ex Vukasinovic)  
 Date of birth: 24 October 1976  
 Location: Belgrade, Serbia  
 Contact: [nevena.vukasinovic@univie.ac.at](mailto:nevena.vukasinovic@univie.ac.at)

### Education

2003 – 2009 Ph.D. Student in Molecular Cell Biology.  
 Department of Molecular Cell Biology, University of Vienna,  
 Austria  
 Supervisor: Prof. Gerhard Wiche  
 28. Mar. 2006 International recognition of academic degree – *Magistra rerum*  
*Naturalium*, NARIC, Austrian Ministry of Education, Vienna,  
 Austria  
 08. Nov. 2002 Graduation, Molecular Biology and Physiology, University of  
 Belgrade. Diploma thesis: "The effect of nucleoside analog  
 Ribavirin on the expression of GFAP and vimentin after the injury  
 of the senso-motor cortex of adult rat"  
 1995 – 2002 Study of Molecular Biology and Physiology at the University of  
 Belgrade, Serbia  
 1991 – 1995 Secondary Grammar School in Belgrade, Serbia

### Work experience

Present inVentivHealth, Inc., Clinical Research Associate (pain  
 management)  
 2014 – 2015 Maternity leave  
 2012 – 2014 inVentivHealth, Inc., Clinical Research Associate (oncology)  
 2011 – 2012 Maternity leave  
 2010 – 2011 i3 Research, Clinical Research Associate (oncology)  
 2009 – 2009 Sick leave  
 2003 – 2009 Ph.D. Student in Molecular Cell Biology  
 Research topic: "Molecular, structural and *in vivo* analysis of  
 dominant plectin mutation EBS- Ogná", Dep. of Molecular Cell  
 Biology, Max F. Perutz Laboratories, University of Vienna,  
 Vienna, Austria  
 2007 – 2009 Research Associate at the Department of Molecular and Cell  
 Biology, MFPL, University of Vienna (Labor Manager, supervisor  
 of mouse genotyping assays and responsible for sequencing)  
 2004 – 2009 Miscellaneous teaching assignments at the University of Vienna  
 (Practical laboratory courses in Biochemistry and Cell Biology;  
 supervision of rotation students)

## Awards/Scholarships

2003 – 2006	Fellowship from the International PhD Program, Vienna Biocenter, (funded by the Austrian Science Research Fund, FWF).
1996 – 2002	Scholarship granted by Ministry of Education of Serbia

## Congresses and workshops

May 2003	Mini Symposium on the Formation, Storage and Retrieval of Memory “Memorize this”, organized by Students of the Vienna Biocenter “International PhD Program”, Vienna, Austria, <i>co-organizer and participant</i>
May 2005	IMP Spring Conference & IMBA Inaugural Conference, Vienna, Austria, <i>participant</i>
Aug. 2005	FEBS ESF Workshop “Integrated Approaches on Cytoskeleton Research”, Luxembourg, Luxembourg, <i>participant, poster presentation</i>
Sep. 2005	Workshop “Coiled-coils, Collagen & Co- proteins: IV”, Alpbach, Austria, <i>participant and poster presentation</i>
Oct. 2005	“6 <sup>th</sup> EMBL Mouse Molecular Genetics Meeting”, Heidelberg, Germany, <i>participant and poster presentation</i>
Nov. 2007	PhD Symposium "Molecules to Mind", <i>participant</i>

## Publications

Walko G, **Vukasinovic N**, Gross K, Fischer I, Sibitz S, Fuchs P, Reipert S, Jungwirth U, Berger W, Salzer U, Carugo O, Castañón MJ and Wiche G. 2011. Targeted Proteolysis of Plectin Isoform 1a Accounts for Hemidesmosome Dysfunction in Mice Mimicking the Dominant Skin Blistering Disease EBS-Ogna. PLoS Genetics 7: pp e1002396

## Posters

**Vukasinovic N**, Fuchs P, Castañón MJ and Wiche G. Molecular, structural, and *in vivo* analysis of the dominant plectin mutation EBS-Ogna. FEBS ESF Workshop “Integrated Approaches on Cytoskeleton Research”, Luxembourg, Luxembourg, 2005.

**Vukasinovic N**, Fuchs P, Castañón MJ and Wiche G. Molecular, structural, and *in vivo* analysis of the dominant plectin mutation EBS-Ogna. 6<sup>th</sup> EMBL Mouse Molecular Genetics Meeting, Heidelberg, Germany, 2005.

**Vukasinovic N** and Wiche G. Dominant plectin mutation EBS-Ogna. Alpbach Workshop “Coiled-coils, Collagen & Co-proteins: IV”, Alpbach, Austria, 2005.

## Miscellaneous skills

Languages	Serbian – native English – proficiency (IELTS 8.0) German – intermediate (speaking, reading), basic (writing)
Courses	English in an European and International Context Course for oral presentation in English Writing Scientific Texts in English
Computer Skills	Microsoft Office, Adobe Illustrator, Adobe Photoshop